Title

Analysis of BRCA1-BARD-1 Function in Caenorhabditis elegans Meiosis

Permalink

https://escholarship.org/uc/item/9gz914fm

Author

Li, Qianyan

Publication Date

2022

Peer reviewed|Thesis/dissertation

Analysis of BRCA1-BARD-1 Function in *Caenorhabditis elegans* Meiosis

By

QIANYAN LI
DISSERTATION

Submitted in partial satisfaction of the requirements for the degree of

DOCTOR OF PHILOSOPHY

in

Biochemistry, Molecular, Cellular and Developmental Biology

in the

OFFICE OF GRADUATE STUDIES

of the

UNIVERSITY OF CALIFORNIA

DAVIS

Approved:

_____

JoAnne Engebrecht, Chair

_____

Daniel A. Starr

_____

Francis J. McNally

Committee in Charge

2022

Abstract

Sexual reproduction relies on successful completion of meiosis, a specialized cell division that produces haploid eggs and sperm; errors in meiosis lead to aneuploid gametes and have devastating consequences on progeny viability. To ensure each gamete receives the correct complement of chromosomes, crossovers are established between each chromosome pair, which along with microtubule attachment, allow for biorientation of the homologous chromosomes across the cell division plane. Many meiotic DNA double strand breaks (DSBs) are purposely introduced in early meiotic prophase to make sure each chromosome pair will receive at least one crossover. The repair of these DSBs by different DNA repair pathways, with homologous recombination (HR) being the major one utilized during meiosis, results in both crossover and non-crossover products. Despite extensive research to understand meiosis, the specific mechanisms for how different repair pathways are utilized for efficient DNA repair, how the position and numbers of crossovers are determined, and how the entire process is orchestrated by different protein players remain elusive. BRCA1 and its binding partner BARD1 are tumor suppressors that play critical roles in maintaining genome integrity by promoting HR in somatic cells. The roles of BRCA1 and BARD1 in meiotic DSB repair, however, are largely unexplored. This is partially due to the two genes being essential in mammals, and null mutations of either gene results in embryonic lethality in mouse models. Further, BRCA1 and BARD1 together form a heterodimer that exhibits E3 ubiquitin ligase activity *in vitro* but it remains controversial whether this enzymatic activity is essential for BRCA1-BARD1 *in vivo* function. To answer these questions, I took advantage of *C. elegans*, a small nematode that contains

evolutionarily conserved BRCA1 and BARD1 orthologs (BRC-1 and BRD-1), to study their functions during spermatogenesis and oogenesis as well as to determine the requirement for E3 ligase activity of this complex in meiosis. By live cell imaging on worms expressing endogenous functional GFP fusions to BRC-1 and BRD-1, I found both proteins localize to DNA damage sites in early meiotic prophase and then concentrate onto a specific chromosome domain defined by crossover sites. Consistent with this localization pattern, I found BRC-1-BRD-1 plays important roles in DNA DSB repair and also influences crossover patterning in the germ line. During oogenesis, this complex stabilizes the RAD-51 filament in late pachytene and promotes the formation of extra crossovers under checkpoint activation conditions. Surprisingly, BRC-1-BRD-1 exhibits opposing functions during spermatogenesis, promoting DNA resection in early pachytene and inhibiting extra crossover formation when meiosis is perturbed. Using a combination of biochemistry and cell biology, I discovered that E3 ligase activity of BRC-1-BRD-1 is specifically required for the recruitment and concentration of the complex to DNA damage sites in the meiotic region of the gonad but not in the mitotic region where germline stem cells actively divide. The physiological substrates of BRC-1-BRD-1 in the germ line remain unknown, and future investigation will determine whether the differential functions observed for BRC-1-BRD-1 during oogenesis and spermatogenesis are results of the complex ubiquitylating different substrates in the female and male germ lines.

Dedication

Dedicated to my parents, Mengzhao Qian and Deshan Li.

Acknowledgement

First and foremost, I would like to thank my thesis advisor Dr. JoAnne Engebrecht for her continuous support and guidance over the years. JoAnne is the most patient and dedicated mentor I have ever met, and I sincerely appreciate her patience and the time she has generously spent to help me overcome the challenges that I encountered as a graduate student. JoAnne has provided me freedom to explore my scientific interest and is always there when I need her support. This work would not have been promptly completed without her guidance and help. I am sincerely grateful to be trained under her mentorship.

I would like to thank my academic advisor, Dr. Qizhi Gong, who has kindly provided me with many suggestions for my academic progress and career plans. Likewise, I would like to extend my gratitude to my thesis committee members, Drs. Daniel Starr and Francis McNally, for providing feedback on my thesis work, evaluating my research progress and sharing scientific expertise.

I would like to thank my lab colleagues Arshdeep Kaur and Sara Hariri for helping me with many experiments, providing the opportunity for me to grow as a mentor, and hanging out outside of the lab between experiments. I would also like to acknowledge previous Engebrecht lab members who helped get me started when I joined. Kate Lawrence provided initial training on using the deconvolution microscopy. Alison Deshong taught me how to microinject and use the 3i spinning disc confocal microscopy. Aleksandra Kuzmanov provided helpful advice from the perspective of an international scholar. Mike Van taught me how to make figures using Illustrator and Braden Larson showed me how to dissect worms.

Table of Contents

Chapter 1

Introduction

BRCA1 and BRCA2 Tumor Suppressor Function in Meiosis

Qianyan Li and JoAnne Engebrecht*

Department of Molecular and Cellular Biology, and Biochemistry, Molecular, Cellular and Developmental Biology Graduate Group, University of California, Davis, Davis, CA, United States

Meiosis is a specialized cell cycle that results in the production of haploid gametes for sexual reproduction. During meiosis, homologous chromosomes are connected by chiasmata, the physical manifestation of crossovers. Crossovers are formed by the repair of intentionally induced double strand breaks by homologous recombination and facilitate chromosome alignment on the meiotic spindle and proper chromosome segregation. While it is well established that the tumor suppressors BRCA1 and BRCA2 function in DNA repair and homologous recombination in somatic cells, the functions of BRCA1 and BRCA2 in meiosis have received less attention. Recent studies in both mice and the nematode *Caenorhabditis elegans* have provided insight into the roles of these tumor suppressors in a number of meiotic processes, revealing both conserved and organism-specific functions. BRCA1 forms an E3 ubiquitin ligase as a heterodimer with BARD1 and appears to have regulatory roles in a number of key meiotic processes. BRCA2 is a very large protein that plays an intimate role in homologous recombination. As women with no indication of cancer but carrying BRCA mutations show decreased ovarian reserve and accumulated oocyte DNA damage, studies in these systems may provide insight into why BRCA mutations impact reproductive success in addition to their established roles in cancer.

Keywords: BARD1, BRCA1, BRCA2, DSBs, meiosis, MSCI, recombination

INTRODUCTION

Homologous recombination (HR) is a high-fidelity pathway that mediates error-free repair of DNA double strand breaks (DSBs) and is essential for maintaining genome integrity. In somatic cells, DSBs can arise when DNA replication is impeded or following exposure to irradiation or other genotoxic stress. Cells deficient for HR show genomic instability including chromosome rearrangements, characteristic of most cancers (Negrini et al., 2010). In contrast to somatic cells, where DSBs pose a risk to genome integrity, during meiosis, hundreds of DSBs are purposely introduced by the topoisomerase-like protein SPO11 in early meiotic prophase and these meiotic DSBs must be accurately repaired for the production of euploid gametes (Lam and Keeney, 2014). As meiosis proceeds, meiotic DSBs are processed by DNA end resection to reveal 3′ overhangs (Garcia et al., 2011). The RAD51 recombinase as well as the meiosis-specific paralog DMC1 assemble on the resulting single strand DNA to form nucleoprotein filaments that mediate strand invasion and homology search for accurate repair (Shinohara and Shinohara, 2004). Meiotic DSB repair occurs concomitantly with the assembly of the synaptonemal complex (SC), the meiosis-specific multi-protein structure that forms between homologous chromosomes. In many

organisms, SC assembly is driven by HR (Zickler and Kleckner, 2015). In the context of full length SC at the pachytene stage of meiotic prophase, a subset of recombination intermediates is processed into inter-homolog crossovers, which are essential for accurate separation of homologous chromosomes at meiosis I (Neale and Keeney, 2006; Baudat and de Massy, 2007). A large number of proteins are critical for HR, including the tumor suppressors BRCA1 and BRCA2, whose functions have been well characterized in somatic cells in the context of DNA damage and carcinogenesis. However, the roles of BRCA1 and BRCA2 during meiotic recombination have received less attention. Although the processing of DSBs by HR is similar in somatic cells and meiosis, meiotic recombination is unique in that SPO11 remains attached to the DNA end following DSB formation. Additionally, meiotic recombination occurs in the context of the SC and both sister and non-sister chromatids can serve as templates for repair. Thus, BRCA1 and BRCA2 function may be modified in meiosis to ensure accurate repair of meiotic DSBs. Studies in model organisms have provided insights into the roles of BRCA1 and BRCA2 in meiosis. This review will summarize the conserved and organism-specific meiotic functions of BRCA1 and BRCA2, focusing on recent studies in mice and *C. elegans*.

BRCA1 IN COMPLEX WITH BARD1 IS AN E3 UBIQUITIN LIGASE CRITICAL FOR GENOME INTEGRITY

Breast cancer susceptibility gene 1 (BRCA1) is a tumor suppressor gene, germline mutations of which are linked to familial breast and ovarian cancers (Hall et al., 1990; Futreal et al., 1994; Godwin et al., 1994; Miki et al., 1994). More than two decades of research has implicated BRCA1 function in multiple cellular pathways, including transcriptional regulation, DNA damage signaling, cell cycle checkpoints, centrosome regulation and in the repair of DNA DSBs through HR (Moynahan et al., 1999; Xu et al., 1999; Deng, 2002, 2006; Yarden et al., 2002; Caestecker and Van de Walle, 2013; Hill et al., 2014; Hatchi et al., 2015). Of critical importance, its role in promoting HR is directly linked to maintenance of genome integrity (Roy et al., 2011; Prakash et al., 2015).

In humans, the 1,863 amino acid BRCA1 protein has an N-terminal RING (Really Interesting New Gene) domain that coordinates two zinc cations in a cross-braced arrangement, a largely unstructured central region encoded by exon11, followed by a coiled coil domain and two C-terminal BRCT repeats (**Figure 1**). RING domains create a platform for binding to E2 ubiquitin conjugating enzymes and facilitate the transfer of ubiquitin from the E2 to substrates, thereby specifying E3 ubiquitin ligase activity (Deshaies and Joazeiro, 2009). The BRCT repeats are phosphopeptide interaction modules for binding to phosphorylated proteins (Manke et al., 2003; Rodriguez et al., 2003; Yu et al., 2003). BRCA1 forms a heterodimer with its obligate binding partner BARD1 (BRCA1-Associated RING Domain protein 1) through their N-terminal regions and the heterodimer exhibits efficient ubiquitin transfer activity (Wu et al., 1996; Meza et al., 1999; Brzovic et al., 2001;

Hashizume et al., 2001; Baer and Ludwig, 2002). The BARD1 protein is 777 amino acids in length and similar to BRCA1, contains a RING domain at its N-terminus and two BRCT repeats at its C-terminus (**Figure 1**). In addition, four ankyrin repeats involved in chromatin recognition of newly replicated sister chromatids are present in the middle of the protein (FoxIII, Le Trong et al., 2008; Nakamura et al., 2019). Most studies indicate that BARD1 is indispensable for BRCA1 function and depletion of BARD1 leads to highly similar phenotypes as observed for BRCA1 mutants. Mutations in BARD1 have been identified in patients with breast, ovarian and other cancer types, although at a lower frequency than BRCA1 mutations (Thai et al., 1998; Ghimenti et al., 2002). Further, as with BRCA1, loss of BARD1 results in embryonic lethality in mice as well as defects in HR leading to chromosomal instability (McCarthy et al., 2003).
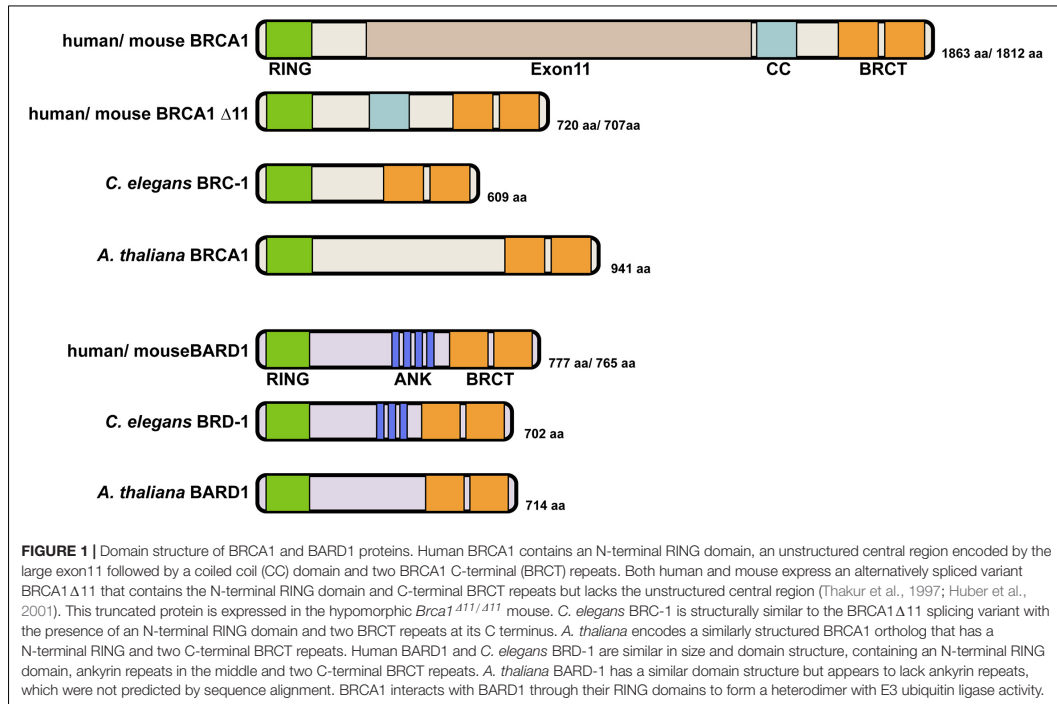
The mechanisms by which BRCA1-BARD1 promotes HR during DSB repair involve multiple steps. First, BRCA1 promotes DNA end resection by antagonizing 53BP1, a DNA damage response protein that promotes error-prone non-homologous end joining (NHEJ) (Bunting et al., 2010; Daley and Sung, 2014). Two, BRCA1 regulates the MRE11-RAD50-NBS1-CtIP complex essential for DNA end processing (Cruz-Garcia et al., 2014; Aparicio et al., 2016). There is also evidence that BRCA1 removes a chromatin barrier for DNA resection through ubiquitylation of histone H2A (Densham et al., 2016). In addition to promoting resection, BRCA1-BARD1 binds to DNA and interacts with RAD51 directly, enhancing RAD51 recombinase activity by promoting homologous strand invasion and synaptic complex formation (Zhao et al., 2017). However, whether BRCA1 functions by similar mechanisms to promote HR during meiosis for the repair of SPO11-induced DSBs has remained elusive.

BRCA1 FUNCTION IN MOUSE MEIOSIS

Mice homozygous for *Brca1* null alleles are embryonic lethal, excluding the possibility to assess BRCA1 function during meiosis (Gowen et al., 1996; Hakem et al., 1996; Liu et al., 1996; Ludwig et al., 1997). To circumvent this limitation, meiosis has been analyzed in mice carrying a hypomorphic mutation that deletes the large exon11 in the heterozygous *Trp53* (encoding p53) mutant background ($Brca1^{\Delta 11/\Delta 11}$ $Trp53^{+/-}$) (Xu et al., 2003; **Figure 1**). These mice develop and survive to adulthood; lethality likely bypassed by the reduced expression of *Trp53* (Cressman et al., 1999).

BRCA1 Is Essential for Meiotic Sex Chromosome Inactivation During Spermatogenesis

Although *Trp53* heterozygosity rescues the embryonic lethality of $Brca1^{\Delta 11/\Delta 11}$ mice, males are infertile as a result of pachytene arrest and apoptotic removal of germ cells (Xu et al., 2003). This observation revealed an essential role of BRCA1 in meiotic sex chromosome inactivation (MSCI). MSCI is a repressive mechanism that occurs during meiotic prophase I and involves elaboration of heterochromatin and transcriptional silencing of non-homologous regions of sex chromosomes (Turner, 2007).

3

FIGURE 1 | Domain structure of BRCA1 and BARD1 proteins. Human BRCA1 contains an N-terminal RING domain, an unstructured central region encoded by the large exon11 followed by a coiled coil (CC) domain and two BRCA1 C-terminal (BRCT) repeats. Both human and mouse express an alternatively spliced variant BRCA1Δ11 that contains the N-terminal RING domain and C-terminal BRCT repeats but lacks the unstructured central region (Thakur et al., 1997; Huber et al., 2001). This truncated protein is expressed in the hypomorphic *Brca1*^Δ11/Δ11 mouse. *C. elegans* BRC-1 is structurally similar to the BRCA1Δ11 splicing variant with the presence of an N-terminal RING domain and two BRCT repeats at its C terminus. *A. thaliana* encodes a similarly structured BRCA1 ortholog that has a N-terminal RING and two C-terminal BRCT repeats. Human BARD1 and *C. elegans* BRD-1 are similar in size and domain structure, containing an N-terminal RING domain, ankyrin repeats in the middle and two C-terminal BRCT repeats. *A. thaliana* BARD-1 has a similar domain structure but appears to lack ankyrin repeats, which were not predicted by sequence alignment. BRCA1 interacts with BARD1 through their RING domains to form a heterodimer with E3 ubiquitin ligase activity.

MSCI is required for efficient meiotic progression in males as failure to repress the X and Y chromosomes results in elevated germline apoptosis (**Figure 2**).
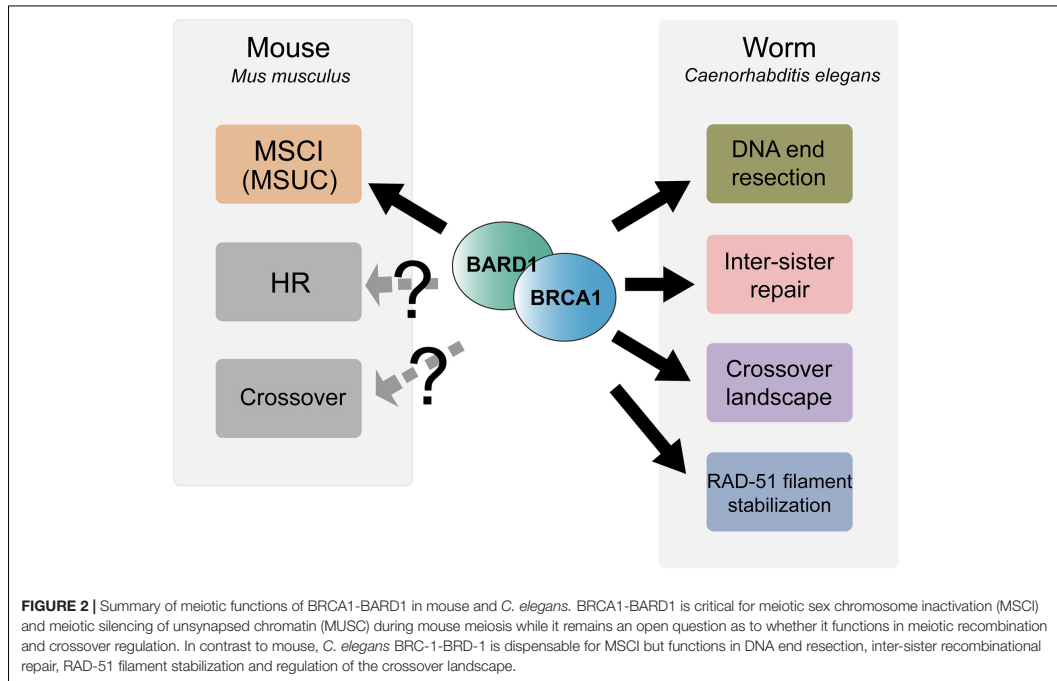
In wild-type spermatocytes, BRCA1 localizes to asynapsed chromosome axes, including the mostly unsynapsed X and Y sex chromosomes (Scully et al., 1997). BRCA1 recruits the checkpoint kinase ataxia telangiectasia and Rad3-related protein (ATR) to the hemizygous regions of sex chromosomes; ATR phosphorylates a histone variant, H2AX, to form γH2AX, leading to sex chromosome compaction and transcriptional silencing (Fernandez-Capetillo et al., 2003; Turner et al., 2004). In the absence of full length BRCA1, ATR and γH2AX localization is disrupted, formation of XY sex body fails, and transcriptional silencing is abolished, leading to ectopic gene transcription from the hemizygous regions of the sex chromosomes (Xu et al., 2003; Turner et al., 2004; Broering et al., 2014). The inability to execute successful MSCI in the *Brca1*^Δ11/Δ11 mutant has been attributed to a direct role of BRCA1 in establishing heterochromatin on the X and Y chromosomes and XY body morphogenesis, rather than an indirect consequence of defective meiotic recombinational repair in the absence of full-length BRCA1 (Broering et al., 2014).

The related process of meiotic silencing of unsynapsed chromatin (MSUC) also requires BRCA1 and operates in both male and female germ cells (Mahadevaiah et al., 2008; Kouznetsova et al., 2009). As with MSCI, MSUC leads to accumulation of repressive chromatin and transcriptional silencing on any asynapsed chromosomal regions. MSUC promotes the elimination of gametes with chromosome asynapsis and is initiated by the recruitment of BRCA1 to unsynapsed chromosomes through the interaction with the SC axial component SYCP3. Interestingly, oocytes have a limited capacity to silence unsynapsed chromosomes and this appears to be a consequence of the amount of BRCA1 available to accumulate on unsynapsed chromosomes. Thus, the role of BRCA1 in transcriptional silencing contributes to ensuring the production of euploid gametes.

Potential BRCA1 Role in Meiotic Recombination

In addition to MSCI failure, spermatocytes from *Brca1*^Δ11/Δ11 Trp53^+/− mice exhibited a prolonged autosomal γH2AX signal with greatly reduced numbers of RAD51 (but not DMC1) and MLH1 foci, suggesting that BRCA1 plays a role in meiotic DSBs repair and crossover formation (Xu et al., 2003). In contrast, a separate study utilizing Cre/LoxP mediated conditional germline-specific deletion of *Brca1* exon11 in the presence of both wild-type *Trp53* alleles showed that RAD51 foci were not reduced, although decreased numbers of MSH4 foci and delayed appearance of MLH1 foci were observed. These authors concluded that while BRCA1 is not essential for meiotic DSB repair, BRCA1 might be involved in the regulation of the

4

FIGURE 2 | Summary of meiotic functions of BRCA1-BARD1 in mouse and *C. elegans*. BRCA1-BARD1 is critical for meiotic sex chromosome inactivation (MSCI) and meiotic silencing of unsynapsed chromatin (MUSC) during mouse meiosis while it remains an open question as to whether it functions in meiotic recombination and crossover regulation. In contrast to mouse, *C. elegans* BRC-1-BRD-1 is dispensable for MSCI but functions in DNA end resection, inter-sister recombinational repair, RAD-51 filament stabilization and regulation of the crossover landscape.

timing of crossover formation (Broering et al., 2014). In a recent study using END-seq on mouse spermatocytes that allows direct examination of meiotic DSB processing at the single nucleotide level, hypomorphic $Brca1^{\Delta11/\Delta11}$ $Trp53^{+/-}$ mice did not exhibit a reduction in resection track length, suggesting that BRCA1 does not promote DNA resection in meiotic DSB repair as in somatic cells (Paiano et al., 2020). Together these results suggest that the critical meiotic role for BRCA1 is in transcriptional silencing; however, it is possible that BRCA1 function in meiotic recombination is obscured by the use of the hypomorphic $Brca1^{\Delta11/\Delta11}$ mutant (**Figure 2**).

Analysis of female meiosis in the hypomorphic $Brca1^{\Delta11/\Delta11}$ mutation revealed no observable phenotypes. Female *Brca1* mutants are fertile and the number of MLH1 foci are comparable to that observed in wild-type oogenesis, suggesting that the region deleted in $Brca1^{\Delta11/\Delta11}$ is not required for meiotic recombination during female meiosis (Xu et al., 2003; Broering et al., 2014). Therefore, the observed sex-specific phenotypes in the hypomorphic $Brca1^{\Delta11/\Delta11}$ mutant are likely a consequence of the presence of unsynapsed sex chromosomes in males. It is also important to note that the region encoded by exon11 is thought to be unstructured with no resemblance to known domain structures (Li and Greenberg, 2012). Future studies focusing on the RING domain, which confers E3 ubiquitin ligase activity, and the BRCT repeats, are necessary to reveal whether these domains play important roles in the repair of meiotic DSBs in both male and female meiosis. Finally, to the best of our

knowledge a functional role of BARD1 in mice gametogenesis has not been examined.

BRCA1 FUNCTION IN *C. ELEGANS* MEIOSIS

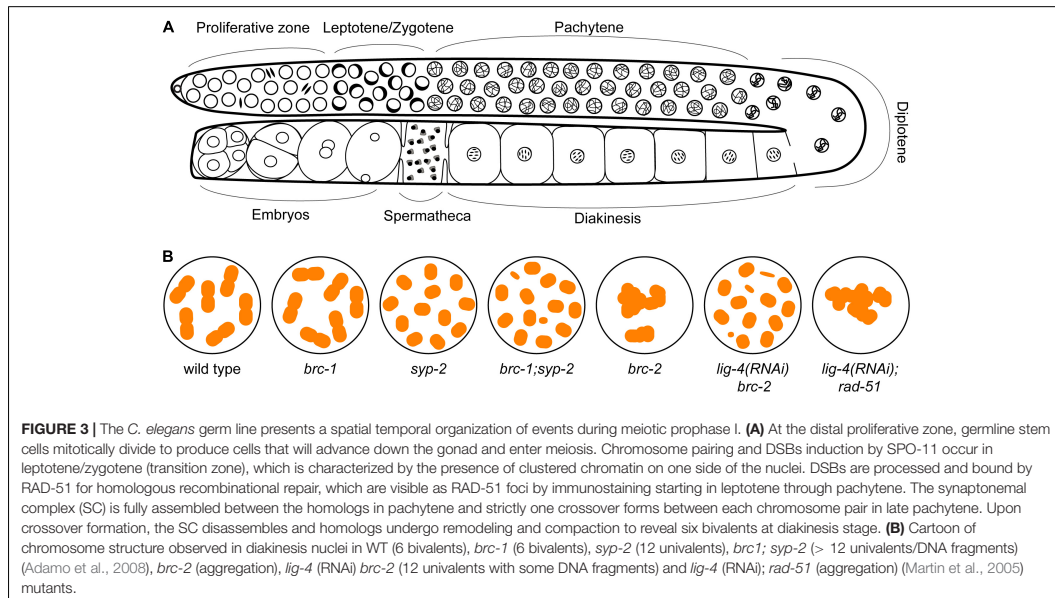### The *C. elegans* Germ Line as a Model for Studying Meiosis and BRCA1-BARD1 Function

Caenorhabditis elegans has emerged as an excellent model for investigating meiosis: many genes required for meiotic recombination are conserved in this metazoan and the animals possess prominent gonads that exhibit a spatial temporal organization of germ cells undergoing meiotic prophase I (**Figure 3A**). At the distal tip, germline stem cells divide to produce cells that will advance down the gonad and enter meiosis. In transition zone (corresponding to leptotene/zygotene), homologous chromosomes are paired together, facilitated by Zn-finger ZIM-1/2/3 and HIM-8 proteins that bind to special sequences present on each homolog pair. Beginning at this stage, SPO-11 induces meiotic DSBs, which are processed and bound by RAD-51 for homologous recombinational repair. In pachytene, the SC is fully assembled between the homologs and within this context strictly one crossover forms between each chromosome pair in late pachytene. Upon crossover formation, the SC

5

disassembles and homologs undergo remodeling and compaction to reveal six bivalents at diakinesis stage, representing the six pairs of homologs connected by chiasmata (**Figure 3B**; Lui and Colaiacovo, 2013; Hillers et al., 2017). Although the overall process is very similar to other systems, it is important to note that there are differences unique to *C. elegans* meiosis. These include the absence of DMC1 in this organism, thus RAD-51 is the sole recombinase acting during both mitotic and meiotic recombination (Brown and Bishop, 2014). Interestingly, *C. elegans* RAD-51 contains three amino acids conserved in the DMC1 lineage that stabilize mismatch-containing heteroduplex DNA, critical for meiotic recombinase function (Steinfeld et al., 2019). Another unique feature of *C. elegans* meiosis is that chromosome synapsis does not depend on meiotic recombination initiation (Dernburg et al., 1998). Nevertheless, the availability of molecular markers combined with genetic and genomic approaches has made the *C. elegans* germ line a powerful system that provides a unique opportunity to dissect gene function at any particular sub-stage of meiotic prophase. Most importantly, proteins with conserved domain structure and sequence similarity to BRCA1 and BARD1, referred to as BRC-1 and BRD-1, are encoded in the *C. elegans* genome. *brc-1* and *brd-1* null mutants exhibit elevated IR sensitivity and a higher incidence of males among self-progeny (a readout of X chromosome non-disjunction) compared to wild type, but are mostly fertile, allowing analysis of meiotic outcomes in the absence of functional BRCA1 and BARD1 (Boulton et al., 2004; Li et al., 2018). Similar to *C. elegans*, *Arabidopsis AtBRCA1* and *AtBARD1* mutants are also fertile, suggesting that the essentiality of mammalian BRCA1-BARD1 is not broadly conserved (Reidt et al., 2006).

C. elegans brc-1 encodes a 609 amino acid protein with highly conserved N-terminal RING domain and C terminal BRCT repeats, similar to the human protein. Structurally, *C. elegans* BRC-1 is analogous to the BRCA1Δ11 splicing variant (**Figure 1**). AtBRCA1 with 941 amino acids is also considerably smaller than the human protein. The *C. elegans* BRD-1 and AtBARD1 proteins are similar in both size and domain architecture to the human protein, although AtBARD1 does not have recognizable ankyrin repeats (**Figure 1**). Interestingly, *C. elegans* BRC-1-BRD-1 exhibits dynamic localization throughout meiotic prophase. Discrete foci of BRC-1-BRD-1 that partially colocalize with RAD-51 are present in both proliferative/mitotic region and early meiotic prophase, from leptotene to early pachytene (Li et al., 2018, 2020). As meiotic prophase progresses, BRC-1-BRD-1 localizes with the SC between the maternal and paternal chromosomes (Polanowska et al., 2006; Janisiw et al., 2018; Li et al., 2018). This localization is in contrast to BRCA1 localization in mammalian meiocytes, where BRCA1 is found on the axes of asynapsed chromosomes (Turner et al., 2004). In late pachytene upon crossover maturation, BRC-1-BRD-1 concentrates on one subdomain of the chromosome pair termed the "short arm", suggesting an intimate connection of BRC-1-BRD-1 to crossover sites and potential involvement in crossover regulation.

BRC-1-BRD-1 Is Not Essential for Meiotic Sex Chromosome Inactivation but Promotes HR in Spermatogenesis

C. elegans BRC-1-BRD-1 is absent from the single asynapsed X chromosome in male germ cells, and consistent with

FIGURE 3 | The *C. elegans* germ line presents a spatial temporal organization of events during meiotic prophase I. **(A)** At the distal proliferative zone, germline stem cells mitotically divide to produce cells that will advance down the gonad and enter meiosis. Chromosome pairing and DSBs induction by SPO-11 occur in leptotene/zygotene (transition zone), which is characterized by the presence of clustered chromatin on one side of the nuclei. DSBs are processed and bound by RAD-51 for homologous recombinational repair, which are visible as RAD-51 foci by immunostaining starting in leptotene through pachytene. The synaptonemal complex (SC) is fully assembled between the homologs in pachytene and strictly one crossover forms between each chromosome pair in late pachytene. Upon crossover formation, the SC disassembles and homologs undergo remodeling and compaction to reveal six bivalents at diakinesis stage. **(B)** Cartoon of chromosome structure observed in diakinesis nuclei in WT (6 bivalents), *brc-1* (6 bivalents), *syp-2* (12 univalents), *brc1; syp-2* (> 12 univalents/DNA fragments) (Adamo et al., 2008), *brc-2* (aggregation), *lig-4* (RNAi) *brc-2* (12 univalents with some DNA fragments) and *lig-4* (RNAi); *rad-51* (aggregation) (Martin et al., 2005) mutants.

6

this observation, BRC-1-BRD-1 is not required for MSCI during spermatogenesis. In *brc-1* and *brd-1* null mutants, deposition of the repressive chromatin mark H3K9me2 and the absence of Pol2-S2P (actively transcribing RNA polymerase II) signal on the X chromosome are indistinguishable from wild-type animals, suggesting that MSCI is successful in these mutants. As such, the null mutants do not exhibit pachytene arrest and germ cells complete meiotic prophase in preparation for the meiotic divisions (Li et al., 2020).

Analysis of RAD-51 immunostaining in the *brc-1* and *brd-1* null male germ lines showed reduced levels of RAD-51 foci in early meiotic prophase and this reduction was suppressed by inhibiting the NHEJ pathway. Moreover, quantification of GFP:RPA-1 foci, indicative of single stranded DNA, showed a significant reduction in overall foci number and intensity in the absence of BRC-1-BRD-1, suggesting that BRC-1-BRD-1 favors HR at the expense of NHEJ through promoting resection of DSBs during male meiosis (Li et al., 2020; **Figure 2**). This role is similar to what is proposed for BRCA1 function in promoting HR in somatic cells.

BRC-1-BRD-1 Promotes Inter-Sister Recombination and Stabilizes the RAD-51 Filament Under Checkpoint Activation in Oogenesis

In contrast to male meiosis, *brc-1* and *brd-1* null mutants exhibited an increased number of RAD-51 foci at late pachytene in oogenic germ lines, with no obvious difference in RAD-51 kinetics in early meiotic prophase as compared to wild-type animals (Adamo et al., 2008; Janisiw et al., 2018; Li et al., 2018). The elevated RAD-51 foci observed in late pachytene suggests that the repair of a subset of DSBs is delayed in the absence of BRC-1-BRD-1. The high fertility and presence of six bivalents, representing the six homologs connected by chiasmata, at diakinesis in *brc-1* and *brd-1* mutants (**Figure 3B**) suggest that BRC-1-BRD-1 is not essential for crossover formation. To test the hypothesis that BRC-1 promotes repair of DSBs by the inter-sister recombination pathway, Adamo and coworkers disrupted SC assembly and thereby inter-homolog crossovers by mutation of *syp-2* (one of six components in the central region of the SC) in the *brc-1* mutant. *syp-2* mutants have twelve intact univalents at diakinesis (**Figure 3B**), suggesting efficient repair of DSBs by the inter-sister pathway. On the other hand, in the *brc-1; syp-2* double mutant more than twelve DAPI staining bodies were often observed (**Figure 3B**), indicating the presence of chromosome fragmentation and failure in inter-sister repair. These results are consistent with BRC-1 playing an important role in inter-sister repair during oogenesis (Adamo et al., 2008). A recent study extended these findings by showing that mutation of *brc-1* enhanced the phenotype of phosphorylation defective mutants in *syp-1* (another component of the central region of the SC), presumably through impairment of inter-sister recombination (Garcia-Muse et al., 2019; **Figure 2**). Importantly, BRC-1-dependent inter-sister repair prevents erroneous recombination

(recombination between heterologous sequences) in meiosis, suggesting one mechanism by which BRC-1 prevents genome instability (Leon-Ortiz et al., 2018).

In addition to promoting inter-sister repair, BRC-1 is required to stabilize the RAD-51 filament from premature disassembly in late pachytene under meiotic checkpoint activation conditions. In *zim-1/2/3* or *syp-1* mutants, which lack crossovers on a subset or all chromosomes, respectively, and activate meiotic checkpoints, extensive RAD-51 foci are present throughout meiotic prophase (Yu et al., 2016). Removing BRC-1 in these mutant backgrounds results in a region in late pachytene with significantly reduced RAD-51 levels, with high levels of RAD-51 both prior to and after this region. Both the number of RAD-51 foci as well as the fluorescence intensity of residual foci was greatly diminished in this region and thus this pattern has been referred to as a RAD-51 "dark zone". Taking advantage of the spatial temporal organization of the germ line, time course analysis of *spo-11; brc-1; syp-1* mutants exposed to irradiation (IR) was performed. The *spo-11* mutant was used so that breaks could be induced uniformly in the germ line at a single point in time by IR and as nuclei moved through the germ line no new breaks were formed. This analysis revealed that RAD-51 installed on processed DSBs in nuclei residing in early prophase at the time of DSB induction was dismantled once the nuclei reached late pachytene, suggesting that BRC-1 promotes the stability of the RAD-51 filament under these conditions (Li et al., 2018). The mechanism underlying BRC-1-dependent RAD-51 stabilization is currently unknown and could be either through direct interaction with RAD-51 to reduce its ATP hydrolysis and/or regulation of helicases which dismantle the RAD-51 filament. Interestingly, the requirement for BRC-1 to stabilize RAD-51 filaments under checkpoint activation conditions is oogenesis-specific, as a RAD-51 dark zone was not observed in the male germ line (Li et al., 2020; **Figure 2**).

Recent studies examining the mutational signatures of *brc-1* and *brd-1* mutants propagated over multiple generations revealed elevated levels of small deletions, deletions-insertions, single nucleotide variants and tandem repeats (Kamp et al., 2020; Volkova et al., 2020). Analysis of *brc-1* and *brd-1* mutants in combination with mutations in different repair pathways provided evidence that theta-mediated end joining (TMEJ), but not NHEJ, was responsible for the mutational profiles observed. TMEJ anneals short regions of microhomology and catalyzes template-dependent DNA synthesis to repair the broken DNA molecule. These results suggest that in the absence of BRC-1-BRD-1, TMEJ repairs inefficiently resected DSBs. It will be important to distinguish whether the mutations are a consequence of repair of meiotic DSBs, or repair of breaks generated during replication prior to meiotic entry or during embryogenesis, to understand the complete spectrum of BRC-1-BRD-1 function in both the soma and in meiosis. Nonetheless, the mutational profile of *C. elegans brc-1* and *brd-1* mutants is very similar to that found in BRCA1-deficient tumor cells, suggesting that TMEJ repair in the absence of BRCA1 contributes to carcinogenesis (Kamp et al., 2020; Volkova et al., 2020).

7

BRC-1-BRD-1 Regulates Crossover Patterning

Given that there are many more DSBs than crossovers, a subset of processed DSBs is chosen to be resolved as crossovers in a process referred to as crossover designation (Gray and Cohen, 2016). To investigate whether BRC-1 plays a role in crossover designation and/or resolution, genetic linkage analysis on meiotic products of *brc-1* mutants was performed and revealed an altered crossover landscape. Although the genetic map length was not significantly different between wild type and *brc-1* mutants, there was a shift in crossover distribution from chromosome arms, which are most often observed in wild-type animals, to more central regions on chromosomes (Li et al., 2018, 2020). Altered crossover distribution to the chromosome center has been observed in many other *C. elegans* mutants defective for various aspects of meiotic recombination (Zetka and Rose, 1995; Wagner et al., 2010; Meneely et al., 2012; Saito et al., 2012, 2013; Chung et al., 2015; Hong et al., 2016; Jagut et al., 2016). While the underlying mechanisms are currently unknown, it has been suggested that this could result from an altered chromatin landscape (Saito and Colaiacovo, 2017). Thus, BRCA1 may regulate chromatin structure in *C. elegans* meiosis, as it does in mouse meiosis (Broering et al., 2014; Densham et al., 2016), although the specific types of chromatin modification regulated by BRCA1 may not be identical in *C. elegans* and mouse.

Surprisingly, in the *zim-1* mutant where two chromosomes fail to pair and synapse, BRC-1-BRD-1 promoted the formation of extra COSA-1 marked crossover designation events on the remaining chromosome pairs during oogenesis. COSA-1 (CrossOver Site Associated protein 1) is generally accepted to mark canonical crossovers in *C. elegans* meiosis (Yokoo et al., 2012); therefore, the number of COSA-1 foci has been used as a cytological readout of the number of genetic crossovers. The reduced COSA-1 foci in the *brc-1; zim-1* double mutant, however, was not accompanied by a smaller genetic map distance, measured by SNP marker-based linkage analysis. These results suggest that not all crossovers are marked by COSA-1 in the *brc-1; zim-1* double mutant. Further, while the map length was similar in the absence of BRC-1, CO patterning was altered such that there were elevated levels of single crossovers (SCOs) with a concomitant reduction in double crossovers (DCOs). As a crossover can form between any two non-sister chromatids within paired homologs, two, three or four-strand DCOs are possible outcomes of elevated crossover formation. However, only DCOs between the same two chromatids can be detected as DCOs in SNP marker-based analysis, because only one sister chromatid is inherited in the product of meiosis. DCOs involving three or four chromatids will be detected as SCOs. Therefore, the aforementioned observation is consistent with a model whereby inactivation of BRC-1 in the *zim-1* mutant results in a shift from two-strand DCOs that are marked by COSA-1 and observed in the DCO class, to three- and four-strand DCOs that lack the COSA-1 marker and are detected as SCOs (Li et al., 2018). In contrast to oogenesis, BRC-1 inhibits the formation of extra COSA-1 marked crossover precursors in spermatogenesis. Elevated levels of COSA-1 foci were observed in the *brc-1; zim-1* double mutant as compared to *zim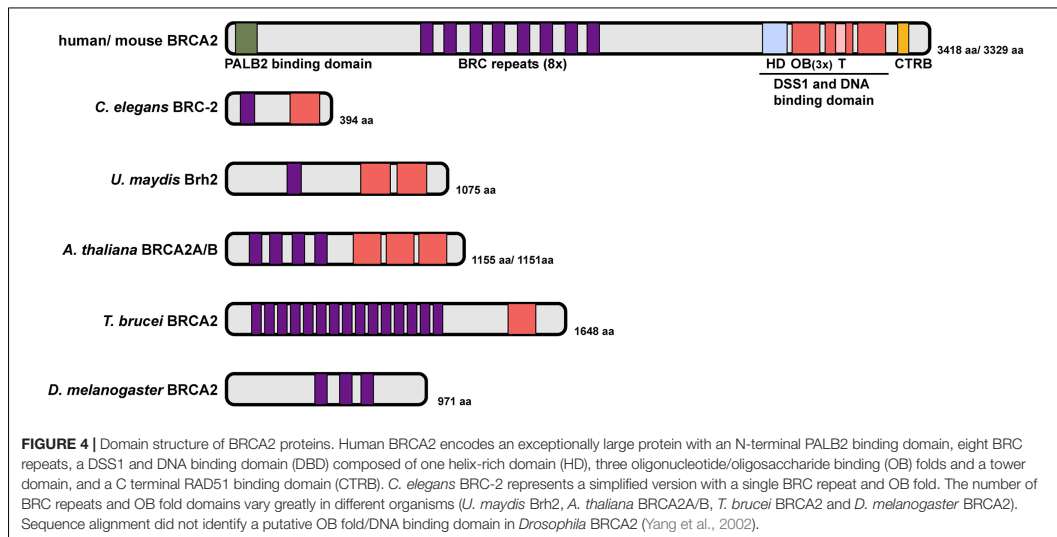-1*. Additionally, the genetic map distance was enlarged in the *brc-1; zim-1* double mutant, suggesting that BRC-1 inhibits the formation of extra canonical crossovers in spermatogenesis (Li et al., 2020). Together, these results suggest that BRC-1 plays a role in CO patterning, perhaps through regulating both canonical and non-canonical CO pathways under conditions of meiotic dysfunction (**Figure 2**).

Why does *brc-1* and *brd-1* mutation exhibit sex-specific phenotypes? One hypothesis is that BRC-1-BRD-1 interacts with unique partners to form different complexes during male and female meiosis. This would be analogous to what has been established for BRCA1 function in somatic cells, where it forms three different complexes with distinct functions under different physiological conditions (Li and Greenberg, 2012). Alternatively, or in addition, the sex-specific phenotypes could be a consequence of BRC-1-BRD-1 being differentially regulated by post-translational modifications in the diverging environments of male and female meiosis. Future studies on BRC-1-BRD-1 interacting proteins and the regulation of complex(es) will provide insight into the functions of BRC-1-BRD-1 during spermatogenesis and oogenesis. These studies may also shed light on the sex-specific regulation of the BRCA1-BARD1 complex in mammals.

BRCA2 FUNCTIONS AS AN ESSENTIAL MEDIATOR FOR HR

Breast cancer susceptibility gene 2 (BRCA2) is an essential mediator of HR (Jensen et al., 2010; Liu et al., 2010; Kowalczykowski, 2015). Similar to *BRCA1,* germline mutations in *BRCA2* predispose patients to breast and ovarian cancer and genome instability (Wooster et al., 1995; Yu et al., 2000; Venkitaraman, 2002; King et al., 2003). Biochemical, cell biological and genetic studies have supported a role of BRCA2 in recruiting the RAD51 recombinase to resected single strand DNA at DSBs and promoting nucleoprotein filament assembly to mediate homology search and strand exchange (Sharan et al., 1997; Wong et al., 1997; Abbott et al., 1998; Chen et al., 1999; Tutt et al., 1999; Yuan et al., 1999; Moynahan et al., 2001; Xu et al., 2001; Jensen et al., 2010; Liu et al., 2010; Thorslund et al., 2010).

Human BRCA2 encodes an exceptionally large protein consisting of 3,418 amino acids with multiple functional domains: an N-terminal domain that facilitates binding with Partner And Localizer of BRCA2 (PALB2), eight BRC repeats that define the RAD51 binding motif, a DSS1 and DNA binding domain (DBD, composed of one helix-rich domain (HD), three oligonucleotide/oligosaccharide binding (OB) folds and a tower domain), and a C terminal RAD51 binding domain (CTRB) (**Figure 4**; Yang et al., 2002; Esashi et al., 2005; Xia et al., 2006; Carreira et al., 2009; Shivji et al., 2009). Given its essential role in HR, it is not surprising that BRCA2 is conserved in fungi, plants and metazoans. While overall similar, BRCA2 orthologs possess different numbers of BRC repeats and OB folds, which are signature domains of BRCA2, and vary considerably in size (Gudmundsdottir and Ashworth, 2004; **Figure 4**). For example, Brh2, the BRCA2 ortholog in the fungus *Ustilago maydis,* contains a single BRC repeat and

8

FIGURE 4 | Domain structure of BRCA2 proteins. Human BRCA2 encodes an exceptionally large protein with an N-terminal PALB2 binding domain, eight BRC repeats, a DSS1 and DNA binding domain (DBD) composed of one helix-rich domain (HD), three oligonucleotide/oligosaccharide binding (OB) folds and a tower domain, and a C terminal RAD51 binding domain (CTRB). *C. elegans* BRC-2 represents a simplified version with a single BRC repeat and OB fold. The number of BRC repeats and OB fold domains vary greatly in different organisms (*U. maydis* Brh2, *A. thaliana* BRCA2A/B, *T. brucei* BRCA2 and *D. melanogaster* BRCA2). Sequence alignment did not identify a putative OB fold/DNA binding domain in *Drosophila* BRCA2 (Yang et al., 2002).

two OB folds (Kojic et al., 2002, 2005). *Drosophila melanogaster* BRCA2 contains three BRC repeats but no recognizable OB fold (Klovstad et al., 2008). Two almost identical BRCA2 orthologs were identified in *Arabidopsis thaliana*, each containing four BRC repeats (Siaud et al., 2004). In contrast, the parasite *Trypanosoma brucei* possess a single BRCA2 ortholog with 15 BRC repeats (Hartley and McCulloch, 2008). The BRC repeat is highly conserved among species; despite the different number of repeats, BRC domains in all BRCA2 orthologs examined so far have been shown to bind RAD51 directly and to promote RAD51 nucleoprotein filament formation on ssDNA, which is essential for homology search and strand exchange during HR. In addition, BRCA2 interaction with the highly conserved DSS1 protein also contributes to HR through promoting RAD51-recruitment activity and stability of BRCA2 (Li et al., 2006; Liu et al., 2010; Siaud et al., 2011). The CTRB domain, while conferring RAD51 binding and stabilizing RAD51 filaments on ssDNA, is not essential for HR (Davies and Pellegrini, 2007; Esashi et al., 2007; Prakash et al., 2015).

C. elegans BRCA2 (BRC-2) contains domain signatures similar to mammalian BRCA2 but is approximately 1/8 the size, with just 394 amino acids. BRC-2 contains a single BRC repeat that directly interacts with RAD51 and a single OB fold that preferentially binds to ssDNA (Martin et al., 2005; Petalcorin et al., 2006; **Figure 4**). The single BRC repeat is comprised of two RAD-51 interaction regions, one that preferentially binds to free RAD-51, and the other to the RAD-51-DNA nucleoprotein filament that exhibits inhibitory activity on RAD-51 ATPase hydrolysis. Together, these two RAD-51 interaction regions within the BRC repeat are proposed to coordinate the activity of BRC-2 for promoting RAD-51 nucleation on ssDNA and stabilizing existing RAD51 filament from disassembly through inhibiting ATP hydrolysis (Petalcorin et al., 2007). Recent single-molecule

analysis has revealed that BRC-2 acts primarily as a RAD-51 nucleation factor on RPA-coated ssDNA (Belan et al., 2021).

BRCA2 Role in Meiotic Recombination

In addition to a role of promoting RAD51 mediated HR in somatic cells, studies on BRCA2 orthologs have revealed a requirement for BRCA2 during meiosis. In *Ustilago maydis,* mutation of Brh2 led to a failure in the formation of meiotic spore products (Kojic et al., 2002). Null mutants of BRCA2 ortholog in *Drosophila* led to sterility in both male and female flies (Klovstad et al., 2008; Weinberg-Shukron et al., 2018). A transgenic mouse line expressing low levels of human BRCA2 in the gonad showed reduced RAD51 and DMC1 foci formation and prophase arrest of spermatocytes, due to the inability to complete meiotic recombination (Sharan et al., 2004). Depletion of *A. thaliana* BRCA2 by RNAi showed meiotic defects similar to *rad51; dmc1* double mutants (Siaud et al., 2004) and *C. elegans brc-2* mutant produced completely inviable progeny (Martin et al., 2005), suggesting an indispensable role of BRCA2 during meiosis. Studies on human and *Arabidopsis* BRCA2 proteins demonstrated that BRCA2 directly binds to the meiosis-specific recombinase DMC1, which functions together with RAD51 to promote strand invasion and joint molecule formation during meiotic recombination (Dray et al., 2006; Thorslund et al., 2007; Jensen et al., 2010; Martinez et al., 2016). As with RAD51, the BRC repeats facilitate binding between BRCA2 and DMC1, although binding affinities for each individual BRC repeat differ between RAD51 and DMC1 (Martinez et al., 2016). Moreover, different mechanisms have been proposed for BRCA2 stimulation of RAD51 versus DMC1 recombinase activity. In the context of RAD51 mediated recombination, BRCA2 and its eight BRC repeats function by a combination of inhibiting RAD51 ATPase activity, promoting RAD51 filament formation
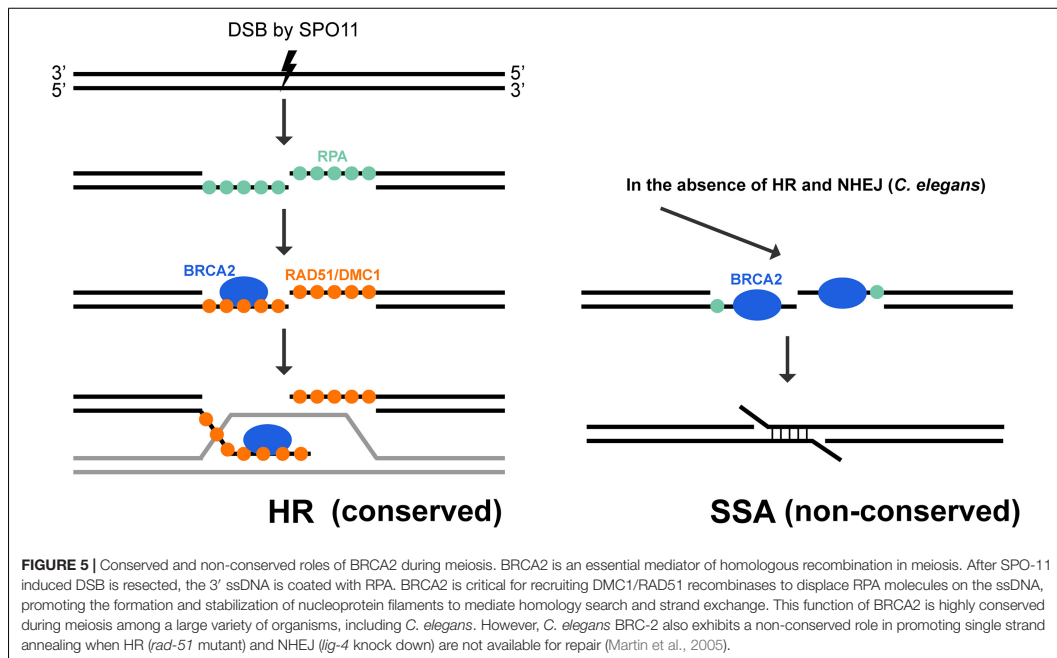
9

on ssDNA but not dsDNA, and enhancing strand exchange activity of RAD51. In contrast, stabilization of DMC1 filament on ssDNA was proposed to be the major mechanism by which BRCA2 functions with DMC1 (Martinez et al., 2016; **Figure 5**).

BRCA2 localization to DSBs in somatic cells depends on PALB2 (Xia et al., 2006). It has remained mysterious until recently, how BRCA2 is recruited to DSBs during meiosis. The Shibuya group identified a BRCA2 localizer in mice, which they named meiotic localizer of BRCA2 (MEILB2). MEILB2 is specifically expressed in germ cells and localizes to meiotic recombination sites on the chromosome axis. In the absence of MEILB2, the recruitment of DMC1 and RAD51 recombinase to meiotic DSBs is abolished, leading to sterility in male mice. Furthermore, MEILB2 directly binds to BRCA2 *in vitro* and is a physiological binding partner of BRCA2 *in vivo*. Removing MEILB2 impairs BRCA2 localization to resected ssDNA in spermatocytes, suggesting that MEILB2 recruits BRCA2 to sites undergoing meiotic recombination (Zhang et al., 2019). In contrast to males, female *Meilb2*$^{-/-}$ mice show only a ∼50% reduction in the localization of DMC1 and RAD51, and are sub-fertile, suggesting that redundant mechanisms exist to localize BRAC2 in oogenesis. One possibility is that PALB2 functions in concert with MEILB2 in female meiosis to localize BRCA2. Interestingly, PALB2 knockout mice show reduced male, but not female, fertility. This reduction in fertility is likely due to PALB2 interaction with BRCA1 (Simhadri et al., 2014). Future studies addressing the roles, redundancies and interconnections between PALB2, BRCA1 and BRCA2 will be important for understanding how meiotic DSBs are processed in male and female meiosis. Recently a third component of the BRCA2 complex, BRCA2 and MEILB2-associating protein 1 (BRME1), was identified. BRME1 forms a ternary complex with BRCA2 and MEILB2 and in the absence of BRME1, meiotic DSB repair, homologous chromosome synapsis and crossover formation were impaired in spermatogenesis (Takemoto et al., 2020; Zhang et al., 2020). MEILB2 is conserved among vertebrate taxa; whether binding partners promote meiotic regulation of BRCA2 in organisms such as worms and plants remain to be investigated.

Non-conserved Role of BRCA2 in *C. elegans* Meiosis

BRCA2's role in promoting RAD51/DMC1 nucleoprotein filament formation for homology search and strand exchange in meiotic recombination is conserved among all organisms where it has been examined. A RAD-51 independent, non-conserved role of BRC-2 was uncovered in *C. elegans* meiosis (Martin et al., 2005; Petalcorin et al., 2006). Without BRC-2, SPO-11 induced DSBs are resected, but RAD-51 is not recruited to the single stranded DNA, blocking strand invasion for error-free repair. As the presence of DSBs is extremely deleterious, alternative repair pathways are engaged to remove any remaining breaks before cells exit meiotic prophase I. In *rad-51* or *brc-2* single mutant, oogenic diakinesis nuclei exhibit aggregated DAPI staining chromosome structures, in contrast to the six

FIGURE 5 | Conserved and non-conserved roles of BRCA2 during meiosis. BRCA2 is an essential mediator of homologous recombination in meiosis. After SPO-11 induced DSB is resected, the 3′ ssDNA is coated with RPA. BRCA2 is critical for recruiting DMC1/RAD51 recombinases to displace RPA molecules on the ssDNA, promoting the formation and stabilization of nucleoprotein filaments to mediate homology search and strand exchange. This function of BRCA2 is highly conserved during meiosis among a large variety of organisms, including *C. elegans*. However, *C. elegans* BRC-2 also exhibits a non-conserved role in promoting single strand annealing when HR (*rad-51* mutant) and NHEJ (*lig-4* knock down) are not available for repair (Martin et al., 2005).

10

morphologically distinct bivalent structures in wild-type animals (**Figure 3B**). Inactivating NHEJ (*lig-4*) in the *brc-2* mutant resulted in mostly twelve DAPI bodies (**Figure 3B**), suggesting that the aggregation observed in *brc-2* is due to inappropriate repair of meiotic DSBs by NHEJ. However, when a functional BRC-2 was present, as in the case of the *lig-4; rad-51* double mutant, diakinesis nuclei contained clumped DAPI structures as seen in *brc-2* and *rad-51* single mutants (**Figure 3B**; Martin et al., 2005). This observation suggests that BRC-2 promotes an alternative repair pathway when both HR and NHEJ fail to be executed in meiocytes. A possible candidate for this repair pathway is single strand annealing (SSA). Indeed, *in vitro* experiments showed that purified *C. elegans* BRC-2 protein promoted annealing of single strand oligonucleotide coated with RPA (Petalcorin et al., 2006), an activity that mammalian BRCA2 does not possess (Jensen et al., 2010; **Figure 5**). It is likely that *C. elegans* BRC-2 has acquired this function to promote SSA during meiosis, as an ortholog of RAD52, which mediates SSA, is missing.

CONCLUSION

That organisms such as mice, *C. elegans*, and *A. thaliana* carrying mutations in their respective BRCA1 and BRCA2 orthologs exhibit meiotic phenotypes is consistent with BRCA1 and BRCA2 playing critical roles in meiosis. While important for meiotic recombination, BRCA1 and BRCA2 orthologs have acquired divergent functions throughout evolution. BRCA1 together with BARD1 functions as an E3 ubiquitin ligase that promotes ubiquitin transfer to a number of substrates and therefore plays regulatory roles in various processes. Not surprisingly, BRCA1 function during meiosis is quite diverse in different organisms (**Figure 2**). For example, BRCA1 is essential for MSCI in mice but is dispensable for MSCI in *C. elegans*, while *C. elegans* BRC-1 promotes DNA end resection, stabilizes the RAD-51 filament and regulates the crossover landscape. It remains an open question whether BRCA1-BARD1 functions in any of these aspects of meiotic recombination in mammals. Future studies taking advantage of conditional expression and genome editing tools should facilitate analyses on the role of E3 ligase activity, including identification of substrates, and the conserved BRCT domains. In contrast to BRCA1, BRCA2 plays a fundamental and conserved role in HR as a mediator to recruit RAD51 and DMC1 for nucleoprotein filament formation and strand

invasion. However, *C. elegans* BRC-2 also uniquely promotes the alternative SSA pathway, perhaps as a consequence of a streamlined set of repair proteins (e.g., absence of DMC1 and RAD52) (**Figure 5**). While not identical, knowledge on meiotic roles of BRCA1 and BRCA2 from model organisms will continue to provide valuable insights into the mechanisms by which these two genes function during human meiosis. Clinical data has shown a correlation between the presence of BRCA1 and BRCA2 mutations in healthy carriers and ovarian aging, which is measured by elevated accumulation of DNA damage in oocytes and reduced primordial follicle reserve (Oktay et al., 2010; Lin et al., 2017; Lambertini et al., 2018). This indicates that the functions of BRCA1 and BRCA2 during human meiosis are likely to influence sperm and egg quality. Interestingly, some cancers inappropriately express meiotic genes and recent evidence suggests that this may lead to altered BRCA2 function (Hosoya et al., 2011; Zhang et al., 2020). HR was inhibited in somatic cells when the SC protein SYCP3 and the meiotic partners of BRCA2, MEILB2 and BRME1, were aberrantly expressed, presumably as a result of BRCA2 protein being sequestered when bound by the meiotic proteins. Future studies focusing on meiotic aspects of BRCA1 and BRCA2 may advance our knowledge in human reproduction as well as tumorigenesis to provide tools for improving fertility and health.

AUTHOR CONTRIBUTIONS

QL wrote the manuscript with content and editorial input from JE. Both authors contributed to the article and approved the submitted version.

FUNDING

ACKNOWLEDGMENTS

REFERENCES

Abbott, D. W., Freeman, M. L., and Holt, J. T. (1998). Double-strand break repair deficiency and radiation sensitivity in BRCA2 mutant cancer cells. *J. Natl. Cancer Inst.* 90, 978–985. doi: 10.1093/jnci/90.13.978

Adamo, A., Montemauri, P., Silva, N., Ward, J. D., Boulton, S. J., and La Volpe, A. (2008). BRC-1 acts in the inter-sister pathway of meiotic double-strand break repair. *EMBO Rep.* 9, 287–292. doi: 10.1038/sj.embor.7401167

Aparicio, T., Baer, R., Gottesman, M., and Gautier, J. (2016). MRN, CtIP, and BRCA1 mediate repair of topoisomerase II-DNA adducts. *J. Cell Biol.* 212, 399–408. doi: 10.1083/jcb.201504005

Baer, R., and Ludwig, T. (2002). The BRCA1/BARD1 heterodimer, a tumor suppressor complex with ubiquitin E3 ligase activity. *Curr. Opin. Genet. Dev.* 12, 86–91. doi: 10.1016/s0959-437x(01)00269-6

Baudat, F., and de Massy, B. (2007). Regulating double-stranded DNA break repair towards crossover or non-crossover during mammalian meiosis. *Chromosome Res.* 15, 565–577. doi: 10.1007/s10577-007-1140-3

Belan, O., Barroso, C., Kaczmarczyk, A., Anand, R., Federico, S., O'reilly, N., et al. (2021). Single-molecule analysis reveals cooperative stimulation of Rad51 filament nucleation and growth by mediator proteins. *Mol. Cell* 81, 1058.e7–1073.e7.

Boulton, S. J., Martin, J. S., Polanowska, J., Hill, D. E., Gartner, A., and Vidal, M. (2004). BRCA1/BARD1 orthologs required for DNA repair in

11

Caenorhabditis elegans. Curr. Biol. 14, 33–39. doi: 10.1016/j.cub.2003.11.029

Broering, T. J., Alavattam, K. G., Sadreyev, R. I., Ichijima, Y., Kato, Y., Hasegawa, K., et al. (2014). BRCA1 establishes DNA damage signaling and pericentric heterochromatin of the X chromosome in male meiosis. *J. Cell Biol.* 205, 663–675. doi: 10.1083/jcb.201311050

Brown, M. S., and Bishop, D. K. (2014). DNA strand exchange and RecA homologs in meiosis. *Cold Spring Harb. Perspect. Biol.* 7:a016659. doi: 10.1101/cshperspect.a016659

Brzovic, P. S., Rajagopal, P., Hoyt, D. W., King, M. C., and Klevit, R. E. (2001). Structure of a BRCA1-BARD1 heterodimeric RING-RING complex. *Nat. Struct. Biol.* 8, 833–837.

Bunting, S. F., Callen, E., Wong, N., Chen, H. T., Polato, F., Gunn, A., et al. (2010). 53BP1 inhibits homologous recombination in Brca1-deficient cells by blocking resection of DNA breaks. *Cell* 141, 243–254. doi: 10.1016/j.cell.2010.03.012

Caestecker, K. W., and Van de Walle, G. R. (2013). The role of BRCA1 in DNA double-strand repair: past and present. *Exp. Cell Res.* 319, 575–587. doi: 10.1016/j.yexcr.2012.11.013

Carreira, A., Hilario, J., Amitani, I., Baskin, R. J., Shivji, M. K., Venkitaraman, A. R., et al. (2009). The BRC repeats of BRCA2 modulate the DNA-binding selectivity of RAD51. *Cell* 136, 1032–1043. doi: 10.1016/j.cell.2009.02.019

Chen, C. F., Chen, P. L., Zhong, Q., Sharp, Z. D., and Lee, W. H. (1999). Expression of BRC repeats in breast cancer cells disrupts the BRCA2-Rad51 complex and leads to radiation hypersensitivity and loss of G(2)/M checkpoint control. *J. Biol. Chem.* 274, 32931–32935. doi: 10.1074/jbc.274.46.32931

Chung, G., Rose, A. M., Petalcorin, M. I., Martin, J. S., Kessler, Z., Sanchez-Pulido, L., et al. (2015). REC-1 and HIM-5 distribute meiotic crossovers and function redundantly in meiotic double-strand break formation in *Caenorhabditis elegans. Genes Dev.* 29, 1969–1979. doi: 10.1101/gad.266056.115

Cressman, V. L., Backlund, D. C., Avrutskaya, A. V., Leadon, S. A., Godfrey, V., and Koller, B. H. (1999). Growth retardation, DNA repair defects, and lack of spermatogenesis in BRCA1-deficient mice. *Mol. Cell Biol.* 19, 7061–7075. doi: 10.1128/mcb.19.10.7061

Cruz-Garcia, A., Lopez-Saavedra, A., and Huertas, P. (2014). BRCA1 accelerates CtIP-mediated DNA-end resection. *Cell Rep.* 9, 451–459. doi: 10.1016/j.celrep.2014.08.076

Daley, J. M., and Sung, P. (2014). 53BP1, BRCA1, and the choice between recombination and end joining at DNA double-strand breaks. *Mol. Cell Biol.* 34, 1380–1388. doi: 10.1128/mcb.01639-13

Davies, O. R., and Pellegrini, L. (2007). Interaction with the BRCA2 C terminus protects RAD51-DNA filaments from disassembly by BRC repeats. *Nat. Struct. Mol. Biol.* 14, 475–483. doi: 10.1038/nsmb1251

Deng, C. X. (2002). Roles of BRCA1 in centrosome duplication. *Oncogene* 21, 6222–6227. doi: 10.1038/sj.onc.1205713

Deng, C. X. (2006). BRCA1: cell cycle checkpoint, genetic instability, DNA damage response and cancer evolution. *Nucleic Acids Res.* 34, 1416–1426. doi: 10.1093/nar/gkl010

Densham, R. M., Garvin, A. J., Stone, H. R., Strachan, J., Baldock, R. A., Daza-Martin, M., et al. (2016). Human BRCA1-BARD1 ubiquitin ligase activity counteracts chromatin barriers to DNA resection. *Nat. Struct. Mol. Biol.* 23, 647–655. doi: 10.1038/nsmb.3236

Dernburg, A. F., Mcdonald, K., Moulder, G., Barstead, R., Dresser, M., and Villeneuve, A. M. (1998). Meiotic recombination in *C. elegans* initiates by a conserved mechanism and is dispensable for homologous chromosome synapsis. *Cell* 94, 387–398. doi: 10.1016/s0092-8674(00)81481-6

Deshaies, R. J., and Joazeiro, C. A. (2009). RING domain E3 ubiquitin ligases. *Annu. Rev. Biochem.* 78, 399–434. doi: 10.1146/annurev.biochem.78.101807.093809

Dray, E., Siaud, N., Dubois, E., and Doutriaux, M. P. (2006). Interaction between *Arabidopsis* Brca2 and its partners Rad51, Dmc1, and Dss1. *Plant Physiol.* 140, 1059–1069. doi: 10.1104/pp.105.075838

Esashi, F., Christ, N., Gannon, J., Liu, Y., Hunt, T., Jasin, M., et al. (2005). CDK-dependent phosphorylation of BRCA2 as a regulatory mechanism for recombinational repair. *Nature* 434, 598–604. doi: 10.1038/nature03404

Esashi, F., Galkin, V. E., Yu, X., Egelman, E. H., and West, S. C. (2007). Stabilization of RAD51 nucleoprotein filaments by the C-terminal region of BRCA2. *Nat. Struct. Mol. Biol.* 14, 468–474. doi: 10.1038/nsmb1245

Fernandez-Capetillo, O., Mahadevaiah, S. K., Celeste, A., Romanienko, P. J., Camerini-Otero, R. D., Bonner, W. M., et al. (2003). H2AX is required for chromatin remodeling and inactivation of sex chromosomes in male mouse meiosis. *Dev. Cell* 4, 497–508. doi: 10.1016/s1534-5807(03)00093-5

Fox, D. III, Le Trong, I., Rajagopal, P., Brzovic, P. S., Stenkamp, R. E., and Klevit, R. E. (2008). Crystal structure of the BARD1 ankyrin repeat domain and its functional consequences. *J. Biol. Chem.* 283, 21179–21186. doi: 10.1074/jbc.m802333200

Futreal, P. A., Liu, Q., Shattuck-Eidens, D., Cochran, C., Harshman, K., Tavtigian, S., et al. (1994). BRCA1 mutations in primary breast and ovarian carcinomas. *Science* 266, 120–122. doi: 10.1126/science.7939630

Garcia, V., Phelps, S. E., Gray, S., and Neale, M. J. (2011). Bidirectional resection of DNA double-strand breaks by Mre11 and Exo1. *Nature* 479, 241–244. doi: 10.1038/nature10515

Garcia-Muse, T., Galindo-Diaz, U., Garcia-Rubio, M., Martin, J. S., Polanowska, J., O'reilly, N., et al. (2019). A meiotic checkpoint alters repair partner bias to permit inter-sister repair of persistent DSBs. *Cell Rep.* 26, 775.e5–787.e5.

Ghimenti, C., Sensi, E., Presciuttini, S., Brunetti, I. M., Conte, P., Bevilacqua, G., et al. (2002). Germline mutations of the BRCA1-associated ring domain (BARD1) gene in breast and breast/ovarian families negative for BRCA1 and BRCA2 alterations. *Genes Chromosomes Cancer* 33, 235–242. doi: 10.1002/gcc.1223

Godwin, A. K., Vanderveer, L., Schultz, D. C., Lynch, H. T., Altomare, D. A., Buetow, K. H., et al. (1994). A common region of deletion on chromosome 17q in both sporadic and familial epithelial ovarian tumors distal to BRCA1. *Am. J. Hum. Genet.* 55, 666–677.

Gowen, L. C., Johnson, B. L., Latour, A. M., Sulik, K. K., and Koller, B. H. (1996). Brca1 deficiency results in early embryonic lethality characterized by neuroepithelial abnormalities. *Nat. Genet.* 12, 191–194. doi: 10.1038/ng0296-191

Gray, S., and Cohen, P. E. (2016). Control of meiotic crossovers: from double-strand break formation to designation. *Annu. Rev. Genet.* 50, 175–210. doi: 10.1146/annurev-genet-120215-035111

Gudmundsdottir, K., and Ashworth, A. (2004). BRCA2 in meiosis: turning over a new leaf. *Trends Cell Biol.* 14, 401–404. doi: 10.1016/j.tcb.2004.07.002

Hakem, R., De La Pompa, J. L., Sirard, C., Mo, R., Woo, M., Hakem, A., et al. (1996). The tumor suppressor gene Brca1 is required for embryonic cellular proliferation in the mouse. *Cell* 85, 1009–1023. doi: 10.1016/s0092-8674(00)81302-1

Hall, J. M., Lee, M. K., Newman, B., Morrow, J. E., Anderson, L. A., Huey, B., et al. (1990). Linkage of early-onset familial breast cancer to chromosome 17q21. *Science* 250, 1684–1689. doi: 10.1126/science.2270482

Hartley, C. L., and McCulloch, R. (2008). Trypanosoma brucei BRCA2 acts in antigenic variation and has undergone a recent expansion in BRC repeat number that is important during homologous recombination. *Mol. Microbiol.* 68, 1237–1251. doi: 10.1111/j.1365-2958.2008.06230.x

Hashizume, R., Fukuda, M., Maeda, I., Nishikawa, H., Oyake, D., Yabuki, Y., et al. (2001). The RING heterodimer BRCA1-BARD1 is a ubiquitin ligase inactivated by a breast cancer-derived mutation. *J. Biol. Chem.* 276, 14537–14540. doi: 10.1074/jbc.c000881200

Hatchi, E., Skourti-Stathaki, K., Ventz, S., Pinello, L., Yen, A., Kamieniarz-Gdula, K., et al. (2015). BRCA1 recruitment to transcriptional pause sites is required for R-loop-driven DNA damage repair. *Mol. Cell* 57, 636–647. doi: 10.1016/j.molcel.2015.01.011

Hill, S. J., Rolland, T., Adelmant, G., Xia, X., Owen, M. S., Dricot, A., et al. (2014). Systematic screening reveals a role for BRCA1 in the response to transcription-associated DNA damage. *Genes Dev.* 28, 1957–1975. doi: 10.1101/gad.241620.114

Hillers, K. J., Jantsch, V., Martinez-Perez, E., and Yanowitz, J. L. (2017). Meiosis. *WormBook* 2017, 1–43. doi: 10.1016/b978-0-12-503365-7.50005-5

Hong, Y., Sonneville, R., Agostinho, A., Meier, B., Wang, B., Blow, J. J., et al. (2016). The SMC-5/6 complex and the HIM-6 (BLM) helicase synergistically promote meiotic recombination intermediate processing and chromosome maturation during *Caenorhabditis elegans* Meiosis. *PLoS Genet.* 12:e1005872. doi: 10.1371/journal.pgen.1005872

Hosoya, N., Okajima, M., Kinomura, A., Fujii, Y., Hiyama, T., Sun, J., et al. (2011). Synaptonemal complex protein SYCP3 impairs mitotic recombination

12

by interfering with BRCA2. *EMBO Rep.* 13, 44–51. doi: 10.1038/embor.2011.221

Huber, L. J., Yang, T. W., Sarkisian, C. J., Master, S. R., Deng, C. X., and Chodosh, L. A. (2001). Impaired DNA damage response in cells expressing an exon 11-deleted murine Brca1 variant that localizes to nuclear foci. *Mol. Cell Biol.* 21, 4005–4015. doi: 10.1128/mcb.21.12.4005-4015.2001

Jagut, M., Hamminger, P., Woglar, A., Millonigg, S., Paulin, L., Mikl, M., et al. (2016). Separable roles for a *Caenorhabditis elegans* RMI1 homolog in promoting and antagonizing meiotic crossovers ensure faithful chromosome inheritance. *PLoS Biol.* 14:e1002412. doi: 10.1371/journal.pbio.1002412

Janisiw, E., Dello Stritto, M. R., Jantsch, V., and Silva, N. (2018). BRCA1-BARD1 associate with the synaptonemal complex and pro-crossover factors and influence RAD-51 dynamics during *Caenorhabditis elegans* meiosis. *PLoS Genet.* 14:e1007653. doi: 10.1371/journal.pgen.1007653

Jensen, R. B., Carreira, A., and Kowalczykowski, S. C. (2010). Purified human BRCA2 stimulates RAD51-mediated recombination. *Nature* 467, 678–683. doi: 10.1038/nature09399

Kamp, J. A., Van Schendel, R., Dilweg, I. W., and Tijsterman, M. (2020). BRCA1-associated structural variations are a consequence of polymerase theta-mediated end-joining. *Nat. Commun.* 11:3615.

King, M. C., Marks, J. H., Mandell, J. B., and New York Breast Cancer Study Group (2003). Breast and ovarian cancer risks due to inherited mutations in BRCA1 and BRCA2. *Science* 302, 643–646. doi: 10.1126/science.1088759

Klovstad, M., Abdu, U., and Schupbach, T. (2008). Drosophila brca2 is required for mitotic and meiotic DNA repair and efficient activation of the meiotic recombination checkpoint. *PLoS Genet.* 4:e31. doi: 10.1371/journal.pgen.0040031

Kojic, M., Kostrub, C. F., Buchman, A. R., and Holloman, W. K. (2002). BRCA2 homolog required for proficiency in DNA repair, recombination, and genome stability in *Ustilago maydis*. *Mol. Cell* 10, 683–691. doi: 10.1016/s1097-2765(02)00632-9

Kojic, M., Zhou, Q., Lisby, M., and Holloman, W. K. (2005). Brh2-Dss1 interplay enables properly controlled recombination in *Ustilago maydis*. *Mol. Cell Biol.* 25, 2547–2557. doi: 10.1128/mcb.25.7.2547-2557.2005

Kouznetsova, A., Wang, H., Bellani, M., Camerini-Otero, R. D., Jessberger, R., and Hoog, C. (2009). BRCA1-mediated chromatin silencing is limited to oocytes with a small number of asynapsed chromosomes. *J. Cell Sci.* 122, 2446–2452. doi: 10.1242/jcs.049353

Kowalczykowski, S. C. (2015). An overview of the molecular mechanisms of recombinational DNA repair. *Cold Spring Harb. Perspect. Biol.* 7:a016410. doi: 10.1101/cshperspect.a016410

Lam, I., and Keeney, S. (2014). Mechanism and regulation of meiotic recombination initiation. *Cold Spring Harb. Perspect. Biol.* 7:a016634. doi: 10.1101/cshperspect.a016634

Lambertini, M., Goldrat, O., Ferreira, A. R., Dechene, J., Azim, H. A. Jr., Desir, J., et al. (2018). Reproductive potential and performance of fertility preservation strategies in BRCA-mutated breast cancer patients. *Ann. Oncol.* 29, 237–243. doi: 10.1093/annonc/mdx639

Leon-Ortiz, A. M., Panier, S., Sarek, G., Vannier, J. B., Patel, H., Campbell, P. J., et al. (2018). A distinct class of genome rearrangements driven by heterologous recombination. *Mol. Cell* 69, 292.e6–305.e6.

Li, J., Zou, C., Bai, Y., Wazer, D. E., Band, V., and Gao, Q. (2006). DSS1 is required for the stability of BRCA2. *Oncogene* 25, 1186–1194. doi: 10.1038/sj.onc.1209153

Li, M. L., and Greenberg, R. A. (2012). Links between genome integrity and BRCA1 tumor suppression. *Trends Biochem. Sci.* 37, 418–424. doi: 10.1016/j.tibs.2012.06.007

Li, Q., Hariri, S., and Engebrecht, J. (2020). Meiotic double-strand break processing and crossover patterning are regulated in a sex-specific manner by BRCA1-BARD1 in *Caenorhabditis elegans*. *Genetics* 216, 359–379. doi: 10.1534/genetics.120.303292

Li, Q., Saito, T. T., Martinez-Garcia, M., Deshong, A. J., Nadarajan, S., Lawrence, K. S., et al. (2018). The tumor suppressor BRCA1-BARD1 complex localizes to the synaptonemal complex and regulates recombination under meiotic dysfunction in *Caenorhabditis elegans*. *PLoS Genet.* 14:e1007701. doi: 10.1371/journal.pgen.1007701

Lin, W., Titus, S., Moy, F., Ginsburg, E. S., and Oktay, K. (2017). Ovarian aging in women with BRCA germline mutations. *J. Clin. Endocrinol. Metab.* 102, 3839–3847. doi: 10.1210/jc.2017-00765

Liu, C. Y., Flesken-Nikitin, A., Li, S., Zeng, Y., and Lee, W. H. (1996). Inactivation of the mouse Brca1 gene leads to failure in the morphogenesis of the egg cylinder in early postimplantation development. *Genes Dev.* 10, 1835–1843. doi: 10.1101/gad.10.14.1835

Liu, J., Doty, T., Gibson, B., and Heyer, W. D. (2010). Human BRCA2 protein promotes RAD51 filament formation on RPA-covered single-stranded DNA. *Nat. Struct. Mol. Biol.* 17, 1260–1262. doi: 10.1038/nsmb.1904

Ludwig, T., Chapman, D. L., Papaioannou, V. E., and Efstratiadis, A. (1997). Targeted mutations of breast cancer susceptibility gene homologs in mice: lethal phenotypes of Brca1, Brca2, Brca1/Brca2, Brca1/p53, and Brca2/p53 nullizygous embryos. *Genes Dev.* 11, 1226–1241. doi: 10.1101/gad.11.10.1226

Lui, D. Y., and Colaiacovo, M. P. (2013). Meiotic development *in Caenorhabditis elegans*. *Adv. Exp. Med. Biol.* 757, 133–170. doi: 10.1007/978-1-4614-4015-4_6

Mahadevaiah, S. K., Bourc'his, D., De Rooij, D. G., Bestor, T. H., Turner, J. M., and Burgoyne, P. S. (2008). Extensive meiotic asynapsis in mice antagonises meiotic silencing of unsynapsed chromatin and consequently disrupts meiotic sex chromosome inactivation. *J. Cell Biol.* 182, 263–276. doi: 10.1083/jcb.200710195

Manke, I. A., Lowery, D. M., Nguyen, A., and Yaffe, M. B. (2003). BRCT repeats as phosphopeptide-binding modules involved in protein targeting. *Science* 302, 636–639. doi: 10.1126/science.1088877

Martin, J. S., Winkelmann, N., Petalcorin, M. I., Mcilwraith, M. J., and Boulton, S. J. (2005). RAD-51-dependent and -independent roles of a *Caenorhabditis elegans* BRCA2-related protein during DNA double-strand break repair. *Mol. Cell Biol.* 25, 3127–3139. doi: 10.1128/mcb.25.8.3127-3139.2005

Martinez, J. S., Von Nicolai, C., Kim, T., Ehlen, A., Mazin, A. V., Kowalczykowski, S. C., et al. (2016). BRCA2 regulates DMC1-mediated recombination through the BRC repeats. *Proc. Natl. Acad. Sci. U.S.A.* 113, 3515–3520. doi: 10.1073/pnas.1601691113

McCarthy, E. E., Celebi, J. T., Baer, R., and Ludwig, T. (2003). Loss of Bard1, the heterodimeric partner of the Brca1 tumor suppressor, results in early embryonic lethality and chromosomal instability. *Mol. Cell Biol.* 23, 5056–5063. doi: 10.1128/mcb.23.14.5056-5063.2003

Meneely, P. M., Mcgovern, O. L., Heinis, F. I., and Yanowitz, J. L. (2012). Crossover distribution and frequency are regulated by him-5 in *Caenorhabditis elegans*. *Genetics* 190, 1251–1266. doi: 10.1534/genetics.111.137463

Meza, J. E., Brzovic, P. S., King, M. C., and Klevit, R. E. (1999). Mapping the functional domains of BRCA1. Interaction of the ring finger domains of BRCA1 and BARD1. *J. Biol. Chem.* 274, 5659–5665.

Miki, Y., Swensen, J., Shattuck-Eidens, D., Futreal, P. A., Harshman, K., Tavtigian, S., et al. (1994). A strong candidate for the breast and ovarian cancer susceptibility gene BRCA1. *Science* 266, 66–71. doi: 10.1126/science.7545954

Moynahan, M. E., Chiu, J. W., Koller, B. H., and Jasin, M. (1999). Brca1 controls homology-directed DNA repair. *Mol. Cell* 4, 511–518. doi: 10.1016/s1097-2765(00)80202-6

Moynahan, M. E., Pierce, A. J., and Jasin, M. (2001). BRCA2 is required for homology-directed repair of chromosomal breaks. *Mol. Cell* 7, 263–272. doi: 10.1016/s1097-2765(01)00174-5

Nakamura, K., Saredi, G., Becker, J. R., Foster, B. M., Nguyen, N. V., Beyer, T. E., et al. (2019). H4K20me0 recognition by BRCA1-BARD1 directs homologous recombination to sister chromatids. *Nat. Cell Biol.* 21, 311–318. doi: 10.1038/s41556-019-0282-9

Neale, M. J., and Keeney, S. (2006). Clarifying the mechanics of DNA strand exchange in meiotic recombination. *Nature* 442, 153–158. doi: 10.1038/nature04885

Negrini, S., Gorgoulis, V. G., and Halazonetis, T. D. (2010). Genomic instability–an evolving hallmark of cancer. *Nat. Rev. Mol. Cell Biol.* 11, 220–228. doi: 10.1038/nrm2858

Oktay, K., Kim, J. Y., Barad, D., and Babayev, S. N. (2010). Association of BRCA1 mutations with occult primary ovarian insufficiency: a possible explanation for the link between infertility and breast/ovarian cancer risks. *J. Clin. Oncol.* 28, 240–244. doi: 10.1200/jco.2009.24.2057

Paiano, J., Wu, W., Yamada, S., Sciascia, N., Callen, E., Paola Cotrim, A., et al. (2020). ATM and PRDM9 regulate SPO11-bound recombination intermediates during meiosis. *Nat. Commun.* 11:857.

13

Petalcorin, M. I., Galkin, V. E., Yu, X., Egelman, E. H., and Boulton, S. J. (2007). Stabilization of RAD-51-DNA filaments via an interaction domain in *Caenorhabditis elegans* BRCA2. *Proc. Natl. Acad. Sci. U.S.A.* 104, 8299–8304. doi: 10.1073/pnas.0702805104

Petalcorin, M. I., Sandall, J., Wigley, D. B., and Boulton, S. J. (2006). CeBRC-2 stimulates D-loop formation by RAD-51 and promotes DNA single-strand annealing. *J Mol. Biol.* 361, 231–242. doi: 10.1016/j.jmb.2006.06.020

Polanowska, J., Martin, J. S., Garcia-Muse, T., Petalcorin, M. I., and Boulton, S. J. (2006). A conserved pathway to activate BRCA1-dependent ubiquitylation at DNA damage sites. *EMBO J.* 25, 2178–2188. doi: 10.1038/sj.emboj.7601102

Prakash, R., Zhang, Y., Feng, W., and Jasin, M. (2015). Homologous recombination and human health: the roles of BRCA1, BRCA2, and associated proteins. *Cold Spring Harb. Perspect. Biol.* 7:a016600. doi: 10.1101/cshperspect.a016600

Reidt, W., Wurz, R., Wanieck, K., Chu, H. H., and Puchta, H. (2006). A homologue of the breast cancer-associated gene BARD1 is involved in DNA repair in plants. *EMBO J.* 25, 4326–4337. doi: 10.1038/sj.emboj.7601313

Rodriguez, M., Yu, X., Chen, J., and Songyang, Z. (2003). Phosphopeptide binding specificities of BRCA1 COOH-terminal (BRCT) domains. *J. Biol. Chem.* 278, 52914–52918. doi: 10.1074/jbc.c300407200

Roy, R., Chun, J., and Powell, S. N. (2011). BRCA1 and BRCA2: different roles in a common pathway of genome protection. *Nat. Rev. Cancer* 12, 68–78. doi: 10.1038/nrc3181

Saito, T. T., and Colaiacovo, M. P. (2017). Regulation of crossover frequency and distribution during meiotic recombination. *Cold Spring Harb. Symp. Quant. Biol.* 82, 223–234. doi: 10.1101/sqb.2017.82.034132

Saito, T. T., Lui, D. Y., Kim, H. M., Meyer, K., and Colaiacovo, M. P. (2013). Interplay between structure-specific endonucleases for crossover control during *Caenorhabditis elegans* meiosis. *PLoS Genet.* 9:e1003586. doi: 10.1371/journal.pgen.1003586

Saito, T. T., Mohideen, F., Meyer, K., Harper, J. W., and Colaiacovo, M. P. (2012). SLX-1 is required for maintaining genomic integrity and promoting meiotic noncrossovers in the *Caenorhabditis elegans* germline. *PLoS Genet.* 8:e1002888. doi: 10.1371/journal.pgen.1002888

Scully, R., Chen, J., Plug, A., Xiao, Y., Weaver, D., Feunteun, J., et al. (1997). Association of BRCA1 with Rad51 in mitotic and meiotic cells. *Cell* 88, 265–275. doi: 10.1016/s0092-8674(00)81847-4

Sharan, S. K., Morimatsu, M., Albrecht, U., Lim, D. S., Regel, E., Dinh, C., et al. (1997). Embryonic lethality and radiation hypersensitivity mediated by Rad51 in mice lacking Brca2. *Nature* 386, 804–810. doi: 10.1038/386804a0

Sharan, S. K., Pyle, A., Coppola, V., Babus, J., Swaminathan, S., Benedict, J., et al. (2004). BRCA2 deficiency in mice leads to meiotic impairment and infertility. *Development* 131, 131–142. doi: 10.1242/dev.00888

Shinohara, A., and Shinohara, M. (2004). Roles of RecA homologues Rad51 and Dmc1 during meiotic recombination. *Cytogenet. Genome Res.* 107, 201–207. doi: 10.1159/000080598

Shivji, M. K., Mukund, S. R., Rajendra, E., Chen, S., Short, J. M., Savill, J., et al. (2009). The BRC repeats of human BRCA2 differentially regulate RAD51 binding on single- versus double-stranded DNA to stimulate strand exchange. *Proc. Natl. Acad. Sci. U.S.A.* 106, 13254–13259. doi: 10.1073/pnas.0906208106

Siaud, N., Barbera, M. A., Egashira, A., Lam, I., Christ, N., Schlacher, K., et al. (2011). Plasticity of BRCA2 function in homologous recombination: genetic interactions of the PALB2 and DNA binding domains. *PLoS Genet.* 7:e1002409. doi: 10.1371/journal.pgen.1002409

Siaud, N., Dray, E., Gy, I., Gerard, E., Takvorian, N., and Doutriaux, M. P. (2004). Brca2 is involved in meiosis in *Arabidopsis thaliana* as suggested by its interaction with Dmc1. *EMBO J.* 23, 1392–1401. doi: 10.1038/sj.emboj.7600146

Simhadri, S., Peterson, S., Patel, D. S., Huo, Y., Cai, H., Bowman-Colin, C., et al. (2014). Male fertility defect associated with disrupted BRCA1-PALB2 interaction in mice. *J. Biol. Chem.* 289, 24617–24629. doi: 10.1074/jbc.m114.566141

Steinfeld, J. B., Belan, O., Kwon, Y., Terakawa, T., Al-Zain, A., Smith, M. J., et al. (2019). Defining the influence of Rad51 and Dmc1 lineage-specific amino acids on genetic recombination. *Genes Dev.* 33, 1191–1207. doi: 10.1101/gad.328062.119

Takemoto, K., Tani, N., Takada-Horisawa, Y., Fujimura, S., Tanno, N., Yamane, M., et al. (2020). Meiosis-Specific C19orf57/4930432K21Rik/BRME1 Modulates Localization of RAD51 and DMC1 to DSBs in mouse meiotic recombination. *Cell Rep.* 31:107686. doi: 10.1016/j.celrep.2020.107686

Thai, T. H., Du, F., Tsan, J. T., Jin, Y., Phung, A., Spillman, M. A., et al. (1998). Mutations in the BRCA1-associated RING domain (BARD1) gene in primary breast, ovarian and uterine cancers. *Hum. Mol. Genet.* 7, 195–202. doi: 10.1093/hmg/7.2.195

Thakur, S., Zhang, H. B., Peng, Y., Le, H., Carroll, B., Ward, T., et al. (1997). Localization of BRCA1 and a splice variant identifies the nuclear localization signal. *Mol. Cell Biol.* 17, 444–452. doi: 10.1128/mcb.17.1.444

Thorslund, T., Esashi, F., and West, S. C. (2007). Interactions between human BRCA2 protein and the meiosis-specific recombinase DMC1. *EMBO J.* 26, 2915–2922. doi: 10.1038/sj.emboj.7601739

Thorslund, T., Mcilwraith, M. J., Compton, S. A., Lekomtsev, S., Petronczki, M., Griffith, J. D., et al. (2010). The breast cancer tumor suppressor BRCA2 promotes the specific targeting of RAD51 to single-stranded DNA. *Nat. Struct. Mol. Biol.* 17, 1263–1265. doi: 10.1038/nsmb.1905

Turner, J. M. (2007). Meiotic sex chromosome inactivation. *Development* 134, 1823–1831. doi: 10.1242/dev.000018

Turner, J. M., Aprelikova, O., Xu, X., Wang, R., Kim, S., Chandramouli, G. V., et al. (2004). BRCA1, histone H2AX phosphorylation, and male meiotic sex chromosome inactivation. *Curr. Biol.* 14, 2135–2142. doi: 10.1016/j.cub.2004.11.032

Tutt, A., Gabriel, A., Bertwistle, D., Connor, F., Paterson, H., Peacock, J., et al. (1999). Absence of Brca2 causes genome instability by chromosome breakage and loss associated with centrosome amplification. *Curr. Biol.* 9, 1107–1110. doi: 10.1016/s0960-9822(99)80479-5

Venkitaraman, A. R. (2002). Cancer susceptibility and the functions of BRCA1 and BRCA2. *Cell* 108, 171–182. doi: 10.1016/s0092-8674(02)00615-3

Volkova, N. V., Gonzalez-Huici, V., Bertolini, S., Gonzalez, S., Vohringer, H., et al. (2020). Mutational signatures are jointly shaped by DNA damage and repair. *Nat. Commun.* 11:2169.

Wagner, C. R., Kuervers, L., Baillie, D. L., and Yanowitz, J. L. (2010). xnd-1 regulates the global recombination landscape in *Caenorhabditis elegans*. *Nature* 467, 839–843. doi: 10.1038/nature09429

Weinberg-Shukron, A., Rachmiel, M., Renbaum, P., Gulsuner, S., Walsh, T., Lobel, O., et al. (2018). Essential role of BRCA2 in ovarian development and function. *N. Engl. J. Med.* 379, 1042–1049.

Wong, A. K., Pero, R., Ormonde, P. A., Tavtigian, S. V., and Bartel, P. L. (1997). RAD51 interacts with the evolutionarily conserved BRC motifs in the human breast cancer susceptibility gene brca2. *J. Biol. Chem.* 272, 31941–31944. doi: 10.1074/jbc.272.51.31941

Wooster, R., Bignell, G., Lancaster, J., Swift, S., Seal, S., Mangion, J., et al. (1995). Identification of the breast cancer susceptibility gene BRCA2. *Nature* 378, 789–792.

Wu, L. C., Wang, Z. W., Tsan, J. T., Spillman, M. A., Phung, A., Xu, X. L., et al. (1996). Identification of a RING protein that can interact in vivo with the BRCA1 gene product. *Nat. Genet.* 14, 430–440. doi: 10.1038/ng1296-430

Xia, B., Sheng, Q., Nakanishi, K., Ohashi, A., Wu, J., Christ, N., et al. (2006). Control of BRCA2 cellular and clinical functions by a nuclear partner. PALB2. *Mol. Cell* 22, 719–729. doi: 10.1016/j.molcel.2006.05.022

Xu, X., Aprelikova, O., Moens, P., Deng, C. X., and Furth, P. A. (2003). Impaired meiotic DNA-damage repair and lack of crossing-over during spermatogenesis in BRCA1 full-length isoform deficient mice. *Development* 130, 2001–2012. doi: 10.1242/dev.00410

Xu, X., Qiao, W., Linke, S. P., Cao, L., Li, W. M., Furth, P. A., et al. (2001). Genetic interactions between tumor suppressors Brca1 and p53 in apoptosis, cell cycle and tumorigenesis. *Nat. Genet.* 28, 266–271. doi: 10.1038/90108

Xu, X., Weaver, Z., Linke, S. P., Li, C., Gotay, J., Wang, X. W., et al. (1999). Centrosome amplification and a defective G2-M cell cycle checkpoint induce genetic instability in BRCA1 exon 11 isoform-deficient cells. *Mol. Cell* 3, 389–395. doi: 10.1016/s1097-2765(00)80466-9

Yang, H., Jeffrey, P. D., Miller, J., Kinnucan, E., Sun, Y., Thoma, N. H., et al. (2002). BRCA2 function in DNA binding and recombination from a BRCA2-DSS1-ssDNA structure. *Science* 297, 1837–1848. doi: 10.1126/science.297.5588.1837

Yarden, R. I., Pardo-Reoyo, S., Sgagias, M., Cowan, K. H., and Brody, L. C. (2002). BRCA1 regulates the G2/M checkpoint by activating Chk1 kinase upon DNA damage. *Nat. Genet.* 30, 285–289. doi: 10.1038/ng837

Yokoo, R., Zawadzki, K. A., Nabeshima, K., Drake, M., Arur, S., and Villeneuve, A. M. (2012). COSA-1 reveals robust homeostasis and separable licensing and

14

reinforcement steps governing meiotic crossovers. *Cell* 149, 75–87. doi: 10. 1016/j.cell.2012.01.052

Yu, V. P., Koehler, M., Steinlein, C., Schmid, M., Hanakahi, L. A., Van Gool, A. J., et al. (2000). Gross chromosomal rearrangements and genetic exchange between nonhomologous chromosomes following BRCA2 inactivation. *Genes Dev.* 14, 1400–1406.

Yu, X., Chini, C. C., He, M., Mer, G., and Chen, J. (2003). The BRCT domain is a phospho-protein binding domain. *Science* 302, 639–642. doi: 10.1126/science. 1088753

Yu, Z., Kim, Y., and Dernburg, A. F. (2016). Meiotic recombination and the crossover assurance checkpoint in *Caenorhabditis elegans*. *Semin. Cell Dev. Biol.* 54, 106–116. doi: 10.1016/j.semcdb.2016.03.014

Yuan, S. S., Lee, S. Y., Chen, G., Song, M., Tomlinson, G. E., and Lee, E. Y. (1999). BRCA2 is required for ionizing radiation-induced assembly of Rad51 complex in vivo. *Cancer Res.* 59, 3547–3551.

Zetka, M. C., and Rose, A. M. (1995). Mutant rec-1 eliminates the meiotic pattern of crossing over in *Caenorhabditis elegans*. *Genetics* 141, 1339–1349. doi: 10. 1093/genetics/141.4.1339

Zhang, J., Fujiwara, Y., Yamamoto, S., and Shibuya, H. (2019). A meiosis-specific BRCA2 binding protein recruits recombinases to DNA double-strand breaks to ensure homologous recombination. *Nat. Commun.* 10:722.

Zhang, J., Gurusaran, M., Fujiwara, Y., Zhang, K., Echbarthi, M., Vorontsov, E., et al. (2020). The BRCA2-MEILB2-BRME1 complex governs meiotic recombination and impairs the mitotic BRCA2-RAD51 function in cancer cells. *Nat. Commun.* 11:2055.

Zhao, W., Steinfeld, J. B., Liang, F., Chen, X., Maranon, D. G., Jian Ma, C., et al. (2017). BRCA1-BARD1 promotes RAD51-mediated homologous DNA pairing. *Nature* 550, 360–365. doi: 10.1038/nature24060

Zickler, D., and Kleckner, N. (2015). Recombination, pairing, and synapsis of homologs during meiosis. *Cold Spring Harb. Perspect. Biol.* 7:a016626. doi: 10.1101/cshperspect.a016626

15

Chapter 2

The tumor suppressor BRCA1-BARD1 complex localizes to the synaptonemal complex and regulates recombination under meiotic dysfunction in *Caenorhabditis elegans*

Qianyan Li, Takamune T. Saito, Marina Martinez-Garcia, Alison J. Deshong, Saravanapriah Nadarajan, Katherine S. Lawrence, Paula M. Checchi, Monica P. Colaiacovo, JoAnne Engebrecht

Takamune Saito and Marina Martinez-Garcia performed the SNP makers based genetic linkage analysis (Figure 8D). Alison Deshong performed live cell imaging (Figure 1A and part of Figure 4). JoAnne Engebrecht performed the viability and apoptosis assays (Figure 5D-5F) and quantified RAD-51 foci (Figure 6B). Katherine Lawrence and Paula Checchi conducted preliminary work leading to the start of this project. QL performed all other experiments.

The tumor suppressor BRCA1-BARD1 complex localizes to the synaptonemal complex and regulates recombination under meiotic dysfunction in *Caenorhabditis elegans*

Qianyan Li[1], Takamune T. Saito[2¤a], Marina Martinez-Garcia[2], Alison J. Deshong[1], Saravanapriah Nadarajan[2], Katherine S. Lawrence[1], Paula M. Checchi[1¤b], Monica P. Colaiacovo[2], JoAnne Engebrecht[1]*

1 Department of Molecular and Cellular Biology, University of California Davis; Davis CA, United States of America, **2** Department of Genetics, Harvard Medical School; Boston, MA, United States of America

¤a Current address: Department of Genetic Engineering, Kindai University, Kinokawa, Wakayama, Japan
¤b Current address: Department of Biology, Marist College, Poughkeepsie, NY, United States of America
* jengebrecht@ucdavis.edu

Abstract

Breast cancer susceptibility gene 1 (BRCA1) and binding partner BRCA1-associated RING domain protein 1 (BARD1) form an essential E3 ubiquitin ligase important for DNA damage repair and homologous recombination. The *Caenorhabditis elegans* orthologs, BRC-1 and BRD-1, also function in DNA damage repair, homologous recombination, as well as in meiosis. Using functional GFP fusions we show that in mitotically-dividing germ cells BRC-1 and BRD-1 are nucleoplasmic with enrichment at foci that partially overlap with the recombinase RAD-51. Co-localization with RAD-51 is enhanced under replication stress. As cells enter meiosis, BRC-1-BRD-1 remains nucleoplasmic and in foci, and beginning in mid-pachytene the complex co-localizes with the synaptonemal complex. Following establishment of the single asymmetrically positioned crossover on each chromosome pair, BRC-1-BRD-1 concentrates to the short arm of the bivalent. Localization dependencies reveal that BRC-1 and BRD-1 are interdependent and the complex fails to properly localize in both meiotic recombination and chromosome synapsis mutants. Consistent with a role for BRC-1-BRD-1 in meiotic recombination in the context of the synaptonemal complex, inactivation of BRC-1 or BRD-1 enhances the embryonic lethality of mutants defective in chromosome synapsis. Our data suggest that under meiotic dysfunction, BRC-1-BRD-1 stabilizes the RAD-51 filament and alters the recombination landscape; these two functions can be genetically separated from BRC-1-BRD-1's role in the DNA damage response. Together, we propose that BRC-1-BRD-1 serves a checkpoint function at the synaptonemal complex where it monitors and modulates meiotic recombination.

17

Author summary

Our genomes are passed down from one generation to the next through the specialized
cell division program of meiosis. Meiosis is highly regulated to coordinate both the large
scale chromosomal and fine scale DNA events to ensure fidelity. While the tumor sup-
pressor BRCA1-BARD1 is essential for genome integrity, its specific role in meiosis has
been difficult to uncover. Taking advantage of attributes of the *Caenorhabditis elegans* sys-
tem, we have analyzed the function of the BRCA1-BARD1 complex in meiosis in this sim-
ple metazoan. We find that BRCA1 and BARD1 localize dynamically to the proteinaceous
structure that aligns maternal and paternal chromosomes, where it regulates homologous
recombination. Although BRCA1 and BARD1 mutants have only subtle meiotic defects,
we show that this complex plays critical roles in meiotic recombination when meiosis is
perturbed, and this is separable from BRCA1-BARD1's function in response to DNA
damage in somatic cells. These results highlight the complexity of ensuring accurate trans-
mission of the genome and uncover the requirement for this conserved complex in
meiosis.

Introduction

BRCA1 was identified twenty-eight years ago as the causative agent of early-onset familial
breast cancer [1]. Subsequently, BRCA1 was shown to interact with BARD1 through their
RING domains [2], to form an E3 ubiquitin ligase, which adds the small polypeptide ubiquitin
to protein substrates [3] (hereafter referred to as BRCA1-BARD1). While BRCA1-BARD1 has
been extensively studied with respect to its crucial tumor suppressor activities, we still do not
fully understand how this protein complex mediates the diverse functions that have been
ascribed to it (*e.g.*, DNA metabolism, checkpoint signaling, chromatin dynamics, centrosome
amplification, and transcriptional and translational regulation [4, 5]). This is due in part to the
diversity of protein-protein interactions involved in generating numerous distinct BRCA1-
BARD1 multi-protein complexes [6]. An additional impediment to understanding BRCA1-
BARD1 function is that the corresponding mouse knockouts are embryonic lethal [7, 8].

The simple metazoan *Caenorhabditis elegans* offers several advantages to the study of this
key complex. First, unlike in mammals, *C. elegans* BRCA1 and BARD1 orthologs, BRC-1 and
BRD-1, are not essential yet play critical roles in DNA replication and the DNA damage
response, as well as in homologous recombination, which is critical for repairing programmed
double strand breaks (DSBs) during meiosis [9–14]. Additionally, attributes of the *C. elegans*
system, including sophisticated genetics, ease of genome editing, and the spatio-temporal
organization of the germ line allow us to overcome some challenges inherent in studying this
complex in mammalian meiosis.

Meiosis is essential for sexual reproduction and results in the precise halving of the genome
for packaging into gametes. During meiosis, homologous chromosomes are connected by
crossover recombination to facilitate their alignment and segregation on the meiotic spindle.
Recombination is integrated and reinforced with chromosome pairing and synapsis, although
the extent of dependencies of these critical meiotic processes are distinct in different organisms
(reviewed in [15, 16]). While it is well established that BRCA1-BARD1 plays an important role
in DNA repair and recombination [5], the specific function of BRCA1-BARD1 in meiotic
recombination is not known. In mice, partial deletions of BRCA1 result in early apoptosis of
male germ cells due to failures in meiotic sex chromosome inactivation [17, 18]. BRCA1 has
been shown to co-localize with RAD51 on asynapsed chromosomes in mouse spermatocytes,

18

suggesting it functions in meiotic recombination [19]. In *C. elegans*, *brc-1* and *brd-1* mutants have mild meiotic phenotypes consistent with a role in some aspect of meiotic recombination [9, 10]. However, the relationship between BRC-1-BRD-1 function in synapsis and recombination has not been explored.

Here, we assessed BRC-1 and BRD-1 dynamics in the *C. elegans* germ line. Surprisingly, BRC-1-BRD-1 localizes to the synaptonemal complex (SC), becomes concentrated onto chromosome regions upon crossover designation, and at late meiotic prophase is restricted to the short arm of each bivalent as defined by the single crossover site on *C. elegans* chromosomes. BRC-1 and BRD-1 are interdependent for localization to the SC and proper localization is dependent on meiotic recombination and chromosome synapsis. Further, our data suggest that the BRC-1-BRD-1 complex promotes homologous recombination under meiotic dysfunction by stabilizing the RAD-51 filament and altering the patterning of crossovers. Similar findings are reported by Janisiw et al. in the accompanying paper.

Results

GFP::BRC-1 and BRD-1::GFP are expressed in embryos and the germ line

To examine BRC-1 and BRD-1 expression and localization in *C. elegans*, we engineered GFP:: BRC-1 and BRD-1::GFP fusions at the endogenous loci using CRISPR-Cas9 [20]. *brc-1* and *brd-1* mutants have low levels of embryonic lethality, produce slightly elevated levels of male progeny (*X0*), a readout of *X* chromosome nondisjunction, and display sensitivity to γ-irradiation (IR) [10]. Worms expressing these fusions as the only source of BRC-1 or BRD-1 produced wild-type levels of viable progeny and males, and were not sensitive to IR (S1A–S1C Fig), suggesting that the fusions are fully functional.

We monitored the localization of GFP::BRC-1 and BRD-1::GFP by live cell imaging. In whole worms, GFP fluorescence was observed in embryos and in the germ line, with very little signal in the soma (note auto-fluorescence of gut granules also observed in wild type; Fig 1A). Immunoblots of whole worm extracts of *gfp::brc-1; fog-2*, which are true females [21] and therefore do not contain embryos, compared to self-fertilizing *gfp::brc-1* hermaphrodites containing embryos, revealed that <10% of the GFP::BRC-1 signal is due to expression in embryos (S1E Fig). Thus, BRC-1 and BRD-1 are expressed predominantly in the germ line.

BRC-1-BRD-1 and RAD-51 become concentrated in foci upon replication stress

The *C. elegans* germ line is arranged in a spatio-temporal gradient, with proliferating germ cells (premeiotic) and all stages of meiosis arrayed from the distal to proximal end [22] (Fig 1B). We first focused on the premeiotic zone, where germ cells are mitotically proliferating. GFP::BRC-1 and BRD-1::GFP were observed diffusely throughout the nucleus, with occasional foci that partially co-localized with the recombinase RAD-51 (Fig 1C and 1D). In mammalian cells RAD51 marks stalled/collapsed replication forks [23], and BRCA1/BRC-1 has been implicated in repair of damaged forks in both mammals and *C. elegans* [14, 24]. To determine whether BRC-1-BRD-1 responds to stalled/collapsed replication forks, we treated worms with the ribonucleotide reductase inhibitor, hydroxyurea (HU). HU slows replication causing fork stalling and collapse, and cell cycle arrest leading to enlarged nuclei [23, 25]. GFP::BRC-1 and BRD-1::GFP fluorescence became enriched in many foci following exposure to HU, and these exhibited substantial co-localization with RAD-51 (Fig 1C and 1D). Consistent with a role in resolving collapsed replication forks, both *brc-1* and *brd-1* mutants were sensitive to HU as measured by embryonic lethality (S1D Fig). These results suggest that BRC-1-BRD-1 responds
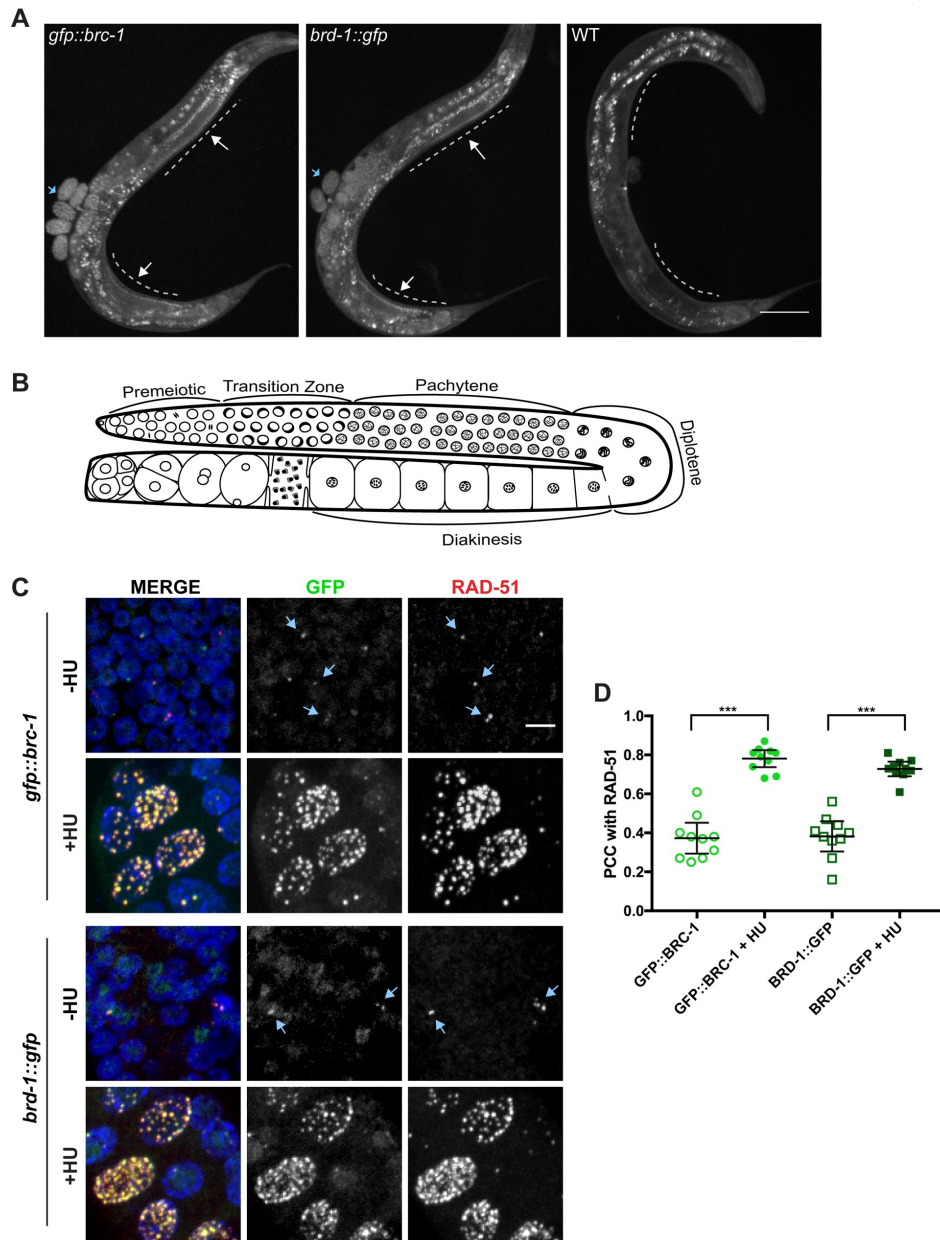
19

Fig 1. GFP::BRC-1 and BRD-1::GFP are expressed in the germ line and respond to stalled/collapsed replication forks. A) GFP fluorescence of whole worms expressing GFP::BRC-1, BRD-1::GFP, or no GFP (WT). Dashed line denotes germ line with arrows to indicate GFP fluorescence;

20

blue arrows denote GFP signal in embryos; gut granules auto-fluoresce. Scale bar = 100μm. B) Schematic of the spatiotemporal organization of the hermaphrodite germ line with meiotic stages indicated. C) Proliferating germ cells (premeiotic) expressing GFP::BRC-1 or BRD-1::GFP (green), stained with antibodies against RAD-51 (red), and counterstained with DAPI (blue) in the absence (-HU) and presence of 5mM hydroxyurea (+HU). Blue arrows denote co-localization between GFP and RAD-51. Images are projections through half of the gonad. Scale bar = 5μm. D) Pearson's Correlation Coefficient (PCC) measurements between RAD-51 and GFP::BRC-1 or BRD-1::GFP in the absence and presence of HU. 95% Confidence Intervals are shown. *** p< 0.0001, Mann-Whitney test; n = 10 nuclei.

to replication stress and concentrates in foci where it co-localizes with RAD-51, presumably to resolve stalled/collapsed replication forks.

BRC-1 and BRD-1 localize to the SC and concentrate to the short arm of the bivalent during meiotic prophase

In early meiotic prophase (transition zone/early pachytene), GFP::BRC-1 and BRD-1::GFP direct fluorescence were observed diffusely on chromatin and in foci (Fig 2A). These foci partially overlapped with RAD-51, which marks meiotic DSBs [26]. We noticed that the relative intensity of the foci was weaker in fixed versus live imaging (see Figs 3 and 4), suggesting that these foci were sensitive to fixation conditions. Beginning at mid-pachytene, GFP::BRC-1 and BRD-1::GFP were observed in tracks along the entire chromosome length, and then concentrated to a portion of each chromosome at late pachytene (Fig 2A). In diplotene and diakinesis, GFP::BRC-1 and BRD-1::GFP were further restricted to six short stretches on the six pairs of homologous chromosomes (Fig 2A). As oocytes continued to mature, GFP::BRC-1 and BRD-1::GFP were disassembled from chromosomes in an asynchronous manner, with some chromosomes losing signal before others. Thus, in diakinesis nuclei we did not always observe six stretches of fluorescence, and the fluorescence intensity varied between chromosomes.

The concentration of BRC-1-BRD-1 into tracks at mid-pachytene suggested that the complex localized to the SC. To investigate this, we co-stained with antibodies against GFP and the SC central region component, SYP-1 [27]. Homologous chromosomes begin synapsing early in meiotic prophase (29); however, GFP::BRC-1 was not observed on tracks until after the SC appeared to be fully formed (Fig 2B). Interestingly, the concentration of GFP::BRC-1 to a portion of each chromosome preceded the relocalization of SYP-1 to the short arm of the bivalent (arrows in late pachytene images of GFP::BRC-1; Fig 2B). As the SC reorganizes as a consequence of crossover maturation [28], we examined worms co-expressing TagRFP-T::BRC-1 (TagRFP-T is a RFP variant with improved photostability [20, 29]) and GFP::COSA-1, a cyclin related protein that marks presumptive crossover sites [30]. TagRFP-T::BRC-1 also appeared to be fully functional (S1A–S1C Fig), although the fluorescent signal was weaker than GFP, and could only be detected in mid-late pachytene through diakinesis. GFP::COSA-1 was observed at one end of each TagRFP-T::BRC-1 stretch (Fig 2C). Thus, BRC-1 and BRD-1 localize to the SC and are redistributed concomitant with crossover designation, suggesting that BRC-1-BRD-1 functions in one or more aspects of meiotic recombination within the context of the SC.

BRC-1 and BRD-1 are interdependent for localization

In both mammalian cells and *C. elegans*, BRCA1/BRC-1 and BARD1/BRD-1 form a stable complex [2, 31]. To probe the relationship between *C. elegans* BRC-1 and BRD-1 *in vivo*, we imaged live worms heterozygous for both TagRFP-T::BRC-1 and BRD-1::GFP (*brc-1* and *brd-1* are linked). In the heterozygous state the TagRFP-T signal could only be detected at late pachytene through early diakinesis when BRC-1 and BRD-1 are concentrated on short tracks.
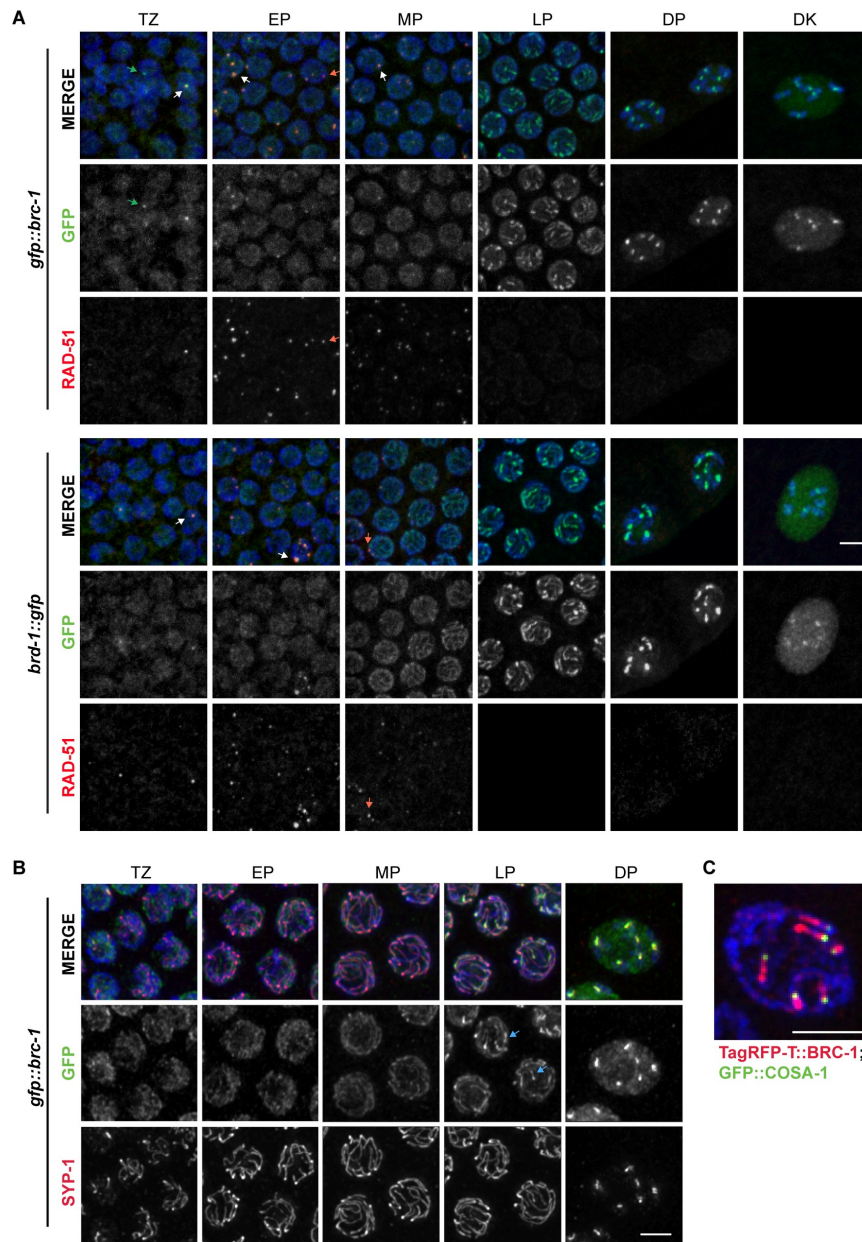
21

Fig 2. GFP::BRC-1 and BRD-1::GFP localize to the SC in meiotic prophase. A) Nuclei from indicated meiotic stages stained with RAD-51 antibodies (red), DAPI (blue) and imaged for GFP fluorescence (green). White arrows demark foci positive for both GFP

22

fluorescence and RAD-51 signal; green arrows demark foci containing GFP but not RAD-51; red arrows demark foci containing only RAD-51. Scale bar = 5 μm. B) Co-localization between GFP::BRC-1 (green) and SC central component SYP-1 (red) by antibody staining; germ lines at indicated stages were counterstained with DAPI. Blue arrows at late pachytene show chromosomal regions where GFP:: BRC-1 concentrates before SYP-1. Scale bar = 2 μm. C) TagRFP-T::BRC-1 (red) and GFP::COSA-1 (green) at late pachytene showing TagRFP-T::BRC-1 on one side of the GFP::COSA-1 focus, which marks the presumptive crossover. Scale bar = 2 μm. Images are projections through half of the gonad. TZ = transition zone; EP = early pachytene; MP = mid pachytene; LP = late pachytene; DP = diplotene; DK = diakinesis.

The TagRFP-T and GFP signals overlapped, suggesting that BRC-1 and BRD-1 are localized together on the SC (Fig 3A).

To examine localization dependencies between BRC-1 and BRD-1 in *C. elegans* germ cells, we monitored GFP::BRC-1 and BRD-1::GFP in the corresponding *brd-1(ok1623)* and *brc-1 (xoe4)* null mutant backgrounds by live cell imaging. In the absence of BRD-1 we observed diffuse GFP::BRC-1 fluorescence within the nucleoplasm from proliferative zone to mid-pachytene, with no evidence of tracks (Fig 3B). In late pachytene, weak GFP::BRC-1 foci were observed; however, in diplotene and diakinesis only a diffuse nucleoplasmic signal was detected, with no concentrated regions of GFP::BRC-1. This result suggests that BRD-1 is required for the correct localization of BRC-1 in meiotic cells. In worms harboring a null allele of *brc-1*, BRD-1::GFP was largely cytosolic, except at diakinesis where it was observed in the nucleoplasm. Analysis of steady state protein levels by immunoblot revealed that BRC-1 and BRD-1 were present, albeit at reduced levels, in the absence of the other partner (in *brc-1 (xoe4)*, BRD-1::GFP = 60% of wild-type levels; in *brd-1(ok1623)*, GFP::BRC-1 = 50% of wild-type levels; Fig 3C). Thus, BRC-1 and BRD-1 are mutually dependent for localization to meiotic chromosomes.

Impairment of either meiotic recombination or synaptonemal complex formation alters GFP::BRC-1 localization

To provide insight into the relationship between BRC-1-BRD-1 and the progression of meiotic recombination, we monitored the localization of GFP::BRC-1 in mutants that impair different steps of meiotic recombination: *spo-11* mutants are unable to form meiotic DSBs [32, 33], *rad-51* mutants are blocked prior to strand invasion [34–36], and *msh-5* mutants fail to form crossovers [37, 38]. In live *spo-11* mutants, we observed many fewer GFP::BRC-1 foci in transition zone and early pachytene compared to WT (TZ: 1.29±0.12 vs. 0.18±0.05; EP: 4.61±0.36 vs. 0.91±0.22 foci/nucleus in WT and *spo-11*, respectively; p <0.0001; S2A Fig). At mid-pachytene GFP::BRC-1 was observed in tracks in the *spo-11* mutant similar to wild type, as synapsis occurs in the absence of meiotic DSB formation in *C. elegans* [32] (Fig 4). In late pachytene, GFP::BRC-1 fluorescence did not concentrate on a portion of each chromosome pair nor retract to the short arm of the bivalent as in wild type, consistent with these events being dependent on meiotic recombination. However, in 20.23±1.78% of nuclei (n = 4 germ lines) there was enrichment of GFP::BRC-1 on one or sometimes two tracks, in addition to weak staining on other tracks. This is similar to what has been previously reported for synapsis markers, including the phosphorylated form of SYP-4 [39–41], and likely represents *spo-11*-independent lesions capable of recruiting meiotic DNA repair components and altering SC properties. Consistent with this, we observed GFP::BRC-1 enrichment on the phospho-SYP-4-marked chromosome in *spo-11* mutants (S2B Fig). However, GFP::BRC-1 did not retract to chromosome subdomains as in wild type in diplotene and diakinesis, suggesting that the relocalization of BRC-1-BRD-1 is dependent on formation of meiotic DSBs. As expected, BRD-1:: GFP was observed in a similar pattern to GFP::BRC-1 in *spo-11* mutants throughout meiotic prophase (S2C Fig).
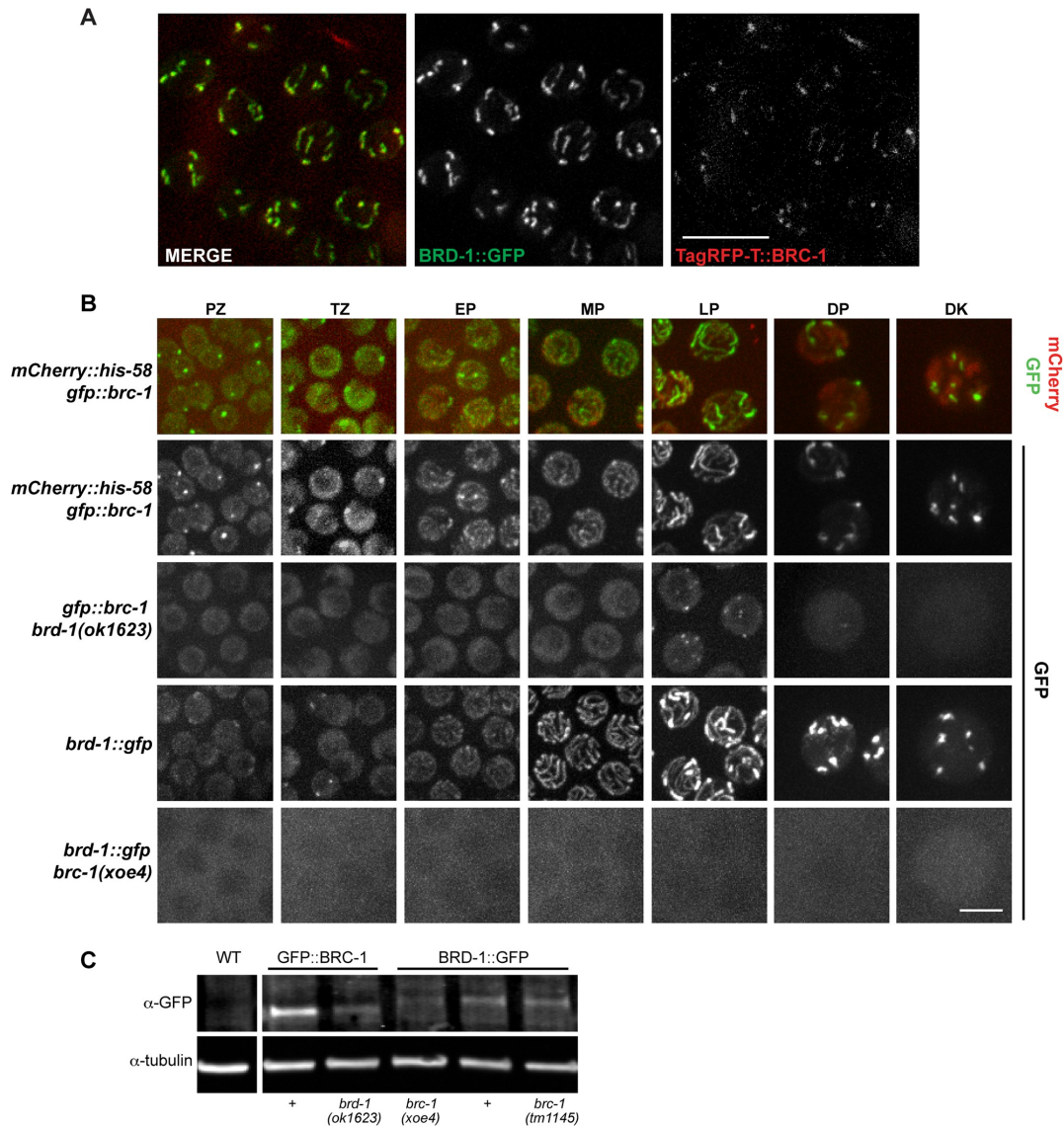
23

Fig 3. BRC-1 and BRD-1 are inter-dependent for localization. A) Co-localization between BRD-1::GFP (green) and TagRFP-T::BRC-1 (red) at late pachytene in live worms. Scale bar = 10 μm. B) Stills of germline nuclei from live worms expressing GFP::BRC-1 and mCherry::Histone H2B (*mCherry::his-58*; *gfp::brc-1*); merge and GFP channel; top two panels, respectively. GFP::BRC-1 expression in *brd-1(ok1623)* mutant at indicated meiotic stages. Bottom two panels show BRD-1::GFP localization in wild type and the *brc-1(xoe4)* mutant. Images are projections through half of the gonad. TZ = transition zone; EP = early pachytene; MP = mid pachytene; LP = late pachytene; DP = diplotene; DK = diakinesis. Scale bar = 5 μm. C) Immunoblot of whole worm extracts from indicated worms probed with anti-GFP and α-tubulin antibodies. Lane 1 = N2: wild type; Lane 2 = JEL515: *gfp::brc-1*; Lane 3 = JEL520: *gfp::brc-1 brd-1(ok1623)*; Lane 4 = JEL744: *brc-1(xoe4) brd-1::gfp*; Lane 5 = JEL657: *brd-1::gfp*; Lane 6 = JEL678: *brc-1(tm1145) brd-1::gfp*.

24
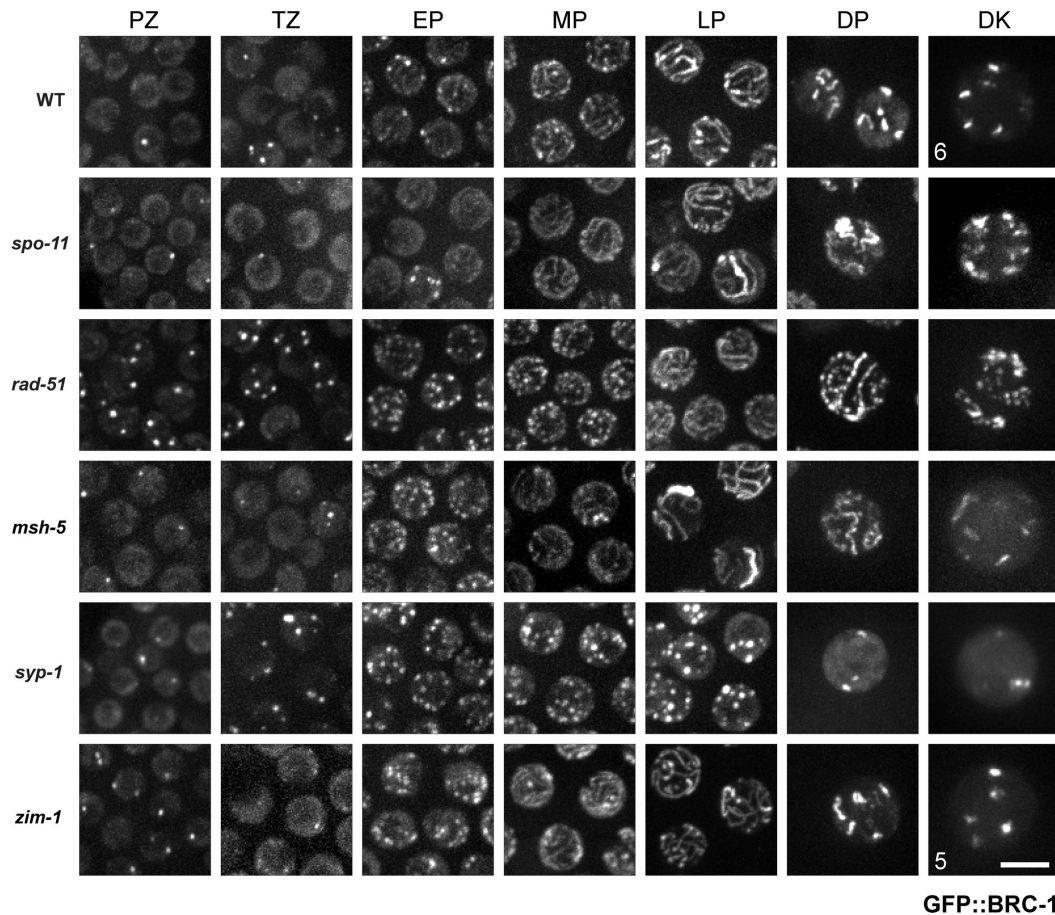
Fig 4. GFP::BRC-1 localization is perturbed when either meiotic recombination or chromosome synapsis is impaired. High-magnification images of live *C. elegans* expressing GFP::BRC-1 from the indicated genetic backgrounds and gonad region (PZ = Proliferative Zone, TZ = Transition Zone, EP = Early Pachytene, MP = Mid Pachytene, LP = Late Pachytene, DP = Diplotene, DK = Diakinesis). In wild-type worms GFP::BRC-1 localizes to chromatin and in a small number of foci in the proliferative and transition zones. GFP::BRC-1 localizes to long tracks corresponding to the SC in mid-pachytene. In late pachytene, GFP::BRC-1 becomes condensed to one side of each chromosome, demarcating what will become the short arms of the six bivalents in diakinesis (WT = 6). This localization pattern is perturbed when synapsis and crossover formation are disrupted. A *zim-1* diakinesis nucleus with 5 GFP::BRC-1 short stretches is shown. Images are projections through half of the gonad. Scale bar = 5 μm.

Following DSB formation and processing, RAD-51 is loaded onto resected single-stranded DNA and facilitates strand exchange [36]. GFP::BRC-1 localization was altered in the *rad-51* mutant (Fig 4). Significantly increased levels of GFP::BRC-1 foci were observed throughout the germ line. In the proliferative zone, wild type had 0.55±0.04, while *rad-51* had 0.96±0.10 foci per nucleus (S2A Fig). These most likely represent concentration of GFP::BRC-1 at

25

stalled/collapsed replication forks. In transition zone, wild type had 1.29±0.12, while *rad-51* had 3.98±0.31 foci/nucleus, and this was further increased in early pachytene (WT: 4.6±0.4 vs. *rad-51*: 13.3±0.7; S2A Fig). These foci presumably represent resected meiotic DSBs that fail to undergo strand invasion in the absence of RAD-51, as they cannot be solely accounted for by the elevated foci observed in proliferating cells. Track-like structures were not observed until late pachytene in the absence of RAD-51. The punctate nature of GFP::BRC-1 was particularly pronounced in diplotene and diakinesis, with no clear concentration to six regions. This is consistent with the disorganized chromatin masses observed in *rad-51* diakinesis nuclei [35], and suggests that RAD-51 is required for the proper organization and retraction of GFP::BRC-1.

In *msh-5* mutants, GFP::BRC-1 appeared similar to wild type from the proliferative zone to mid pachytene, localizing in the nucleoplasm and concentrating in foci before converging on tracks (Fig 4; S2A Fig). Similar to *spo-11*, 26.27±2.25% of *msh-5* late pachytene nuclei (n = 4 germ lines) contained enrichment of GFP::BRC-1 on one or occasionally two chromosomes. In diplotene, GFP::BRC-1 was observed in long tracks, with no evidence of retraction. The presence of more than six stretches of GFP::BRC-1 in diakinesis suggests that BRC-1 remains associated with the univalents in *msh-5* mutants. Taken together, our data suggest that GFP::BRC-1 localizes to the SC and its retraction to the short arm of the bivalent is dependent on processing of meiotic DSBs into crossovers.

We also examined localization of GFP::BRC-1 when synapsis is blocked by mutation of a component of the central region of the SC, *syp-1* [27]. GFP::BRC-1 in *syp-1* looked similar to wild type in proliferating germ cells (Fig 4). However, as cells entered meiosis GFP::BRC-1 was observed in many foci (in TZ, WT: 1.29±0.12 vs. *syp-1*: 7.29±0.36 foci/nucleus; S2A Fig). The number of foci increased through early and mid pachytene but GFP::BRC-1 never attained nuclear track staining, supporting a dependency on the SC for track localization. Similarly, the GFP::BRC-1 signal did not localize to sub-regions of condensed (DP and DK) chromosomes, but rather was found in a small number of nuclear foci. Thus, GFP::BRC-1 localization to tracks is dependent on SC formation.

To examine localization under conditions where a subset of chromosomes fail to synapse and recombine, we monitored GFP::BRC-1 localization in the *zim-1* mutant, in which chromosomes *II* and *III* cannot synapse [42]. In transition zone and early pachytene, GFP::BRC-1 was observed in many foci in the *zim-1* mutant, similar to the *syp-1* mutant (TZ: WT: 1.29±0.12 vs. *zim-1*: 4.5±0.36 foci/nucleus; Fig 4; S2A Fig). However, as meiosis progressed GFP::BRC-1 was observed on tracks that condensed to the short arm of the bivalent on multiple chromosomes. Many times we observed more than four stretches of GFP::BRC-1 fluorescence at diplotene/diakinesis (Fig 4), suggesting that there are more than four chiasmata in the *zim-1* mutant. We address the role of BRC-1 in chiasmata formation in the *zim-1* mutant below.

The BRC-1-BRD-1 complex is important when chromosome synapsis and crossover formation are perturbed

Given the association of GFP::BRC-1 and BRD-1::GFP with the SC (Fig 4), we next examined the functional consequence of removing BRC-1-BRD-1 when synapsis is perturbed. For these studies we focused on the *zim-1* mutant, as the appearance of more than four short tracks of GFP::BRC-1 at diplotene/diakinesis (Fig 4) suggested that these BRC-1-BRD-1-associated regions were altered in the absence of *zim-1*. Additionally, unlike mutants such as *syp-1* that result in a complete failure in synapsis and therefore 95% embryonic lethality [27], loss of ZIM-1 results in 73.9% inviable progeny [42], allowing us to determine whether removal of BRC-1-BRD-1 enhances embryonic lethality.

26

In the course of our experiments we discovered that strain DW102 [31] harbors mutations in both *brc-1* and *brd-1*; sequence analysis revealed that *brc-1(tm1145)* is an in-frame deletion, removing 71 amino acids (116–186) C-terminal to the predicted RING domain, which in the mammalian ortholog is responsible for E3 ubiquitin ligase activity and dimerization with BARD1 [3, 43, 44] (Fig 5A). The *brd-1* mutation in DW102 is identical to *brd-1(dw1)* [31]; cDNA analysis revealed that the mutation results in the use of an alternative splice site to generate a protein missing 327 amino acids, leaving the RING domain intact (Fig 5A and S3A Fig). To discern the contributions of BRC-1 and BRD-1 we used CRISPR-Cas9 to generate a complete deletion of BRC-1, *brc-1(xoe4)* (Fig 5A and S3A Fig). We also examined the *brc-1 (tm1145)* and *brd-1(dw1)* single mutants, the *brc-1(tm1145) brd-1(dw1)* double mutant and *brd-1(ok1623)*, which results in the removal of 359 amino acids C terminal of the RING domain (Fig 5A and S3A Fig). As expected, *brc-1(xoe4)*, *brd-1(dw1)*, *brc-1(tm1145) brd-1 (dw1)*, and *brd-1(ok1623)* displayed slightly elevated embryonic lethality (Fig 5B), male progeny (Fig 5C), and IR sensitivity (Fig 5D). On the other hand, *brc-1(tm1145)* was not statistically different from wild type for embryonic lethality, production of male progeny or IR sensitivity, suggesting that this allele is not a null mutation (Fig 5B–5D). Consistent with this, BRD-1:: GFP was stable (Fig 3C) and localized similarly to wild type in the *brc-1(tm1145)* mutant background (S3B Fig).

In contrast to the differential impact of the alleles on embryonic lethality, male progeny, and IR sensitivity, loss of *zim-1* in any of the *brc-1* or *brd-1* mutants resulted in enhanced embryonic lethality compared to the single *zim-1* mutant (p<0.0001; Fig 5E). These results suggest that the region C-terminal to the BRC-1 RING domain, which is deleted in *brc-1 (tm1145)*, is important for promoting embryonic viability when chromosome pairing and synapsis are perturbed.

To determine the nature of the enhanced embryonic lethality of *zim-1* mutants when BRC-1-BRD-1 is impaired, we first monitored germline apoptosis. Apoptosis is an output of checkpoint signaling and is important for culling defective germ cells [45–47]. Previous studies had established that both *brc-1* [9] and *zim-1* [48] have elevated checkpoint-dependent germline apoptosis. We found that all *brc-1* and *brd-1* alleles, including *brc-1(tm1145)*, had elevated apoptosis (Fig 5F). Loss of *zim-1* resulted in higher levels of apoptosis than *brc-1* and *brd-1* mutants; however, the levels of apoptosis in the double *brc-1; zim-1* and *brd-1; zim-1* mutants were not significantly different than *zim-1* alone. We also analyzed SUN-1 phosphorylated on Serine12 (Sun-1 S12P), which is dephosphorylated following establishment of the obligate crossover, and serves as a readout of meiotic progression [49]. Loss of ZIM-1 resulted in persistent SUN-1 S12P, which was unaltered in the absence of BRC-1 (S3C Fig). These results suggest that BRC-1-BRD-1 does not function in known signaling pathways responsible for monitoring unrepaired DSBs or crossovers leading to apoptosis or cell cycle delay.

We next monitored RAD-51 assembly/disassembly in the spatiotemporal organization of the germ line. Previous analyses revealed that *brc-1* and *brd-1* mutant hermaphrodites have elevated RAD-51 foci in late pachytene, suggesting that repair of a subset of meiotic DSBs is delayed in the absence of BRC-1-BRD-1 [9]; this was also observed in the *brc-1(tm1145) brd-1 (dw1)* and *brd-1(ok1623)* mutants (S4A Fig). Further, blocking synapsis on some or all chromosomes results in elevated RAD-51 levels genome wide [26, 50], as observed in the *zim-1* mutant (Fig 6A and 6B). Surprisingly, *brc-1; zim-1* and *brd-1; zim-1* double mutants resulted in fewer RAD-51 at mid-late pachytene: RAD-51 foci appeared at similar levels compared to the *zim-1* single mutant early in meiotic prophase, but in the latter half of pachytene many fewer RAD-51 were detected on chromosomes (Fig 6A and 6B and S4B Fig). High levels of RAD-51 were observed again at the gonad bend, as nuclei exited pachytene and entered diplotene (Fig 6A and 6B and S4B Fig). Similar patterns were observed when BRC-1-BRD-1 was
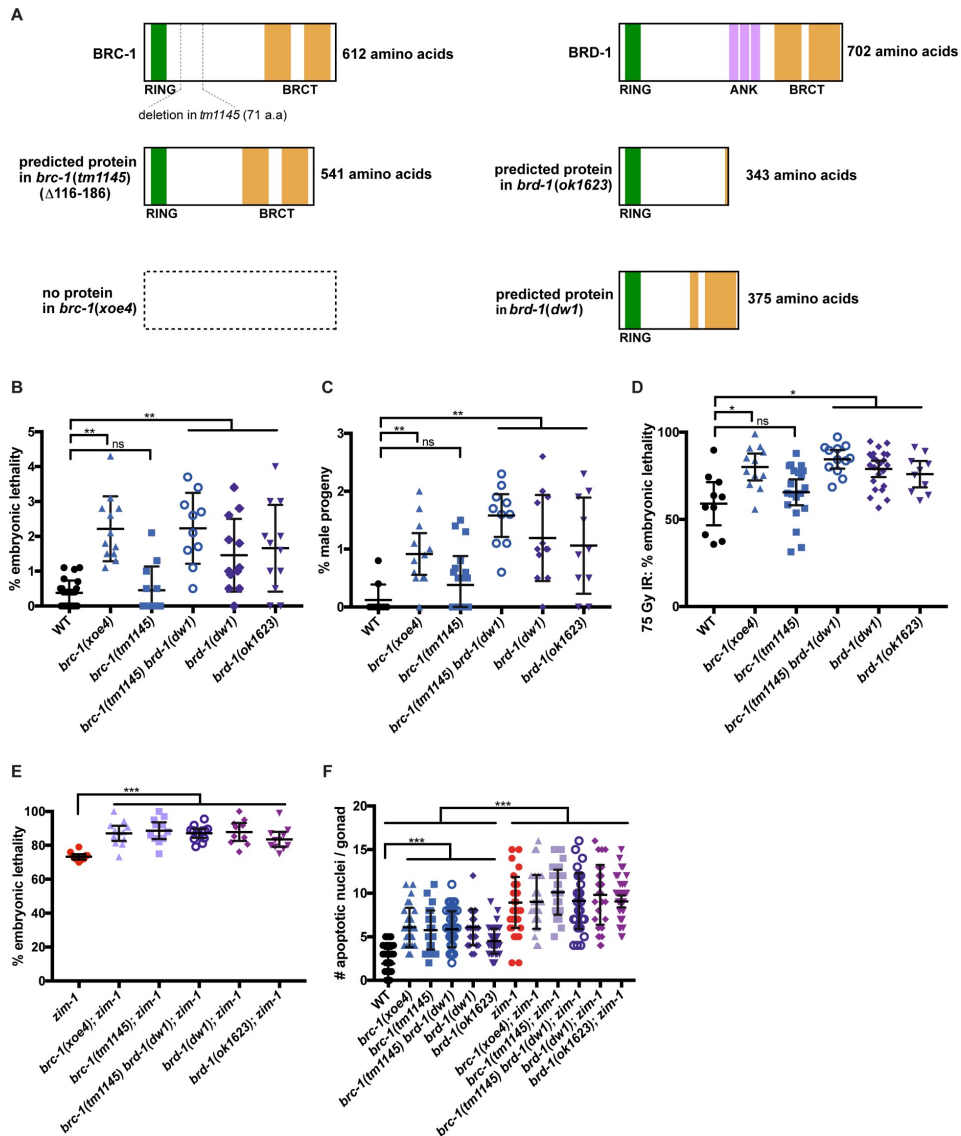
27

Fig 5. Differential effect of *brc-1* and *brd-1* alleles on the DNA damage response and meiosis. A) Cartoon of predicted proteins produced from the different *brc-1* and *brd-1* mutant alleles based on cDNA analysis (see also S3A Fig). RING (green), BRCT (gold) and Ankyrin (ANK; purple) domains are indicated. B) % embryonic lethality of *brc-1* and *brd-1* mutants; numbers of animals scored: WT = 26; *brc-1(xoe4)* = 12; *brc-1(tm1145)* = 12; *brc-1(tm1145) brd-1(dw1)* = 10; *brd-1(dw1)* = 12; *brd-1(ok1623)* = 12. C) % male progeny produced from *brc-1* and *brd-1* mutants; numbers of animals scored: WT = 10; *brc-1(xoe4)* = 12; *brc-1(tm1145)* = 22; *brc-1(tm1145) brd-1(dw1)* = 10; *brd-1(dw1)* = 12; *brd-1(ok1623)* = 10. D) % embryonic lethality following 75 Gy IR; numbers of animals scored: WT = 10; *brc-1(xoe4)* = 12; *brc-1(tm1145)* = 20; *brc-1(tm1145) brd-1(dw1)* = 12; *brd-1(dw1)* = 23; *brd-1(ok1623)* = 10. E) % embryonic lethality of *zim-1* in the presence and absence of BRC-1-BRD-1. Numbers of animals

28

removed in other mutants that perturb synapsis (i.e., *syp-1*; S4B Fig). These results suggest that when synapsis and therefore crossover formation is impaired, BRC-1-BRD-1 plays a role in DSB formation, DNA end resection, RAD-51 loading, and/or stabilization of the RAD-51 filament in mid-late pachytene.

To differentiate between these possible meiotic functions of BRC-1-BRD-1, we analyzed the pattern of the single-stranded binding protein RPA-1 (GFP::RPA-1; [51]). RPA-1 binds resected ends prior to RAD-51 loading [52, 53] and is also associated with recombination events at a post-strand-exchange step, which can be observed in chromosome spreads [54]. In the *brc-1(tm1145); zim-1* germ line we observed an inverse pattern between RAD-51 and RPA-1 at mid-late pachytene: GFP::RPA-1 foci were prevalent in the region where RAD-51 foci were reduced (Fig 6A). In the *zim-1* single mutant, fewer GFP::RPA-1 foci were observed at this stage, while RAD-51 remained prevalent. We also observed very few RPA-1 foci at mid-late pachytene in wild type or *brc-1(tm1145) brd-1(dw1)* double mutant whole mount gonads (S4C Fig). These results suggest that BRC-1-BRD-1 is not required for DSB formation *per se* in this region of the germ line, as we observed an increase in GFP::RPA-1 foci, not a decrease as would be expected if BRC-1-BRD-1 mediates DSB formation. Additionally, this result argues against a role for BRC-1-BRD-1 in promoting resection as RPA-1 loads on exposed single stranded DNA [52]. Thus, at mid to late pachytene BRC-1-BRD-1 either facilitates the assembly of RAD-51 on new breaks, and/or stabilizes the RAD-51 filament.

BRC-1-BRD-1 stabilizes the RAD-51 filament when crossover formation is impaired

The lack of RAD-51 in mid to late pachytene in *brc-1; zim-1* and *brd-1; zim-1* mutants is reminiscent of the RAD-51 "dark zone" observed in the *rad-50* mutant following exposure to IR, which likely reflects a requirement for RAD-50 in loading RAD-51 at resected DSBs on meiotic chromosomes [55]. However, the distal boundary of the dark zone in the *brc-1; zim-1* double mutant is distinct from the *rad-50* mutant: the dark zone in *rad-50* extends from meiotic entry to late pachytene [55], while in the *brc-1; zim-1* and *brd-1; zim-1* mutants reduction in RAD-51 was limited to mid-late pachytene (Fig 6A and 6B and S4B Fig), suggesting that the nature of the dark zone is different in these mutant situations. If BRC-1-BRD-1 is required for loading RAD-51 on breaks in mid-late pachytene, then a time course analysis would reveal a diminution of the dark zone by twelve hours following IR exposure, as was observed for *rad-50* mutants (Fig 7A, loading defect on left) [55]. On the other hand, if BRC-1-BRD-1 was important for protecting RAD-51 from disassembly, then the dark zone should be maintained throughout the time course as RAD-51 would be disassembled as nuclei with pre-installed RAD-51 move through the mid-late pachytene region of the germ line (Fig 7A, stabilization defect on right). SPO-11 remains active under conditions where crossovers have not formed on all chromosomes [56, 57], making it difficult to distinguish a RAD-51 loading defect onto new breaks in this region of the germ line versus a defect in RAD-51 stability. Therefore, we performed these experiments in the *spo-11* mutant background [32], as IR will induce breaks uniformly in the germ line at a single point in time and as nuclei move through the germ line, no new breaks will be formed. *spo-11* is tightly linked to *zim-1*; consequently, we used RNAi
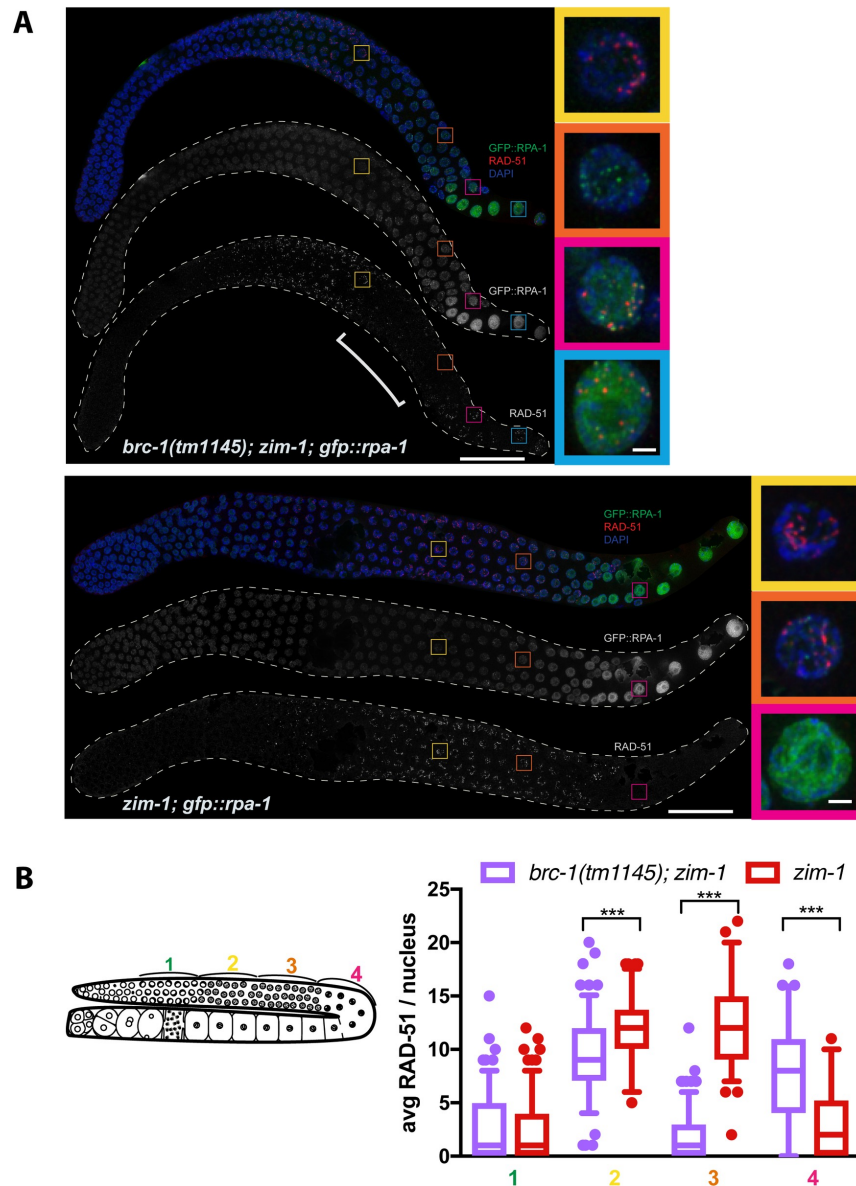
29

Fig 6. Inactivation of BRC-1-BRD-1 alters the pattern of RAD-51 foci in the *zim-1* mutant. A) Dissected germ lines from *brc-1 (tm1145); zim-1; gfp::rpa-1* and *zim-1; gfp::rpa-1* worms stained with anti-RAD-51 (red), counterstained with DAPI (blue) imagined for GFP::RPA-1 fluorescence (green). Scale bar = 20 μm. Insets show selected nuclei from different regions of the germ line; bracket indicates RAD-51 "dark zone". Images are projections through half of the gonad. A minimum of 3 germ lines were examined for each genotype. Scale bar = 1 μm. B) Schematic of germ line indicating zones for analysis of RAD-51 foci. Box whisker plots show
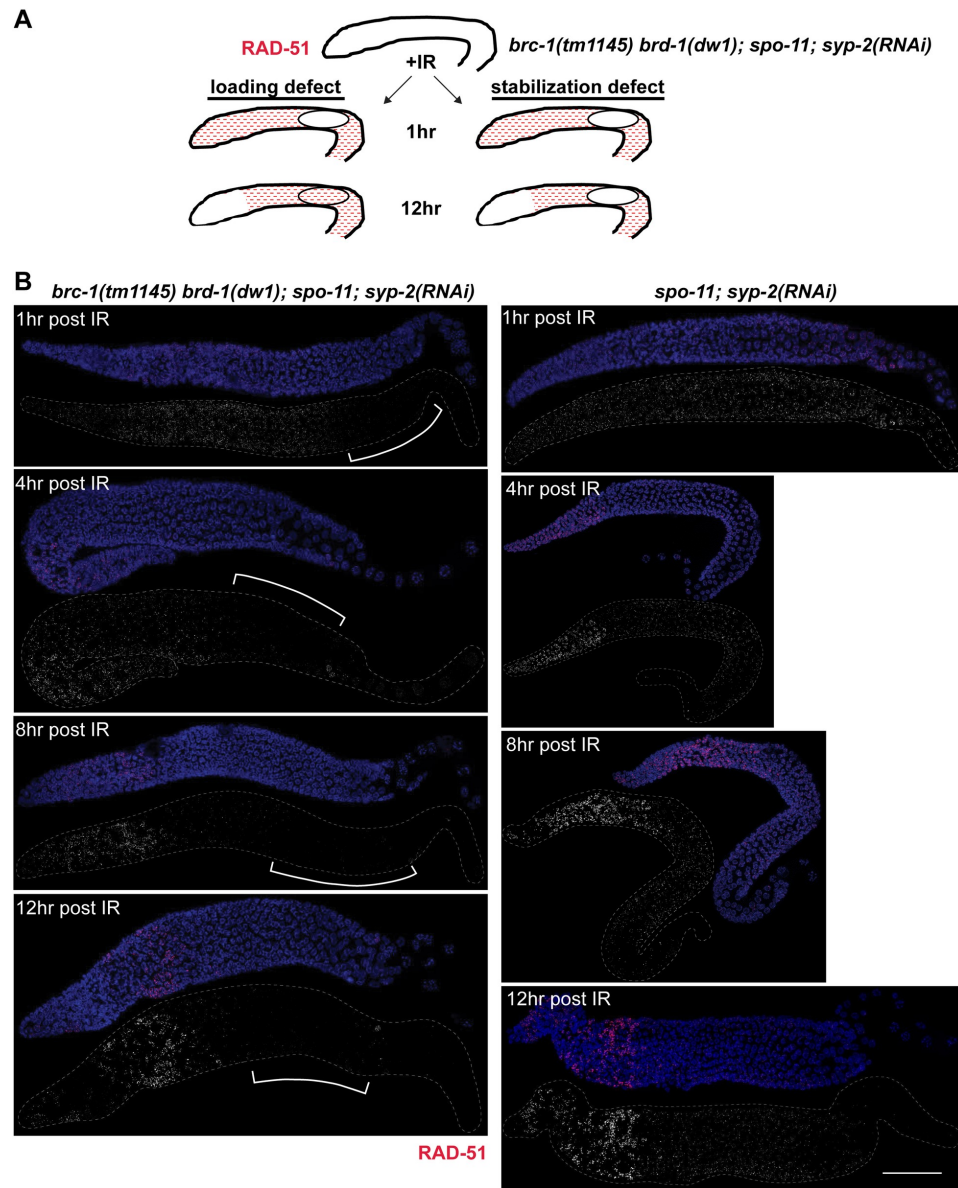
30

against SYP-2, which in our hands is more efficient than *zim-1*(RNAi), to block synapsis and crossover formation. To that end, we exposed *spo-11* and *brc-1(tm1145) brd-1(dw1); spo-11* mutants depleted for SYP-2 to 10 Gy of IR and examined RAD-51 over time. At one, four, eight, and twelve hours following IR, the dark zone was maintained in the absence of BRC-1-BRD-1 (Fig 7B). This result is consistent with the hypothesis that BRC-1-BRD-1 stabilizes the RAD-51 filament rather than facilitates loading of RAD-51 on new DSBs at mid-late pachytene.

BRC-1-BRD-1 alters recombination patterning under meiotic dysfunction

A subset of RAD-51 strand invasions are processed into crossovers, which are marked by CNTD1/COSA-1 [30, 58]. Given the reduction in RAD-51 in mid-late pachytene in *brc-1; zim-1* and *brd-1; zim-1* mutant hermaphrodites, we next analyzed crossover precursor formation in the various mutants. In *C. elegans*, each of the six chromosome pairs forms a single crossover; consequently, there are six COSA-1 foci in hermaphrodite germ cells at late pachytene [30] (Fig 8A). We also observed six COSA-1 foci in late pachytene nuclei in the *brc-1* and *brd-1* mutants (Fig 8A), indicating that breaks are efficiently processed into crossovers in the absence of BRC-1-BRD-1 in an otherwise wild-type worm. This is consistent with the presence of six bivalents at diakinesis and the low embryonic lethality of *brc-1* and *brd-1* [9, 10] (Fig 5B). In *zim-1* mutants we expected to observe four COSA-1 foci per nucleus, one on each of the four paired chromosomes, but not on the unpaired chromosomes *II* and *III*. Contrary to our expectations, *zim-1* had an average of 6.12±0.12 COSA-1 foci (χ^2: p<0.005), with a very broad distribution ranging from 2 to 9 foci; such a wide distribution is never observed in wild type [30] (Fig 8A; S5 Fig). Inactivation of BRC-1 and/or BRD-1 in *zim-1* reduced the number of GFP::COSA-1 foci to a range of 4.3–4.8 in the various mutants, closer to expectations although still significantly different than expected (χ^2: p<0.005), and the distribution remained broad (p <0.0001; Fig 8A). These results suggest that when crossovers are unable to form between some homologs, additional COSA-1-marked crossover precursors are generated, and some of these are dependent on BRC-1-BRD-1.

The higher than expected numbers of COSA-1 foci observed in *zim-1* mutants could reflect recombination intermediates that do not go on to form chiasmata (i.e., non-crossovers or inter-sister crossovers). Alternatively, COSA-1 could mark *bona fide* inter-homolog crossovers, such that some chromosomes have more than one chiasma, as has been observed in mutants where the *X* chromosomes fail to pair and synapse [50]. As these two possibilities are not mutually exclusive, the extra COSA-1 foci could be due to a combination of both recombination outcomes. To provide insight into the nature of the extra COSA-1 foci, we analyzed COSA-1 in *syp-1* mutants, where no chiasmata can form as all chromosomes fail to synapse, and found that there were on average 4.85±0.07 COSA-1 foci at late pachytene (Fig 8A; S5 Fig). These results suggest that under conditions of meiotic dysfunction when chromosomes are unable to pair/synapse, COSA-1 is recruited to recombination intermediates that are processed into non-crossovers and/or inter-sister crossovers. Similar numbers of COSA-1 foci, associated with MSH-5, were observed in *syp-3* mutants; high resolution cytological analyses indicated that these recombination sites are non-randomly distributed but with some
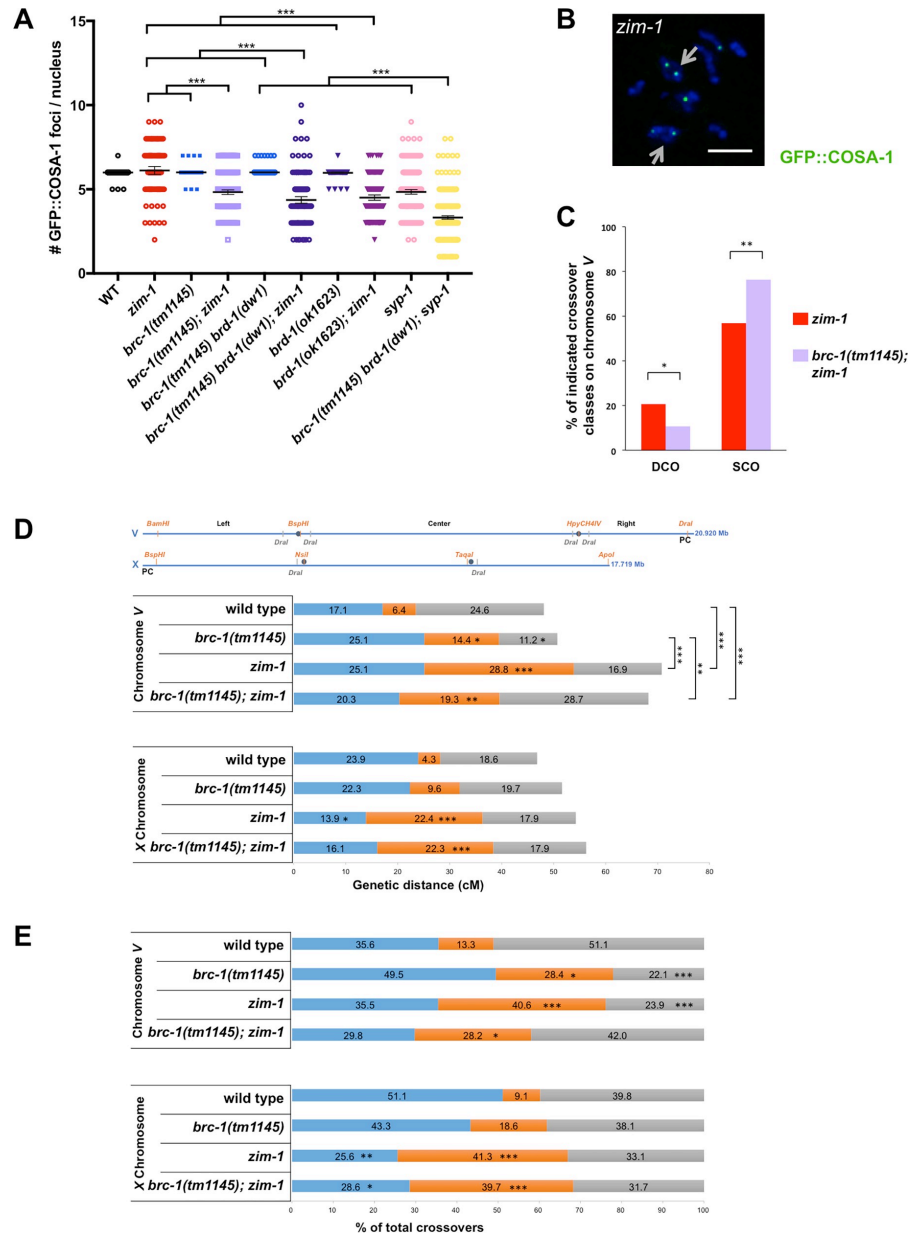
31

Fig 7. BRC-1 promotes the stability of RAD-51 filaments when crossover formation is impaired. A) Schematic of potential outcomes of IR-induced RAD-51 (red) over time in *brc-1(tm1145) brd-1(dw1); spo-11; syp-2*(RNAi) worms: a defect in RAD-51 loading would result in loss of the "dark zone" (circle) by 12 hrs (left), while a defect in RAD-51 stabilization would manifest in the maintenance of the dark zone over 12 hrs (right). B) Projections of whole germ lines at indicated times after IR treatment in *brc-1(tm1145) brd-1(dw1); spo-11; syp-2*(RNAi) (left) and *spo-11; syp-2* (RNAi) (right). DAPI (blue), RAD-51 (red). A minimum of 3 germ lines were imaged for each condition. Scale bar = 30 μm.

32

Fig 8. BRC-1-BRD-1 alters the crossover landscape when meiosis is impaired. A) Number of GFP::COSA-1 foci in mid-late pachytene in indicated mutants. Number of nuclei from a minimum of 4 germ lines scored: *gfp::cosa-1* = 458, *brc-1(tm1145) brd-1(dw1); gfp::cosa-1* =

33

abnormalities, consistent with the formation of nonproductive intermediates or inter-sister crossovers [59]. As with *zim-1* mutants, inactivation of BRC-1-BRD-1 in the *syp-1* mutant background led to fewer COSA-1 foci (Fig 8A; S5 Fig), suggesting that BRC-1-BRD-1 promotes COSA-1-associated recombination processing when chiasma formation is impaired.

To determine whether the extra COSA-1 foci on synapsed chromosomes could form chiasmata, we examined *zim-1* and *brc-1(tm1145); zim-1* diplotene/diakinesis nuclei, where chromosomes are individualized and cross-shaped structures indicative of crossovers between homologs can be observed. Consistent with the formation of extra chiasmata in the *zim-1* mutant background, we observed 52% of diplotene/diakinesis nuclei (n = 52) containing at least one ring-shaped structure, and six had two ring-shaped structures. The simplest interpretation is that there was a chiasma on each end of the chromosome pair (arrow; Fig 8B). This was reduced to 21% of diplotene/diakinesis nuclei (n = 43) containing ring-shaped chromosomes in the *brc-1(tm1145); zim-1* double mutant (*zim-1* vs. *brc-1(tm1145); zim-1*, p = 0.0028 Mann-Whitney). These results suggest that BRC-1-BRD-1 promotes chiasma formation when some chromosomes are unable to interact with their partner.

To examine genetic crossovers, we monitored linkage between SNP markers on chromosomes *V* and *X* in Bristol/Hawaiian hybrid strains to assess both crossover numbers and distribution. While inactivation of *brc-1* had no effect on crossover numbers on chromosome *V* (WT = 48.1cM; *brc-1* = 50.8cM), we observed an altered distribution compared to wild type (Fig 8D and 8E; S1 Table). In *C. elegans*, crossovers are enriched on the arms [28, 60–62]; in the *brc-1(tm1145)* mutant we observed a more even distribution, with more crossovers in the center and fewer on the right arm (Fig 8E; S1 Table). On the other hand, in *brc-1(tm1145)*, neither crossover frequency nor distribution were significantly different on the *X* chromosome (Fig 8D and 8E), which has an altered crossover landscape compared to the autosomes [63, 64].

We next monitored linkage between SNP markers in the *zim-1* and *brc-1(tm1145); zim-1* mutants. We observed a significant increase in the recombination map on chromosome *V* in *zim-1* (70.8cM), and multiple double crossovers were observed (Fig 8D; S1 Table). Extra crossovers were also observed on autosomes in worms unable to pair and synapse *X* chromosomes [50]. Inactivation of BRC-1 in the *zim-1* background resulted in significantly fewer double crossovers (DCOs) on chromosome *V* (p = 0.0242; Fig 8C, S1 Table), although the overall genetic map length was not significantly different compared to the *zim-1* single mutant (68.2cM; Fig 8D). This is most likely a consequence of an increase in the single crossover class (SCO; *zim-1* vs. *brc-1(tm1145); zim-1*, p = 0.0007; Fig 8C, S1 Table). On the *X* chromosome crossover frequency and distribution were altered in the center region in both *zim-1* and *brc-1 (tm1145); zim-1* and in the left interval in *zim-1*; however, the overall map lengths were not statistically different between any of the strains.

34

C. elegans exhibits strong interference, which is the phenomenon that a crossover at one position on a chromosome decreases the probability of formation of a crossover nearby, resulting in a single crossover per chromosome [62]. Given the detection of DCOs on chromosome *V* in the *zim-1* and *brc-1(tm1145); zim-1* mutants, we calculated the interference ratio. While wild type and *brc-1* had absolute intereference of 1, as no double crossovers were observed, the *zim-1* mutant displayed reduced interference in the left-center and left-right intervals and negative interference in the center-right interval (Table 1). Inactivation of BRC-1 in the *zim-1* mutant restored positive interference in the center-right interval; however, this fell short of statistical significant (p = 0.064). In addition to the non-randomness in the number and position of crossovers, interference also operates on the level of chromatids such that a crossover between any two non-sister chromatids can affect the probability of those chromatids being involved in other crossovers [65]. Chromatid interference has been shown to occur in fungi, Drosophila, maize and humans [65–70]. Since we assayed single products of meiosis, the SCO class includes single crossovers as well as recombinants that are the result of three- or four-strand double crossovers, while only two strand-events can be detected as DCOs. The elevated numbers of SCOs and reduction in two-strand DCOs on chromosome *V* in the *brc-1(tm1145); zim-1* mutant compared to the *zim-1* single mutant (Fig 8C), suggest that there may be more three- and/or four-strand double crossovers when BRC-1 is inactivated. Thus, BRC-1 may counteract chromatid interference under meiotic dysfunction, such that more two-strand double crossovers occur. Taken together, the reduced number of COSA-1 foci and alteration in the genetic map in the *brc-1(tm1145); zim-1* mutant suggest that BRC-1-BRD-1 modifies recombination patterning under meiotic dysfunction.

Discussion

Here we show that *C. elegans* BRC-1 and BRD-1 orthologs localize to the SC and regulate recombination when meiosis is perturbed. Our results suggest that BRC-1-BRD-1 plays an

Table 1. Crossover interference on chromosome *V*.

WT (V)	expected DCO	observed DCO	c.o.c.	interference
LC	0.011	0.00	0.00	1.00
CR	0.016	0.00	0.00	1.00
LR	0.042	0.00	0.00	1.00
brc-1 (V)	expected DCO	observed DCO	c.o.c.	interference
LC	0.036	0.00	0.00	1.00
CR	0.016	0.00	0.00	1.00
LR	0.028	0.00	0.00	1.00
zim-1(V)	expected DCO	observed DCO	c.o.c.	interference
LC	0.072	0.055	0.75	0.25
CR	0.049	0.087	1.79	-0.79
LR	0.042	0.018	0.43	0.57
brc-1;zim-1(V)	expected DCO	observed DCO	c.o.c.	interference
LC	0.039	0.026	0.67	0.33
CR	0.055	0.031	0.57	0.43
LR	0.058	0.031	0.54	0.46

LC = left-center interval; CR = center-right interval; LR = left-right interval. DCO: double crossover; expected DCO: (crossover frequency at interval "A") x (crossover frequency at interval "B"). c.o.c. (coefficient of coincidence) = actual DCO frequency/ expected DCO frequency; Interference = 1- c.o.c. See S1 Table for data used for calculations. Statistical analyses of interference using χ^2 on 2-by-2 contingency tables of observed and expected DCOs [119], indicated that interference in the CR interval fell short of statistical significance between *zim-1* and *brc-1(tm1145); zim-1*, p = 0.064.

35

important role in monitoring and modulating processing of meiotic DSBs into crossovers in the context of the specialized meiotic chromosome structure.

BRC-1-BRD-1 undergoes dynamic localization that is coupled to crossover recombination

In mouse spermatocytes BRCA1 is associated with RAD51 and enriched on asynapsed regions of meiotic chromosomes, including the X-Y sex body [18, 19]. Here we show that *C. elegans* BRC-1 and BRD-1 partially co-localize with RAD-51 in early meiotic prophase, but become enriched on synapsed chromosomes as meiosis progresses, co-localizing with SYP-1, a SC central region component (Fig 2B). The enrichment of mammalian BRCA1 on asynapsed chromosomes versus BRC-1 on synapsed chromosomes in *C. elegans* most likely reflects alteration in the relationship between meiotic recombination and SC formation in these organisms. Meiotic chromosomes can pair and synapse in the absence of meiotic recombination in *C. elegans* [32], while these events are interdependent in mammals [15, 16]. The HORMAD axial components also show differences in chromosome association in mice and worms: in mice, HORMAD1 and HORMAD2 are enriched on asynapsed chromosomes [71, 72], while *C. elegans* HORMADS, HIM-3, HTP-1/2, and HTP-3, remain associated with synapsed chromosomes [73–76]. However, the function of HORMADs in preventing inter-sister recombination and in checkpoint signaling appears to be similar in these different organisms [77–82]. Thus, the association of BRC-1-BRD-1 to the SC in *C. elegans* is likely a consequence of the inter-relationship between SC formation and meiotic recombination in this organism and not due to different functions for this complex in worm versus mammalian meiosis.

Another difference between *C. elegans* and mammals is the nature of the kinetochore. *C. elegans* chromosomes are holocentric while in many organisms, including yeast and mice, chromosomes are monocentric. Holocentricity dictates that a single off-centered crossover is formed on each homolog pair to define the long and short arms necessary to ensure regulated sister chromatid cohesion release at meiosis I and II [60–62, 83]. Interestingly, BRC-1-BRD-1 becomes restricted to the short arm of the bivalent, as defined by the crossover site, and this precedes SC reorganization. While the absence of BRC-1-BRD-1 alone does not affect crossover formation on chromosome *V* and the *X* chromosome, it does have a subtle effect on the distribution of crossovers along chromosome *V* such that more occur in the middle of the chromosome (Fig 8D and 8E). The change in crossover distribution in *brc-1* mutants may contribute to the slightly increased nondisjunction observed in the absence of the BRC-1-BRD-1 complex.

We show that the concentration of BRC-1-BRD-1 to a portion of each chromosome track in late pachytene is dependent on meiotic DSB formation and processing into crossovers (*spo-11*, *rad-51* and *msh-5*; Fig 4). Interestingly, in both *spo-11* and *msh-5* mutants there are occasional chromosomal tracks in late pachytene, which are highly enriched for BRC-1. While synapsis markers also show occasional enrichment to single tracks in the absence of *spo-11*, and these partially overlap with BRC-1 (S2B Fig), no enrichment of synapsis markers is observed when crossover factors (i.e., *msh-5*, *cosa-1 or zhp-3*) are removed [39–41]. While it has been proposed that *spo-11*-independent lesions can recruit meiotic DNA repair components [39–41], the enrichment of BRC-1 in the absence of such crossover factors suggests that BRC-1-BRD-1 can respond to other repair intermediates in addition to those leading to inter-homolog crossovers. One possibility is that when inter-homolog crossover formation is blocked, DSBs are repaired through site-specific nucleases [84–86], a subset of which leads to the concentration of BRC-1-BRD-1 on chromosomes in late pachytene. This is also consistent with the observation that BRC-1 is maintained on chromosomes in *spo-11*, *rad-51* and *msh-5*

36

mutants in diakinesis nuclei. Perhaps the failure to form interhomolog crossovers in these mutants leads to continued association of BRC-1-BRD-1 on chromosomes.

BRC-1 and BRD-1 associate and are mutually dependent for localization to meiotic chromosomes

BRCA1 forms a potent E3 ubiquitin ligase only in complex with its partner BARD1 [2, 3]. Biochemical and structural studies have defined the RING domains and associated helices of these proteins as critical for catalytic activity and BRCA1-BARD1 interaction [43]. However, while the BRCA1-BARD1 heterodimer exhibits substantially greater E3 ligase activity *in vitro* than BRCA1 alone, only the BRCA1 RING domain interacts with the E2 for ubiquitin transfer, suggesting that BRCA1 is the critical subunit for E3 ubiquitin ligase activity [3, 87]. Structure-function analysis of the BARD1 RING domain suggests that BARD1 may serve to attenuate BRCA1 E3 ligase activity [88]. Interestingly, while the localization of BRC-1 and BRD-1 were interdependent (Fig 3B), BRD-1 appeared to be excluded from the nucleus in the absence of BRC-1, while BRC-1 was nucleoplasmic and formed foci in late pachytene in the absence of BRD-1 (Fig 3B). These differences may reflect the nature of the alleles examined: *brc-1(xoe4)* produces no protein, while the two *brd-1* alleles are predicted to produce truncated proteins, where the RING domain and associated helices remain intact (Fig 5A). In humans, BRCA1 nuclear localization signals in the middle of the protein can directly mediate nuclear import, or import can occur indirectly through interaction with BARD1 [89]. Thus, the truncated BRD-1 protein produced from the *brd-1(ok1623)* allele could associate with BRC-1 and facilitate nuclear localization of the albeit nonfunctional complex. Alternatively, *C. elegans* BRC-1 may be uniquely required for nuclear localization or retention, and in its absence BRD-1 cannot enter or be retained in the nucleus. The weak nucleoplasmic BRD-1 signal observed at the end of meiotic prophase in the absence of BRC-1 most likely reflects differences in the nuclear membrane as oogenesis proceeds [90, 91].

In addition to the N-terminal RING domains, both BRC-1 and BRD-1 contain long linker and phosphoprotein binding BRCA1 C-terminal (BRCT) domains. BRCT domains are phosphorylation-dependent interacting modules that have been implicated in tumor suppressor activity [92]. Interestingly, only BRD-1 contains Ankyrin (ANK) repeat interaction domains. Recent structural and functional analyses of the ANK domain in TONSL-MMS22L, a complex involved in homologous recombination, revealed that the ANK domain interacts with histone H4 tails [93]. The BARD1 ANK domains have a very similar fold [93], suggesting that BARD1 ANK domains may be important for association with chromatin. The predicted truncated proteins produced in the *brd-1* mutants, which behave as nulls (Fig 5 and S4 Fig), lack at least part of the BRCT domains and all of the ANK domains, suggesting that some combination of these domains are critical for BRD-1 function with respect to both DNA damage signaling and meiosis.

BRC-1-BRD-1 function in meiotic recombination can be genetically separated from its established role in the DDR

It has long been appreciated that BRCA1-BARD1 mediates its tumor suppressor activity at least in part through regulating homologous recombination [6]. Given the importance of homologous recombination in repairing DSBs during meiosis, it is not surprising that removing BRC-1-BRD-1 impinges on meiotic recombination. Unexpectedly, we identified a small region C-terminal to the BRC-1 RING and associated helices as being important specifically for meiosis, suggesting that the function of BRC-1-BRD-1 in DNA damage response and meiosis are distinct. While containing no specific fold or homology, this region has several potential

37

phosphorylation sites based on prediction algorithms that may mediate its interaction with key meiotic proteins.

BRCA1-BARD1 associates with the recombinase RAD51 in both mammals and *C. elegans* [19, 31, 94]. BRCA1 has also been shown to be required for the assembly of DNA damage induced RAD51 foci on chromatin [95], and this has been interpreted as a requirement for BRCA1 in RAD51 filament assembly. However, recent biochemical analyses using purified proteins found that BRCA1 is not required for RAD51 assembly on RPA coated single stranded DNA and instead promotes DNA strand invasion [94]. Further, a BARD1 mutant that cannot interact with RAD51 does not promote DNA strand invasion, and also does not form foci *in vivo*. Thus, it is likely that BRCA1-BARD1 is not required for RAD51 filament assembly *per se*. Our IR time course analysis of *C. elegans brc-1 brd-1* mutants is consistent with a function for this complex in stabilizing the RAD-51 filament. It is possible that similar to the mammalian complex, BRC-1-BRD-1 promotes RAD-51 strand invasion; however, *in vivo* the RAD-51 filament may be subject to disassembly by other proteins in the absence of BRC-1-BRD-1, which would not be recapitulated *in vitro*. One such protein is the FANCJ/ DOG-1 helicase, which interacts with BRCA1 [96], and can disassemble RAD51 on ssDNA *in vitro* [97]. It is also likely that BRCA1-BARD1 plays multiple roles during homologous recombination and interacts with, and coordinates the activity, of many proteins, including RAD51, and these interactions are modulated under different conditions, including DNA damage, meiosis, meiotic dysfunction, as well as at different stages of the cell cycle. Consistent with this, Janisiw et al. found that BRC-1 associates with the pro-crossover factor MSH-5.

BRCA1-BARD1 and meiotic checkpoint signaling

brc-1 and *brd-1* mutants have very subtle defects in meiosis. These include low levels of X chromosome nondisjunction [10] (Fig 5C), a delay in repair of a subset of DSBs through the intersister pathway [9], and elevated heterologous recombination [12]. However, removing BRC-1-BRD-1 when meiosis is perturbed in mutants that impair chromosome pairing, synapsis and crossover recombination leads to enhanced meiotic dysfunction, including elevated embryonic lethality (Fig 5E), impaired RAD-51 stability (Fig 7), and alteration of COSA-1 numbers and the crossover landscape (Fig 8). These results suggest that BRC-1-BRD-1 plays a critical role in meiotic recombination when meiosis is impaired.

In both *C. elegans* and *Drosophila melanogaster*, preventing crossover formation on a subset of chromosomes leads to additional events on other chromosomes, and is referred to as the interchromosomal effect [50, 98–101]. There is also evidence in humans that Robertsonian translocations elicit the interchromosomal effect [102]. Our analyses of the *zim-1* mutant, where chromosomes *II* and *III* fail to recombine, revealed elevated COSA-1 foci genome wide and an increase in genetic crossovers on chromosome *V* (but not the *X* chromosome, Fig 8), consistent with the interchromosomal effect. Further, our data suggest that when meiosis is impaired as in *syp-1*, and perhaps *zim-1* mutants, COSA-1 can mark events that do not ultimately become interhomolog crossovers (see also [59]). Interestingly, removal of BRC-1-BRD-1 in *zim-1* and *syp-1* mutants decreased the number of COSA-1 foci. On the other hand, in the *brc-1(tm1145); zim-1* mutant we detected elevated levels of single crossovers but reduced levels of two-strand double crossovers on chromosome *V* compared to the *zim-1* single mutant, with no change in the overall map length (Fig 8D). One possibility to explain the observed COSA-1 and crossover pattern is that COSA-1 does not become enriched on a subset of crossovers in *brc-1; zim-1* mutants even though these events are dependent on the canonical meiotic crossover pathway, as observed in the *rtel-1* and *dyp-28* mutants [30, 103–105]. Alternatively, the extra crossovers that are not marked by COSA-1 in the absence of BRC-1-BRD-1 may be the

38

result of activation of alternative crossover formation pathways. In either scenario, BRC-1, and presumably BRD-1, appear to dictate the patterning of crossovers among non-sister chromatids. As interference is mediated by meiotic chromosome structure [106], perhaps SC-associated BRC-1-BRD-1 counteracts chromatid interference in the context of meiotic dysfunction.

In conclusion, our results suggest that BRC-BRD-1 serves a critical role in monitoring the progression of meiotic recombination in the context of the SC when meiosis cannot proceed normally, suggesting that BRC-1-BRD-1 serves a checkpoint function. When cross-over formation is blocked, BRC-1-BRD-1 stabilizes the RAD-51 filament and promotes processing of recombination intermediates marked by COSA-1. In this context, BRC-1-BRD-1 joins a growing list of proteins that monitor meiotic recombination to promote accurate chromosome segregation, including protein kinases and ubiquitin/SUMO E3 ligases [39, 56, 57, 107–110]. Future work will examine the relationship between BRC-1-BRD-1 and other meiotic checkpoint pathways and identify substrates of BRC-1-BRD-1-ubiquitination to understand how this complex modulates recombination under conditions when meiosis is perturbed.

Materials and methods

Generation of *gfp::brc-1*, *tag-rfp-T::brc-1*, *brd-1::gfp* and *brc-1(xoe4)*

Fluorescent protein knock-ins were generated using CRISPR-mediated homology dependent repair with self-excising cassette containing hygromycin resistant as selection [20]. The *brc-1 (xoe4)* deletion allele was generated using Cas9-snRNPs and an single strand oligonucleotide repair template [111]. Cas9 protein was purchased from Innovative Genomics Institute, UC Berkeley. For a list of sgRNAs and repair templates refer to S2 Table. All CRISPR-generated lines were back crossed a minimum of three times, with the exception of JEL744 *brc-1(xoe4) brd-1::gfp*, which was only back crossed once.

Genetics

C. elegans var. Bristol (N2), was used as the wild-type strain. Other strains used in this study are listed in S3 Table. Some nematode strains were provided by the Caenorhabditis Genetics Center, which is funded by the National Institutes of Health National Center for Research Resources. Strains were maintained at 20˚C.

Embryonic lethality and production of male progeny

Embryonic lethality in the absence or presence of 5mM hydroxyurea (HU) (16 hrs), or 75 Grays (Gy) of γ-irradiation (IR) from a ^{137}Cs source, was determined over 3 days by counting eggs and hatched larvae 24 hr after removing the hermaphrodite and calculating percent as eggs/ (eggs + larvae); male progeny was assessed 48 hr after removing the hermaphrodite. A minimum of 10 worms were scored for each condition.

Apoptosis assay

Acridine orange (AO) staining of apoptotic germ cells in WT (N2), *brc-1* and *brd-1* alleles as well as *zim-1* and corresponding double and triple mutants were performed as in [48]. Briefly, 0.5 ml of 50 mg/ml AO (Molecular Probes, Invitrogen; Carlsbad, CA) in M9 was added to 60-mm plates containing 48 hr post L4 worms and incubated at room temperature for 1 hr. Worms were transferred to new 60-mm plates, allowed to recover 15 min, and then mounted

39

under coverslips in M9 on 3% agarose pads containing 1 mM tetramisole (Sigma-Aldrich; St. Louis). Apoptotic bodies were scored by fluorescence microscopy and DIC.

Cytological analysis

Gonads were dissected and fixed with 1% paraformaldehyde in egg buffer plus 0.01% Tween20 for 5 min, freeze-cracked and post-fixed in either ice-cold 100% methanol for indirect immunofluorescence, or ice-cold 100% ethanol for direct fluorescence (GFP::BRC-1, TagRFP-T:: BRC-1, BRD-1::GFP, GFP::RPA-1, GFP::COSA-1) for 1 min [112]. For staining with antibodies against phospho-SYP-4, gonads were dissected, freeze-cracked, incubated in 100% methanol for 1 min and post-fixed in 4% paraformaldehyde in PBS, 80mM HEPES(pH7.4), 0.8mM EDTA, 1.6mM MgS0$_4$ for 30 min [40]. The following primary antibodies were used at the indicated dilutions: rabbit anti-RAD-51 (1:10,000; Catalog #29480002; Novus Biologicals, Littleton, CO), rabbit anti-GFP (1:500; NB600-308; Novus Biologicals, Littleton, CO), goat anti-SYP-1 (1:200; generously provided by Anne Villeneuve); rabbit anti-phospho-SYP-4 (1:100; [40]), and guinea pig anti-SUN-1 S12P (1:1,000; generously provided by Verena Jantsch). Secondary antibodies Alexa Fluor 594 donkey anti-rabbit IgG, Alexa Fluor 555 donkey anti-goat IgG, Alexa Fluor 488 donkey anti-rabbit IgG, Alexa Fluor 488 goat anti-guinea pig IgG from Life Technologies were used at 1:500 dilutions. DAPI (2μg/ml; Sigma-Aldrich) was used to counterstain DNA.

Collection of fixed images was performed using an API Delta Vision deconvolution microscope, a Nikon TiE inverted microscope stand equipped with an 60x, NA 1.49 objective lens and Andor Clara interline camera, or were captured on a spinning-disk module of an inverted objective fluorescence microscope [Marianas spinning-disk confocal (SDC) real-time 3D Confocal-TIRF (total internal reflection) microscope; Intelligent Imaging Innovations] equipped with an 63x, NA 1.46 objective lens using a Photometrics QuantiEM electron multiplying charge-coupled device (EMCCD) camera. Z stacks (0.2 μm) were collected from the entire gonad. A minimum of three germ lines was examined for each condition. Images were deconvolved using Applied Precision SoftWoRx or Nikon NIS Elements Offline batch deconvolution software employing either "Automatic3D" or "Richardson-Lucy" deconvolution modes and subsequently processed and analyzed using Fiji (ImageJ) (Wayne Rasband, NIH).

RAD-51 foci were quantified in a minimum of three germ lines of age-matched hermaphrodites (18–24 hr post-L4). As *zim-1* mutants have an extended transition zone [42], we divided germ lines into four equal zones from the beginning of the transition zone (leptotene/zygotene), as counted from the first row with three or more crescent-shaped nuclei, through diplotene (Fig 6B). The number of foci per nucleus was scored for each region.

To assess formation of RAD-51 foci following IR treatment, 18–24 hrs post-L4 worms were exposed to 10 Gy of IR; gonads were dissected 1, 4, 8, and 12 hr following IR treatment and fixed for immunofluorescence as above.

GFP::COSA-1 foci were quantified from deconvolved 3D data stacks; nuclei were scored individually through z-stacks to ensure that all foci within each individual nucleus were counted. Nuclei with features indicative of apoptosis (compact and DAPI-bright) were excluded. Foci were counted in the last five rows of pachytene nuclei as in [30].

For live cell imaging, 18–24 hr post L4 hermaphrodites were anesthetized in 1mM tetramisole and immobilized between a coverslip and an 2% agarose pad on a glass slide. Z-stacks (0.33 μm) were captured on a spinning-disk module of an inverted objective fluorescence microscope (NIH 1S10RR024543) with a 100×, NA 1.46 objective, and EMCCD camera. Z-projections of stacks were generated, cropped, and adjusted for brightness in Fiji.

40

Pearson's Correlation Coefficient (PCC) was determined by drawing a Region of Interest (ROI) around a nucleus and using the co-localization function in Fiji.

Immunoblot analysis

Whole worm lysates were generated from indicated worms; unmated *fog-2(q71)* worms were used to eliminate embryos. ~100 worms were collected, washed in M9 buffer and resuspended in equal volume of 2X Laemmli sample buffer (Bio-RAD). Lysates were resolved on 4–15% SDS-PAGE gradient gels (Bio-RAD) and transferred to Millipore Immobilon-P PVDF membranes. Membranes were blocked with 5% nonfat milk and probed with rabbit anti-GFP (1:1000; NB600-308; Novus Biologicals, Littleton, CO) and mouse anti-α-tubulin (1:1000; Sigma-Aldrich; T9026) as loading control, followed by IRDye680LT- and IRDye800-conjugated anti-rabbit and anti-mouse IgG secondary antibodies (1:20000; LI-COR Bioscience Lincoln, NE). Immunoblots were imaged on a LI-COR Odyssey Infrared Imager, signal was quantified using Fiji and normalized with the α-tubulin signal.

RNA-mediated interference analysis

RNA-mediated interference (RNAi) was performed at 20˚C, using the feeding method [113]. Cultures were plated onto NGM plates containing 25 μg/ml carbenicillin and 1 mM IPTG and were used within 2 weeks. L4 worms were transferred to RNAi plates, and resulting progeny were exposed to IR as described above. The efficiency of RNAi was tested in parallel by examining embryonic lethality.

Meiotic mapping

Meiotic crossover frequencies and distribution were assayed utilizing single-nucleotide polymorphism (SNP) markers as in [114]. The SNP markers located at the boundaries of the chromosome domains were chosen based on data from WormBase (WS231) and [64], and are indicated in Fig 8D. The SNP markers and primers used are listed in [86]. PCR and restriction digests of single embryo lysates were performed and confirmed with additional SNPs as described in [115, 116] (Fig 8D). Statistical analyses were performed using the two-tailed Fisher's Exact test, 95% C.I., as in [117, 118]. For statistical analyses of interference we conducted χ^2 tests on 2-by-2 contingency tables of observed and expected DCOs [119].

Supporting information

S1 Table. Genetic mapping data.
(XLSX)

S2 Table. Reagents used for generating CRISPR/Cas9 edited worms.
(DOCX)

S3 Table. Strains used in this study.
(DOCX)

S1 Fig. GFP::BRC-1, TagRFP-T::BRC-1 and BRD-1::GFP are functional and expressed predominantly in the germ line. A) % embryonic lethality; B) % male progeny; C) % embryonic lethality following 75 Gy IR; D) % embryonic lethality following treatment with 5mM HU for 16 hrs of indicated strains. 95% Confidence Intervals shown; * p<0.05; ** p<0.001; *** p<0.0001. *gfp::brc-1*, *tag-rfp-t::brc-1* and *brd-1::gfp* are not statistically different compared to WT. A minimum of 10 worms were analyzed for each condition. E) Immunoblot of whole worm extracts from WT, *gfp::brc-1* and *gfp::brc-1; fog-2* probed with rabbit anti-GFP and

41

mouse anti-α-tubulin. Ratio determined by fluorescent intensities from three independent experiments.
(TIF)

S2 Fig. In the absence of SPO-11, GFP::BRC-1 and BRD-1::GFP are enriched on a subset of chromosomes. A) Number of GFP::BRC-1 foci in indicated mutants in Proliferative Zone, Transition Zone and Early Pachytene. Number of foci examined in a minimum of 3 germ lines: PZ: WT (n = 412); *spo-11* (n = 177); *rad-51*(n = 114); *msh-5* (n = 175); *syp-1* (n = 140); *zim-1* (n = 142); TZ: WT (n = 287); *spo-11* (n = 103); *rad-51*(n = 52); *msh-5* (n = 94); *syp-1* (n = 83); *zim-1* (n = 112); EP: WT (n = 202); *spo-11* (n = 106); *rad-51*(n = 57); *msh-5* (n = 57); *syp-1* and *zim-1* had too many foci to accurately count. *** p<0.0001. B) Late pachytene region of the germ line stained with anti-GFP (green) and anti-phosphoSYP-4 (SYP-4P) (red) and counterstained with DAPI. Scale bar = 10 μm. C) High-magnification images of live *C. elegans* expressing BRD-1::GFP in the *spo-11* background. Images are projections through half of the gonad. PZ = Proliferative Zone, TZ = Transition Zone, EP = Early Pachytene, MP = Mid Pachytene, LP = Late Pachytene, DP = Diplotene, DK = Diakinesis. Scale bar = 5 μm.
(TIF)

S3 Fig. *brc-1* and *brd-1* mutant alleles and meiotic progression. A) Genomic regions of *brc-1* and *brd-1* from WormBase Version: WS265 (https://wormbase.org/#012-34-5), with the region deleted in the different alleles indicated. Color dotted lines indicate the resulting splicing of *brd-1(ok1623)* (pink; splicing of exon 7–12, which introduces a stop codon and results in a 343 a. a. protein) and *brd-1(dw1)* (orange; cryptic splice site within intron 11 spliced to exon 12, resulting in a 375 a. a. protein) as determined by cDNA analysis. B) High-magnification images of live *brc-1(tm1145)* worms expressing BRD-1::GFP (PZ = Proliferative Zone, TZ = Transition Zone, EP = Early Pachytene, MP = Mid Pachytene, LP = Late Pachytene, DP = Diplotene, DK = Diakinesis). Scale bar = 5 μm. C) Indicated germ lines stained with antibodies against SUN-1 S12P (green) and counterstained with DAPI (blue). Numbers beneath genotype indicate the percentage of cell rows with SUN-1 S12P staining normalized to gonad length as in [49]; 3 germ lines were examined. Images are projections through half of the gonad. Scale bar = 20 μm.
(TIF)

S4 Fig. Inactivation of *brc-1* or *brd-1* alters pattern of RAD-51 foci in mid-late pachytene in chromosome synapsis mutants. A) Box whisker plots show average number of RAD-51 foci per nucleus in the different zones of meiotic prophase (see Fig 6B). Horizontal line of each box indicates the median, the top and bottom of the box indicates medians of upper and lower quartiles, lines extending above and below boxes indicate standard deviation and individual data points are outliers from 5–95%. Numbers of nuclei scored in each zone for WT: 1 = 186; 2 = 343; 3 = 292; 4 = 166; *brc-1(tm1145) brd-1(dw1)*: 1 = 233; 2 = 303; 3 = 261; 4 = 68; *brd-1 (ok1623)*: 1 = 186; 2 = 135; 3 = 162; 4 = 117. * p<0.05; ** p<0.001; *** p<0.0001. B) Dissected germ lines from *brd-1(ok1623); zim-1, brc-1(tm1145) brd-1(dw1); syp-1, syp-1, brd-1(dw1); zim-1, brc-1(tm1145) brd-1(dw1); zim-1*, and *brc-1(xoe4); zim-1* worms stained with anti-RAD-51 (red) and counterstained with DAPI (blue); white bracket indicates region of reduced RAD-51 foci. A minimum of 4 germ lines were imaged for each genotype. Full projections of the gonads are shown. Scale bar = 20 μm. C) Mid-late pachytene region of gonad from *gfp:: rpa-1* and *brc-1(tm1145) brd-1(dw1); gfp::rpa-1* worms stained with anti-RAD-51 (red) and imaged for GFP::RPA-1 fluorescence (green), counterstained with DAPI (blue). Images are projections through half of the gonad. Scale bar = 8 μm.
(TIF)

42

S5 Fig. COSA-1 foci in synapsis mutants in the presence and absence of BRC-1. Late pachytene region of the germ line in indicated mutants expressing GFP::COSA-1 (green) and counterstained with DAPI (blue). Images are projections through half of the gonad. Scale bar = 5 μm.
(TIF)

Acknowledgments

Author Contributions

Conceptualization: Katherine S. Lawrence, Paula M. Checchi, JoAnne Engebrecht.

Funding acquisition: Monica P. Colaiacovo, JoAnne Engebrecht.

Investigation: Qianyan Li, Takamune T. Saito, Marina Martinez-Garcia, Alison J. Deshong, Saravanapriah Nadarajan, Katherine S. Lawrence, Paula M. Checchi, JoAnne Engebrecht.

Methodology: Qianyan Li, Takamune T. Saito, JoAnne Engebrecht.

Resources: Saravanapriah Nadarajan.

Supervision: Monica P. Colaiacovo, JoAnne Engebrecht.

Visualization: Qianyan Li, Takamune T. Saito, Alison J. Deshong, JoAnne Engebrecht.

Writing – original draft: JoAnne Engebrecht.

Writing – review & editing: Qianyan Li, Takamune T. Saito, Marina Martinez-Garcia, Alison J. Deshong, Saravanapriah Nadarajan, Katherine S. Lawrence, Paula M. Checchi, Monica P. Colaiacovo, JoAnne Engebrecht.

References

1. Hall JM, Lee MK, Newman B, Morrow JE, Anderson LA, Huey B, et al. Linkage of early-onset familial breast cancer to chromosome 17q21. Science. 1990; 250(4988):1684–9. PMID: 2270482.

2. Wu LC, Wang ZW, Tsan JT, Spillman MA, Phung A, Xu XL, et al. Identification of a RING protein that can interact in vivo with the BRCA1 gene product. Nat Genet. 1996; 14(4):430–40. https://doi.org/10.1038/ng1296-430 PMID: 8944023.

3. Hashizume R, Fukuda M, Maeda I, Nishikawa H, Oyake D, Yabuki Y, et al. The RING heterodimer BRCA1-BARD1 is a ubiquitin ligase inactivated by a breast cancer-derived mutation. J Biol Chem. 2001; 276(18):14537–40. https://doi.org/10.1074/jbc.C000881200 PMID: 11278247.

4. Kais Z, Parvin JD. Regulation of centrosomes by the BRCA1-dependent ubiquitin ligase. Cancer Biol Ther. 2008; 7(10):1540–3. PMID: 18927495; PubMed Central PMCID: PMCPMC2628548.

5. Savage KI, Harkin DP. BRCA1, a 'complex' protein involved in the maintenance of genomic stability. FEBS J. 2015; 282(4):630–46. https://doi.org/10.1111/febs.13150 PMID: 25400280.

6. Li ML, Greenberg RA. Links between genome integrity and BRCA1 tumor suppression. Trends Biochem Sci. 2012; 37(10):418–24. https://doi.org/10.1016/j.tibs.2012.06.007 PMID: 22836122; PubMed Central PMCID: PMCPMC3459146.

43

7. Ludwig T, Chapman DL, Papaioannou VE, Efstratiadis A. Targeted mutations of breast cancer susceptibility gene homologs in mice: lethal phenotypes of Brca1, Brca2, Brca1/Brca2, Brca1/p53, and Brca2/p53 nullizygous embryos. Genes Dev. 1997; 11(10):1226–41. PMID: 9171368.

8. McCarthy EE, Celebi JT, Baer R, Ludwig T. Loss of Bard1, the heterodimeric partner of the Brca1 tumor suppressor, results in early embryonic lethality and chromosomal instability. Mol Cell Biol. 2003; 23(14):5056–63. https://doi.org/10.1128/MCB.23.14.5056-5063.2003 PMID: 12832489; PubMed Central PMCID: PMCPMC162231.

9. Adamo A, Montemauri P, Silva N, Ward JD, Boulton SJ, La Volpe A. BRC-1 acts in the inter-sister pathway of meiotic double-strand break repair. EMBO Rep. 2008; 9(3):287–92. https://doi.org/10.1038/sj.embor.7401167 PMID: 18219312; PubMed Central PMCID: PMCPMC2267377.

10. Boulton SJ, Martin JS, Polanowska J, Hill DE, Gartner A, Vidal M. BRCA1/BARD1 orthologs required for DNA repair in Caenorhabditis elegans. Curr Biol. 2004; 14(1):33–9. PMID: 14711411.

11. Hong Y, Sonneville R, Agostinho A, Meier B, Wang B, Blow JJ, et al. The SMC-5/6 complex and the HIM-6 (BLM) helicase synergistically promote meiotic recombination intermediate processing and chromosome maturation during Caenorhabditis elegans meiosis. PLoS Genet. 2016; 12(3):e1005872. https://doi.org/10.1371/journal.pgen.1005872 PMID: 27010650; PubMed Central PMCID: PMCPMC4807058.

12. Leon-Ortiz AM, Panier S, Sarek G, Vannier JB, Patel H, Campbell PJ, et al. A Distinct class of genome rearrangements driven by heterologous recombination. Mol Cell. 2018; 69(2):292–305 e6. Epub 2018/01/21. https://doi.org/10.1016/j.molcel.2017.12.014 PMID: 29351848.

13. Pontier DB, Tijsterman M. A robust network of double-strand break repair pathways governs genome integrity during C. elegans development. Curr Biol. 2009; 19(16):1384–8. Epub 2009/08/04. https://doi.org/10.1016/j.cub.2009.06.045 PMID: 19646877.

14. Wolters S, Ermolaeva MA, Bickel JS, Fingerhut JM, Khanikar J, Chan RC, et al. Loss of Caenorhabditis elegans BRCA1 promotes genome stability during replication in smc-5 mutants. Genetics. 2014; 196(4):985–99. https://doi.org/10.1534/genetics.113.158295 PMID: 24424777; PubMed Central PMCID: PMCPMC3982690.

15. Cahoon CK, Hawley RS. Regulating the construction and demolition of the synaptonemal complex. Nat Struct Mol Biol. 2016; 23(5):369–77. Epub 2016/05/05. https://doi.org/10.1038/nsmb.3208 PMID: 27142324.

16. Zickler D, Kleckner N. A few of our favorite things: Pairing, the bouquet, crossover interference and evolution of meiosis. Semin Cell Dev Biol. 2016; 54:135–48. Epub 2016/03/02. https://doi.org/10.1016/j.semcdb.2016.02.024 PMID: 26927691; PubMed Central PMCID: PMCPMC4867269.

17. Broering TJ, Alavattam KG, Sadreyev RI, Ichijima Y, Kato Y, Hasegawa K, et al. BRCA1 establishes DNA damage signaling and pericentric heterochromatin of the X chromosome in male meiosis. J Cell Biol. 2014; 205(5):663–75. https://doi.org/10.1083/jcb.201311050 PMID: 24914237; PubMed Central PMCID: PMCPMC4050732.

18. Turner JM, Aprelikova O, Xu X, Wang R, Kim S, Chandramouli GV, et al. BRCA1, histone H2AX phosphorylation, and male meiotic sex chromosome inactivation. Curr Biol. 2004; 14(23):2135–42. https://doi.org/10.1016/j.cub.2004.11.032 PMID: 15589157.

19. Scully R, Chen J, Plug A, Xiao Y, Weaver D, Feunteun J, et al. Association of BRCA1 with Rad51 in mitotic and meiotic cells. Cell. 1997; 88(2):265–75. PMID: 9008167.

20. Dickinson DJ, Pani AM, Heppert JK, Higgins CD, Goldstein B. Streamlined genome engineering with a self-excising drug selection cassette. Genetics. 2015; 200(4):1035–49. https://doi.org/10.1534/genetics.115.178335 PMID: 26044593; PubMed Central PMCID: PMCPMC4574250.

21. Schedl T, Kimble J. fog-2, a germ-line-specific sex determination gene required for hermaphrodite spermatogenesis in Caenorhabditis elegans. Genetics. 1988; 119(1):43–61. PMID: 3396865; PubMed Central PMCID: PMCPMC1203344.

22. Hillers KJ, Jantsch V, Martinez-Perez E, Yanowitz JL. Meiosis. WormBook. 2015:1–54. https://doi.org/10.1895/wormbook.1.178.1 PMID: 26694509; PubMed Central PMCID: PMCPMC5215044.

23. Petermann E, Orta ML, Issaeva N, Schultz N, Helleday T. Hydroxyurea-stalled replication forks become progressively inactivated and require two different RAD51-mediated pathways for restart and repair. Mol Cell. 2010; 37(4):492–502. https://doi.org/10.1016/j.molcel.2010.01.021 PMID: 20188668; PubMed Central PMCID: PMCPMC2958316.

24. Pathania S, Nguyen J, Hill SJ, Scully R, Adelmant GO, Marto JA, et al. BRCA1 is required for postreplication repair after UV-induced DNA damage. Mol Cell. 2011; 44(2):235–51. https://doi.org/10.1016/j.molcel.2011.09.002 PMID: 21963239; PubMed Central PMCID: PMCPMC3200447.

25. MacQueen AJ, Villeneuve AM. Nuclear reorganization and homologous chromosome pairing during meiotic prophase require C. elegans chk-2. Genes Dev. 2001; 15(13):1674–87. https://doi.org/10.1101/gad.902601 PMID: 11445542; PubMed Central PMCID: PMCPMC312723.

44

26. Colaiacovo MP, MacQueen AJ, Martinez-Perez E, McDonald K, Adamo A, La Volpe A, et al. Synaptonemal complex assembly in *C. elegans* is dispensable for loading strand-exchange proteins but critical for proper completion of recombination. Dev Cell. 2003; 5(3):463–74. PMID: 12967565.

27. MacQueen AJ, Colaiacovo MP, McDonald K, Villeneuve AM. Synapsis-dependent and -independent mechanisms stabilize homolog pairing during meiotic prophase in *C. elegans*. Genes Dev. 2002; 16 (18):2428–42. https://doi.org/10.1101/gad.1011602 PMID: 12231631; PubMed Central PMCID: PMCPMC187442.

28. Nabeshima K, Villeneuve AM, Colaiacovo MP. Crossing over is coupled to late meiotic prophase bivalent differentiation through asymmetric disassembly of the SC. J Cell Biol. 2005; 168(5):683–9. Epub 2005/03/02. https://doi.org/10.1083/jcb.200410144 PMID: 15738262; PubMed Central PMCID: PMCPMC2171829.

29. Liu R, Liang QN, Du SQ, Hu XJ, Ding Y. The crystal structure of red fluorescent protein TagRFP-T reveals the mechanism of its superior photostability. Biochem Biophys Res Commun. 2016; 477 (2):229–34. https://doi.org/10.1016/j.bbrc.2016.06.047 PMID: 27297107.

30. Yokoo R, Zawadzki KA, Nabeshima K, Drake M, Arur S, Villeneuve AM. COSA-1 reveals robust homeostasis and separable licensing and reinforcement steps governing meiotic crossovers. Cell. 2012; 149(1):75–87. https://doi.org/10.1016/j.cell.2012.01.052 PMID: 22464324; PubMed Central PMCID: PMCPMC3339199.

31. Polanowska J, Martin JS, Garcia-Muse T, Petalcorin MI, Boulton SJ. A conserved pathway to activate BRCA1-dependent ubiquitylation at DNA damage sites. EMBO J. 2006; 25(10):2178–88. https://doi.org/10.1038/sj.emboj.7601102 PMID: 16628214; PubMed Central PMCID: PMCPMC1462971.

32. Dernburg AF, McDonald K, Moulder G, Barstead R, Dresser M, Villeneuve AM. Meiotic recombination in *C. elegans* initiates by a conserved mechanism and is dispensable for homologous chromosome synapsis. Cell. 1998; 94(3):387–98. PMID: 9708740.

33. Keeney S, Giroux CN, Kleckner N. Meiosis-specific DNA double-strand breaks are catalyzed by Spo11, a member of a widely conserved protein family. Cell. 1997; 88(3):375–84. PMID: 9039264.

34. Alpi A, Pasierbek P, Gartner A, Loidl J. Genetic and cytological characterization of the recombination protein RAD-51 in *Caenorhabditis elegans*. Chromosoma. 2003; 112(1):6–16. https://doi.org/10.1007/s00412-003-0237-5 PMID: 12684824.

35. Rinaldo C, Bazzicalupo P, Ederle S, Hilliard M, La Volpe A. Roles for *Caenorhabditis elegans rad-51* in meiosis and in resistance to ionizing radiation during development. Genetics. 2002; 160(2):471–9. PMID: 11861554; PubMed Central PMCID: PMCPMC1461995.

36. Shinohara A, Ogawa H, Ogawa T. Rad51 protein involved in repair and recombination in *S. cerevisiae* is a RecA-like protein. Cell. 1992; 69(3):457–70. PMID: 1581961.

37. Hollingsworth NM, Ponte L, Halsey C. MSH5, a novel MutS homolog, facilitates meiotic reciprocal recombination between homologs in *Saccharomyces cerevisiae* but not mismatch repair. Genes Dev. 1995; 9(14):1728–39. PMID: 7622037.

38. Kelly KO, Dernburg AF, Stanfield GM, Villeneuve AM. *Caenorhabditis elegans msh-5* is required for both normal and radiation-induced meiotic crossing over but not for completion of meiosis. Genetics. 2000; 156(2):617–30. PMID: 11014811; PubMed Central PMCID: PMCPMC1461284.

39. Machovina TS, Mainpal R, Daryabeigi A, McGovern O, Paouneskou D, Labella S, et al. A surveillance system ensures crossover formation in *C. elegans*. Curr Biol. 2016; 26(21):2873–84. Epub 2016/10/11. https://doi.org/10.1016/j.cub.2016.09.007 PMID: 27720619; PubMed Central PMCID: PMCPMC5104180.

40. Nadarajan S, Lambert TJ, Altendorfer E, Gao J, Blower MD, Waters JC, et al. Polo-like kinase-dependent phosphorylation of the synaptonemal complex protein SYP-4 regulates double-strand break formation through a negative feedback loop. Elife. 2017; 6. https://doi.org/10.7554/eLife.23437 PMID: 28346135; PubMed Central PMCID: PMCPMC5423773.

41. Pattabiraman D, Roelens B, Woglar A, Villeneuve AM. Meiotic recombination modulates the structure and dynamics of the synaptonemal complex during *C. elegans* meiosis. PLoS Genet. 2017; 13(3): e1006670. https://doi.org/10.1371/journal.pgen.1006670 PMID: 28339470; PubMed Central PMCID: PMCPMC5384771.

42. Phillips CM, Dernburg AF. A family of zinc-finger proteins is required for chromosome-specific pairing and synapsis during meiosis in *C. elegans*. Dev Cell. 2006; 11(6):817–29. https://doi.org/10.1016/j.devcel.2006.09.020 PMID: 17141157.

43. Brzovic PS, Rajagopal P, Hoyt DW, King MC, Klevit RE. Structure of a BRCA1-BARD1 heterodimeric RING-RING complex. Nat Struct Biol. 2001; 8(10):833–7. https://doi.org/10.1038/nsb1001-833 PMID: 11573085.

45

44. Lorick KL, Jensen JP, Fang S, Ong AM, Hatakeyama S, Weissman AM. RING fingers mediate ubiquitin-conjugating enzyme (E2)-dependent ubiquitination. Proc Natl Acad Sci U S A. 1999; 96 (20):11364–9. PMID: 10500182; PubMed Central PMCID: PMCPMC18039.

45. Bhalla N, Dernburg AF. A conserved checkpoint monitors meiotic chromosome synapsis in *Caenorhabditis elegans*. Science. 2005; 310(5754):1683–6. https://doi.org/10.1126/science.1117468 PMID: 16339446.

46. Gartner A, Milstein S, Ahmed S, Hodgkin J, Hengartner MO. A conserved checkpoint pathway mediates DNA damage—induced apoptosis and cell cycle arrest in *C. elegans*. Mol Cell. 2000; 5(3):435–43. Epub 2000/07/06. PMID: 10882129.

47. Gumienny TL, Lambie E, Hartwieg E, Horvitz HR, Hengartner MO. Genetic control of programmed cell death in the *Caenorhabditis elegans* hermaphrodite germline. Development. 1999; 126(5):1011–22. Epub 1999/02/03. PMID: 9927601.

48. Jaramillo-Lambert A, Engebrecht J. A single unpaired and transcriptionally silenced X chromosome locally precludes checkpoint signaling in the *Caenorhabditis elegans* germ line. Genetics. 2010; 184 (3):613–28. https://doi.org/10.1534/genetics.109.110338 PMID: 20008570; PubMed Central PMCID: PMCPMC2845332.

49. Woglar A, Daryabeigi A, Adamo A, Habacher C, Machacek T, La Volpe A, et al. Matefin/SUN-1 phosphorylation is part of a surveillance mechanism to coordinate chromosome synapsis and recombination with meiotic progression and chromosome movement. PLoS Genet. 2013; 9(3):e1003335. Epub 2013/03/19. https://doi.org/10.1371/journal.pgen.1003335 PMID: 23505384; PubMed Central PMCID: PMCPMC3591285.

50. Carlton PM, Farruggio AP, Dernburg AF. A link between meiotic prophase progression and crossover control. PLoS Genet. 2006; 2(2):e12. https://doi.org/10.1371/journal.pgen.0020012 PMID: 16462941; PubMed Central PMCID: PMCPMC1359072.

51. Sonneville R, Querenet M, Craig A, Gartner A, Blow JJ. The dynamics of replication licensing in live *Caenorhabditis elegans* embryos. J Cell Biol. 2012; 196(2):233–46. https://doi.org/10.1083/jcb.201110080 PMID: 22249291; PubMed Central PMCID: PMCPMC3265957.

52. Garcia-Muse T, Boulton SJ. Distinct modes of ATR activation after replication stress and DNA double-strand breaks in *Caenorhabditis elegans*. EMBO J. 2005; 24(24):4345–55. Epub 2005/12/02. https://doi.org/10.1038/sj.emboj.7600896 PMID: 16319925; PubMed Central PMCID: PMCPMC1356337.

53. Koury E, Harrell K, Smolikove S. Differential RPA-1 and RAD-51 recruitment *in vivo* throughout the *C. elegans* germline, as revealed by laser microirradiation. Nucleic Acids Res. 2018; 46(2):748–64. Epub 2017/12/16. https://doi.org/10.1093/nar/gkx1243 PMID: 29244155; PubMed Central PMCID: PMCPMC5778493.

54. Woglar A, Villeneuve AM. Dynamic architecture of DNA repair complexes and the synaptonemal complex at sites of meiotic recombination. Cell 2018;1678–1691.e16. Epub 2018/5/10. https://doi.org/10.1016/j.cell.2018.03.066 PMID: 29754818.

55. Hayashi M, Chin GM, Villeneuve AM. *C. elegans* germ cells switch between distinct modes of double-strand break repair during meiotic prophase progression. PLoS Genet. 2007; 3(11):e191. https://doi.org/10.1371/journal.pgen.0030191 PMID: 17983271; PubMed Central PMCID: PMCPMC2048528.

56. Rosu S, Zawadzki KA, Stamper EL, Libuda DE, Reese AL, Dernburg AF, et al. The C. elegans DSB-2 protein reveals a regulatory network that controls competence for meiotic DSB formation and promotes crossover assurance. PLoS Genet. 2013; 9(8):e1003674. https://doi.org/10.1371/journal.pgen.1003674 PMID: 23950729; PubMed Central PMCID: PMCPMC3738457.

57. Stamper EL, Rodenbusch SE, Rosu S, Ahringer J, Villeneuve AM, Dernburg AF. Identification of DSB-1, a protein required for initiation of meiotic recombination in *Caenorhabditis elegans*, illuminates a crossover assurance checkpoint. PLoS Genet. 2013; 9(8):e1003679. https://doi.org/10.1371/journal.pgen.1003679 PMID: 23990794; PubMed Central PMCID: PMCPMC3749324.

58. Holloway JK, Sun X, Yokoo R, Villeneuve AM, Cohen PE. Mammalian CNTD1 is critical for meiotic crossover maturation and deselection of excess precrossover sites. J Cell Biol. 2014; 205(5):633–41. https://doi.org/10.1083/jcb.201401122 PMID: 24891606; PubMed Central PMCID: PMCPMC4050721.

59. Woglar A, Villeneuve AM. Dynamic Architecture of DNA repair complexes and the synaptonemal complex at sites of meiotic recombination. Cell. 2018; 173(7):1678–91 e16. Epub 2018/05/15. https://doi.org/10.1016/j.cell.2018.03.066 PMID: 29754818; PubMed Central PMCID: PMCPMC6003859.

60. Albertson DG, Rose AM, Villeneuve AM. Chromosome Organization, Mitosis, and Meiosis. In: nd, Riddle DL, Blumenthal T, Meyer BJ, Priess JR, editors. C elegans II. Cold Spring Harbor (NY)1997.

61. de Carvalho CE, Zaaijer S, Smolikov S, Gu Y, Schumacher JM, Colaiacovo MP. LAB-1 antagonizes the Aurora B kinase in *C. elegans*. Genes Dev. 2008; 22(20):2869–85. Epub 2008/10/17. https://doi.org/10.1101/gad.1691208 PMID: 18923084; PubMed Central PMCID: PMCPMC2569883.

46

62. Hillers KJ, Villeneuve AM. Chromosome-wide control of meiotic crossing over in *C. elegans*. Curr Biol. 2003; 13(18):1641–7. Epub 2003/09/19. PMID: 13678597.

63. Lim JG, Stine RR, Yanowitz JL. Domain-specific regulation of recombination in *Caenorhabditis elegans* in response to temperature, age and sex. Genetics. 2008; 180(2):715–26. Epub 2008/09/11. https://doi.org/10.1534/genetics.108.090142 PMID: 18780748; PubMed Central PMCID: PMCPMC2567375.

64. Rockman MV, Kruglyak L. Recombinational landscape and population genomics of *Caenorhabditis elegans*. PLoS Genet. 2009; 5(3):e1000419. Epub 2009/03/14. https://doi.org/10.1371/journal.pgen.1000419 PMID: 19283065; PubMed Central PMCID: PMCPMC2652117.

65. Teuscher F, Brockmann GA, Rudolph PE, Swalve HH, Guiard V. Models for chromatid interference with applications to recombination data. Genetics. 2000; 156(3):1449–60. PMID: 11063716; PubMed Central PMCID: PMCPMC1461339.

66. Hawthorne DC, Mortimer RK. Chromosome mapping in *Saccharomyces*: centromere-linked genes. Genetics. 1960; 45(8):1085–110. PMID: 17247984; PubMed Central PMCID: PMCPMC1210110.

67. Hou Y, Fan W, Yan L, Li R, Lian Y, Huang J, et al. Genome analyses of single human oocytes. Cell. 2013; 155(7):1492–506. https://doi.org/10.1016/j.cell.2013.11.040 PMID: 24360273.

68. Li X, Li L, Yan J. Dissecting meiotic recombination based on tetrad analysis by single-microspore sequencing in maize. Nat Commun. 2015; 6:6648. https://doi.org/10.1038/ncomms7648 PMID: 25800954; PubMed Central PMCID: PMCPMC4383000.

69. Strickland WN. An analysis of interference in *Aspergillus nidulans*. Proc R Soc Lond B Biol Sci. 1958; 149(934):82–101. PMID: 13554433.

70. Strickland WN. Tetrad analysis of short chromosome regions of *Neurospora crassa*. Genetics. 1961; 46:1125–41. PMID: 13917785; PubMed Central PMCID: PMCPMC1210263.

71. Fukuda T, Daniel K, Wojtasz L, Toth A, Hoog C. A novel mammalian HORMA domain-containing protein, HORMAD1, preferentially associates with unsynapsed meiotic chromosomes. Exp Cell Res. 2010; 316(2):158–71. Epub 2009/08/19. https://doi.org/10.1016/j.yexcr.2009.08.007 PMID: 19686734.

72. Wojtasz L, Daniel K, Roig I, Bolcun-Filas E, Xu H, Boonsanay V, et al. Mouse HORMAD1 and HORMAD2, two conserved meiotic chromosomal proteins, are depleted from synapsed chromosome axes with the help of TRIP13 AAA-ATPase. PLoS Genet. 2009; 5(10):e1000702. Epub 2009/10/24. https://doi.org/10.1371/journal.pgen.1000702 PMID: 19851446; PubMed Central PMCID: PMCPMC2758600.

73. Couteau F, Zetka M. HTP-1 coordinates synaptonemal complex assembly with homolog alignment during meiosis in *C. elegans*. Genes Dev. 2005; 19(22):2744–56. Epub 2005/11/18. https://doi.org/10.1101/gad.1348205 PMID: 16291647; PubMed Central PMCID: PMCPMC1283966.

74. Goodyer W, Kaitna S, Couteau F, Ward JD, Boulton SJ, Zetka M. HTP-3 links DSB formation with homolog pairing and crossing over during *C. elegans* meiosis. Dev Cell. 2008; 14(2):263–74. Epub 2008/02/13. https://doi.org/10.1016/j.devcel.2007.11.016 PMID: 18267094.

75. Martinez-Perez E, Villeneuve AM. HTP-1-dependent constraints coordinate homolog pairing and synapsis and promote chiasma formation during *C. elegans* meiosis. Genes Dev. 2005; 19(22):2727–43. Epub 2005/11/18. https://doi.org/10.1101/gad.1338505 PMID: 16291646; PubMed Central PMCID: PMCPMC1283965.

76. Zetka MC, Kawasaki I, Strome S, Muller F. Synapsis and chiasma formation in *Caenorhabditis elegans* require HIM-3, a meiotic chromosome core component that functions in chromosome segregation. Genes Dev. 1999; 13(17):2258–70. Epub 1999/09/15. PMID: 10485848; PubMed Central PMCID: PMCPMC317003.

77. Couteau F, Nabeshima K, Villeneuve A, Zetka M. A component of *C. elegans* meiotic chromosome axes at the interface of homolog alignment, synapsis, nuclear reorganization, and recombination. Curr Biol. 2004; 14(7):585–92. Epub 2004/04/06. https://doi.org/10.1016/j.cub.2004.03.033 PMID: 15062099.

78. Daniel K, Lange J, Hached K, Fu J, Anastassiadis K, Roig I, et al. Meiotic homologue alignment and its quality surveillance are controlled by mouse HORMAD1. Nat Cell Biol. 2011; 13(5):599–610. Epub 2011/04/12. https://doi.org/10.1038/ncb2213 PMID: 21478856; PubMed Central PMCID: PMCPMC3087846.

79. Kim Y, Rosenberg SC, Kugel CL, Kostow N, Rog O, Davydov V, et al. The chromosome axis controls meiotic events through a hierarchical assembly of HORMA domain proteins. Dev Cell. 2014; 31 (4):487–502. Epub 2014/12/03. https://doi.org/10.1016/j.devcel.2014.09.013 PMID: 25446517; PubMed Central PMCID: PMCPMC4254552.

80. Kogo H, Tsutsumi M, Ohye T, Inagaki H, Abe T, Kurahashi H. HORMAD1-dependent checkpoint/surveillance mechanism eliminates asynaptic oocytes. Genes Cells. 2012; 17(6):439–54. Epub 2012/04/26. https://doi.org/10.1111/j.1365-2443.2012.01600.x PMID: 22530760.

47

81. Shin YH, McGuire MM, Rajkovic A. Mouse HORMAD1 is a meiosis I checkpoint protein that modulates DNA double- strand break repair during female meiosis. Biol Reprod. 2013; 89(2):29. Epub 2013/06/14. https://doi.org/10.1095/biolreprod.112.106773 PMID: 23759310; PubMed Central PMCID: PMCPMC4076362.

82. Silva N, Ferrandiz N, Barroso C, Tognetti S, Lightfoot J, Telecan O, et al. The fidelity of synaptonemal complex assembly is regulated by a signaling mechanism that controls early meiotic progression. Dev Cell. 2014; 31(4):503–11. Epub 2014/12/03. https://doi.org/10.1016/j.devcel.2014.10.001 PMID: 25455309.

83. Ferrandiz N, Barroso C, Telecan O, Shao N, Kim HM, Testori S, et al. Spatiotemporal regulation of Aurora B recruitment ensures release of cohesion during *C. elegans* oocyte meiosis. Nat Commun. 2018; 9(1):834. Epub 2018/02/28. https://doi.org/10.1038/s41467-018-03229-5 PMID: 29483514; PubMed Central PMCID: PMCPMC5827026.

84. Agostinho A, Meier B, Sonneville R, Jagut M, Woglar A, Blow J, et al. Combinatorial regulation of meiotic holliday junction resolution in *C. elegans* by HIM-6 (BLM) helicase, SLX-4, and the SLX-1, MUS-81 and XPF-1 nucleases. PLoS Genet. 2013; 9(7):e1003591. Epub 2013/08/01. https://doi.org/10.1371/journal.pgen.1003591 PMID: 23901331; PubMed Central PMCID: PMCPMC3715425.

85. O'Neil NJ, Martin JS, Youds JL, Ward JD, Petalcorin MI, Rose AM, et al. Joint molecule resolution requires the redundant activities of MUS-81 and XPF-1 during *Caenorhabditis elegans* meiosis. PLoS Genet. 2013; 9(7):e1003582. Epub 2013/07/23. https://doi.org/10.1371/journal.pgen.1003582 PMID: 23874209; PubMed Central PMCID: PMCPMC3715453.

86. Saito TT, Lui DY, Kim HM, Meyer K, Colaiacovo MP. Interplay between structure-specific endonucleases for crossover control during *Caenorhabditis elegans* meiosis. PLoS Genet. 2013; 9(7):e1003586. Epub 2013/07/23. https://doi.org/10.1371/journal.pgen.1003586 PMID: 23874210; PubMed Central PMCID: PMCPMC3715419.

87. Brzovic PS, Keeffe JR, Nishikawa H, Miyamoto K, Fox D 3rd, Fukuda M, et al. Binding and recognition in the assembly of an active BRCA1/BARD1 ubiquitin-ligase complex. Proc Natl Acad Sci U S A. 2003; 100(10):5646–51. https://doi.org/10.1073/pnas.0836054100 PMID: 12732733; PubMed Central PMCID: PMCPMC156255.

88. Stewart MD, Duncan ED, Coronado E, DaRosa PA, Pruneda JN, Brzovic PS, et al. Tuning BRCA1 and BARD1 activity to investigate RING ubiquitin ligase mechanisms. Protein Sci. 2017; 26(3):475–83. https://doi.org/10.1002/pro.3091 PMID: 27977889; PubMed Central PMCID: PMCPMC5326557.

89. Thompson ME. BRCA1 16 years later: nuclear import and export processes. FEBS J. 2010; 277(15):3072–8. https://doi.org/10.1111/j.1742-4658.2010.07733.x PMID: 20608972

90. Link J, Paouneskou D, Velkova M, Daryabeigi A, Laos T, Labella S, et al. Transient and partial nuclear lamina disruption promotes chromosome movement in early meiotic prophase. Dev Cell. 2018; 45(2):212–25 e7. https://doi.org/10.1016/j.devcel.2018.03.018 PMID: 29689196; PubMed Central PMCID: PMCPMC5920155.

91. VanGompel MJ, Nguyen KC, Hall DH, Dauer WT, Rose LS. A novel function for the *Caenorhabditis elegans* torsin OOC-5 in nucleoporin localization and nuclear import. Mol Biol Cell. 2015; 26(9):1752–63. https://doi.org/10.1091/mbc.E14-07-1239 PMID: 25739455; PubMed Central PMCID: PMCPMC4436785.

92. Wu Q, Jubb H, Blundell TL. Phosphopeptide interactions with BRCA1 BRCT domains: More than just a motif. Prog Biophys Mol Biol. 2015; 117(2–3):143–8. https://doi.org/10.1016/j.pbiomolbio.2015.02.003 PMID: 25701377; PubMed Central PMCID: PMCPMC4728184.

93. Saredi G, Huang H, Hammond CM, Alabert C, Bekker-Jensen S, Forne I, et al. H4K20me0 marks post-replicative chromatin and recruits the TONSL-MMS22L DNA repair complex. Nature. 2016; 534(7609):714–8. https://doi.org/10.1038/nature18312 PMID: 27338793; PubMed Central PMCID: PMCPMC4939875.

94. Zhao W, Steinfeld JB, Liang F, Chen X, Maranon DG, Jian Ma C, et al. BRCA1-BARD1 promotes RAD51-mediated homologous DNA pairing. Nature. 2017; 550(7676):360–5. Epub 2017/10/05. https://doi.org/10.1038/nature24060 PMID: 28976962; PubMed Central PMCID: PMCPMC5800781.

95. Bhattacharyya A, Ear US, Koller BH, Weichselbaum RR, Bishop DK. The breast cancer susceptibility gene BRCA1 is required for subnuclear assembly of Rad51 and survival following treatment with the DNA cross-linking agent cisplatin. J Biol Chem. 2000; 275(31):23899–903. Epub 2000/06/14. https://doi.org/10.1074/jbc.C000276200 PMID: 10843985.

96. Cantor SB, Bell DW, Ganesan S, Kass EM, Drapkin R, Grossman S, et al. BACH1, a novel helicase-like protein, interacts directly with BRCA1 and contributes to its DNA repair function. Cell. 2001; 105(1):149–60. PMID: 11301010.

97. Sommers JA, Rawtani N, Gupta R, Bugreev DV, Mazin AV, Cantor SB, et al. FANCJ uses its motor ATPase to destabilize protein-DNA complexes, unwind triplexes, and inhibit RAD51 strand exchange.

48

J Biol Chem. 2009; 284(12):7505–17. https://doi.org/10.1074/jbc.M809019200 PMID: 19150983; PubMed Central PMCID: PMCPMC2658046.

98. Crown KN, Miller DE, Sekelsky J, Hawley RS. Local inversion heterozygosity alters recombination throughout the Genome. Curr Biol. 2018. https://doi.org/10.1016/j.cub.2018.07.004 PMID: 30174188.

99. Joyce EF, McKim KS. Chromosome axis defects induce a checkpoint-mediated delay and interchromosomal effect on crossing over during Drosophila meiosis. PLoS Genet. 2010; 6(8). Epub 2010/08/17. https://doi.org/10.1371/journal.pgen.1001059 PMID: 20711363; PubMed Central PMCID: PMCPMC2920846.

100. Roberts P. Interchromosomal effects and the relation between crossing-over and nondisjunction. Genetics. 1962; 47:1691–709. Epub 1962/12/01. PMID: 13974320; PubMed Central PMCID: PMCPMC1210314.

101. Suzuki DT. Interchromosomal effects on crossing over in *Drosophila melanogaster*. Ii.A reexamination of X chromosome inversion effects. Genetics. 1963; 48:1605–17. Epub 1963/12/01. PMID: 14102803; PubMed Central PMCID: PMCPMC1210445.

102. Anton E, Vidal F, Blanco J. Interchromosomal effect analyses by sperm FISH: incidence and distribution among reorganization carriers. Syst Biol Reprod Med. 2011; 57(6):268–78. Epub 2011/11/19. https://doi.org/10.3109/19396368.2011.633682 PMID: 22092077.

103. Barber LJ, Youds JL, Ward JD, McIlwraith MJ, O'Neil NJ, Petalcorin MI, et al. RTEL1 maintains genomic stability by suppressing homologous recombination. Cell. 2008; 135(2):261–71. Epub 2008/10/30. https://doi.org/10.1016/j.cell.2008.08.016 PMID: 18957201; PubMed Central PMCID: PMCPMC3726190.

104. Tsai CJ, Mets DG, Albrecht MR, Nix P, Chan A, Meyer BJ. Meiotic crossover number and distribution are regulated by a dosage compensation protein that resembles a condensin subunit. Genes Dev. 2008; 22(2):194–211. https://doi.org/10.1101/gad.1618508 PMID: 18198337; PubMed Central PMCID: PMCPMC2192754.

105. Youds JL, Mets DG, McIlwraith MJ, Martin JS, Ward JD, NJ ON, et al. RTEL-1 enforces meiotic crossover interference and homeostasis. Science. 2010; 327(5970):1254–8. Epub 2010/03/06. https://doi.org/10.1126/science.1183112 PMID: 20203049; PubMed Central PMCID: PMCPMC4770885.

106. Libuda DE, Uzawa S, Meyer BJ, Villeneuve AM. Meiotic chromosome structures constrain and respond to designation of crossover sites. Nature. 2013; 502(7473):703–6. Epub 2013/10/11. https://doi.org/10.1038/nature12577 PMID: 24107990; PubMed Central PMCID: PMCPMC3920622.

107. Deshong AJ, Ye AL, Lamelza P, Bhalla N. A quality control mechanism coordinates meiotic prophase events to promote crossover assurance. PLoS Genet. 2014; 10(4):e1004291. Epub 2014/04/26. https://doi.org/10.1371/journal.pgen.1004291 PMID: 24762417; PubMed Central PMCID: PMCPMC3998905.

108. Kim Y, Kostow N, Dernburg AF. The chromosome axis mediates feedback control of CHK-2 to ensure crossover formation in *C. elegans*. Dev Cell. 2015; 35(2):247–61. Epub 2015/10/28. https://doi.org/10.1016/j.devcel.2015.09.021 PMID: 26506311; PubMed Central PMCID: PMCPMC4624198.

109. Mateo AR, Kessler Z, Jolliffe AK, McGovern O, Yu B, Nicolucci A, et al. The p53-like protein CEP-1 Is required for meiotic fidelity in *C. elegans*. Curr Biol. 2016; 26(9):1148–58. Epub 2016/05/07. https://doi.org/10.1016/j.cub.2016.03.036 PMID: 27151662; PubMed Central PMCID: PMCPMC5215890.

110. Zhang L, Kohler S, Rillo-Bohn R, Dernburg AF. A compartmentalized signaling network mediates crossover control in meiosis. Elife. 2018; 7. https://doi.org/10.7554/eLife.30789 PMID: 29521627; PubMed Central PMCID: PMCPMC5906097.

111. Paix A, Folkmann A, Rasoloson D, Seydoux G. High Efficiency, Homology-directed genome editing in *Caenorhabditis elegans* ssing CRISPR-Cas9 ribonucleoprotein complexes. Genetics. 2015; 201 (1):47–54. https://doi.org/10.1534/genetics.115.179382 PMID: 26187122; PubMed Central PMCID: PMCPMC4566275.

112. Jaramillo-Lambert A, Ellefson M, Villeneuve AM, Engebrecht J. Differential timing of S phases, X chromosome replication, and meiotic prophase in the *C. elegans* germ line. Dev Biol. 2007; 308(1):206–21. https://doi.org/10.1016/j.ydbio.2007.05.019 PMID: 17599823.

113. Timmons L, Court DL, Fire A. Ingestion of bacterially expressed dsRNAs can produce specific and potent genetic interference in *Caenorhabditis elegans*. Gene. 2001; 263(1–2):103–12. PMID: 11223248.

114. Nabeshima K, Villeneuve AM, Hillers KJ. Chromosome-wide regulation of meiotic crossover formation in *Caenorhabditis elegans* requires properly assembled chromosome axes. Genetics. 2004; 168 (3):1275–92. Epub 2004/12/08. https://doi.org/10.1534/genetics.104.030700 PMID: 15579685; PubMed Central PMCID: PMCPMC1448768.

49

115. Davis MW, Hammarlund M, Harrach T, Hullett P, Olsen S, Jorgensen EM. Rapid single nucleotide polymorphism mapping in *C. elegans*. BMC Genomics. 2005; 6:118. Epub 2005/09/15. https://doi.org/10.1186/1471-2164-6-118 PMID: 16156901; PubMed Central PMCID: PMCPMC1242227.

116. Smolikov S, Schild-Prufert K, Colaiacovo MP. CRA-1 uncovers a double-strand break-dependent pathway promoting the assembly of central region proteins on chromosome axes during *C. elegans* meiosis. PLoS Genet. 2008; 4(6):e1000088. Epub 2008/06/07. https://doi.org/10.1371/journal.pgen.1000088 PMID: 18535664; PubMed Central PMCID: PMCPMC2408554.

117. Meneely PM, McGovern OL, Heinis FI, Yanowitz JL. Crossover distribution and frequency are regulated by *him-5* in *Caenorhabditis elegans*. Genetics. 2012; 190(4):1251–66. Epub 2012/01/24. https://doi.org/10.1534/genetics.111.137463 PMID: 22267496; PubMed Central PMCID: PMCPMC3316641.

118. Mets DG, Meyer BJ. Condensins regulate meiotic DNA break distribution, thus crossover frequency, by controlling chromosome structure. Cell. 2009; 139(1):73–86. https://doi.org/10.1016/j.cell.2009.07.035 PMID: 19781752; PubMed Central PMCID: PMCPMC2785808.

119. Brady MM, McMahan S, Sekelsky J. Loss of Drosophila Mei-41/ATR Alters Meiotic Crossover Patterning. Genetics. 2018; 208(2):579–88. https://doi.org/10.1534/genetics.117.300634 PMID: 29247012; PubMed Central PMCID: PMCPMC5788523.

50

Chapter 3

Meiotic double-strand break processing and crossover patterning are regulated in a

sex-specific manner by BRCA1-BARD1 in *Caenorhabditis elegans*

Qianyan Li, Sara Hariri, JoAnne Engebrecht

Sara Hariri measured GFP::COSA-1 foci in *zim-2* and *him-8* mutants (part of Figure 6A) and co-performed SNP markers based genetic linkage analysis (Figure 7B). JoAnne Engebrecht quantified GFP::RPA-1 and GFP::BRC-1 foci (Figure 3B and 3D) and performed viability assay for male-sired progeny (Figure 5A). QL performed all other experiments.

Meiotic Double-Strand Break Processing and Crossover Patterning Are Regulated in a Sex-Specific Manner by BRCA1–BARD1 in *Caenorhabditis elegans*

Qianyan Li, Sara Hariri, and JoAnne Engebrecht[1]

Department of Molecular and Cellular Biology, and Biochemistry, Molecular, Cellular and Developmental Biology Graduate Group,
University of California, Davis, California 95616

ORCID IDs: 0000-0003-4865-0101 (Q.L.); 0000-0002-2733-7506 (J.E.)

ABSTRACT Meiosis is regulated in a sex-specific manner to produce two distinct gametes, sperm and oocytes, for sexual reproduction. To determine how meiotic recombination is regulated in spermatogenesis, we analyzed the meiotic phenotypes of mutants in the tumor suppressor E3 ubiquitin ligase BRC-1-BRD-1 complex in *Caenorhabditis elegans* male meiosis. Unlike in mammals, this complex is not required for meiotic sex chromosome inactivation, the process whereby hemizygous sex chromosomes are transcriptionally silenced. Interestingly, *brc-1* and *brd-1* mutants show meiotic recombination phenotypes that are largely opposing to those previously reported for female meiosis. Fewer meiotic recombination intermediates marked by the recombinase RAD-51 were observed in *brc-1* and *brd-1* mutants, and the reduction in RAD-51 foci could be suppressed by mutation of nonhomologous-end-joining proteins. Analysis of GFP::RPA-1 revealed fewer foci in the *brc-1 brd-1* mutant and concentration of BRC-1-BRD-1 to sites of meiotic recombination was dependent on DNA end resection, suggesting that the complex regulates the processing of meiotic double-strand breaks to promote repair by homologous recombination. Further, BRC-1-BRD-1 is important to promote progeny viability when male meiosis is perturbed by mutations that block the pairing and synapsis of different chromosome pairs, although the complex is not required to stabilize the RAD-51 filament as in female meiosis under the same conditions. Analyses of crossover designation and formation revealed that BRC-1-BRD-1 inhibits supernumerary COs when meiosis is perturbed. Together, our findings suggest that BRC-1-BRD-1 regulates different aspects of meiotic recombination in male and female meiosis.

KEYWORDS BRC-1-BRD-1; crossovers; meiosis; recombination; sex; Genetics of Sex

MEIOSIS is essential for sexual reproduction and results in the precise halving of the genome for packaging into gametes. Chromosomes must be accurately segregated during meiosis to ensure that the next generation has the correct genomic complement. In metazoans with defined sexes, the products of meiosis—sperm and oocytes—contribute not only haploid genomes but also unique cellular components to support embryonic development. In addition to the striking morphological differences between sperm and oocytes, the process of meiosis itself exhibits extensive sexual dimorphism with respect to the temporal program of events, the extent and placement of recombination, checkpoint signaling, chromosome segregation, and sex chromosome behavior (Morelli and Cohen 2005; Turner 2007; Nagaoka *et al.* 2012; Bury *et al.* 2016; Cahoon and Libuda 2019). However, the underlying mechanisms governing these differences are not well understood.

Meiotic chromosome segregation relies on establishing connections between homologous chromosomes. In most organisms, this is accomplished by the intentional induction of hundreds of double-strand breaks (DSBs) by the conserved topoisomerase Spo11 (Keeney *et al.* 1997; Dernburg *et al.* 1998). A subset of meiotic DSBs use a nonsister chromatid as template for repair by homologous recombination (HR) to generate crossovers (COs) that ensure disjunction and

promote genetic variation. In almost all animals and plants where it has been examined, COs differ in number, placement, and spacing in the sexes (Lenormand and Dutheil 2005; Gruhn *et al.* 2013; Stapley *et al.* 2017; Kianian *et al.* 2018; Lloyd and Jenczewski 2019).

Knowledge is lacking with respect to the contributions of different pathways to repair of DSBs not destined to form COs and whether their use differs in the sexes. During *Caenorhabditis elegans* and *Drosophila* oogenesis, the non-homologous end joining (NHEJ) pathway for DSB repair is actively inhibited early in meiosis (Joyce *et al.* 2012; Lemmens *et al.* 2013; Yin and Smolikove 2013; Lawrence *et al.* 2016; Girard *et al.* 2018) but NHEJ and other pathways, including theta-mediated end-joining and single-strand annealing, serve as backups to ensure that all DSBs are repaired in late pachytene before the meiotic divisions (Smolikov *et al.* 2007; Macaisne *et al.* 2018). A recent study examining the repair of DNA breaks induced by radiation suggests that mouse spermatocytes switch to a somatic-like repair mode at pachytene, temporarily engaging NHEJ and then HR to repair the damage (Enguita-Marruedo *et al.* 2019). Interestingly, studies in juvenile male mice suggest that structure-specific nucleases may resolve processed DSBs at the expense of the canonical CO pathway, leading to higher levels of meiotic chromosome mis-segregation (Zelazowski *et al.* 2017).

Male meiosis in many species has the added challenge of the presence of heteromorphic sex chromosomes. Meiotic DSBs are induced on hemizygous regions of sex chromosomes (Ashley *et al.* 1995; Moens *et al.* 1997; Sciurano *et al.* 2006; Jaramillo-Lambert and Engebrecht 2010), yet they are unable to participate in CO formation due to a lack of a homolog. In *C. elegans* and the related nematode, *Caenorhabditis briggsae*, HR using the sister chromatid as repair template, and alternative repair pathways are engaged to repair meiotic DSBs induced on the completely hemizygous *X* chromosome of males (Checchi *et al.* 2014; Van *et al.* 2016). The presence of hemizygous sex chromosomes also complicates analyses of meiotic recombination in mammals as inactivation of many recombination genes impairs meiotic sex chromosome inactivation (MSCI). MSCI is the process whereby hemizygous regions of sex chromosomes acquire heterochromatin marks and are transcriptionally silenced (Turner 2007). MSCI is required for efficient meiotic progression in males, as failure to inactivate sex chromosomes results in elevated apoptosis and elimination of germ cells (Mahadevaiah *et al.* 2008; Royo *et al.* 2010).

C. elegans has emerged as an excellent model for meiotic studies, including investigations into the sex-specific regulation of meiotic events. Both the *C. elegans* hermaphrodite and male germ lines are arranged in a spatiotemporal gradient that in combination with available molecular markers enables recombination progression to be monitored through all stages of meiotic prophase (Shakes *et al.* 2009; Lui and Colaiacovo 2013; Hillers *et al.* 2015) (Figure 2A). Additionally, the lack of absolute interdependence of recombination initiation and chromosome synapsis also facilitates analyses of meiotic mutants. *C. elegans* exists predominantly as a self-fertilizing hermaphrodite (*XX*); during development, hermaphrodites initially produce sperm and then switch to oocyte production, and thus as adults are functionally female. Males (*X0*) arise spontaneously due to *X* chromosome nondisjunction.

The hemizygous *X* chromosome of *C. elegans* male germ cells undergoes modifications similar to the hemizygous regions of the X and Y of mammalian spermatocytes, including accumulation of repressive chromatin marks resulting in transcriptional silencing (Kelly *et al.* 2002; Reuben and Lin 2002; Bean *et al.* 2004; Maine 2010). A *C. elegans* SETBD1 histone methyltransferase—an ortholog of which has been shown to mediate MSCI in mammals (Hirota *et al.* 2018)—and a small RNA pathway are important for silencing the *X* chromosome of male germ cells (She *et al.* 2009; Bessler *et al.* 2010; Checchi and Engebrecht 2011). However, the role of many components required for MSCI in mammals, including the tumor suppressor E3 ubiquitin ligase BRCA1 and master checkpoint kinase ATR (Turner *et al.* 2004; Royo *et al.* 2013; Broering *et al.* 2014), have not been analyzed in *C. elegans*. Here, we examined the requirement for BRCA1-BARD1 (BRC-1-BRD-1) and ATR (ATL-1) in meiotic silencing in *C. elegans*. Surprisingly our studies revealed that in contrast to mammals, *C. elegans* BRC-1-BRD-1 is not essential for MSCI. However, *X* chromosome transcriptional silencing is impaired in the absence of ATL-1, suggesting that while meiotic silencing is conserved, the pathways mediating MSCI have evolved independently. We also found that the meiotic phenotypes of male *brc-1* and *brd-1* mutants are different than those previously reported in female meiosis (Boulton *et al.* 2004; Adamo *et al.* 2008; Janisiw *et al.* 2018; Li *et al.* 2018), providing further evidence that recombination is regulated differently in spermatogenic *vs.* oogenic germ cells (Jaramillo-Lambert and Engebrecht 2010; Checchi *et al.* 2014). We propose that BRC-1-BRD-1 functions at an early step of meiotic DSB repair in male meiosis, which is similar to one of its established somatic roles in promoting HR at the expense of NHEJ. Additionally, this complex alters the CO landscape when meiosis is perturbed by inhibiting supernumerary COs, rather than promoting extra COs as in female meiosis. Together, our findings indicate that the processing of meiotic DSBs and the regulation of CO patterning are regulated in a sex-specific manner in *C. elegans*.

Materials and Methods

Genetics

C. elegans var. Bristol (N2), was used as the wild-type strain. Other strains used in this study are listed in Supplemental Materials, Table S1. Some nematode strains were provided by the Caenorhabditis Genetics Center, which is funded by the National Institutes of Health National Center for Research Resources (NIH NCRR). Strains were maintained at 20°.

CRISPR-mediated generation of alleles

zim-3(xoe15) was generated in the Bristol background using guides tacgcctgagaacatgtttt and aaaagatcgtgtgatggtcc with repair template: gtaaataacggttgtcgatacgcctgagaacatgtttttg gacatttatcttttctagtaggtttttccatatactttattttattctgaagtttag to delete most of the coding sequence except for exon 7 and 8. External primers cacgacgacaccctcatgta and ttgtgcagagtcg tagcgaa and internal primers cacgacgacaccctcatgta and gctcgtgtacattgagccct were used to genotype for *zim-3(xoe15)*. *brc-1(xoe4)* was introduced into the Hawaiian background (CB4856) using primers, guides and repair template as described (Li *et al.* 2018). *zim-1(xoe6) was* generated in the Bristol and Hawaiian background using guides tccaatcatcacaagtcatc and attcgatgagcttcgtcgtc with repair template tttaaaaatgcagttt-taaaagtgtttcattgtcattttatattttccaggcttcgtcgtcgggccgtctgcttttt gtaaattgtgtctcatgtgttat to delete the entire coding sequence. External primers cacacatttggctggggtct and atgggcagcagcaagaaagt, and internal primers gctccgtctgcacaaatcct and gttgaaaagcggg gaacacc were used to identify *zim-1(xoe6)*. Worms were outcrossed a minimum of two times and analyzed phenotypically by examining progeny viability to confirm correct editing.

Embryonic lethality of male-sired progeny

A single *fog-2(q71)* female was mated with three males of indicated genotypes on small *Escherichia coli* OP-50 spots. The mated female was transferred to new plates every 24 hr. Embryonic lethality was determined over 3 days by counting eggs and hatched larvae 24 hr after removing the female and calculating percent as eggs/(eggs + larvae). The progeny of a minimum of 10 mated females were scored.

Cytological analyses

Immunostaining of germ lines was performed as described (Jaramillo-Lambert *et al.* 2007) except that slides were incubated in 100% ethanol instead of 100% methanol for direct green fluorescent protein (GFP) fluorescence of GFP::COSA-1. The following primary antibodies were used at the indicated dilutions: rabbit anti-Pol2-S2P (1:500; cat #ab5059; RRID: AB_304749; Abcam, Cambridge, MA), rabbit anti-HIM-8 (1:500; cat #4198.00.02; SDIX; Newark, DE; RRID: AB_2616418), rabbit anti-histone H3K4me2 (1:500; cat# 9725; Cell Signaling Technology; Danvers, MA; RRID: AB_10205451), mouse anti-histone H3K9me2 (1:500; Cat# 9753; RRID: AB_659848; AbCam), mouse anti-Pol2-S5P H14 (1:500; cat# MMS-134R; RRID: AB_10119940; Covance, Princeton, NJ), rabbit anti-RAD-51 (1:10,000; cat #2948.00.02; SDIX; RRID: AB_2616441), mouse anti-GFP (1:500; cat #632375; BD Biosciences; San Jose, CA). Secondary antibodies Alexa Fluor 594 donkey anti-rabbit IgG, Alexa Fluor 594 goat anti-mouse IgG, Alexa Fluor 488 goat anti-rabbit IgG, and Alexa Fluor 488 goat anti-mouse IgG from Life Technologies were used at 1:500 dilutions. DAPI (4′,6-diamidino-2-phenylindole; 2 μg/ml; Sigma-Aldrich) was used to counterstain DNA.

Collection of fixed images was performed using an API Delta Vision or an API Delta Vision Ultra deconvolution microscope equipped with an 60×, NA 1.49 objective lens, and appropriate filters for epifluorescence. Z stacks (0.2 μm) were collected from the entire gonad. A minimum of three germ lines was examined for each condition. Images were deconvolved using Applied Precision SoftWoRx batch deconvolution software and subsequently processed and analyzed using Fiji (ImageJ) (Wayne Rasband, NIH).

Quantification of H3K9me2 enrichment on the *X* chromosome was performed by examining deconvolved three-dimensional (3D) data stacks and binning mid- to late-pachytene nuclei into three categories: enrichment = single strong track of H3K9me2 associated with HIM-8; partial enrichment = diffuse H3K9me2 signal associated with HIM-8; no enrichment = multiple H3K9me2 signals with no HIM-8 association. To quantitate the transcriptional status of the *X* chromosome in wild type (three germ lines) and the *atl-1* mutant (six germ lines), mid- to late pachytene nuclei with a single HIM-8-marked chromosome were examined in deconvolved 3D data stacks for the presence of Pol2-S5P labeling.

RAD-51 foci were quantified in a minimum of three germ lines of age-matched males (18–24 hr post-L4). We divided germ lines into the transition zone (leptotene/zygotene), as counted from the first and last row with two or more crescent-shaped nuclei, and then divided pachytene into three equal parts: early, mid and late (Figure 2A). RAD-51 were quantified from half projections of the germ lines. The number of foci per nucleus was scored for each region.

To assess formation of RAD-51 foci following ionizing radiation (IR) treatment, 18–24 hr post-L4 male worms were exposed to 10 Grays (Gys) of IR; 1 hr post-IR, worms were dissected and gonads fixed for immunofluorescence as above.

GFP::COSA-1 foci were quantified from deconvolved 3D data stacks; late pachytene nuclei were scored individually through z-stacks to ensure that all foci within each individual nucleus were counted.

For live cell imaging (Figure 3, A and C), 18–24 hr post L4 males were anesthetized in 1 mM tetramisole (Sigma-Aldrich) and immobilized between a coverslip and a 2.5% agarose pad on a glass slide. Z-stacks (0.33 μm) were captured on a spinning-disk module of an inverted objective fluorescence microscope [Marianas spinning-disk confocal (SDC) real-time 3D Confocal-TIRF (total internal reflection) microscope; Intelligent Imaging Innovations] with a 100×, 1.46 numerical aperture objective, and a Photometrics QuantiEM electron multiplying charge-coupled device (EMCCD) camera. Z-projections of ∼20–30 z-slices were generated, cropped, and adjusted for brightness in Fiji. GFP::RPA-1 fluorescence was quantified by measuring the mean fluorescence intensity and SD in Fiji for individual nuclei [region of interest (ROI)] in transition zone to mid-pachytene. Coefficient of variation (CV) is defined as SD of intensity divided by mean intensity (Bishop *et al.* 2015). The CV describes the dispersion of pixel intensity values from a 2D ROI around the mean pixel intensity such that nuclei with more distinct foci will have high CV values, whereas

nuclei with more uniform fluorescence will have low CV values.

Meiotic mapping

Meiotic CO frequencies and distribution were assayed using single-nucleotide polymorphism (SNP) markers as in Nabeshima *et al.* (2004). The SNP markers located at the boundaries of the chromosome domains were chosen based on data from WormBase (WS231), Bazan and Hillers (2011) and Saito *et al.* (2013). Markers and primers used are listed in Table S2. Hawaiian strain CB4856 males carrying each mutation were crossed to the same mutant strain in the Bristol background. Among the progeny of this cross, male worms were plated individually and crossed to two *fog-2(q71)* female worms in the Bristol background. Upon successful mating, embryos (Smolikov *et al.* 2008) together with larva up to L4 stage were collected individually and stored at $-80°$. Since all three mutant (*brc-1*, *zim-1*, *brc-1;zim-1*) hermaphrodites produce self-fertilized male progeny, the identity of the hybrid Bristol/Hawaiian male was confirmed by PCR, and restriction digest before the collected samples were used for further analysis: individuals were lysed in 5 µl of lysis buffer (50 mM KCl, 10 mM Tris pH 8.2, 2.5 mM MgCl$_2$, 0.45% NP-40, 0.45% Tween20, 0.01% gelatin; 60 µg of proteinase K/ml was added before use) and diluted to 50 µl volume with molecular biology grade water. PCR was performed using 3–5 µl diluted lysate with Phusion or *Taq* polymerase in a 15 µl reaction. Half volume of the PCR products was digested overnight with appropriate restriction enzyme and analyzed on 1–2.5% agarose gels. Double crossovers (DCOs) were confirmed either with additional SNPs by a distinctive restriction enzyme digest or by repeating PCR and digestion if no additional SNPs were available for the marker as described in Saito *et al.* (2013) (Table S2).

Statistical analyses

Statistical analyses and figures were prepared using GraphPad Prism version 8.0 (GraphPad Software). Statistical comparisons of H3K9me2 association with HIM-8 (Figure 1C), absence of Pol2-S5P on HIM-8-marked chromosomes (Figure 1E), RAD-51 (Figure 2B and Figure 5B, and Figure S1A), GFP::RPA-1 fluorescence (Figure 3B), GFP::BRC-1 (Figure 3D), and GFP::COSA-1 foci numbers (Figure 6A) were analyzed by Mann-Whitney. Embryonic lethality (Figure 5A) was analyzed by one-way ANOVA. Fisher exact test on a 2×2 contingency table was used for statistical analyses on genetic map distance, distribution and % multi-COs (Figure 7, B–D). For statistical analyses of interference, $\chi2$ tests on 2×2 contingency tables of observed and expected DCOs were performed (Brady *et al.* 2018). Detailed descriptions of statistical analyses are indicated in figure legends.

Data availability

Strains and reagents are available upon request. The authors affirm that all data necessary for confirming the conclusions of this article are represented fully within the article and its tables and figures. Supplemental material available at figshare: https://doi.org/10.25386/genetics.12730904.

Results

C. elegans BRC-1-BRD-1 is not required for MSCI

During *C. elegans* meiosis, the *X* chromosome accumulates the repressive chromatin mark histone H3 lysine nine dimethylation (H3K9me2) and is transcriptionally silenced similar to MSCI in mammals (Kelly *et al.* 2002; Reuben and Lin 2002; Bean *et al.* 2004; Checchi and Engebrecht 2011). In mice, the E3 ubiquitin ligase BRCA1, critical for DNA damage response, is essential for MSCI. As a result, *brca1*$^{-/-}$ mutant male germ cells inappropriately express X-linked genes leading to pachytene arrest, apoptosis of spermatocytes and infertility (Xu *et al.* 2003; Turner *et al.* 2004; Broering *et al.* 2014). To determine whether *C. elegans* BRC-1 or its binding partner BRD-1 (Boulton *et al.* 2004) plays a role in MSCI, we labeled male *brc-1*, *brd-1*, and *brc-1 brd-1* double mutant germ lines [*brc-1(xoe4)*, *brd-1(ok1623)*, *brc-1(xoe4) brd-1(dw1)* and *brc-1(tm1145) brd-1(dw1)* (Polanowska *et al.* 2006; Janisiw *et al.* 2018; Li *et al.* 2018)] with antibodies against H3K9me2 and the *X*-specific pairing center binding protein HIM-8 (Phillips and Dernburg 2006). The *X* chromosome, marked by HIM-8, was highly enriched for H3K9me2 in all of the *brc-1* and *brd-1* mutant combinations, as in wild type, suggesting that enrichment of this repressive chromatin mark on the *X* chromosome occurs in the absence of BRC-1 and/or BRD-1 (Figure 1, A and C). To examine the transcriptional status of the *X* chromosome, we colabeled germ lines with antibodies that recognize H3K9me2 and RNA polymerase II phosphorylated on serine 2 (Pol2-S2P), which is associated with transcriptional elongation (Hsin and Manley 2012), and for which we and others previously showed is excluded from the single *X* chromosome in male germ cells (Kelly *et al.* 2002; Larson *et al.* 2016). Pol2-S2P was present throughout the nucleus except for a single track, marked by H3K9me2, in all *brc-1* and *brd-1* mutants (Figure 1B), suggesting that the *X* chromosome is transcriptionally silenced in the absence of BRC-1-BRD-1.

In mammals, BRCA1 is observed on asynapsed axes and is enriched on the X–Y sex body (Turner *et al.* 2004). In *C. elegans* hermaphrodites, BRC-1 and BRD-1 become associated with fully synapsed chromosomes in pachytene (Polanowska *et al.* 2006; Janisiw *et al.* 2018; Li *et al.* 2018). We examined the localization of BRC-1 in male germ lines expressing an endogenously tagged and fully functional GFP fusion (GFP::BRC-1; Li *et al.* 2018) and found that it was also associated with tracks corresponding to synapsed chromosomes at pachytene. However, in contrast to the six tracks observed in oocytes, only five tracks were present in spermatocytes, suggesting that BRC-1-BRD-1 does not localize to the asynapsed *X* chromosome. To verify this, we colabeled male germ lines with antibodies against GFP, to detect GFP::BRC-1, and the activating chromatin mark, H3K4me2, which is enriched on all chromosomes except the *X* (Reuben
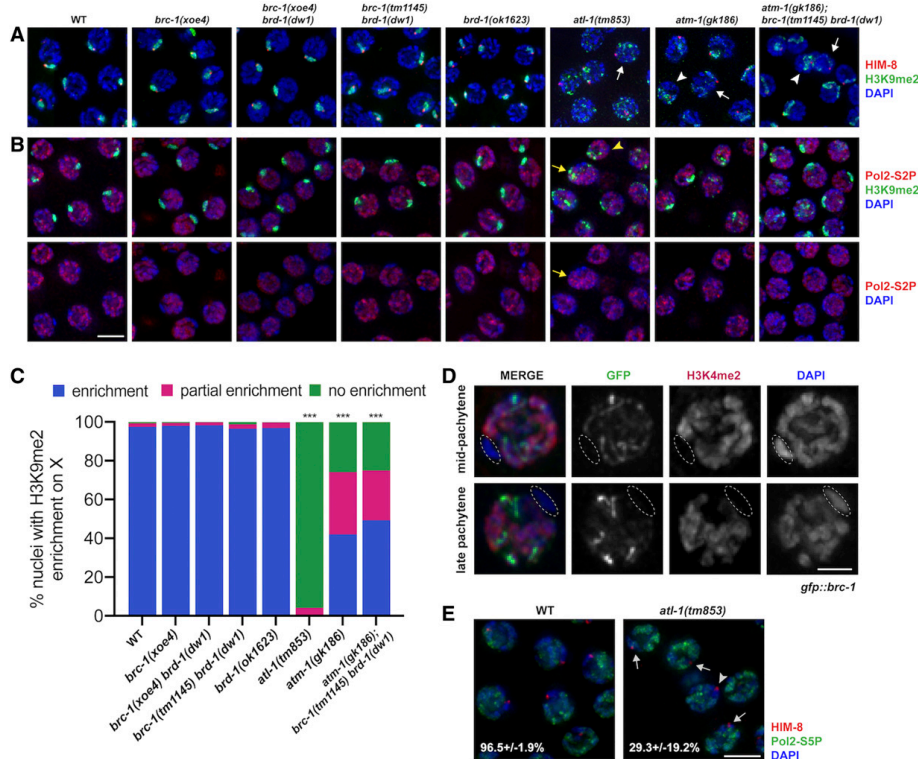
Figure 1 BRC-1-BRD-1 is not required for MSCI. Pachytene nuclei from *C. elegans* wild-type and indicated mutant male germ lines labeled with (A) anti-H3K9me2 (green; repressive chromatin), anti-HIM-8 (red; *X* chromosome marker), and counterstained with DAPI (blue); white arrows mark HIM-8 chromosomes largely lacking H3K9me2 while white arrowheads mark HIM-8 chromosomes with diffuse H3K9me2 labeling, or (B) anti-H3K9me2 (green), anti-Pol2-S2P (red; actively transcribing RNA polymerase II), and counterstained with DAPI (blue); lower panel shows anti-Pol2-S2P and DAPI; yellow arrows mark chromatin with both H3K9me2 and Pol2-S2P labeling while yellow arrowheads mark chromatin with neither H3K9me2 nor Pol2-S2p labeling. Images are projections through half of the gonad. Bar, 5 μm. (C) Quantification of enrichment of H3K9me2 on the *X* chromosome; enrichment = single strong track of H3K9me2 associated with HIM-8 (blue); partial enrichment = diffuse H3K9me2 signal associated with HIM-8 [arrowhead in (A)] (red); no enrichment = multiple H3K9me2 signals with no clear HIM-8 association [arrow in (A)] (green). Statistical comparisons between WT and mutants by Mann-Whitney: ***$P < 0.0001$. *atm-1(gk186)* and *atm-1(gk186)*; *brc-1(tm1145) brd-1(dw1)* were also statistically different from *atl-1(tm853)* ($P < 0.0001$). Number of germ lines, nuclei scored: WT = 3, 433; *brc-1(xoe4)* = 5, 398; *brc-1(xoe4) brd-1(dw1)* = 6, 654; *brc-1(tm1145) brd-1(dw1)* = 3, 257; *brd-1(ok1623)* = 6, 816; *atl-1(tm853)* = 4, 341; *atm-1(gk186)* = 3, 333; *atm-1(gk186)*; *brc-1(tm1145) brd-1(dw1)* = 7, 613. (D) GFP::BRC-1 (green) only localizes to synapsed chromosomes and does not localize to the single *X* chromosome in male meiotic nuclei. *X* chromosome (circled) identified by chromosome morphology and lack of anti-H3K4me2 staining (red); nuclei counterstained with DAPI (blue). Bar, 2 μm. (E) Pachytene nuclei labeled with anti-HIM-8 (red; *X* chromosome marker), anti-Pol2-S5P (green; marking transcriptionally competent chromatin) and counterstained with DAPI (blue); %± SD nuclei containing a *X* chromosome lacking Pol2-S5P labeling is indicated [arrowhead denotes nucleus without Pol2-S5P on *X* chromosome; arrows denote nuclei with *X* chromosome containing Pol2-S5P labeling in *atl-1(tm853)*)]. Bar, 5 μm. Number of germ lines, nuclei scored: WT = 3, 162; *atl-1(tm853)* = 6, 182. Statistical comparisons between WT and *atl-1(tm853)* by Mann-Whitney, $P = 0.0121$.

and Lin 2002; Bean *et al.* 2004; Jaramillo-Lambert and Engebrecht 2010; Checchi and Engebrecht 2011), and found that the chromosome lacking H3K4me2 also lacked GFP::BRC-1 (Figure 1D). Thus, contrary to mammals, *C. elegans* BRC-1-BRD-1 is not enriched on asynapsed sex chromosomes in male germ cells.

During mammalian MSCI, BRCA1 facilitates the recruitment of the phosphoinositide 3-kinase ataxia telangiectasia and RAD3-related (ATR) kinase to sex chromosomes; ATR in turn phosphorylates the histone variant H2AX (γ-H2AX) to facilitate chromosome compaction. Consequently, inactivation of either ATR or H2AX also results in MSCI failure (Fernandez-Capetillo *et al.* 2003; Turner *et al.* 2004; Royo *et al.* 2013). Given that BRC-1-BRD-1 is not essential for MSCI, and no H2AX variant has been identified in the *C. elegans* genome (Boulton 2006), we next addressed
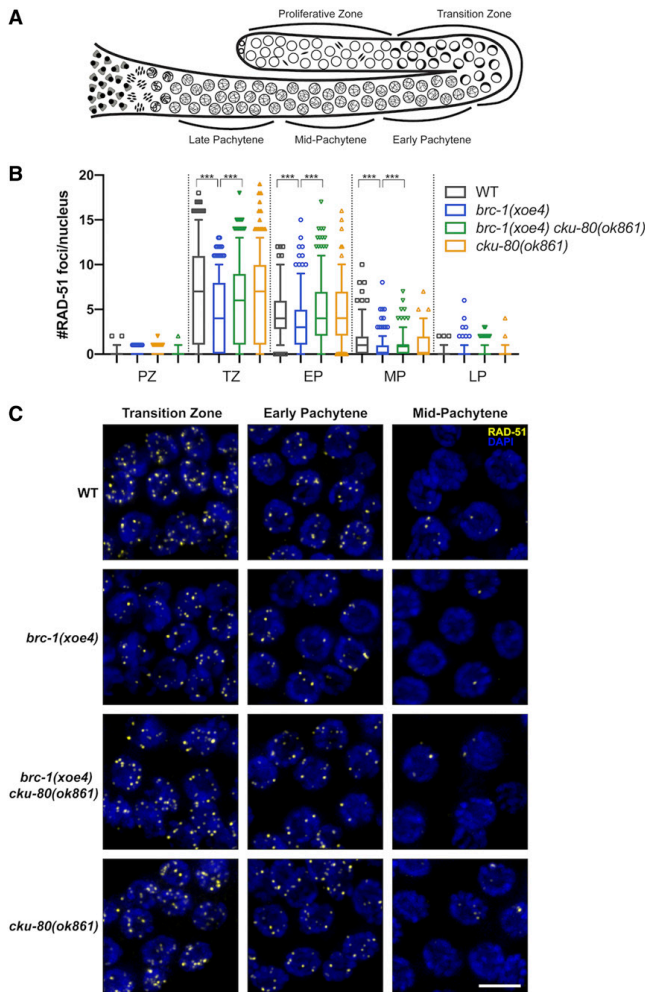
Figure 2 BRC-1-BRD-1 promotes HR at the expense of NHEJ in the male germ line. (A) Cartoon of the spatio-temporal organization of the *C. elegans* male germ line, modified from Van *et al.* (2016). (B) Quantification of RAD-51 in indicated regions of the germ line. Box whisker plots show number of RAD-51 foci per nucleus in the different regions. Horizontal line of each box represents the median, top and bottom of each box represents medians of upper and lower quartiles, lines extending above and below boxes indicate SD, and individual data points are outliers from 5 to 95%. Statistical comparisons by Mann–Whitney of WT *vs. brc-1(xoe4)* and *brc-1(xoe4) vs. brc-1(xoe4) cku-80(ok861)* in the different regions of the germ line; ***$P <$ 0.0001. All statistical comparisons are shown in Table S3. PZ, prolifer-ative zone; TZ, transition zone; EP, early pachytene; MP, mid-pachytene; LP, late pachytene. Number of germ lines and nuclei scored in each region: WT = 6, PZ = 958; TZ = 413; EP = 266; MP = 252; LP = 219; *brc-1(xoe4)* = 6, PZ = 848; TZ = 343; EP = 320; MP = 330; LP = 287; *brc-1(xoe4) cku-80(ok861)* = 6, PZ = 905; TZ = 316; EP = 296; MP = 329; LP = 289; *cku-80(ok861)* = 4, PZ = 814; TZ = 287; EP = 202; MP = 230; LP = 217. (C) Representative images of nuclei from indicated genotypes and regions of the germ line stained with antibodies against RAD-51 (yellow) and counterstained with DAPI (blue). Images are projections through half of the gonad. Bar, 5 μm.

whether the ATR ortholog, ATL-1, is required for enrichment of repressive chromatin on the *X* chromosome. To that end, we monitored the localization of H3K9me2 and HIM-8 in *atl-1(tm853)* deletion mutant male germ lines. In contrast to *brc-1* or *brd-1* mutants, mutation of *atl-1* resulted in altered distribution of H3K9me2. In most nuclei (95.9%), there was no clear association between HIM-8 and H3K9me2 (white arrow; Figure 1, A and C), indicating that the *X* chromosome was not specifically enriched for H3K9me2, and in the remaining nuclei (4.1%), H3K9me2 was associated with HIM-8 but had a much less compact signal (white arrow-head; Figure 1, A and C). Colabeling for Pol2-S2P and H3K9me2 revealed regions of the genome that were enriched for

both repressive chromatin and Pol2-S2P (yellow arrow; Figure 1B), as well as regions that were enriched for neither Pol2-S2P nor H3K9me2 (yellow arrowhead; Figure 1B), suggesting that the absence of ATL-1 disrupts the association between repressive chromatin and transcriptional silencing. As H3K9me2 is not a reliable marker of the *X* chromosome in the *atl-1* mutant, we next colabeled wild type and *atl-1* mutants with antibodies against HIM-8 and RNA Pol II phosphorylated on serine 5 (Pol2-S5P), which marks transcriptionally competent chromatin (Hsin and Manley 2012), to specifically examine the tran-scriptional status of the *X* chromosome. As previously report-ed (Checchi and Engebrecht 2011), Pol2-S5P is enriched on all chromosomes but the *X* in wild-type male germ lines.
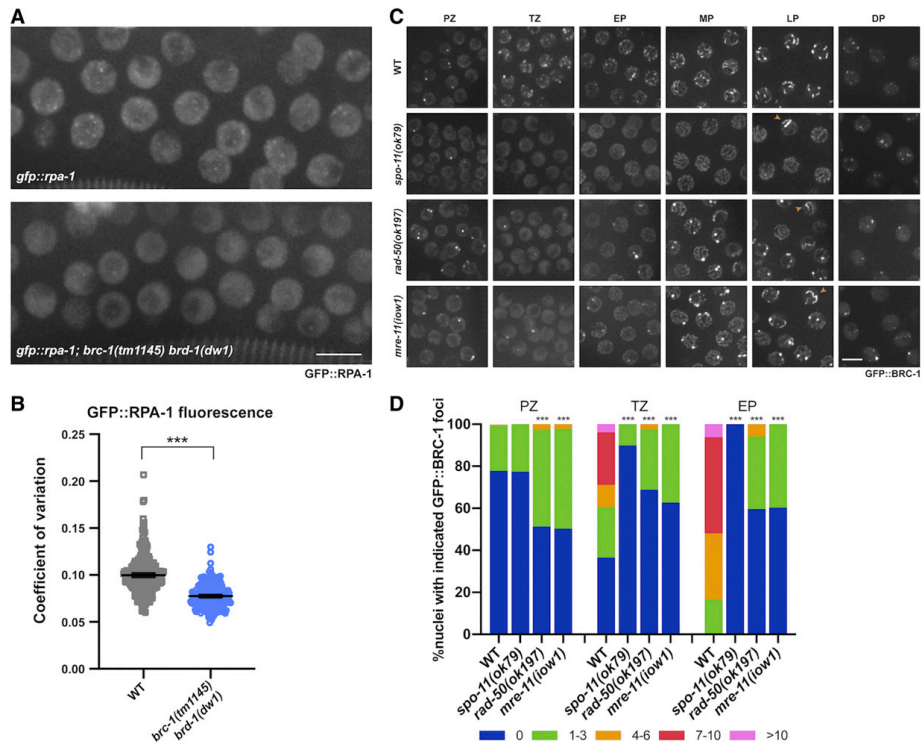
Figure 3 GFP::RPA-1 foci are reduced in the *brc-1 brd-1* mutant and GFP::BRC-1 concentration at foci in early meiotic prophase is dependent on meiotic DSB resection. (A) High-magnification images of wild-type and *brc-1(tm1145) brd-1(dw1)* transition zone/early pachytene nuclei in live worms expressing GFP::RPA-1. Images are projections through half of the gonad. Bar, 5 μm. (B) Coefficient of variation (SD/mean fluorescent intensity) of GFP::RPA-1 fluorescence is shown; six germ lines were analyzed for each genotype. Statistical comparisons between WT and *brc-1(tm1145) brd-1(dw1)* by Mann–Whitney: ***P < 0.0001. (C) Images of germ cells from live worms expressing GFP::BRC-1 from the indicated genetic backgrounds and gonad regions (PZ, proliferative zone; TZ, transition zone; EP, early pachytene; MP, mid-pachytene, LP, late pachytene, DP, diplotene). Images are projections through half of the gonad. Bar, 5 μm. (D) Number of GFP::BRC-1 foci in PZ, TZ, and EP in wild type and mutants. Numbers were binned as 0, 1–3, 4–6, 7–10, >10. A minimum of three germ lines were quantified for each genotype. Statistical comparisons between WT and mutants by Mann–Whitney: ***P < 0.0001. *spo-11(ok79)* is statistically different than either *rad-50(ok197)* or *mre-11(iow1)*: PZ: *P* < 0.0001; TZ: *spo-11(ok79) vs. rad-50(ok197) P* = 0.0002; *spo-11(ok79) vs. mre-11(iow1) P* < 0.0001; EP: *spo-11(ok79) vs. rad-50(ok197) P* < 0.0001; *spo-11(ok79) vs. mre-11(iow1) P* = 0.0004.

However, in only 29.3 ± 19.2% of *atl-1* nuclei Pol2-S5P was not observed on the *X* chromosome (*vs.* 96.5 ± 1.9% in wild type; *P* = 0.0121; arrowhead; Figure 1E). Thus, although BRC-1-BRD-1 does not appear to play a role in MSCI, ATL-1 is important for the correct targeting of H3K9me2 and transcriptional silencing of the *X* chromosome during *C. elegans* male meiosis.

ATR participates with the related and partially redundant kinase, ataxia-telangiectasia mutated (ATM) during DNA damage signaling (Abraham 2001). In mice, ATM does not play a role in MSCI (Royo *et al.* 2013). To determine whether ATM functions in targeting repressive chromatin to the *X* chromosome in *C. elegans*, we monitored H3K9me2 and HIM-8 in germ lines of the *atm-1(gk186)* deletion mutant. While 42.1% of nuclei were wild type with respect to

association between HIM-8 and H3K9me2, 32.1% of nuclei showed association between the signals but much more diffuse H3K9me2 labeling, and 25.8% showed no association between HIM-8 and H3K9me2 (Figure 1, A and C). Similarly, Pol2-S2P showed a variable staining pattern with some nuclei containing a single track lacking Pol2-S2P and enriched for H3K9me2, which presumably corresponds to the *X* chromosome, while in other nuclei no clear chromosome lacking Pol2-S2P was detected (Figure 1B). Thus, in *C. elegans*, ATL-1, and to a lesser extent ATM-1, are important for accumulation of repressive chromatin and transcriptional silencing of the *X* chromosome.

To determine whether a function for BRC-1-BRD-1 in the correct targeting of repressive chromatin and transcriptional silencing of the *X* chromosome can be uncovered in the
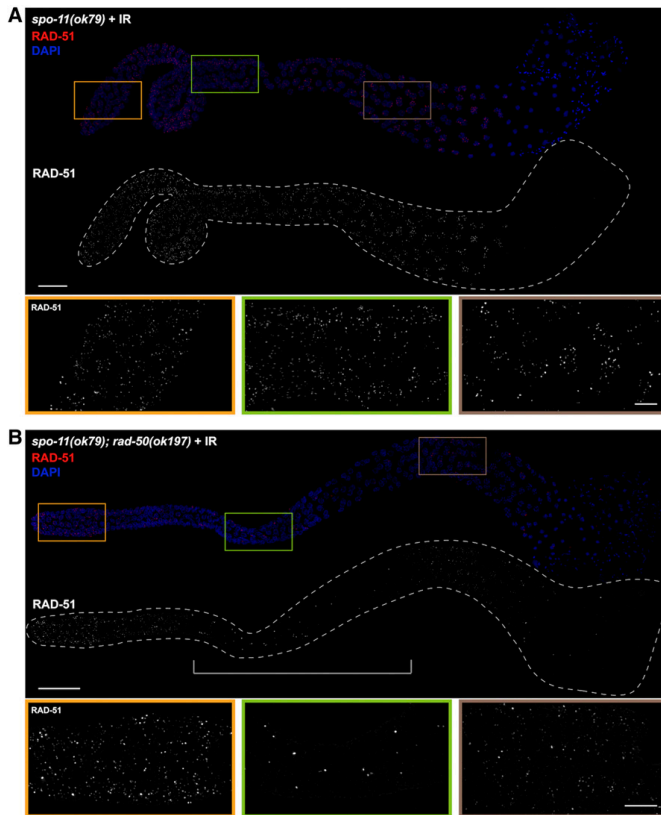
Figure 4 RAD-51 loading is dependent on RAD-50 in male meiotic germ cells. (A) *spo-11(ok79)* and (B) *spo-11(ok79)*; *rad-50(ok197)* male gonads fixed and dissected 1 hr after exposure to 10 Gys IR, stained with RAD-51 antibody (red), and counterstained with DAPI (blue). In the *spo-11*; *rad-50* mutant RAD-51 foci are largely absent in most nuclei in the central portion of the gonad, indicated by the bracket, from the onset of meiotic prophase to mid-pachytene. Images are projections through the entire gonad. Four germ lines were examined. Bar, 20 μm. Insets show selected nuclei from different regions of the germ line; Bar, 5 μm.

sensitized *atm-1* mutant background, we examined H3K9me2 and HIM-8 as well as H3K9me2 and Pol2-S2P in the *atm-1(gk186)*; *brc-1(tm1145) brd-1(dw1)* triple mutant (Figure 1, A–C). We found no difference in either H3K9me2 or Pol2-S2P localization between *atm-1(gk186)* and *atm-1(gk186)*; *brc-1(tm1145) brd-1 (dw1)*, consistent with BRC-1-BRD-1 being dispensable for transcriptional silencing of the *X* chromosome in *C. elegans* male germ cells.

A subset of meiotic DSBs is repaired by NHEJ in the absence of BRC-1-BRD-1 in male germ cells

BRCA1-BARD1 has been implicated in promoting HR repair in somatic cells; however, its role in meiotic recombination has been controversial and is complicated by the pachytene arrest and apoptotic removal of *brca1* mutant spermatocytes due to MSCI failure (Xu *et al.* 2003; Broering *et al.* 2014). The finding that neither *brc-1* nor *brd-1* mutants impair *X* chromosome transcriptional silencing in *C. elegans* prompted us to examine the role of BRC-1-BRD-1 in meiotic recombination in the absence of the complications associated with MSCI failure. To that end, we monitored meiotic DSB repair by

examining the assembly and disassembly of the recombinase RAD-51 (Rinaldo *et al.* 2002) in the spatiotemporal organization of the *C. elegans* male germ line using antibodies against RAD-51 (Colaiácovo *et al.* 2003; Checchi *et al.* 2014) (Figure 2A).

brc-1 and *brd-1* mutant hermaphrodites exhibit a slight increase in embryonic lethality and male progeny (a readout of *X* chromosome nondisjunction), and some RAD-51 foci perdure in late meiotic prophase, suggesting that repair of a subset of meiotic DSBs is delayed in the absence of BRC-1-BRD-1 (Boulton *et al.* 2004; Adamo *et al.* 2008; Janisiw *et al.* 2018; Li *et al.* 2018). In contrast to the appearance of more RAD-51 foci in mid and late pachytene in female germ cells, fewer RAD-51 foci were observed in *brc-1*, *brd-1* or *brc-1 brd-1* male germ cells compared to wild type in early meiotic prophase (transition zone) through mid-pachytene (Figure 2, B and C and Figure S1). These results suggest that, in the absence of BRC-1-BRD-1, fewer DSBs are induced, a subset of DSBs is repaired without loading RAD-51, RAD-51 loading is impaired, and/or repair occurs with faster kinetics than wild type. Given a
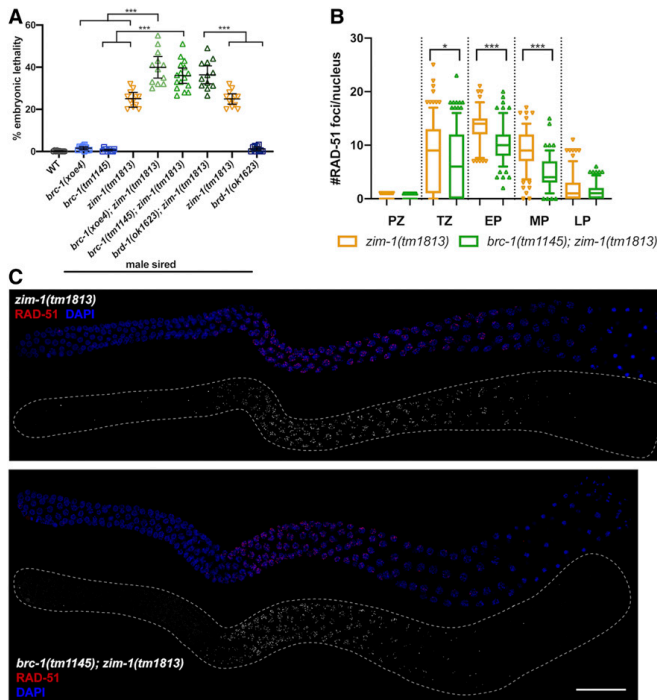
Figure 5 Progeny embryonic lethality is enhanced when sired by *brc-1*; *zim-1* or *brd-1*; *zim-1* double mutant males but RAD-51 stability in not impaired. (A) Embryonic lethality of *fog-2(q71)* progeny sired by *brc-1(xoe4)*, *brc-1(tm1145)*, *zim-1(tm1813)*, *brc-1(xoe4)*; *zim-1(tm1813)*, *brc-1(tm1145)*; *zim-1(tm1813)*, *brd-1(ok1623)*; *zim-1(tm1813)*, *brd-1(ok1623)* males. Mean and 95% confidence intervals are shown. The genetic interaction between *brc-1* or *brd-1* and *zim-1* is significant by a one-way ANOVA (***$P < 0.0001$). A minimum of 10 worms were scored for each genotype. (B) Box whisker plots show average number of RAD-51 foci per nucleus in the different zones. Horizontal line of each box indicates the median, the top and bottom of the box indicates medians of upper and lower quartiles, lines extending above and below boxes indicate SD and individual data points are outliers from 5 to 95%. Statistical comparisons by Mann–Whitney of *zim-1(tm1813)* *vs.* *brc-1(tm1145)*; *zim-1(tm1813)* in the different regions of the germ line: *$P < 0.05$; ***$P < 0.0001$. PZ, proliferative zone; TZ, transition zone; EP, early pachytene; MP, mid-pachytene; LP, late pachytene. Numbers of nuclei scored from four germ lines in each zone for *zim-1*: PZ = 668; TZ = 237; EP = 111; MP = 151; LP = 167 and *brc-1*; *zim-1*: PZ = 545; TZ = 318; EP = 155; MP = 137; LP = 149. (C) *zim-1(tm1813)* and *brc-1(tm1145)*; *zim-1(tm1813)* mutant germ lines stained with anti-RAD-51 antibody (red) and counterstained with DAPI (blue). Images are projections through half of the gonad. A minimum of four germ lines were imaged. Bar, 20 μm.

role of BRCA1 in promoting HR at the expense of NHEJ in somatic cells (Daley and Sung 2014), we tested the hypothesis that some meiotic DSBs are repaired by NHEJ in the absence of BRC-1-BRD-1 in male germ cells. To that end, we simultaneously inactivated BRC-1 or BRD-1 and CKU-80 or CKU-70, the *C. elegans* KU80/KU70 orthologs that mediate NHEJ, and monitored RAD-51 foci throughout the germ line (Figure 2, B and C and Figure S1). When NHEJ was inactivated in the *brc-1* or *brd-1* mutants, RAD-51 foci were restored to wild-type levels in the transition zone through mid-pachytene in male germ cells. We also observed a small, but statistically significant elevation of RAD-51 foci in late pachytene when both BRC-1-BRD-1 and NHEJ were mutated, suggesting that both of these complexes contribute to repair of lesions at late pachytene (Figure S1B and Table S3), similar to what has been observed in oogenesis (Smolikov *et al.* 2007; Adamo *et al.* 2008). Together, these results suggest that BRC-1-BRD-1 functions at, or prior to, RAD-51 assembly to facilitate repair by HR in male germ cells, similar to its proposed role in somatic cells, and, in its absence, some breaks are channeled through NHEJ in early meiotic prophase.

BRC-1-BRD-1 promotes the early processing of meiotic DSBs in male germ cells

Following DSB formation, DNA end resection reveals 3′ single-stranded tails that promote homology search and strand invasion (Ranjha *et al.* 2018). To examine a potential role of BRC-1-BRD-1 in DNA end resection, we analyzed the localization pattern of RPA-1 (GFP::RPA-1; Sonneville *et al.* 2012) by live cell imaging. RPA-1 binds single-stranded DNA ends, and its recruitment to DSBs is dependent on resection (Garcia-Muse and Boulton 2005; Sartori *et al.* 2007; Koury *et al.* 2018). RPA-1 also associates with post-strand-exchange intermediates (Woglar and Villeneuve 2018). In transition zone to mid-pachytene, where DSBs are formed and processed, we observed abundant foci in addition to strong nucleoplasmic fluorescence in wild-type male germ lines. In *brc-1(tm1145) brd-1(dw1)* male germ lines, we observed fewer and less intense foci above the nucleoplasmic signal (Figure 3A). To quantify this, we calculated the CV (CV = SD/mean fluorescence intensity), which provides a measure of the extent of foci above the nucleoplasmic signal. Wild type had a significantly higher CV compared to the *brc-1 brd-1* mutant ($P < 0.0001$; Figure 3B), suggesting that fewer RPA-1 molecules accumulated at processed DSBs in the mutant. Taken together, the alteration in both RAD-51 and RPA-1 suggests that BRC-1-BRD-1 facilitates the repair of DSBs by HR most likely through promoting DNA end resection.

To determine whether BRC-1-BRD-1 localizes to DSBs, we examined the localization of GFP::BRC-1 by live cell imaging.
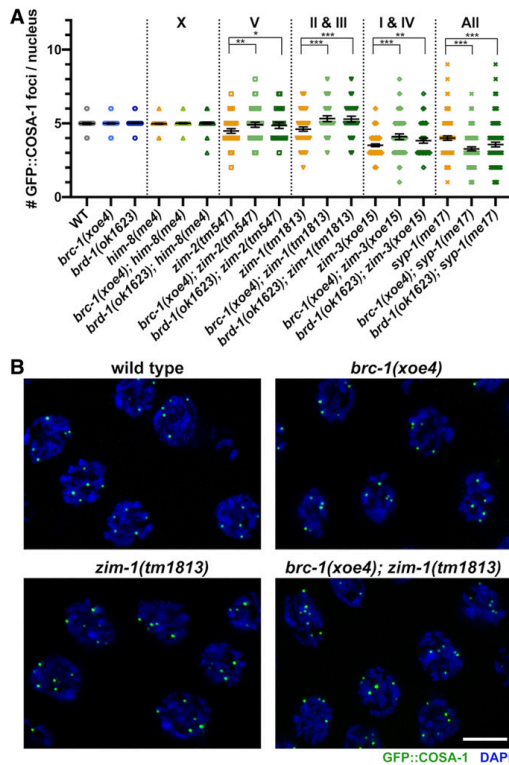
Figure 6 BRC-1-BRD-1 inhibits GFP::COSA-1 marked crossover (CO) precursors when a subset of chromosomes fails to form COs. (A) Number of COSA-1 foci in mid- to late-pachytene in indicated mutants; mean and 95% confidence intervals are shown. Letters/numbers above graph indicate which chromosomes are asynapsed in the different mutants. Statistical comparisons by Mann–Whitney *$P <$ 0.05; **$P <$ 0.001; ***$P <$ 0.0001. Number of nuclei scored: *gfp::cosa-1* = 97, *gfp::cosa-1; brc-1(xoe4)* = 194, *gfp::cosa-1; brd-1(ok1623)* = 103, *gfp::cosa-1; him-8(me4)* = 151, *gfp::cosa-1; brc-1(xoe4); him-8(me4)* = 183, *gfp::cosa-1; brd-1(ok1623); him-8(me4)* = 172, *gfp::cosa-1; zim-2(tm547)* = 125, *gfp::cosa-1; brc-1(xoe4); zim-2(tm547)* = 128, *gfp::cosa-1; brd-1(ok1623); zim-2* = 84, *gfp::cosa-1; zim-1(tm1813)* = 120, *gfp::cosa-1; brc-1(xoe4); zim-1(tm1813)* = 100, *gfp::cosa-1; brd-1(ok1623); zim-1(tm1813)* = 97, *gfp::cosa-1; zim-3(xoe15)* = 308, *gfp::cosa-1; brc-1(xoe4); zim-3(xoe15)* = 133, *gfp::cosa-1; brd-1(ok1623); zim-3(xoe15)* = 145, *gfp::cosa-1; syp-1(me17)* = 271, *gfp::cosa-1; brc-1(xoe4); syp-1(me17)* = 281, *gfp::cosa-1; brd-1(ok1623); syp-1(me17)* = 344. (B) Half projections of late pachytene region showing GFP::COSA-1 (green) and DAPI (blue) in wild type, *brc-1(xoe4)*, *zim-1(tm1813)* and *brc-1(xoe4); zim-1(tm1813)*. Bar, 5 μm.

In wild-type male germ lines, GFP::BRC-1 was nucleoplasmic and formed a small number of bright foci in proliferating germ cells (Figure 3, C and D). As cells progressed into meiosis, GFP::BRC-1 was observed in multiple foci at transition zone and early pachytene; tracks of fluorescence were also beginning to form at early pachytene (Figure 3, C and D). At

mid-pachytene, GFP::BRC-1 was predominantly in tracks, which had begun to concentrate on a chromosomal subdomain. Further concentration into five stretches and then puncta were observed in late pachytene through diplotene. The dynamic localization of GFP::BRC-1 in the male germ line is similar to the hermaphroditic germ line: GFP::BRC-1 foci partially overlap with RAD-51 (Figure S2A), suggesting they mark sites of ongoing meiotic recombination, and the GFP::BRC-1 tracks in pachytene colocalize with the synaptonemal complex (SC) that become concentrated on the short arm, dependent on CO formation (Li *et al.* 2018).

To test the dependencies of BRC-1 localization on DSB formation and processing, we examined GFP::BRC-1 in *spo-11*, *rad-50* and *mre-11* mutants. *spo-11* mutants are unable to form meiotic DSBs (Dernburg *et al.* 1998), and very few GFP::BRC-1 foci were present in transition zone and early pachytene compared to wild type (Figure 3, C and D). At early to mid-pachytene GFP::BRC-1 was observed in tracks in the *spo-11* mutant similar to wild type (Figure 3C), as synapsis occurs in the absence of recombination in *C. elegans* (Dernburg *et al.* 1998). In late pachytene, GFP::BRC-1 fluorescence did not concentrate on a portion of each chromosome pair as in wild type, consistent with these events being dependent on CO formation. However, in 10.7 $\pm$ 3.2% of pachytene nuclei there was enrichment of GFP::BRC-1 on a chromosome track (Figure 3C, arrowhead) with weak fluorescence on the other synapsed chromosomes. This has been observed for GFP::BRC-1 and other synapsis markers in oogenesis and likely represents *spo-11*-independent lesions capable of recruiting meiotic DNA repair components and altering SC properties (Machovina *et al.* 2016; Nadarajan *et al.* 2017; Pattabiraman *et al.* 2017; Li *et al.* 2018).

We next examined the requirement for RAD-50 and MRE-11 in recruitment of GFP::BRC-1 to early meiotic foci. RAD-50 and MRE-11 form a complex with NBS-1 (MRX/N complex) and are required for both DSB formation and processing for repair through HR in meiotic cells, in addition to playing a role in repair of lesions generated during DNA replication (Chin and Villeneuve 2001; Hayashi *et al.* 2007; Girard *et al.* 2018). In *rad-50(ok197)* and *mre-11(ok179)* null mutants, GFP::BRC-1 was observed in fewer foci compared to wild type in transition zone and early pachytene (Figure 3, C and D and Figure S2B). However, in contrast to *spo-11*, an increased number of nuclei with 1–3 GFP::BRC-1 foci were present in proliferating germ cells and throughout meiotic prophase (Figure 3, C and D), suggesting GFP::BRC-1 is enriched at lesions generated during S phase in these mutant backgrounds. We also observed an earlier appearance and higher percentage of nuclei showing concentrated signal on a subset of chromosomes (*rad-50(ok197)*, 21.17 $\pm$ 4.6%), consistent with recruitment of recombination proteins and alteration of the SC properties at mitotic lesions as they progress through meiosis. Together, these results suggest that the enrichment of GFP::BRC-1 to abundant foci in early meiotic prophase is dependent on meiotic DSB formation.
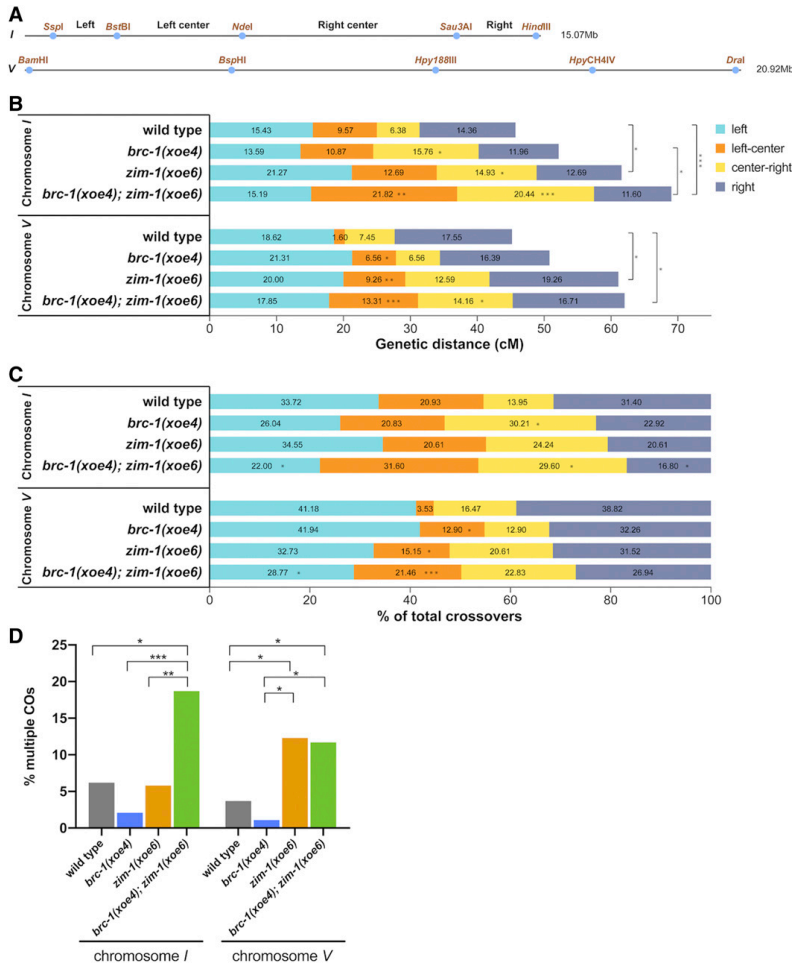
Figure 7 BRC-1 alters the CO landscape in the *zim-1* mutant during male meiosis. (A) SNP markers on chromosome *I* and *V* used for genotyping; primers and additional information are included in Table S2. (B) CO frequency on chromosome *I* in wild type (*n* = 188), *brc-1(xoe4)* (*n* = 184), *zim-1(xoe6)* (*n* = 268) and *brc-1(xoe4)*; *zim-1(xoe6)* (*n* = 362) mutants and on chromosome *V* in wild type (*n* = 188), *brc-1(xoe4)* (*n* = 183), *zim-1(xoe6)* (*n* = 270) and *brc-1(xoe4)*; *zim-1(xoe6)* mutants. *n* = number of individuals analyzed per genotype. (C) CO distribution among recombinants on chromosome *I* and *V* in wild type, *brc-1(xoe4)*, *zim-1(xoe6)*, and *brc-1(xoe4)*; *zim-1(xoe6)* mutants. (D) Percent of recombinant chromosomes containing multiple COs calculated as 100 × (DCO + TCOs)/(SCO + DCOs + TCOs). Statistical analyses were conducted using Fisher exact test on 2 × 2 contingency tables, *$P < 0.05$; **$P < 0.001$; ***$P < 0.0001$.

To determine the requirement for DSB end processing in recruiting GFP::BRC-1 to sites of meiotic recombination, we took advantage of a separation-of-function allele, *mre-11(iow1)*; worms harboring this allele are competent for meiotic DSB formation but defective in resection (Yin and Smolikove 2013). As with *rad-50(ok197)* and *mre-11(ok179)* null mutants, there was a reduction in meiotic GFP::BRC-1 foci in *mre-11(iow1)* mutant germ lines (Figure 3, C and D) and a similar number of pachytene nuclei showing concentration of GFP::BRC-1 on a subset of chromosomes [*mre-11(iow1)*, 19.23 ± 2.8%]. These results suggest that accumulation of GFP::BRC-1 into foci in early meiotic prophase requires DSB resection, consistent with BRC-1-BRD-1 functioning at an early step of meiotic DSB processing to promote HR.

RAD-51 loading is dependent on RAD-50 in male meiotic germ cells

Meiotic recombination occurs in the context of specialized chromosome structure, the chromosomal axes, and fully formed SC, to promote interhomolog COs. Previous analyses in oogenic germ lines revealed a requirement for RAD-50 in loading RAD-51 at DSBs in meiotic prophase (Hayashi *et al.* 2007). Given the somatic-like role of BRC-1-BRD-1 in promoting HR at the expense of NHEJ in meiotic male germ cells, and the dependency of BRC-1 localization at meiotic DSBs on RAD-50, we next addressed whether male meiosis also requires RAD-50 for loading RAD-51 in the context of synapsed chromosomes. To that end, we analyzed RAD-51 localization in *spo-11(ok79)* and *spo-11(ok79)*; *rad-50(ok197)* male germ

Table 1 Crossover (CO) interference on chromosome *I* and *V*

WT (*I*)	exp DCO freq	obs DCO freq	c.o.c	interference
L - LC	0.0148	0.0160	1.0805	−0.0805
L - CR	0.0098	0.0000	0.0000	1.0000
L - R	0.0222	0.0106	0.4802	0.5198
LC - R	0.0138	0.0000	0.0000	1.0000
CR - R	0.0092	0.0000	0.0000	1.0000
LC - CR	0.0061	0.0000	0.0000	1.0000

WT (*V*)	exp DCO freq	obs DCO freq	c.o.c	interference
L - LC	0.0030	0.0000	0.0000	1.0000
L - CR	0.0139	0.0000	0.0000	1.0000
L- R	0.0327	0.0106	0.3255	0.6745
LC - R	0.0028	0.0000	0.0000	1.0000
CR - R	0.0131	0.0053	0.4069	0.5931
LC- CR	0.0012	0.0000	0.0000	1.0000

brc-1 (*I*)	exp DCO freq	obs DCO freq	c.o.c	interference
L - LC	0.0148	0.0000	0.0000	1.0000
L - CR	0.0214	0.0054	0.2538	0.7462
L - R	0.0162	0.0054	0.3345	0.6655
LC - R	0.0130	0.0000	0.0000	1.0000
CR - R	0.0188	0.0000	0.0000	1.0000
LC - CR	0.0171	0.0000	0.0000	1.0000

brc-1 (*V*)	exp DCO freq	obs DCO freq	c.o.c	interference
L - LC	0.0140	0.0000	0.0000	1.0000
L - CR	0.0140	0.0000	0.0000	1.0000
L - R	0.0349	0.0055	0.1564	0.8436
LC - R	0.0107	0.0000	0.0000	1.0000
CR - R	0.0107	0.0000	0.0000	1.0000
LC - CR	0.0043	0.0000	0.0000	1.0000

zim-1 (*I*)	exp DCO freq	obs DCO freq	c.o.c	interference
L - LC	0.0270	0.0000	0.0000	1.0000
L - CR	0.0317	0.0149	0.4702	0.5298
L - R	0.0270	0.0112	0.4149	0.5851
LC - R	0.0161	0.0037	0.2318	0.7682
CR - R	0.0189	0.0037	0.1971	0.8029
LC - CR	0.0189	0.0000	0.0000	1.0000

zim-1 (*V*)	exp DCO freq	obs DCO freq	c.o.c	interference
L - LC	0.0185	0.0037	0.2000	0.8000
L - CR	0.0252	0.0148	0.5882	0.4118
L - R	0.0385	0.0333	0.8654	0.1346
LC - R	0.0178	0.0111	0.6231	0.3769
CR - R	0.0243	0.0037	0.1527	0.8473
LC - CR	0.0117	0.0074	0.6353	0.3647

brc-1; zim-1 (*I*)	exp DCO freq	obs DCO freq	c.o.c	interference
L - LC	0.0332	0.0138	0.4166	0.5834
L - CR	0.0311	0.0304	0.9784	0.0216
L - R	0.0176	0.0110	0.6268	0.3732
LC - R	0.0253	0.0193	0.7637	0.2363
CR - R	0.0237	0.0110	0.4659	0.5341
LC - CR	0.0446	0.0331	0.7431	0.2569

brc-1; zim-1 (*V*)	exp DCO freq	obs DCO freq	c.o.c	interference
L - LC	0.0238	0.0170	0.7153	0.2847
L - CR	0.0253	0.0085	0.3362	0.6638
L - R	0.0298	0.0227	0.7598	0.2402

(continued)

Table 1, *continued*

brc-1; zim-1 (*V*)	exp DCO freq	obs DCO freq	c.o.c	interference
LC - R	0.0223	0.0057	0.2546	0.7454
CR - R	0.0237	0.0085	0.3590	0.6410
LC - CR	0.0189	0.0028	0.1502	0.8498

L, left interval; LC, left-center interval; CR, center-right interval; R, right interval; DCO, double crossover; expected DCO: (crossover frequency at interval "A") × (crossover frequency at interval "B"). c.o.c. (coefficient of coincidence) = actual DCO frequency/expected DCO frequency; Interference = 1- c.o.c. See Table S4 for data used for calculations.

cells. DNA breaks were induced by exposing worms to 10 Gys of IR; 1 hr post-IR, gonads were dissected and labeled with antibodies against RAD-51 (Hayashi *et al.* 2007). Abundant RAD-51 foci were observed throughout the germ line in the *spo-11* worms, indicating proficient loading of RAD-51 on IR-induced DSBs (Figure 4A). Abundant RAD-51 foci were also observed in irradiated *spo-11*; *rad-50* double mutant germ lines in proliferating germ cells and in mid- to late pachytene/ diplotene spermatocytes (Figure 4B). However, in a region extending from the transition zone to mid- to late pachytene very few foci were observed in the irradiated *spo-11*; *rad-50* double-mutant germ lines. Thus, similar to oogenesis, RAD-51 loading is dependent on RAD-50 during meiotic prophase in spermatogenic germ lines. Together, our genetic and cell biological analyses of BRC-1-BRD-1 and DSB processing factors suggest that properties of both somatic and meiotic repair modes exist in male germ cells.

BRC-1-BRD-1 is important when CO formation is blocked on a subset of chromosomes during spermatogenesis

In somatic cells, BRCA1 plays a critical role when errors in the cell cycle occur (Takaoka and Miki 2018) and we previously found that removal of BRC-1-BRD-1 during oogenesis impairs progeny viability and RAD-51 stabilization when CO formation is blocked on a subset of chromosomes (Li *et al.* 2018). To examine the consequence of inactivating BRC-1-BRD-1 under similar conditions during male meiosis, we monitored the viability of progeny sired by mutant *zim-1(tm1813)* [chromosomes *II* and *III* fail to pair and synapse (Phillips and Dernburg 2006)], *brc-1(xoe4)*; *zim-1(tm1813)*, *brc-1(tm1145)*; *zim-1(tm1813)* and *brd-1(ok1623)*; *zim-1 (tm1813)* males. *brc-1(tm1145)* is a hypomorphic allele that we previously showed impairs recombination under meiotic checkpoint activating conditions in oogenesis (Li *et al.* 2018). We used worms carrying the *fog-2(q71)* mutation for these experiments to eliminate hermaphrodite spermatogenesis, rendering *XX* animals self-sterile (Schedl and Kimble 1988), so that the contribution of the male parent to embryonic lethality could be assessed unambiguously. Similar to our findings in hermaphrodites (Li *et al.* 2018), removal of BRC-1 or BRD-1 enhanced the embryonic lethality of *zim-1* mutants when mutant sperm were used to fertilize *fog-2* ova (Figure 5A; *P* < 0.0001 by one-way ANOVA). These results suggest that BRC-1-BRD-1 plays important roles to enhance
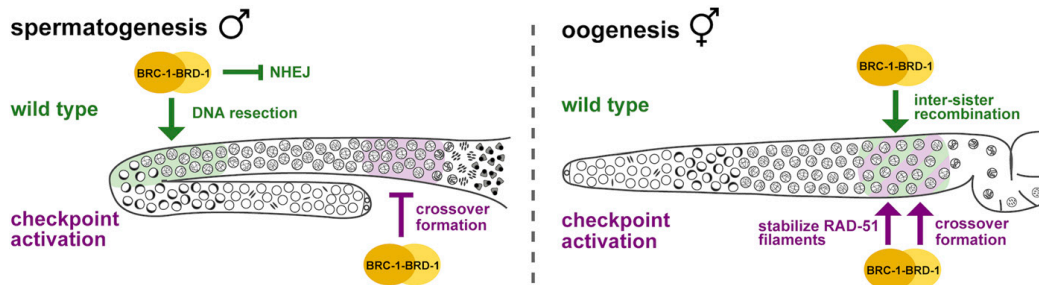
Figure 8 BRC-1-BRD-1 function in spermatogenesis and oogenesis. Model of proposed function of BRC-1-BRD-1 in male and female (hermaphrodite) germ lines. Wild type (green) and checkpoint activation conditions (*e.g.*, *zim-1*; purple) are shown. During spermatogenesis BRC-1-BRD-1 promotes HR at the expense of NHEJ presumably through regulating DNA end resection in early meiotic prophase, while the complex promotes intersister recombination in late meiotic prophase during oogenesis. Under checkpoint activation, BRC-1-BRD-1 inhibits COSA-1-marked COs in male meiosis, either directly or as a consequence of a role for BRC-1-BRD-1 in promoting intersister repair. In female meiosis, BRC-1-BRD-1 mediates the stability of the RAD-51 filament and promotes COSA-1-marked COs. The different phenotypes observed in *brc-1* and *brd-1* mutants are likely a consequence of the complex ubiquitinating different substrates dependent on the distinctive temporal regulation of spermatogenesis *vs.* oogenesis.

the quality of male germ cells under meiotic checkpoint activating conditions.

Previous analyses in the hermaphrodite germ line revealed that RAD-51 levels are elevated genome wide when the obligate CO is not established on any or all chromosome pairs (Colaiácovo *et al.* 2003; Carlton *et al.* 2006; Mets and Meyer 2009). Removal of BRC-1-BRD-1 under these conditions resulted in a "dark zone" of RAD-51 in mid- to late pachytene, which is likely a consequence of premature RAD-51 disassembly (Li *et al.* 2018). To determine whether BRC-1-BRD-1 promotes RAD-51 filament stability in male germ lines when not all chromosomes are connected by a CO, we monitored RAD-51 levels in *zim-1* mutants in the presence and absence of BRC-1-BRD-1. Similar to oogenic germ lines, blocking CO formation on a subset of chromosomes resulted in elevated levels of RAD-51 foci throughout meiotic prophase in male germ lines (Figure 5, B and C). However, in the absence of BRC-1, we did not observe a RAD-51 "dark zone," suggesting that BRC-1-BRD-1 does not play a role in stabilizing the RAD-51 filament under checkpoint activating conditions in male germ cells (Figure 5C). Quantification of foci revealed reduced RAD-51 levels in *brc-1*; *zim-1* compared to *zim-1* (Figure 5B), similar to the reduction in RAD-51 foci observed in *brc-1* or *brd-1* mutants alone compared to wild-type males (Figure 2B). However, the RAD-51 levels in *brc-1*; *zim-1* were still higher throughout pachytene than in wild-type male germ lines (compare Figure 2B and Figure 5B). These results suggest that BRC-1-BRD-1 promotes meiotic recombination in spermatogenesis using different mechanisms than in oogenesis under meiotic checkpoint activation.

BRC-1-BRD-1 inhibits COSA-1-marked CO designation sites when meiosis is perturbed in male germ cells

In addition to stabilizing the RAD-51 filament, BRC-1-BRD-1 promotes formation of CO precursors marked by the cyclin related COSA-1 (Yokoo *et al.* 2012) in the *zim-1* mutant

background in hermaphrodites (Li *et al.* 2018). To determine whether BRC-1-BRD-1 influences CO designation in male germ cells, we monitored GFP::COSA-1 (Yokoo *et al.* 2012) in *brc-1*, *brd-1*, *zim-1*, *brc-1*; *zim-1* and *brd-1*; *zim-1* mutant germ lines. Wild-type males mostly exhibit five COSA-1 foci, one on each of the five pairs of autosomes but not on the single *X* chromosome (Checchi *et al.* 2014). This pattern was unaltered by removal of either BRC-1 or BRD-1 [WT = 4.99 ± 0.30; *brc-1(xoe4)* = 4.99 ± 0.30; *brd-1(ok1623)* = 5.02 ± 0.28; Figure 6A]. As *zim-1* mutants have two asynapsed chromosome pairs, we expected to observe three COSA-1 foci; however, we observed an average of 4.61 ± 1.12 COSA-1 foci (Figure 6A). Further, removing BRC-1 or BRD-1 in *zim-1* males resulted in significantly more COSA-1 foci (*brc-1(xoe4)*; *zim-1(tm1813)* = 5.32 ± 0.97; *brd-1(ok1623)*; *zim-1(tm1813)* = 5.29 ± 0.99) (Figure 6, A and B). This is opposite to what we observed in hermaphrodites, where reduced levels of GFP::COSA-1 was observed in the absence of BRC-1 or BRD-1 in *zim-1* mutants (Li *et al.* 2018).

To examine this further, we monitored GFP::COSA-1 foci in additional mutants that lead to asynapsis of different chromosome pairs. Pairing and synapsis of the *X* chromosome is impaired in *him-8* mutants, *zim-2* mutants have asynapsed chromosome *Vs* and two chromosome pairs, *I* and *IV*, fail to pair and synapse in *zim-3* mutants (Phillips *et al.* 2005; Phillips and Dernburg 2006). As expected, mutation of *him-8* had no effect on GFP::COSA-1 levels either in the presence or absence of BRC-1-BRD-1, presumably due to the presence of the single *X* chromosome in male germ cells (Figure 6A). *zim-2* and *zim-3* mutants showed higher than expected numbers of COSA-1 foci (*zim-2(tm547)* = 4.48 ± 0.85 observed *vs.* four expected, *zim-3(xoe15)* = 3.52 ± 0.80 observed *vs.* three expected), similar to what we observed in the *zim-1* mutant and the number was further increased upon removal of BRC-1-BRD-1 [*brc-1(xoe4)*; *zim-2(tm574)* = 4.91 ± 0.96, *brd-1(ok1623)*; *zim-2(tm574)* = 4.86 ± 0.93, *brc-1(xoe4)*; *zim-3(xoe15)* = 4.09 ± 1.12,

brd-1(ok1623); *zim-3(xoe15)* = 3.83 ± 1.10] (Figure 6A). Thus, BRC-1-BRD-1 limits the number of CO precursors in spermatogenesis under circumstances where asynapsed chromosomes are present.

Previous analyses in oogenesis had indicated that when CO formation is completely blocked by mutation of central components of the SC, COSA-1 accumulates at foci that represent aberrant recombination sites (Li *et al.* 2018; Woglar and Villeneuve 2018; Cahoon *et al.* 2019; Hurlock *et al.* 2020). We next examined GFP::COSA-1 in *syp-1* mutant males, in which germ cells fail to undergo chromosome synapsis and therefore do not form any interhomolog COs (MacQueen *et al.* 2002). As observed in hermaphrodites, *syp-1* mutant males exhibited a significant number of COSA-1 foci (4.0 ± 1.20) (Figure 6A). However, in the absence of BRC-1 or BRD-1, fewer GFP::COSA-1 foci were observed [*brc-1(xoe4)*; *syp-1(me17)*=3.27 ± 1.15, *brd-1(ok1623)*; *syp-1(me17)*=3.56 ± 1.51]. This suggests that unlike the situation where CO formation is inhibited on only a subset of chromosomes, BRC-1-BRD-1 promotes the localization of COSA-1 at recombination sites when no interhomolog COs can form.

BRC-1 influences the CO landscape

Given the effect of BRC-1-BRD-1 on COSA-1 foci in the different mutants, we monitored genetic linkage between SNP markers on chromosomes *I* and *V* in male Bristol/Hawaiian hybrid strains to assess whether BRC-1-BRD-1 alters the formation of *bona fide* COs (Figure 7A). Inactivation of BRC-1 had little effect on the genetic map length of either chromosome *I* or *V* [*I*: WT = 45.74 cM; *brc-1(xoe4)* = 52.17 cM; *V*: WT = 45.21 cM; *brc-1(xoe4)* = 50.82 cM; Figure 7B and Table S4]. In *C. elegans*, COs are not evenly distributed along the length of the chromosomes but are enriched on the gene-poor arms (Barnes *et al.* 1995; Lim *et al.* 2008; Rockman and Kruglyak 2009). Similar to what we reported for oocytes (Li *et al.* 2018), there is a statistically significant alteration in the distribution of COs in the *brc-1* mutant on both chromosomes *I* and *V* compared to wild-type males (Figure 7C and Table S4). In the *brc-1* mutant, we observed an expansion in the center of the chromosome, with more COs in the center-right interval on chromosome *I* (30.21% *vs.* 13.95%; *P* = 0.0123) and the left-center interval on chromosome *V* compared to wild type (12.9% *vs.* 3.53%; *P* = 0.0304) (Figure 7C and Table S4).

We next monitored linkage between SNP markers in the *zim-1* and *brc-1*; *zim-1* mutant males. We observed a significant increase in the genetic map length on both chromosomes *I* and *V* in *zim-1* and *brc-1*; *zim-1* compared to wild-type males [*I*: *zim-1(xoe6)*=61.57 cM *P* = 0.0014, *brc-1(xoe4)*; *zim-1(xoe6)*=69.06 cM *P* = 0.0001; *V*: *zim-1(xoe6)*=61.11 cM *P* = 0.0089, *brc-1(xoe4)*; *zim-1(xoe6)*=62.04 cM *P* = 0.0024; Figure 7B and Table S4]. In addition to the expanded genetic maps, CO distributions were also altered. The percentage of COs on the left and right arms of chromosome *I* were reduced in *brc-1*; *zim-1* compared to wild type (left: 22% *vs.* 33.7% *P* = 0.0426; right: 16.8% *vs.* 31.4% *P* = 0.0053), while the

right-center interval was expanded in *brc-1*; *zim-1* compared to wild-type males (29.6% *vs.* 13.9% *P* = 0.004; Figure 7C and Table S4). On chromosome *V* there was an increased percentage of COs in the left-center interval in *zim-1* compared to wild-type males (15.2% *vs.* 3.5% *P* = 0.0053), and it was further expanded in *brc-1*; *zim-1* (21.5% *P* = 0.0001), while the right-center interval had significantly more COs in *brc-1*; *zim-1* compared to *brc-1* males (22.83% *vs.* 12.9% *P* = 0.045; Figure 7C and Table S4).

A unique feature of *C. elegans* oogenic meiosis is that, on average, there is a single CO per chromosome pair per meiosis (Albertson *et al.* 1997; Hillers and Villeneuve 2003; Hammarlund *et al.* 2005). This is attributed to very strong interference, which is the phenomenon that the presence of one CO at one position decreases the probability of formation of another CO nearby. Analyses in spermatocytes also suggested that there is usually a single CO per chromosome pair (Meneely *et al.* 2002; Kaur and Rockman 2014); however, Lim *et al.* (2008) reported that interference was not as strong in male meiosis due to the appearance of closely spaced DCOs. We detected five DCOs on chromosome *I* and three DCOs on chromosome *V* in a total of 188 wild-type spermatocytes, which corresponds to 6.2% and 3.7% of total CO events (Figure 7D and Table S4). Fewer DCOs were detected in the *brc-1* mutant males, although this was not statistically different (chromosome *I*: 2 DCO/184, 2.1%; chromosome *V*: 1 DCO/183, 1.1%; Figure 7D and Table S4). In contrast, we previously detected no DCOs in 187 oocytes in either wild type or *brc-1* oocytes (Li *et al.* 2018). In the *zim-1* mutant, we detected nine DCOs in 268 spermatocytes on chromosome *I*, which corresponds to 5.8% of total CO events and is not significantly different compared to wild type; however, in the *brc-1*; *zim-1* double mutant, a significantly higher percentage of COs were DCOs and triple crossovers (TCOs): 37 DCOs and two TCOs were detected in 362 spermatocytes, which collectively is 18.7% of total CO events (Figure 7D and Table S4). On chromosome *V*, *zim-1* had elevated levels of DCOs and TCOs (18/270, 12.3%) compared to wild type and *brc-1* spermatocytes, but this was not further increased in the *brc-1*; *zim-1* double mutant (23/353, 11.7%; Figure 7D and Table S4).

Given the increased frequency of DCOs, we calculated interference. While most intervals had absolute interference of 1 in wild type and *brc-1*, the detection of DCOs resulted in decreased interference in two intervals on both chromosome *I* and chromosome *V* (Table 1). *zim-1* mutant males displayed reduced interference in all intervals except the left to left center and left center to right center intervals on chromosome *I*. Inactivation of BRC-1 in the *zim-1* mutant further impaired interference in all intervals on chromosome *I*, but had a variable effect on chromosome *V*, although they did not reach statistical significance (Table 1). Taken together, the elevated number of COSA-1 foci and increased numbers of DCOs and TCOs in the *brc-1*; *zim-1* mutant on chromosome *I* suggest that BRC-1-BRD-1 inhibits supernumerary COs under checkpoint activating conditions.

Discussion

We show here that the BRC-1-BRD-1 complex functions in early processing of meiotic DSBs to promote HR and also inhibits supernumerary COs when some chromosomes are unable to form COs in male meiosis. These functions are distinct from previous analyses in oogenesis and suggests that this complex is differently regulated during male and female meiosis to optimize sperm *vs.* oocyte production (Figure 8).

Overlapping but distinct meiotic silencing pathways in *C. elegans* and mammals

Mouse BRCA1 is essential for MSCI, recruiting ATR for H2AX phosphorylation and chromosome compaction (Turner *et al.* 2004). ATR, in turn, promotes the accumulation of additional BRCA1 and other DNA damage signaling proteins to hemizygous regions of sex chromosomes, perhaps in response to unrepaired meiotic DSBs (Royo *et al.* 2013; Lu and Yu 2015). Accumulation of DNA damage response components are linked to the recruitment of SETDB1 methyltransferase for H3K9me3 enrichment and gene silencing (Hirota *et al.* 2018). While *C. elegans* ATR ortholog and, to a lesser extent, the related ATM checkpoint kinases are critical for targeting H3K9me2 to the hemizygous *X* chromosome in male germ cells, removal of BRC-1-BRD-1 had no effect on either the deposition of H3K9me2 or lack of transcription on the *X* chromosome (Figure 1), suggesting that BRC-1-BRD-1 does not mediate MSCI in *C. elegans* male meiosis.

As master regulators, ATR and ATM phosphorylate a large number of substrates (Matsuoka *et al.* 2007; Mu *et al.* 2007); consequently, the observed effect on meiotic silencing is likely to be indirect. Indeed, a recent study revealed that these kinases function in multiple aspects of meiotic recombination during *C. elegans* oogenesis (Li and Yanowitz 2019). We have shown that the *X* chromosome in males is refractory to ATM-dependent meiotic DSB formation feedback mechanisms (Checchi *et al.* 2014), suggesting that the defect in accumulation of H3K9me2 may not be through unrepaired DSBs, as is proposed in mammals. In addition, ATR is normally present at very low levels in the male germ line and accumulates genome-wide in response to exogenous DNA damage or in mutants impaired for recombination or synapsis but is not enriched on the *X* chromosome (Jaramillo-Lambert *et al.* 2010), implying an indirect role for this kinase in MSCI. Further, a *C. elegans* H2AX ortholog has not been identified that can be phosphorylated by ATR/ATM (Boulton 2006). On the other hand, the SETDB1 methyltransferase, MET-2, mediates H3K9me2 deposition and gene silencing of the *X* chromosome in male germ cells (Bessler *et al.* 2010; Checchi and Engebrecht 2011), analogous to SETDB1 function in mammals (Hirota *et al.* 2018). However, in contrast to mice, MET-2 does not accumulate on the *X* chromosome of male germ cells (Yang *et al.* 2019). Thus, the mechanisms whereby ATL-1/ATM-1 promote accumulation of

H3K9me2 via MET-2 on the *X* chromosome of males remains to be elucidated but perhaps is linked to a small RNA pathway that is required for meiotic silencing (She *et al.* 2009). Nonetheless, the overlapping but distinct requirements for components that mediate MSCI in worms and mammals suggest that meiotic silencing is a conserved feature of meiosis in metazoans; however, the pathways used to target repressive chromatin marks have evolved independently.

BRC-1-BRD-1 regulates DSB processing to promote HR in male germ cells

In somatic cells, BRCA1-BARD1 functions in DNA damage signaling and repair to promote genome integrity (Kouznetsova *et al.* 2009; Li and Greenberg 2012; Savage and Harkin 2015; Takaoka and Miki 2018). Critical to the maintenance of the genome is the choice of pathways for repair of DSBs: HR, NHEJ and other error-prone pathways including microhomology mediated end joining. Whether HR or error-prone pathways are used is largely driven by DNA end resection. Several studies support the hypothesis that BRCA1-BARD1 regulates the choice between repair by HR and NHEJ. Initial evidence for this was based on the observation that *brca1*$^{-/-}$ embryonic lethality can be rescued by removal of 53BP1, a DNA damage response protein that promotes NHEJ (Cao *et al.* 2009; Bouwman *et al.* 2010; Bunting *et al.* 2010). More recent work has suggested that BRCA1-BARD1 promotes DNA end resection by removing a chromatin barrier through ubiquitination of histone H2A (Densham *et al.* 2016) and/or through speeding up resection by interaction with CtIP, a protein that promotes end resection (Cruz-García *et al.* 2014). Studies by other groups also showed that BRCA1 and CtIP work together with the MRX/N complex to mediate resection of complex breaks, and may be important at Spo11-dependent meiotic DSBs (Hartsuiker *et al.* 2009; Aparicio *et al.* 2016).

Our analysis of male meiosis reveals that similar to the role of BRCA1-BARD1 in somatic cells, this complex regulates the processing of meiotic DSB to promote repair by HR (Figure 8). First, in the absence of BRC-1-BRD-1, fewer RPA-1 and RAD-51 foci were observed in meiotic prophase (Figure 2 and Figure 3), suggesting BRC-1-BRD-1 functions at or prior to RPA-1/RAD-51 loading onto resected ends. We show that the reduction in RAD-51 foci can be suppressed by mutation of NHEJ proteins, consistent with a role of BRC-1-BRD-1 in regulating the choice between HR and NHEJ. However, a recent study provides evidence that accumulation of deletions in *C. elegans* *brc-1* and *brd-1* mutants is a consequence of theta-mediated end joining (Kamp *et al.* 2020), suggesting that additional error-prone pathways are activated in the absence of BRC-1-BRD-1. Additionally, the localization of BRC-1 to foci in early meiotic prophase, which presumably represent sites of ongoing recombination, is dependent on DNA resection (Figure 3). These findings point to a role for BRC-1-BRD-1 in promoting repair by HR, likely by regulating resection (Figure 8). In mouse spermatocytes, no defect in end resection was detected in a *brca1* hypomorphic allele also

mutant for p53 (Paiano *et al.* 2020); thus, it is not clear whether BRCA1-BARD1 function in end resection is a conserved feature of male meiosis. It is also important to note that *brc-1* and *brd-1* mutants exhibit only subtle meiotic phenotypes, in contrast to the phenotypic consequence of removing components of the resection machinery. Mutation of CtIP (*C. elegans* COM-1) or components of the MRX/N complex leads to high levels of embryonic lethality and almost a complete absence of RAD-51 loading (Chin and Villeneuve 2001; Hayashi *et al.* 2007; Lemmens *et al.* 2013; Girard *et al.* 2018). Thus, while BRC-1-BRD-1 is not essential for resection, our data are consistent with this complex regulating resection speed or extent, as in somatic cells.

In addition to promoting the processing of DSBs for homologous recombination, BRC-1 also plays a role in CO distribution. Analysis of genetic COs on chromosome *I* and *V* revealed that more COs occurred at the chromosome center, and fewer on the arms, as was previously observed in oogenesis (Li *et al.* 2018). Alteration in CO distribution in the *brc-1* mutant may result from changes in the chromatin landscape, which has been linked to BRCA1 function in mammals (Broering *et al.* 2014; Densham *et al.* 2016), and has been shown to alter CO patterning (Mézard *et al.* 2015; Yu *et al.* 2016). A surprising number of *C. elegans* meiotic mutants display altered CO distribution (Zetka and Rose 1995; Wagner *et al.* 2010; Meneely *et al.* 2012; Saito *et al.* 2012, 2013; Chung *et al.* 2015; Hong *et al.* 2016; Jagut *et al.* 2016; Janisiw *et al.* 2020). While the underlying mechanisms are not clear, one possibility is that CO *vs.* non-CO outcomes are driven by a particular chromatin environment as suggested by Saito and Colaiacovo (2017).

BRC-1-BRD-1 function when male meiosis is perturbed

We show that BRC-1-BRD-1 functions to promote progeny viability when male meiosis is perturbed under conditions when some chromosome pairs fail to pair, synapse, and form a CO (Figure 5). While this is also true for female meiosis, the phenotypic consequences of mutating BRC-1 or BRD-1 when meiosis is perturbed are distinct in the sexes (Figure 8). During female meiosis, removal of BRC-1 or BRD-1 under checkpoint activating conditions leads to premature disassembly of the RAD-51 filament resulting in a "dark zone" of RAD-51 (Li *et al.* 2018); however, no "dark zone" was observed during male meiosis (Figure 5). While fewer RAD-51 foci were observed in the absence of BRC-1-BRD-1 when meiosis was impaired, this is likely a consequence of the role of BRC-1-BRD-1 in DSB end processing and not in promoting RAD-51 stability, although a subtle role in RAD-51 stability cannot be ruled out. Additionally, while the CO landscape is altered in both male and female meiosis, opposite effects of removing BRC-1-BRD-1 in the *zim-1* mutant were observed. In female meiosis, mutation of *brc-1* or *brd-1* in the *zim-1* background led to fewer COSA-1-marked CO designation events, while during male meiosis the numbers increased. One possibility to explain this observation is that destabilization of the RAD-51 filament in the absence of BRC-1-BRD-1 in mid- to late

pachytene in female meiosis leads to fewer meiotic recombination intermediates that can be processed into COSA-1-marked CO precursors. On the other hand, the RAD-51 filament remains stable during male meiosis under these conditions such that more recombination intermediates can be processed into COSA-1 marked COs.

In the *zim-1* and *brc-1*; *zim-1* mutants, we observed an increase in both the number of CO designation sites (COSA-1 foci) as well as *bona fide* COs; however, there is no direct correlation between COSA-1 foci and genetic COs. We expected to see three GFP::COSA-1 foci in *zim-1* if each chromosome received a single CO as in wild type; we observed an average of 4.6 (note the wide distribution from 3 to 8). This is a 53% increase in COSA-1-marked events genome-wide. If those events were evenly distributed between the three paired chromosomes, we would expect a 17% increase/chromosome. The genetic map distance for both chromosomes *I* and *V* was 61 cM in *zim-1*, compared to 45 cM for wild type, which represents a 35% increase on both chromosomes *I* and *V*. Assuming the CO landscape of chromosome *IV* is similarly altered as chromosomes *I* and *V* in the *zim-1* mutant, and each CO site is marked by COSA-1, we would expect ∼100% increase in COSA-1 foci. Alternatively, if the chromosome *IV* CO landscape was unaltered, we would still expect an increase in COSA-1 foci of ∼70%. In either situation, we observed fewer COSA-1 foci than genetic COs, suggesting that not all of the extra COs are marked by COSA-1. In *brc-1*; *zim-1* we observed a 15% increase in COSA-1 foci but only a subtle increase in the genetic map distance compared to *zim-1*, suggesting that more COs are marked by COSA-1 in the absence of BRC-1. Thus, we propose that BRC-1 alters the type of CO events when some chromosomes cannot achieve a CO. Perhaps under checkpoint-signaling conditions, BRC-1-BRD-1 promotes intersister repair in male meiosis, and, in its absence, more intermediates are channeled into interhomolog COs, similar to the role of BRC-1-BRD-1 in intersister recombination in female meiosis (Adamo *et al.* 2008; Garcia-Muse *et al.* 2019). Alternatively, or in addition, BRC-1-BRD-1 may play a direct role in inhibiting interhomolog COs under checkpoint activating conditions.

The alteration in the CO landscape is also reflected in the levels of SCOs and DCOs. On chromosome *I*, the *zim-1* mutant had elevated SCOs, but not DCOs compared to wild type, while removal of BRC-1 in the *zim-1* mutant resulted in elevated levels of DCOs at the expense of SCOs. We propose that this reflects a shift from three- and four-strand DCOs, which are included in the SCO class and are presumably not marked by COSA-1, in *zim-1*, to two-strand DCOs marked by COSA-1 in *brc-1*; *zim-1*. In contrast, on chromosome *V*, the *zim-1* mutant showed significantly higher levels of DCOs compared to wild type, but removing BRC-1 had little effect. During female meiosis, inactivation of BRC-1 in the *zim-1* mutant background had the opposite effect, *i.e.*, decreasing numbers of DCOs and elevated numbers of SCOs were observed on chromosome *V*, presumably due to a shift from two-strand

DCOs to three- and four-strand DCOs (Li *et al.* 2018). Thus, there are both chromosome-specific and sex-specific effects on CO patterning when BRC-1 is inactivated. The sex-specific effect is likely due to RAD-51 stability and CO pathway usage. The chromosome-specific effect may be a consequence of size; chromosome *I* is one of the smallest chromosomes, while chromosome *V* is the largest chromosome. Recent work in yeast suggests that small chromosomes use multiple mechanisms to ensure the formation of the obligate CO (Murakami *et al.* 2020). Therefore, the differential impact on chromosome *I vs. V* may be due to the mechanisms in place to promote CO formation on small chromosomes. Alternatively, other chromosome-specific features may influence which DSBs are converted into COs when BRC-1-BRD-1 is not present to constrain extra CO formation during male meiosis.

Why does removal of BRC-1-BRD-1 enhance embryonic lethality when a subset of chromosomes fails to form a CO? Due to feedback mechanisms, more DSBs are induced when not all homologs are connected by COs (Rosu *et al.* 2013; Stamper *et al.* 2013), and, in the absence of BRC-1-BRD-1, more breaks may be repaired through error-prone pathways, potentially leading to an increase in mutations. Additionally, mutation of *brc-1* enhanced CO distribution defects as well as the number of DCOs on some chromosomes in the *zim-1* mutant background (Figure 7). Alteration in CO position (Altendorfer *et al.* 2020) as well as elevated CO numbers (Hollis *et al.* 2020) are deleterious during *C. elegans* meiosis. This is likely a consequence of the holocentric nature of *C. elegans* chromosomes and the requirement to establish asymmetric domains as defined by the single CO site for accurate cohesion release and chromosome segregation (de Carvalho *et al.* 2008; Ferrandiz *et al.* 2018). Additionally, DSBs on chromosomes that cannot undergo CO formation during male meiosis may fail to be repaired prior to the meiotic divisions due to defects in BRC-1-BRD-1-dependent intersister repair, leading to chromosome fragmentation, loss of genetic material and aneuploid gametes.

Sex-specific regulation of meiosis

Our analyses of BRC-1-BRD-1 reveals several differences between male and female meiosis. First, while there is currently no direct measure of DSB formation in *C. elegans*, we detected more RAD-51 foci in male *vs.* female germ cells, suggesting that more DSBs are induced in spermatocytes (Figure 2) (Checchi *et al.* 2014). Usage of DSBs hotspots in mice has also revealed sex-specific differences (Brick *et al.* 2018). Second, BRC-1-BRD-1 functions at different steps of meiotic recombination in the sexes in wild-type worms (Figure 8). In males, BRC-1-BRD-1 influences the early processing of DSBs to promote HR, while in females, BRC-1-BRD-1 is engaged in mid- to late pachytene to promote repair of breaks processed and assembled with RAD-51 by intersister recombination (Adamo *et al.* 2008). How BRC-1-BRD-1 is differentially regulated in the sexes is not known, but the spatiotemporal pattern of BRC-1-BRD-1 function mirrors MAP kinase activation in the male (transition zone/early pachytene) and female (mid-

to late-pachytene) germ lines (Lee *et al.* 2007). Thus, MAP kinase and/or other signaling pathways could regulate the complex in a sex-specific manner to drive ubiquitination of different substrates in spermatogenesis *vs.* oogenesis.

Overall, *C. elegans* male meiosis appears to be less tightly regulated compared to female meiosis. For example, we detected DCOs in wild-type male meiosis (Figure 7), but none in oocytes (Li *et al.* 2018). Further, previous analyses have shown that males undergo meiosis faster and lack germ line apoptosis, one mechanism to enhance gamete quality by removing defective or damaged germ cells (Gartner *et al.* 2000; Jaramillo-Lambert *et al.* 2007, 2010). Despite faster kinetics and lack of germline apoptosis, male meiosis has a higher fidelity compared to female meiosis (Jaramillo-Lambert *et al.* 2010). Why male meiosis appears to lack some regulatory mechanisms yet has a reduced frequency of meiotic errors compared to oogenesis is currently unknown. Future analyses of *C. elegans* male meiosis may provide insight into the mechanisms that contribute to the fidelity of male gametes.

Literature Cited

Abraham, R. T., 2001 Cell cycle checkpoint signaling through the ATM and ATR kinases. Genes Dev. 15: 2177–2196. https://doi.org/10.1101/gad.914401

Adamo, A., P. Montemauri, N. Silva, J. D. Ward, S. J. Boulton *et al.*, 2008 BRC-1 acts in the inter-sister pathway of meiotic double-strand break repair. EMBO Rep. 9: 287–292. https://doi.org/10.1038/sj.embor.7401167

Albertson, D. G., A. M. Rose, and A. M. Villeneuve, 1997 Chromosome organization, mitosis, and meiosis, in *C. elegans II*, edited by D. L. Riddle, T. Blumenthal, B. J. Meyer, and J. R. Priess, Cold Spring Harbor, NY.

Altendorfer, E., L. I. Lascarez-Lagunas, S. Nadarajan, I. Mathieson and M. P. Colaiacovo, 2020 Crossover position drives chromosome remodeling for accurate meiotic chromosome segregation. Curr. Biol. 30: 1329–1338.e7. https://doi.org/10.1016/j.cub.2020.01.079

Aparicio, T., R. Baer, M. Gottesman, and J. Gautier, 2016 MRN, CtIP, and BRCA1 mediate repair of topoisomerase II-DNA adducts. J. Cell Biol. 212: 399–408. https://doi.org/10.1083/jcb.201504005

Ashley, T., A. W. Plug, J. Xu, A. J. Solari, G. Reddy *et al.*, 1995 Dynamic changes in Rad51 distribution on chromatin during meiosis in male and female vertebrates. Chromosoma 104: 19–28. https://doi.org/10.1007/BF00352222

Barnes, T. M., Y. Kohara, A. Coulson, and S. Hekimi, 1995 Meiotic recombination, noncoding DNA and genomic organization in *Caenorhabditis elegans*. Genetics 141: 159–179.

Bazan, G. C., and K. J. Hillers, 2011 SNP-based mapping of crossover recombination in *Caenorhabditis elegans*. Methods Mol. Biol. 745: 207–222. https://doi.org/10.1007/978-1-61779-129-1_13

Bean, C. J., C. E. Schaner, and W. G. Kelly, 2004 Meiotic pairing and imprinted X chromatin assembly in *Caenorhabditis elegans*. Nat. Genet. 36: 100–105. https://doi.org/10.1038/ng1283

Bessler, J. B., E. C. Andersen, and A. M. Villeneuve, 2010 Differential localization and independent acquisition of the H3K9me2 and H3K9me3 chromatin modifications in the *Caenorhabditis elegans* adult germ line. PLoS Genet. 6: e1000830. https://doi.org/10.1371/journal.pgen.1000830

Bishop, H. I., D. Guan, E. Bocksteins, L. K. Parajuli, K. D. Murray *et al.*, 2015 Distinct cell- and layer-specific expressionpatterns and independent regulation of Kv2 channel subtypes in cortical pyramidal neurons. J. Neurosci. 35: 14922–14942. https://doi.org/10.1523/JNEUROSCI.1897-15.2015

Boulton, S. J., 2006 BRCA1-mediated ubiquitylation. Cell Cycle 5: 1481–1486. https://doi.org/10.4161/cc.5.14.2930

Boulton, S. J., J. S. Martin, J. Polanowska, D. E. Hill, A. Gartner *et al.*, 2004 BRCA1/BARD1 orthologs required for DNA repair in *Caenorhabditis elegans*. Curr. Biol. 14: 33–39. https://doi.org/10.1016/j.cub.2003.11.029

Bouwman, P., A. Aly, J. M. Escandell, M. Pieterse, J. Bartkova *et al.*, 2010 53BP1 loss rescues BRCA1 deficiency and is associated with triple-negative and BRCA-mutated breast cancers. Nat. Struct. Mol. Biol. 17: 688–695. https://doi.org/10.1038/nsmb.1831

Brady, M. M., S. McMahan, and J. Sekelsky, 2018 Loss of Drosophila Mei-41/ATR alters meiotic crossover patterning. Genetics 208: 579–588. https://doi.org/10.1534/genetics.117.300634

Brick, K., S. Thibault-Sennett, F. Smagulova, K. G. Lam, Y. Pu *et al.*, 2018 Extensive sex differences at the initiation of genetic recombination. Nature 561: 338–342. https://doi.org/10.1038/s41586-018-0492-5

Broering, T. J., K. G. Alavattam, R. I. Sadreyev, Y. Ichijima, Y. Kato *et al.*, 2014 BRCA1 establishes DNA damage signaling and pericentric heterochromatin of the X chromosome in male meiosis. J. Cell Biol. 205: 663–675. https://doi.org/10.1083/jcb.201311050

Bunting, S. F., E. Callen, N. Wong, H. T. Chen, F. Polato *et al.*, 2010 53BP1 inhibits homologous recombination in Brca1-deficient cells by blocking resection of DNA breaks. Cell 141: 243–254. https://doi.org/10.1016/j.cell.2010.03.012

Bury, L., P. A. Coelho, and D. M. Glover, 2016 From meiosis to mitosis: the astonishing flexibility of cell division mechanisms in early mammalian development. Curr. Top. Dev. Biol. 120: 125–171. https://doi.org/10.1016/bs.ctdb.2016.04.011

Cahoon, C. K., and D. E. Libuda, 2019 Leagues of their own: sexually dimorphic features of meiotic prophase I. Chromosoma 128: 199–214.

Cahoon, C. K., J. M. Helm, and D. E. Libuda, 2019 Synaptonemal complex central region proteins promote localization of procrossover factors to recombination events during *Caenorhabditis elegans* meiosis. Genetics 213: 395–409. https://doi.org/10.1534/genetics.119.302625

Cao, L., X. Xu, S. F. Bunting, J. Liu, R. H. Wang *et al.*, 2009 A selective requirement for 53BP1 in the biological response to genomic instability induced by Brca1 deficiency. Mol. Cell 35: 534–541. https://doi.org/10.1016/j.molcel.2009.06.037

Carlton, P. M., A. P. Farruggio, and A. F. Dernburg, 2006 A link between meiotic prophase progression and crossover control. PLoS Genet. 2: e12. https://doi.org/10.1371/journal.pgen.0020012

Checchi, P. M., and J. Engebrecht, 2011 *Caenorhabditis elegans* histone methyltransferase MET-2 shields the male X chromosome from checkpoint machinery and mediates meiotic sex chromosome inactivation. PLoS Genet. 7: e1002267. https://doi.org/10.1371/journal.pgen.1002267

Checchi, P. M., K. S. Lawrence, M. V. Van, B. J. Larson, and J. Engebrecht, 2014 Pseudosynapsis and decreased stringency of meiotic repair pathway choice on the hemizygous sex chromosome of *Caenorhabditis elegans* males. Genetics 197: 543–560. https://doi.org/10.1534/genetics.114.164152

Chin, G. M., and A. M. Villeneuve, 2001 *C. elegans mre-11* is required for meiotic recombination and DNA repair but is dispensable for the meiotic G(2) DNA damage checkpoint. Genes Dev. 15: 522–534. https://doi.org/10.1101/gad.864101

Chung, G., A. M. Rose, M. I. Petalcorin, J. S. Martin, Z. Kessler *et al.*, 2015 REC-1 and HIM-5 distribute meiotic crossovers and function redundantly in meiotic double-strand break formation in *Caenorhabditis elegans*. Genes Dev. 29: 1969–1979. https://doi.org/10.1101/gad.266056.115

Colaiácovo, M. P., A. J. MacQueen, E. Martinez-Perez, K. McDonald, A. Adamo *et al.*, 2003 Synaptonemal complex assembly in *C. elegans* is dispensable for loading strand-exchange proteins but critical for proper completion of recombination. Dev. Cell 5: 463–474. https://doi.org/10.1016/S1534-5807(03)00232-6

Cruz-García, A., A. Lopez-Saavedra, and P. Huertas, 2014 BRCA1 accelerates CtIP-mediated DNA-end resection. Cell Rep. 9: 451–459. https://doi.org/10.1016/j.celrep.2014.08.076

Daley, J. M., and P. Sung, 2014 53BP1, BRCA1, and the choice between recombination and end joining at DNA double-strand breaks. Mol. Cell. Biol. 34: 1380–1388. https://doi.org/10.1128/MCB.01639-13

de Carvalho, C. E., S. Zaaijer, S. Smolikov, Y. Gu, J. M. Schumacher *et al.*, 2008 LAB-1 antagonizes the Aurora B kinase in *C. elegans*. Genes Dev. 22: 2869–2885. https://doi.org/10.1101/gad.1691208

Densham, R. M., A. J. Garvin, H. R. Stone, J. Strachan, R. A. Baldock *et al.*, 2016 Human BRCA1-BARD1 ubiquitin ligase activity counteracts chromatin barriers to DNA resection. Nat. Struct. Mol. Biol. 23: 647–655. https://doi.org/10.1038/nsmb.3236

Dernburg, A. F., K. McDonald, G. Moulder, R. Barstead, M. Dresser *et al.*, 1998 Meiotic recombination in *C. elegans* initiates by a conserved mechanism and is dispensable for homologous chromosome synapsis. Cell 94: 387–398. https://doi.org/10.1016/S0092-8674(00)81481-6

Enguita-Marruedo, A., M. Martin-Ruiz, E. Garcia, A. Gil-Fernandez, M. T. Parra *et al.*, 2019 Transition from a meiotic to a somatic-like DNA damage response during the pachytene stage in mouse meiosis. PLoS Genet. 15: e1007439. https://doi.org/10.1371/journal.pgen.1007439

Fernandez-Capetillo, O., S. K. Mahadevaiah, A. Celeste, P. J. Romanienko, R. D. Camerini-Otero *et al.*, 2003 H2AX is required for chromatin remodeling and inactivation of sex chromosomes in male mouse meiosis. Dev. Cell 4: 497–508. https://doi.org/10.1016/S1534-5807(03)00093-5

Ferrandiz, N., C. Barroso, O. Telecan, N. Shao, H. M. Kim *et al.*, 2018 Spatiotemporal regulation of Aurora B recruitment ensures release of cohesion during *C. elegans* oocyte meiosis. Nat. Commun. 9: 834 (erratum: Nat. Commun. 9: 3558). https://doi.org/10.1038/s41467-018-03229-5

Garcia-Muse, T., and S. J. Boulton, 2005 Distinct modes of ATR activation after replication stress and DNA double-strand breaks in *Caenorhabditis elegans*. EMBO J. 24: 4345–4355. https://doi.org/10.1038/sj.emboj.7600896

Garcia-Muse, T., U. Galindo-Diaz, M. Garcia-Rubio, J. S. Martin, J. Polanowska *et al.*, 2019 A meiotic checkpoint alters repair partner bias to permit Inter-sister repair of persistent DSBs. Cell Rep. 26: 775–787.e5. https://doi.org/10.1016/j.celrep.2018.12.074

Gartner, A., S. Milstein, S. Ahmed, J. Hodgkin, and M. O. Hengartner, 2000 A conserved checkpoint pathway mediates DNA damage–induced apoptosis and cell cycle arrest in *C. elegans*. Mol. Cell 5: 435–443. https://doi.org/10.1016/S1097-2765(00)80438-4

Girard, C., B. Roelens, K. A. Zawadzki, and A. M. Villeneuve, 2018 Interdependent and separable functions of *Caenorhabditis elegans* MRN-C complex members couple formation and repair of meiotic DSBs. Proc. Natl. Acad. Sci. USA 115: E4443–E4452. https://doi.org/10.1073/pnas.1719029115

Gruhn, J. R., C. Rubio, K. W. Broman, P. A. Hunt, and T. Hassold, 2013 Cytological studies of human meiosis: sex-specific differences in recombination originate at, or prior to, establishment of double-strand breaks. PLoS One 8: e85075. https://doi.org/10.1371/journal.pone.0085075

Hammarlund, M., M. W. Davis, H. Nguyen, D. Dayton, and E. M. Jorgensen, 2005 Heterozygous insertions alter crossover distribution but allow crossover interference in *Caenorhabditis elegans*. Genetics 171: 1047–1056. https://doi.org/10.1534/genetics.105.044834

Hartsuiker, E., K. Mizuno, M. Molnar, J. Kohli, K. Ohta *et al.*, 2009 Ctp1CtIP and Rad32Mre11 nuclease activity are required for Rec12Spo11 removal, but Rec12Spo11 removal is dispensable for other MRN-dependent meiotic functions. Mol. Cell. Biol. 29: 1671–1681. https://doi.org/10.1128/MCB.01182-08

Hayashi, M., G. M. Chin, and A. M. Villeneuve, 2007 *C. elegans* germ cells switch between distinct modes of double-strand break repair during meiotic prophase progression. PLoS Genet. 3: e191. https://doi.org/10.1371/journal.pgen.0030191

Hillers, K. J., and A. M. Villeneuve, 2003 Chromosome-wide control of meiotic crossing over in *C. elegans*. Curr. Biol. 13: 1641–1647. https://doi.org/10.1016/j.cub.2003.08.026

Hillers, K. J., V. Jantsch, E. Martinez-Perez and J. L. Yanowitz, 2015 Meiosis. (May 4, 2017), *WormBook*, ed. The C. elegans Research Community, WormBook, doi/10.1895/wormbook.1.178.1, http://www.wormbook.org.

Hirota, T., P. Blakeley, M. N. Sangrithi, S. K. Mahadevaiah, V. Encheva *et al.*, 2018 SETDB1 links the meiotic DNA damage response to sex chromosome silencing in mice. Dev. Cell 47: 645–659.e6. https://doi.org/10.1016/j.devcel.2018.10.004

Hollis, J. A., M. L. Glover, A. Schlientz, C. K. Cahoon, B. Bowerman *et al.*, 2020 Excess crossovers impede faithful meiotic chromosome segregation in *C. elegans*. bioRxiv doi: 10.1101/2020.01.30.927640 (Preprint posted January 31, 2020).

Hong, Y., R. Sonneville, A. Agostinho, B. Meier, B. Wang *et al.*, 2016 The SMC-5/6 complex and the HIM-6 (BLM) helicase synergistically promote meiotic recombination intermediate processing and chromosome maturation during *Caenorhabditis elegans* meiosis. PLoS Genet. 12: e1005872. https://doi.org/10.1371/journal.pgen.1005872

Hsin, J. P., and J. L. Manley, 2012 The RNA polymerase II CTD coordinates transcription and RNA processing. Genes Dev. 26: 2119–2137. https://doi.org/10.1101/gad.200303.112

Hurlock, M. E., I. Cavka, L. E. Kursel, J. Haversat, M. Wooten *et al.*, 2020 Identification of novel synaptonemal complex components in *C. elegans*. J. Cell Biol. 219: e201910043. https://doi.org/10.1083/jcb.201910043

Jagut, M., P. Hamminger, A. Woglar, S. Millonigg, L. Paulin *et al.*, 2016 Separable roles for a *Caenorhabditis elegans* RMI1 homolog in promoting and antagonizing meiotic crossovers ensure faithful fhromosome inheritance. PLoS Biol. 14: e1002412. https://doi.org/10.1371/journal.pbio.1002412

Janisiw, E., M. R. Dello Stritto, V. Jantsch, and N. Silva, 2018 BRCA1-BARD1 associate with the synaptonemal complex and pro-crossover factors and influence RAD-51 dynamics during *Caenorhabditis elegans* meiosis. PLoS Genet. 14: e1007653. https://doi.org/10.1371/journal.pgen.1007653

Janisiw, E., M. Raices, F. Balmir, L. P. Paz, A. Baudrimont *et al.*, 2020 Poly(ADP-ribose) glycohydrolase promotes formation and homology-directed repair of meiotic DNA double-strand breaks independent of its catalytic activity. bioRxiv doi: 10.1101/2020.03.12.988840 (Preprint posted March 13, 2020)

Jaramillo-Lambert, A., and J. Engebrecht, 2010 A single unpaired and transcriptionally silenced X chromosome locally precludes checkpoint signaling in the *Caenorhabditis elegans* germ line. Genetics 184: 613–628. https://doi.org/10.1534/genetics.109.110338

Jaramillo-Lambert, A., M. Ellefson, A. M. Villeneuve, and J. Engebrecht, 2007 Differential timing of S phases, X chromosome replication, and meiotic prophase in the *C. elegans* germ line. Dev. Biol. 308: 206–221. https://doi.org/10.1016/j.ydbio.2007.05.019

Jaramillo-Lambert, A., Y. Harigaya, J. Vitt, A. Villeneuve, and J. Engebrecht, 2010 Meiotic errors activate checkpoints that improve gamete quality without triggering apoptosis in male germ cells. Curr. Biol. 20: 2078–2089. https://doi.org/10.1016/j.cub.2010.10.008

Joyce, E. F., A. Paul, K. E. Chen, N. Tanneti, and K. S. McKim, 2012 Multiple barriers to nonhomologous DNA end joining during meiosis in Drosophila. Genetics 191: 739–746. https://doi.org/10.1534/genetics.112.140996

Kamp, J. A., R. van Schendel, I. W. Dilweg, and M. Tijsterman, 2020 BRCA1-associated structural variations are a consequence of polymerase theta-mediated end-joining. Nat. Commun. 11: 3615. https://doi.org/10.1038/s41467-020-17455-3

Kaur, T., and M. V. Rockman, 2014 Crossover heterogeneity in the absence of hotspots in *Caenorhabditis elegans*. Genetics 196: 137–148. https://doi.org/10.1534/genetics.113.158857

Keeney, S., C. N. Giroux, and N. Kleckner, 1997 Meiosis-specific DNA double-strand breaks are catalyzed by Spo11, a member of a widely conserved protein family. Cell 88: 375–384. https://doi.org/10.1016/S0092-8674(00)81876-0

Kelly, W. G., C. E. Schaner, A. F. Dernburg, M. H. Lee, S. K. Kim *et al.*, 2002 X-chromosome silencing in the germline of *C. elegans*. Development 129: 479–492.

Kianian, P. M. A., M. Wang, K. Simons, F. Ghavami, Y. He *et al.*, 2018 High-resolution crossover mapping reveals similarities and differences of male and female recombination in maize. Nat. Commun. 9: 2370. https://doi.org/10.1038/s41467-018-04562-5

Koury, E., K. Harrell, and S. Smolikove, 2018 Differential RPA-1 and RAD-51 recruitment in vivo throughout the *C. elegans* germline, as revealed by laser microirradiation. Nucleic Acids Res. 46: 748–764. https://doi.org/10.1093/nar/gkx1243

Kouznetsova, A., H. Wang, M. Bellani, R. D. Camerini-Otero, R. Jessberger *et al.*, 2009 BRCA1-mediated chromatin silencing is limited to oocytes with a small number of asynapsed chromosomes. J. Cell Sci. 122: 2446–2452. https://doi.org/10.1242/jcs.049353

Larson, B. J., M. V. Van, T. Nakayama, and J. Engebrecht, 2016 Plasticity in the meiotic epigenetic landscape of sex chromosomes in *Caenorhabditis* species. Genetics 203: 1641–1658. https://doi.org/10.1534/genetics.116.191130

Lawrence, K. S., E. C. Tapley, V. E. Cruz, Q. Li, K. Aung *et al.*, 2016 LINC complexes promote homologous recombination in part through inhibition of nonhomologous end joining. J. Cell Biol. 215: 801–821. https://doi.org/10.1083/jcb.201604112

Lee, M. H., M. Ohmachi, S. Arur, S. Nayak, R. Francis *et al.*, 2007 Multiple functions and dynamic activation of MPK-1 extracellular signal-regulated kinase signaling in *Caenorhabditis elegans* germline development. Genetics 177: 2039–2062. https://doi.org/10.1534/genetics.107.081356

Lemmens, B. B., N. M. Johnson, and M. Tijsterman, 2013 COM-1 promotes homologous recombination during *Caenorhabditis elegans* meiosis by antagonizing Ku-mediated non-homologous end joining. PLoS Genet. 9: e1003276. https://doi.org/10.1371/journal.pgen.1003276

70

Lenormand, T., and J. Dutheil, 2005 Recombination difference between sexes: a role for haploid selection. PLoS Biol. 3: e63. https://doi.org/10.1371/journal.pbio.0030063

Li, M. L., and R. A. Greenberg, 2012 Links between genome integrity and BRCA1 tumor suppression. Trends Biochem. Sci. 37: 418–424. https://doi.org/10.1016/j.tibs.2012.06.007

Li, Q., T. T. Saito, M. Martinez-Garcia, A. J. Deshong, S. Nadarajan et al., 2018 The tumor suppressor BRCA1-BARD1 complex localizes to the synaptonemal complex and regulates recombination under meiotic dysfunction in Caenorhabditis elegans. PLoS Genet. 14: e1007701. https://doi.org/10.1371/journal.pgen.1007701

Li, W., and J. L. Yanowitz, 2019 ATM and ATR influence meiotic crossover formation through antagonistic and overlapping functions in Caenorhabditis elegans. Genetics 212: 431–443. https://doi.org/10.1534/genetics.119.302193

Lim, J. G., R. R. Stine, and J. L. Yanowitz, 2008 Domain-specific regulation of recombination in Caenorhabditis elegans in response to temperature, age and sex. Genetics 180: 715–726. https://doi.org/10.1534/genetics.108.090142

Lloyd, A., and E. Jenczewski, 2019 Modelling sex-specific crossover patterning in Arabidopsis. Genetics 211: 847–859. https://doi.org/10.1534/genetics.118.301838

Lu, L. Y., and X. Yu, 2015 Double-strand break repair on sex chromosomes: challenges during male meiotic prophase. Cell Cycle 14: 516–525. https://doi.org/10.1080/15384101.2014.998070

Lui, D. Y., and M. P. Colaiacovo, 2013 Meiotic development in Caenorhabditis elegans. Adv. Exp. Med. Biol. 757: 133–170. https://doi.org/10.1007/978-1-4614-4015-4_6

Macaisne, N., Z. Kessler, and J. L. Yanowitz, 2018 Meiotic double-strand break proteins influence repair pathway utilization. Genetics 210: 843–856. https://doi.org/10.1534/genetics.118.301402

Machovina, T. S., R. Mainpal, A. Daryabeigi, O. McGovern, D. Paouneskou et al., 2016 A surveillance system ensures crossover formation in C. elegans. Curr. Biol. 26: 2873–2884. https://doi.org/10.1016/j.cub.2016.09.007

MacQueen, A. J., M. P. Colaiacovo, K. McDonald, and A. M. Villeneuve, 2002 Synapsis-dependent and -independent mechanisms stabilize homolog pairing during meiotic prophase in C. elegans. Genes Dev. 16: 2428–2442. https://doi.org/10.1101/gad.1011602

Mahadevaiah, S. K., D. Bourc'his, D. G. de Rooij, T. H. Bestor, J. M. Turner et al., 2008 Extensive meiotic asynapsis in mice antagonises meiotic silencing of unsynapsed chromatin and consequently disrupts meiotic sex chromosome inactivation. J. Cell Biol. 182: 263–276. https://doi.org/10.1083/jcb.200710195

Maine, E. M., 2010 Meiotic silencing in Caenorhabditis elegans. Int. Rev. Cell Mol. Biol. 282: 91–134. https://doi.org/10.1016/S1937-6448(10)82002-7

Matsuoka, S., B. A. Ballif, A. Smogorzewska, E. R. McDonald, 3rd, K. E. Hurov et al., 2007 ATM and ATR substrate analysis reveals extensive protein networks responsive to DNA damage. Science 316: 1160–1166. https://doi.org/10.1126/science.1140321

Meneely, P. M., A. F. Farago, and T. M. Kauffman, 2002 Crossover distribution and high interference for both the X chromosome and an autosome during oogenesis and spermatogenesis in Caenorhabditis elegans. Genetics 162: 1169–1177.

Meneely, P. M., O. L. McGovern, F. I. Heinis, and J. L. Yanowitz, 2012 Crossover distribution and frequency are regulated by him-5 in Caenorhabditis elegans. Genetics 190: 1251–1266. https://doi.org/10.1534/genetics.111.137463

Mets, D. G., and B. J. Meyer, 2009 Condensins regulate meiotic DNA break distribution, thus crossover frequency, by controlling chromosome structure. Cell 139: 73–86. https://doi.org/10.1016/j.cell.2009.07.035

Mézard, C., M. T. Jahns, and M. Grelon, 2015 Where to cross? New insights into the location of meiotic crossovers. Trends Genet. 31: 393–401. https://doi.org/10.1016/j.tig.2015.03.008

Moens, P. B., D. J. Chen, Z. Shen, N. Kolas, M. Tarsounas et al., 1997 Rad51 immunocytology in rat and mouse spermatocytes and oocytes. Chromosoma 106: 207–215. https://doi.org/10.1007/s004120050241

Morelli, M. A., and P. E. Cohen, 2005 Not all germ cells are created equal: aspects of sexual dimorphism in mammalian meiosis. Reproduction 130: 761–781. https://doi.org/10.1530/rep.1.00865

Mu, J. J., Y. Wang, H. Luo, M. Leng, J. Zhang, et al., 2007 A proteomic analysis of ataxia telangiectasia-mutated (ATM)/ATM-Rad3-related (ATR) substrates identifies the ubiquitin-proteasome system as a regulator for DNA damage checkpoints. J. Biol. Chem. 282: 17330–17334. https://doi.org/10.1074/jbc.C700079200

Murakami, H., I. Lam, P. C. Huang, J. Song, M. van Overbeek, et al., 2020 Multilayered mechanisms ensure that short chromosomes recombine in meiosis. Nature 582: 124–128. https://doi.org/10.1038/s41586-020-2248-2

Nabeshima, K., A. M. Villeneuve, and K. J. Hillers, 2004 Chromosome-wide regulation of meiotic crossover formation in Caenorhabditis elegans requires properly assembled chromosome axes. Genetics 168: 1275–1292. https://doi.org/10.1534/genetics.104.030700

Nadarajan, S., T. J. Lambert, E. Altendorfer, J. Gao, M. D. Blower et al., 2017 Polo-like kinase-dependent phosphorylation of the synaptonemal complex protein SYP-4 regulates double-strand break formation through a negative feedback loop. eLife 6: e23437. https://doi.org/10.7554/eLife.23437

Nagaoka, S. I., T. J. Hassold, and P. A. Hunt, 2012 Human aneuploidy: mechanisms and new insights into an age-old problem. Nat. Rev. Genet. 13: 493–504. https://doi.org/10.1038/nrg3245

Paiano, J., W. Wu, S. Yamada, N. Sciascia, E. Callen et al., 2020 ATM and PRDM9 regulate SPO11-bound recombination intermediates during meiosis. Nat. Commun. 11: 857. https://doi.org/10.1038/s41467-020-14654-w

Pattabiraman, D., B. Roelens, A. Woglar, and A. M. Villeneuve, 2017 Meiotic recombination modulates the structure and dynamics of the synaptonemal complex during C. elegans meiosis. PLoS Genet. 13: e1006670. https://doi.org/10.1371/journal.pgen.1006670

Phillips, C. M., and A. F. Dernburg, 2006 A family of zinc-finger proteins is required for chromosome-specific pairing and synapsis during meiosis in C. elegans. Dev. Cell 11: 817–829. https://doi.org/10.1016/j.devcel.2006.09.020

Phillips, C. M., C. Wong, N. Bhalla, P. M. Carlton, P. Weiser et al., 2005 HIM-8 binds to the X chromosome pairing center and mediates chromosome-specific meiotic synapsis. Cell 123: 1051–1063. https://doi.org/10.1016/j.cell.2005.09.035

Polanowska, J., J. S. Martin, T. Garcia-Muse, M. I. Petalcorin, and S. J. Boulton, 2006 A conserved pathway to activate BRCA1-dependent ubiquitylation at DNA damage sites. EMBO J. 25: 2178–2188. https://doi.org/10.1038/sj.emboj.7601102

Ranjha, L., S. M. Howard, and P. Cejka, 2018 Main steps in DNA double-strand break repair: an introduction to homologous recombination and related processes. Chromosoma 127: 187–214. https://doi.org/10.1007/s00412-017-0658-1

Reuben, M., and R. Lin, 2002 Germline X chromosomes exhibit contrasting patterns of histone H3 methylation in Caenorhabditis elegans. Dev. Biol. 245: 71–82. https://doi.org/10.1006/dbio.2002.0634

Rinaldo, C., P. Bazzicalupo, S. Ederle, M. Hilliard, and A. La Volpe, 2002 Roles for Caenorhabditis elegans rad-51 in meiosis and in resistance to ionizing radiation during development. Genetics 160: 471–479.

Rockman, M. V., and L. Kruglyak, 2009 Recombinational landscape and population genomics of Caenorhabditis elegans. PLoS Genet. 5: e1000419. https://doi.org/10.1371/journal.pgen.1000419

Rosu, S., K. A. Zawadzki, E. L. Stamper, D. E. Libuda, A. L. Reese *et al.*, 2013 The *C. elegans* DSB-2 protein reveals a regulatory network that controls competence for meiotic DSB formation and promotes crossover assurance. PLoS Genet. 9: e1003674. https://doi.org/10.1371/journal.pgen.1003674

Royo, H., G. Polikiewicz, S. K. Mahadevaiah, H. Prosser, M. Mitchell *et al.*, 2010 Evidence that meiotic sex chromosome inactivation is essential for male fertility. Curr. Biol. 20: 2117–2123. https://doi.org/10.1016/j.cub.2010.11.010

Royo, H., H. Prosser, Y. Ruzankina, S. K. Mahadevaiah, J. M. Cloutier *et al.*, 2013 ATR acts stage specifically to regulate multiple aspects of mammalian meiotic silencing. Genes Dev. 27: 1484–1494. https://doi.org/10.1101/gad.219477.113

Saito, T. T., and M. P. Colaiacovo, 2017 Regulation of crossover frequency and distribution during meiotic recombination. Cold Spring Harb. Symp. Quant. Biol. 82: 223–234. https://doi.org/10.1101/sqb.2017.82.034132

Saito, T. T., F. Mohideen, K. Meyer, J. W. Harper, and M. P. Colaiacovo, 2012 SLX-1 is required for maintaining genomic integrity and promoting meiotic noncrossovers in the *Caenorhabditis elegans* germline. PLoS Genet. 8: e1002888. https://doi.org/10.1371/journal.pgen.1002888

Saito, T. T., D. Y. Lui, H. M. Kim, K. Meyer, and M. P. Colaiacovo, 2013 Interplay between structure-specific endonucleases for crossover control during *Caenorhabditis elegans* meiosis. PLoS Genet. 9: e1003586. https://doi.org/10.1371/journal.pgen.1003586

Sartori, A. A., C. Lukas, J. Coates, M. Mistrik, S. Fu *et al.*, 2007 Human CtIP promotes DNA end resection. Nature 450: 509–514. https://doi.org/10.1038/nature06337

Savage, K. I., and D. P. Harkin, 2015 BRCA1, a 'complex' protein involved in the maintenance of genomic stability. FEBS J. 282: 630–646. https://doi.org/10.1111/febs.13150

Schedl, T., and J. Kimble, 1988 *fog-2*, a germ-line-specific sex determination gene required for hermaphrodite spermatogenesis in *Caenorhabditis elegans*. Genetics 119: 43–61.

Sciurano, R. B., M. I. Rahn, M. I. Pigozzi, S. B. Olmedo, and A. J. Solari, 2006 An azoospermic man with a double-strand DNA break-processing deficiency in the spermatocyte nuclei: case report. Hum. Reprod. 21: 1194–1203. https://doi.org/10.1093/humrep/dei479

Shakes, D. C., J. C. Wu, P. L. Sadler, K. Laprade, L. L. Moore *et al.*, 2009 Spermatogenesis-specific features of the meiotic program in *Caenorhabditis elegans*. PLoS Genet. 5: e1000611. https://doi.org/10.1371/journal.pgen.1000611

She, X., X. Xu, A. Fedotov, W. G. Kelly, and E. M. Maine, 2009 Regulation of heterochromatin assembly on unpaired chromosomes during *Caenorhabditis elegans* meiosis by components of a small RNA-mediated pathway. PLoS Genet. 5: e1000624. https://doi.org/10.1371/journal.pgen.1000624

Smolikov, S., A. Eizinger, A. Hurlburt, E. Rogers, A. M. Villeneuve *et al.*, 2007 Synapsis-defective mutants reveal a correlation between chromosome conformation and the mode of double-strand break repair during *Caenorhabditis elegans* meiosis. Genetics 176: 2027–2033. https://doi.org/10.1534/genetics.107.076968

Smolikov, S., K. Schild-Prufert, and M. P. Colaiacovo, 2008 CRA-1 uncovers a double-strand break-dependent pathway promoting the assembly of central region proteins on chromosome axes during *C. elegans* meiosis. PLoS Genet. 4: e1000088. https://doi.org/10.1371/journal.pgen.1000088

Sonneville, R., M. Querenet, A. Craig, A. Gartner, and J. J. Blow, 2012 The dynamics of replication licensing in live *Caenorhabditis elegans* embryos. J. Cell Biol. 196: 233–246. https://doi.org/10.1083/jcb.201110080

Stamper, E. L., S. E. Rodenbusch, S. Rosu, J. Ahringer, A. M. Villeneuve *et al.*, 2013 Identification of DSB-1, a protein required for initiation of meiotic recombination in *Caenorhabditis elegans*, illuminates a crossover assurance checkpoint. PLoS Genet. 9: e1003679. https://doi.org/10.1371/journal.pgen.1003679

Stapley, J., P. G. D. Feulner, S. E. Johnston, A. W. Santure, and C. M. Smadja, 2017 Variation in recombination frequency and distribution across eukaryotes: patterns and processes. Philos. Trans. R. Soc. Lond. B Biol. Sci. 372: 20160455 [corrigenda: Philos. Trans. R. Soc. Lond. B Biol. Sci. 373: 20170360 (2018)].

Takaoka, M., and Y. Miki, 2018 BRCA1 gene: function and deficiency. Int. J. Clin. Oncol. 23: 36–44. https://doi.org/10.1007/s10147-017-1182-2

Turner, J. M., 2007 Meiotic sex chromosome inactivation. Development 134: 1823–1831. https://doi.org/10.1242/dev.000018

Turner, J. M., O. Aprelikova, X. Xu, R. Wang, S. Kim *et al.*, 2004 BRCA1, histone H2AX phosphorylation, and male meiotic sex chromosome inactivation. Curr. Biol. 14: 2135–2142. https://doi.org/10.1016/j.cub.2004.11.032

Van, M. V., B. J. Larson, and J. Engebrecht, 2016 To break or not to break: sex chromosome hemizygosity during meiosis in *Caenorhabditis*. Genetics 204: 999–1013. https://doi.org/10.1534/genetics.116.194308

Wagner, C. R., L. Kuervers, D. L. Baillie and J. L. Yanowitz, 2010 xnd-1 regulates the global recombination landscape in *Caenorhabditis elegans*. Nature 467: 839–843. https://doi.org/10.1038/nature09429

Woglar, A., and A. M. Villeneuve, 2018 Dynamic architecture of DNA repair complexes and the synaptonemal complex at sites of meiotic recombination. Cell 173: 1678–1691.e16. https://doi.org/10.1016/j.cell.2018.03.066

Xu, X., O. Aprelikova, P. Moens, C. X. Deng, and P. A. Furth, 2003 Impaired meiotic DNA-damage repair and lack of crossing-over during spermatogenesis in BRCA1 full-length isoform deficient mice. Development 130: 2001–2012. https://doi.org/10.1242/dev.00410

Yang, B., X. Xu, L. Russell, M. T. Sullenberger, J. L. Yanowitz *et al.*, 2019 A DNA repair protein and histone methyltransferase interact to promote genome stability in the *Caenorhabditis* elegans germ line. PLoS Genet. 15: e1007992. https://doi.org/10.1371/journal.pgen.1007992

Yin, Y., and S. Smolikove, 2013 Impaired resection of meiotic double-strand breaks channels repair to nonhomologous end joining in *Caenorhabditis elegans*. Mol. Cell. Biol. 33: 2732–2747. https://doi.org/10.1128/MCB.00055-13

Yokoo, R., K. A. Zawadzki, K. Nabeshima, M. Drake, S. Arur *et al.*, 2012 COSA-1 reveals robust homeostasis and separable licensing and reinforcement steps governing meiotic crossovers. Cell 149: 75–87. https://doi.org/10.1016/j.cell.2012.01.052

Yu, Z., Y. Kim, and A. F. Dernburg, 2016 Meiotic recombination and the crossover assurance checkpoint in *Caenorhabditis elegans*. Semin. Cell Dev. Biol. 54: 106–116. https://doi.org/10.1016/j.semcdb.2016.03.014

Zelazowski, M. J., M. Sandoval, L. Paniker, H. M. Hamilton, J. Han *et al.*, 2017 Age-dependent alterations in meiotic recombination cause chromosome segregation errors in spermatocytes. Cell 171: 601–614.e13. https://doi.org/10.1016/j.cell.2017.08.042

Zetka, M. C., and A. M. Rose, 1995 Mutant *rec-1* eliminates the meiotic pattern of crossing over in *Caenorhabditis elegans*. Genetics 141: 1339–1349.

Communicating editor: A. MacQueen

Chapter 4

Inducible degradation of dosage compensation protein DPY-27 facilitates isolation of

***Caenorhabditis elegans* males for molecular and biochemical analyses**

Qianyan Li, Arshdeep Kaur, Benjamin Mallory, Sara Hariri, JoAnne Engebrecht

Arshdeep Kaur performed genetic crosses to generate most of the strains used in this study, conducted small scale auxin-induced degradation of DPY-27, and measured GFP::COSA-1 foci (Figure 2b). Benjamin Mallory performed microinjection to generate the *dpy-27::AID brd-1::gfp* strain. JoAnne Engebrecht performed assays for sperm activation, male-sired progeny viability and sperm competition (Figure 3b-3e). QL performed all other experiments.

Inducible degradation of dosage compensation protein DPY-27 facilitates isolation of *Caenorhabditis elegans* males for molecular and biochemical analyses

Qianyan Li [1,2], Arshdeep Kaur [1], Benjamin Mallory [1,†], Sara Hariri [1,2], JoAnne Engebrecht [1,2,*]

[1]Department of Molecular and Cellular Biology, University of California, Davis, Davis, CA 95616, USA
[2]Biochemistry, Molecular, Cellular and Developmental Biology Graduate Group, University of California, Davis, Davis, CA 95616, USA

*Corresponding author: University of California, Davis, One Shields Avenue, Davis, CA 95616, USA. Email: jengebrecht@ucdavis.edu
†Present address: Genome Sciences Program, University of Washington, Seattle, WA 98195, USA.

Abstract

Biological sex affects numerous aspects of biology, yet how sex influences different biological processes have not been extensively studied at the molecular level. *Caenorhabditis elegans*, with both hermaphrodites (functionally females as adults) and males, is an excellent system to uncover how sex influences physiology. Here, we describe a method to isolate large quantities of *C. elegans* males by conditionally degrading DPY-27, a component of the dosage compensation complex essential for hermaphrodite, but not male, development. We show that germ cells from males isolated following DPY-27 degradation undergo meiosis and spermiogenesis like wild type and these males are competent to mate and sire viable offspring. We further demonstrate the efficacy of this system by analyzing gene expression and performing affinity pull-downs from male worm extracts.

Keywords: *Caenorhabditis elegans*; dosage compensation; DPY-27; males; meiosis; spermiogenesis; Genetics of Sex

Introduction

In metazoans, sex has evolved multiple times and influences most biological processes. Gonochoristic species have 2 biological sexes, defined by the production of differentiated gametes: sperm (males) and ova (females). Somatic tissues also display sexually dimorphic features, the most obvious being those important for mating. Furthermore, studies in mammals have highlighted the impact of sex on physiological processes including metabolism, cardiac, and neuronal functions (Miller 2014). The molecular mechanisms underlying how biological processes are modulated by sex remain largely unknown.

In addition to gonochorism, other reproductive strategies exist. For example, hermaphrodism is common in many species including snails, worms, echinoderms, fish, and plants, where both sperm and ova are produced in the same organism. The nematode *Caenorhabditis elegans* is an androdioecious species with both hermaphrodites and males and has been an excellent model to study sex-specific morphological adaptations and production of sperm and ova. In *C. elegans* hermaphrodites (*XX*), the first wave of germ cells undergoes spermatogenesis; as adults, hermaphrodites exclusively produce ova and thus are functionally female (Hubbard and Greenstein 2000). Males (*XO*) arise spontaneously at a low frequency (~0.2%) because of meiotic chromosome nondisjunction and exclusively produce sperm. The morphological features that differentiate the *C. elegans* male from the hermaphrodite arise during postembryonic development.

Most prominent is the tail structure and associated male-specific neuronal wiring required for mating (Sulston *et al.* 1980). Males can be propagated by crossing with hermaphrodites, which will preferentially use male sperm to fertilize ova, leading to a 1:1 hermaphrodite: male ratio in the offspring (Ward and Carrel 1979; LaMunyon and Ward 1995; LaMunyon and Ward 1998).

Caenorhabditis elegans is a facile genetic model due in part to its facultative hermaphroditic lifestyle, which greatly simplifies genetic analysis. The wealth of genetic mutants available and in-depth understanding of how sex is determined, facilitates mechanistic studies of how sex affects biological processes. For example, *fog-2* loss-of-function mutants block spermatogenesis specifically in hermaphrodites, leading to true female worms (Schedl and Kimble 1988). These mutant worms have been used to distinguish sperm vs ova contributions to euploid progeny (Jaramillo-Lambert *et al.* 2010; Checchi *et al.* 2014; Li *et al.* 2020). Several genes required for spermatogenesis (*spe* genes) have been identified. Most *spe* genes are required for spermatogenesis in both hermaphrodites and males (Nishimura and L'Hernault 2010). Conditional depletion of one of these, *spe-44*, has been developed for mating and longevity studies (Kasimatis *et al.* 2018). Interestingly, the *spe-8* group is specifically required for activation of hermaphrodite, but not male, sperm (L'Hernault *et al.* 1988). Additionally, mutations in genes that are important for *X* chromosome disjunction in meiosis leads to the Him (High incidence of males) phenotype, such that up to 40% of self-progeny are males (Hodgkin *et al.* 1979).

Caenorhabditis elegans has prominent gonads where germ cells are organized in a linear assembly line fashion and reproduces prolifically, making *C. elegans* an outstanding system to investigate meiosis and fertilization. To date, most meiotic studies have focused on oogenesis in hermaphrodites due to the ease of isolating meiotic mutants and performing molecular analyses. A few studies focusing on male meiosis have revealed that while the basic processes are similar, the regulation of meiosis is distinct in spermatogenesis vs oogenesis (Jaramillo-Lambert *et al.* 2007; Shakes *et al.* 2009; Jaramillo-Lambert *et al.* 2010; Checchi *et al.* 2014; Kurhanewicz *et al.* 2020). However, a complete understanding of how sex influences meiosis, gametogenesis, and biology more generally is still lacking.

While hermaphrodites are easy to propagate and collect in large numbers, it has been more difficult to propagate and collect large numbers of males. Most strategies rely on maintaining mated cultures (~50% males) or using *him-8* mutants (~40% males; Hodgkin *et al.* 1979) and then manually picking males. Alternatively, males can be separated from hermaphrodites using filters, which take advantage of the different size of adult hermaphrodites (1 mm × 80 μm) and males (0.8 mm × 50 μm; Chu *et al.* 2006). However, this requires synchronized cultures as larvae are smaller and will filter with males regardless of sex. Additionally, filtering requires extensive labor and in our hands is not very efficient, making it difficult to collect large quantities required for biochemical analyses.

Here, we describe a new method to isolate relatively pure populations of males in large numbers. This method takes advantage of the inducible degradation of DPY-27, a component of the dosage compensation complex (DCC; Plenefisch *et al.* 1989). In *C. elegans*, the DCC downregulates gene expression from the 2 *X* chromosomes in hermaphrodites such that the overall level is comparable to the expression from the single *X* chromosome in males. Consequently, the DCC is essential for embryonic development in hermaphrodites but not in males. Worms defective for the DCC are therefore hermaphrodite-specific lethal (Meyer 2005). Using the auxin-inducible degradation system that has been adapted for *C. elegans* (Zhang *et al.* 2015; Ashley *et al.* 2021), we fused a degron tag to DPY-27 and constructed strains also expressing TIR1 in the *him-8* mutant background, which produces male self-progeny (Hodgkin *et al.* 1979). We show that males collected after auxin treatment exhibit normal meiosis and spermiogenesis and that these males are proficient for mating and sire viable progeny. We demonstrate the effectiveness of this method by analyzing gene expression and performing affinity pull-downs followed by mass spectrometry from male worm extracts.

Materials and methods
Genetics
Caenorhabditis elegans var. Bristol (N2) was used as the wild-type strain. The following strains were constructed:

> JEL1197: *sun-1p::TIR1 II; dpy-27::AID::MYC (xoe41) III; him-8(me4) IV*
> JEL991: *sun-1p::TIR1 II; dpy-27::AID::MYC(xoe41) brd-1::gfp::3xflag (xoe14) III; him-8(me4) IV*
> JEL1217: *sun-1p::TIR1 II; gfp(glo)::3xflag::cosa-1(xoe44) dpy-27::AID:: MYC (xoe41) III; him-8(me4) IV*
> JEL1214: *mex-5p::TIR1 I; dpy-27::AID::MYC (xoe41) III; him-8(me4) IV*

sun-1p::TIR1 and *mex-5p::TIR1* strains were graciously provided by Jordan Ward (UCSC; Ashley *et al.* 2021). Some nematode strains were provided by the Caenorhabditis Genetics Center, which is funded by the National Institutes of Health National

Center for Research Resources (NIH NCRR). Strains were maintained at 20°C.

CRISPR-mediated generation of alleles
dpy-27::AID::MYC(xoe41) and *gfp(glo)::3xflag::cosa-1(xoe44)* were generated using the co-CRISPR method as described (Paix *et al.* 2015). GermLine Optimized GFP sequence was used to enhance germline expression and prevent potential silencing (Fielmich *et al.* 2018). Guide sequence, repair template, and genotyping primers are provided in Supplementary File 1. Correct editing was verified by Sanger sequencing. Worms generated by CRISPR were outcrossed a minimum of 4 times.

Auxin treatment to generate male cultures
Synchronized L1 larvae were placed on NGM plates containing 1 mM auxin (Naphthaleneacetic Acid; K-NAA; PhytoTech #N610) and maintained at 20°C until adulthood. Worms were washed off plates and bleached in a final concentration of 0.5 N NaOH and 1% bleach (Porta-de-la-Riva *et al.* 2012). Embryos were collected by centrifugation at 1,300 g for 1 min and washed 3× with M9 buffer supplemented with 1 mM auxin. Embryos were transferred to a new tube with M9 buffer + 1 mM auxin and kept on a rocker for 24 h. L1 larvae together with unhatched embryos were washed with M9 buffer and plated onto NGM plates without auxin. Approximately two and half days later, viable worms were quantified for % males and used for downstream analyses. A detailed protocol for large-scale collection of male worms is provided in Supplementary File 2.

Cytological analyses
Immunostaining of germlines was performed as described (Jaramillo-Lambert *et al.* 2007) except slides were fixed in 100% ethanol instead of 100% methanol for direct GFP fluorescence of GFP::COSA-1. Rabbit anti-RAD-51 (1:10,000; cat #2948.00.02; SDIX; RRID: AB_2616441), mouse anti-Tubulin (1:500; cat# T9026, Sigma-Aldrich; RRID: AB_477593), and secondary antibodies Alexa Fluor 488 donkey anti-mouse and 594 donkey anti-rabbit IgG (1:500) from Life Technologies were used. DAPI (2 μg/ml; Sigma-Aldrich) was used to counterstain DNA.

Collection of fixed images was performed using an API Delta Vision Ultra deconvolution microscope equipped with a 60×, NA 1.49 objective lens, and appropriate filters for epi-fluorescence. Z-stacks (0.2 μm) were collected from the entire gonad. A minimum of 3 germlines was examined for each condition. Images were deconvolved using Applied Precision SoftWoRx batch deconvolution software and subsequently processed and analyzed using Fiji (ImageJ) (Wayne Rasband, NIH).

RAD-51 foci were quantified in germlines of age-matched males (18–24 h post-L4). Germlines were separated into the transition zone (leptotene/zygotene), as counted from the first and last row with 2 or more crescent-shaped nuclei, and pachytene, which was further divided into 3 equal parts: early, mid, and late pachytene. RAD-51 foci were quantified from half projections of the germlines. The number of foci per nucleus was scored for each region.

GFP::COSA-1 foci were quantified from deconvolved 3D data stacks; mid-late pachytene nuclei were scored individually through z-stacks to ensure that all foci within each individual nucleus were counted.

The number of spermatocytes at metaphase and anaphase, which were identified by spindle shape and orientation (anti-Tubulin) in combination with chromosome morphology (DAPI), in the division zone were quantified.

Spermiogenesis was monitored by releasing sperm into sperm medium (50 mM HEPES, 25 mM KCl, 45 mM NaCl, 1 mM MgSO₄, 5 mM CaCl₂, 10 mM Dextrose; pH 7.8) in the absence and presence of 200 μg/ml Pronase E (MedChemExpress HY-114158A), 0.4 μg/ml Trypsin (Promega V511A), 1 mM ZnCl₂ (Singaravelu *et al.* 2011; Liu *et al.* 2014), and imaged on a Leica DM4B microscope with differential interference contrast optics and a 63× Plan Apo 1.40 NA objective, a Leica K5 cMOS camera, and Leica Application Suite X version 3.7 software. Percent sperm activation (activated sperm/ total) was counted from sperm released from a minimum of 10 worms.

Analyses of male-sired progeny and sperm competitiveness

A single *fog-2(q71)* female and a single male of indicated genotype/condition were allowed to mate for 16 h on small *Escherichia coli* OP50 spots and then the female was transferred to new plates every 24 h up to 96 h. The total number of progeny (eggs + worms) from 6 mated females was scored 24 h after removing the female. Viability of male-sired progeny was determined by mating a single *fog-2(q71)* female with 3 males of indicated genotypes/conditions on small *E. coli* OP50 spots for 24 h. The mated female was transferred to new plates every 24 h. Progeny viability was determined over 3 days by counting eggs and hatched larvae 24 h after removing the female and calculating % as larvae/(eggs + larvae). The progeny of a minimum of 8 mated females were scored.

To test sperm competitiveness, late L4 *unc-119(ed3)* hermaphrodites and males of indicated genotypes/conditions were allowed to mate for 16 h. Hermaphrodites were transferred to fresh plates every 24 h, and upon reaching adulthood, offspring were scored as either Unc (self) or non-Unc (cross) progeny and counted (Hansen *et al.* 2015).

RT-PCR

Total RNA was isolated from 50 to 100 μl of packed worms from indicated genotypes/conditions using the RNeasy Mini Kit (Qiagen, Catalog #74104) and QIAshredder (Qiagen, Catalog #79654). One microgram of RNA was converted to cDNA using SuperScript III First-Strand Synthesis System for RT-PCR (Invitrogen, Catalog #18080-051) primed with Oligo(dT)₂₀. qPCR reactions were prepared with SsoAdvanced Universal SYBR Green Supermix (Bio-Rad, Catalog #1725271) using cDNA and the following primers (final concentration, 400 nM): *ama-1* (Housekeeping) Fwd: 5′GACGAGTCCAACGTACTCTCCAAC-3′, Rev: 5′TACTTGGGGCTCGATGGGC-3′; *vit-2* (female-enriched) Fwd: 5′GCCAGAAGAACCAGAGAAGCC-3′, Rev: 5′–TGTTGTTGCT GCTCGACCTC-3′; *sncp-1.3* (male-enriched) Fwd: 5′-TCCTTCATGC GAATGACCCG-3′, Rev: 5′-GCGCTTTGAATCTACCCAGC-3′; Cq values were determined for each primer pair and normalized to the *ama-1* control. The fold change between—or + auxin and wild type was analyzed using the $2^{-\Delta\Delta Ct}$ method. Raw Cq values and calculations are provided in Supplementary File 3.

Pull-down assays

Male worms were collected following auxin treatment as described above and resuspended in H100 lysis buffer (50 mM HEPES, pH 7.4, 1 mM EGTA, 1 mM MgCl₂, 100 mM KCl, 10% glycerol, 0.05% NP-40) + protease inhibitors (Complete Ultra Tablets, Mini Protease Inhibitor Cocktail; Roche #05892791001 and 1 mM PMSF; Sigma). Worms were allowed to settle at the bottom of the tube and the lysis buffer was removed until there was 0.5–1 ml buffer covering the worm pellet. Worms were resuspended and

flash frozen as "worm popcorns" by pipetting into liquid nitrogen. Worm popcorns were ground into fine powder using a SPEX SamplePrep 6970 FreezerMill and immediately stored at -80°C.

Approximately 1 ml of worm powder was thawed on ice and brought to 4 ml with H100 + protease inhibitors. The lysate was passed through a glass tissue grinder multiple times on ice and then centrifuged at 13,000 rpm for 20 min at 4°C to remove insoluble debris. Fifty microliters of anti-FLAG M2 magnetic beads (Millipore Sigma M8823) were prepared for each pull-down assay by washing with 1 ml H100 + protease inhibitors 4× using a magnetic rack separator. The soluble fraction was incubated with the washed beads for 3 h with constant rotation at 4°C. Beads were washed with 1 ml lysis buffer + protease inhibitors 4× and then washed in lysis buffer without protease inhibitors 7×. Approximately 10% of beads was analyzed by immunoblot to check efficiency of pull-down and the remaining processed for mass spectrometry.

Mass spectrometry analyses

Processing and proteomic profiling were performed at the University of California, Davis Proteomics Core Facility (https:// proteomics.ucdavis.edu). Protein samples on magnetic beads were washed 4× with 200 μl 50 mM Triethyl ammonium bicarbonate (TEAB) for 20 min each at 4°C with shaking. Two micrograms of trypsin was added to the bead/TEAB mixture and the samples were digested overnight at 4°C with shaking at 800 rpm. The supernatant was then removed, and the beads washed once with enough 50 mM ammonium bicarbonate to cover. After 20 min with gentle shaking, the wash was removed and combined with the initial supernatant. The peptide extracts were reduced in volume by vacuum centrifugation and a small portion of the extract was used for fluorometric peptide quantification (Thermo Scientific Pierce). One microgram was loaded for each LC-MS (liquid chromatography–mass spectrometry) analysis.

LC-MS/MS was performed on an ultra-high-pressure nanoflow Nanoelute (Bruker Daltonics) at 40°C with a constant flow of 400 nl/min on a PepSep 150 μm × 25 cm C18 column (PepSep, Denmark) with 1.5 μm particle size (100 Å pores) and a ZDV captive spray emitter (Bruker Daltonics). Mobile phases A and B were water with 0.1% formic acid (v/v) and 80/20/0.1% ACN/water/formic acid (v/v/vol), respectively. Peptides were separated using a 30 min gradient. Eluting peptides were then further separated using TIMS (trapped ion mobility spectrometry) on a Bruker timsTOF Pro 2 mass spectrometer. Mass spectrometry data were acquired using the dda PASEF method (Meier et al., 2018). The acquisition scheme used was 100 ms accumulation, 100 ms PASEF ramp (at 100% duty cycle) with up to 10 PASEF-MS/MS scans per topN acquisition cycle. The capillary voltage was set at 1,700 V, Capillary gas temp 200°C. The target value was set to 20,000 a.u. with the intensity threshold set at 500 a.u. The m/z range surveyed was between 100 and 1,700. Precursor ions for PASEF-MS/ MS were selected in real time from a TIMS-MS survey scan using a nonlinear PASEF scheduling algorithm. The polygon filter (200– 1,700 m/z) was designed to cover ions within a specific m/z and ion mobility plane to select multiply charged peptide features rather than singly charged background ions. The quadrupole isolation width was set to 2 Th for m/z < 700 and 3 Th for m/z 800.

Mass spectrometry raw files were searched using Fragpipe 16.0 (Kong *et al.* 2017) against the UniProt *C. elegans*; UP000001940 database. Decoy sequences were generated, appended, and laboratory contaminates added within Fragpipe. Default search settings were used. Carbamidomethylation of cysteine residues was set as a fixed modification, and methionine oxidation and

acetylation of protein N termini as variable modifications. Decoy false discovery rates were controlled at 1% maximum using both the Peptide and Protein prophet algorithms. Label-free protein quantification was performed with the IonQuant algorithm (default settings; Yu *et al.* 2020).

Search results were loaded into Scaffold (version Scaffold_5.0.1, Proteome Software Inc., Portland, OR, USA) for visualization purposes. Proteins that contained similar peptides and could not be differentiated based on MS/MS analysis alone were grouped to satisfy the principles of parsimony. Proteins sharing significant peptide evidence were grouped into clusters. The complete list of proteins identified from the control and the unique proteins identified from the BRD-1::GFP::3xFLAG pulldowns are provided in Supplementary File 4.

Statistical analyses

Statistical analyses and figures were prepared using GraphPad Prism version 9.0 (GraphPad Software). Statistical comparisons of % males (Fig. 1c), RAD-51 (Fig. 2a) and GFP::COSA-1 foci numbers (Fig. 2b), meiotic divisions (Fig. 2c), sperm activation (Fig. 3b), progeny numbers (Fig. 3c), progeny viability (Fig. 3d), sperm competitiveness (Fig. 3e), and fold change in *vit-2* and *sncp*-1.3 expression (Fig. 4a) were analyzed by Mann–Whitney. Detailed descriptions of statistical analyses are indicated in figure legends.

Results and discussion

Conditional degradation of DPY-27

The development of the auxin-inducible degradation system in *C. elegans* has facilitated analyses of many biological processes, including meiosis, spermatogenesis, mating, and aging (Zhang *et al.* 2015; Kasimatis *et al.* 2018; Ragle *et al.* 2020; Cahoon and Libuda 2021). The system requires the introduction of a short amino acid sequence, auxin-inducible degron (AID), onto a target protein,

Fig. 1. Enrichment of male worms by conditional degradation of DPY-27. a) Strategy for isolation of male cultures. b) Plate phenotype following auxin degradation of DPY-27, where greater than 98% of the worms are males. c) Quantification of male enrichment in WT, *him-8(me4)*, *sun-1p::TIR1; dpy-27::AID; him-8(me4)* and *mex-5p::TIR1; dpy-27::AID; him-8(me4)* in the absence (−auxin) and presence (+auxin) of 1 mM auxin. A minimum of 5 plates were counted for males; mean and 95% confidence intervals are shown. Statistical comparisons between + and − auxin for *sun-1p::TIR1; dpy-27::AID; him-8(me4)*: P = 0.001 and *mex-5p::TIR1; dpy-27::AID; him-8(me4)*: P = 0.0005 by Mann–Whitney.

expression of the plant F-box protein TIR1, and the presence of the plant hormone auxin (Nishimura *et al.* 2009). TIR1 interacts with endogenous SKP1 and CUL1 proteins to form an SCF E3 ubiquitin ligase complex. In the presence of auxin, TIR1 recognizes and binds the AID sequence, leading to ubiquitination and subsequent degradation of the AID-tagged protein (Ruegger *et al.* 1998; Gray *et al.* 1999). We inserted an AID sequence together with an MYC tag at the C-terminus of DPY-27 (abbreviated as DPY-27::AID), which is a component of the DCC essential for embryonic development in hermaphrodites (Plenefisch *et al.* 1989), and generated *dpy-27::AID* strains that also expressed TIR1 under the control of the *sun-1* or *mex-5* promoter, which drive expression in germ cells and during early embryogenesis when dosage compensation is established (Zhang *et al.* 2015; Ashley *et al.* 2021). Additionally, these strains contain a mutation in *him-8*, which leads to the production of male self-progeny (Hodgkin *et al.* 1979; Fig. 1a). The AID tag does not interfere with DPY-27 function, as in the absence of auxin, there was no increase in male self-progeny (or decrease in hermaphrodite self-progeny) between AID-tagged and nontagged strains, indicating that DPY-27::AID is functional (*sun-1p::TIR1* or *mex-5p::TIR1; dpy-27::AID; him-8* vs *him-8*; Fig. 1c). In the presence of 1 mM auxin beginning at the L1 larval stage, the viable progeny of *sun-1p::TIR1; dpy-27::AID; him-8* hermaphrodites were almost exclusively males and the rare surviving hermaphrodites were dumpy, suggesting that dosage compensation was efficiently disrupted (Fig. 1, b and c). Treatment of L4 larvae also resulted in the production of almost all males (∼95%). In contrast, strains expressing the *mex-5* driven TIR1 did not result in as effective killing of hermaphrodite progenies (Fig. 1c). Therefore, all subsequent analyses were performed using strains expressing the *sun-1* promoter-driven TIR1.

DPY-27 depletion does not affect male meiosis or spermiogenesis

To determine whether meiosis was affected in males isolated following DPY-27 degradation, we examined meiotic recombination and the meiotic divisions. We first monitored meiotic double-strand break (DSB) repair by examining the assembly and disassembly of the recombinase RAD-51 (Rinaldo *et al.* 2002) in the spatiotemporal organization of the *C. elegans* male germline using antibodies against RAD-51 (Colaiácovo *et al.* 2003; Checchi *et al.* 2014). RAD-51 loads onto resected DSBs destined for repair by homologous recombination beginning in leptotene/zygotene (transition zone) and is largely removed by mid-late pachytene. We had previously shown that *him-8* mutant males had wild-type levels of RAD-51 foci throughout the germline (Jaramillo-Lambert and Engebrecht 2010). Comparison of wild type, *him-8*, and *sun-1p::TIR1; dpy-27::AID; him-8* without and with auxin treatment revealed no differences, suggesting that DPY-27 does not play a role in the assembly or disassembly of RAD-51 on meiotic DSBs (Fig. 2a). To determine whether DSBs are accurately processed into crossovers, we monitored GFP::COSA-1, a cytological marker of crossover precursor sites (Yokoo *et al.* 2012). Wild-type males mostly exhibit 5 COSA-1 foci in pachytene nuclei, 1 on each of the 5 pairs of autosomes but not on the single *X* chromosome (Checchi *et al.* 2014). This pattern was unaltered by the degradation of DPY-27 (WT = 4.99 ± 0.30, *him-8* = 4.97 ± 0.20, *sun-1p::TIR1; dpy-27::AID; him-8* -auxin = 5.00 ± 0.13, +auxin = 5.02 ± 0.17; Fig. 2b). Together, these results suggest that degradation of DPY-27 has no effect on DSB repair and crossover designation in male meiosis.

As germ cells progress down the gonad, they enter the division zone and undergo meiosis I and II divisions to produce haploid
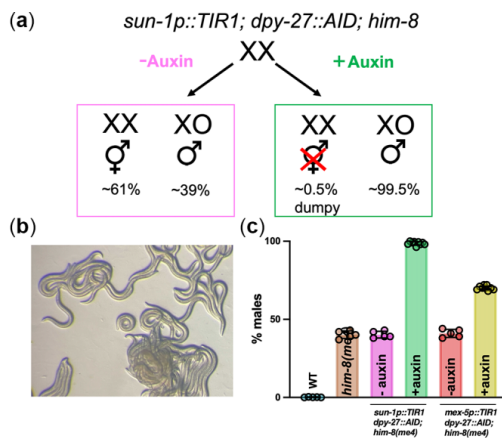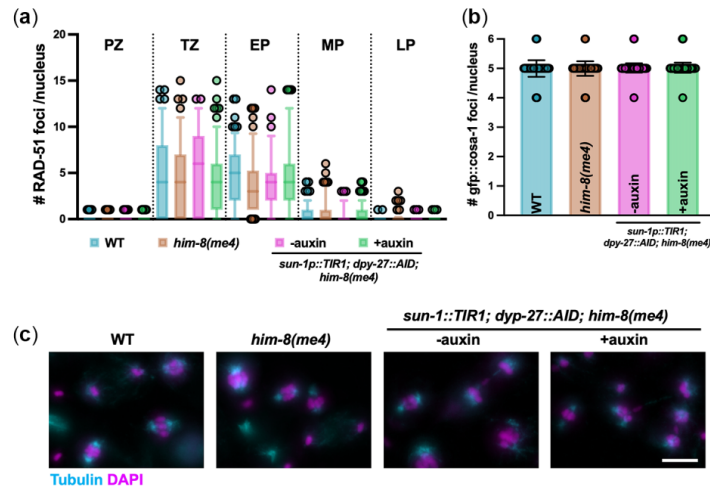
Fig. 2. DPY-27 depletion does not affect male meiosis. a) Quantification of RAD-51 in indicated regions of the germline. Box whisker plots show number of RAD-51 foci per nucleus. Horizontal line of each box represents the median, top and bottom of each box represent medians of upper and lower quartiles, lines extending above and below boxes indicate SD, and individual data points are outliers from 5% to 95%. Comparisons by Mann–Whitney revealed no statistical differences between the strains. PZ, proliferative zone; TZ, transition zone; EP, early pachytene; MP, mid-pachytene; LP, late pachytene. Three germlines were scored for each strain/condition. Number of nuclei scored in each region: WT, PZ = 559; TZ =136; EP = 132; MP = 175; LP = 132; *him-8(me4)*, PZ = 452; TZ = 115; EP = 134; MP = 141; LP = 135; *sun-1p::TIR1; dpy-27::AID; him-8(me4)* − auxin, PZ = 391; TZ = 126; EP = 117; MP = 155; LP = 168; *sun-1p::TIR1; dpy-27::AID,; him-8(me4)* + auxin, PZ = 671; TZ = 187; EP = 197; MP = 209; LP = 206. b) Number of COSA-1 foci in mid-late-pachytene in indicated strains/conditions; mean and 95% confidence intervals are shown. Comparisons by Mann–Whitney revealed no statistical differences between the strains. Number of nuclei analyzed: wild type = 189 (from 3 worms); *him-8(me4)* = 182 (from 3 worms); *sun-1p::TIR1; dpy-27::AID; him-8(me4)* −auxin = 549 (from 8 worms); *sun-1p::TIR1; dpy-27::AID; him-8(me4)* +auxin = 584 (from 8 worms). c) Images of the division zone of male gonads labeled with anti-tubulin (cyan) to visualize the spindle and DAPI (magenta) to visualize the DNA from WT (N2), *him-8(me4)* and *sun-1p::TIR1; dpy-27::AID; him-8(me4)* – and + auxin. Scale bar = 5 microns. There was no significant difference in the number of metaphase and anaphase meiosis I and II spindles/gonad in the different genotypes/conditions (N2 = 13.5 ± 3.7; *him-8(me4)*=12.83 ± 2.1; *sun-1p::TIR1; dpy-27::AID; him-8(me4)* − auxin = 11.83 ± 2.3 and + auxin = 13.5 ± 1.9/gonad) by Mann–Whitney.

spermatids (Shakes *et al.* 2009). To examine the meiotic divisions, we labeled dissected and fixed gonads with antibodies directed against tubulin to visualize the spindle, in combination with DAPI to examine chromosome morphology. Both the spindles and chromosomes appeared similar in all genotypes and conditions examined (Fig. 2c). Additionally, we saw no difference in the number of meiotic divisions in the different strains and conditions (N2 = 13.5 ± 3.7; *him-8(me4)*=12.83 ± 2.1; *sun-1p::TIR1; dpy-27::AID; him-8(me4)*—auxin = 11.83 ± 2.3 and + auxin = 13.5 ± 1.9/gonad). Together, these results indicate that degradation of DPY-27 by the AID system does not affect male meiosis. A previous study showed that *dpy-27* depletion also had no effect on female meiosis (Tsai *et al.* 2008).

Following meiosis, sperm undergo postmeiotic differentiation, sperm activation, or spermiogenesis. During spermiogenesis, round spermatids become motile and competent for fertilization through fusion of membranous organelles with the plasma membrane and formation of a pseudopod (Ward and Carrel 1979). To examine sperm morphology and activation, we released spermatids from male worms and examined their morphology under differential interference contrast microscopy in WT, *him-8* and *sun-1p::TIR1; dpy-27::AID; him-8* in the absence and presence of auxin. We observed no difference in the morphology of the spermatids (Fig. 3a). We also examined sperm activation by releasing spermatids into a solution containing Pronase E, which has previously been shown to induce differentiation into spermatozoa (Singaravelu *et al.* 2011). Activation of spermatids achieved a level greater than 80% in all genotypes and conditions examined (Fig. 3, a and b).

To monitor the quantity, quality, and competitiveness of sperm produced following DPY-27 depletion, we performed mating experiments. To examine quantity and quality, we used the *fog-2(q71)* mutant to eliminate hermaphrodite spermatogenesis, rendering XX animals self-sterile (Schedl and Kimble 1988), so that the contribution of the male parent to progeny number and viability could be assessed unambiguously. We observed no difference between wild type, *him-8* and *sun-1p::TIR1; dpy-27::AID; him-8* in the absence or presence of auxin for either the total number of progeny sired or the ability to produce euploid gametes as indicated by embryonic viability (Fig. 3, c and d). The latter is important as *C. elegans* anucleate sperm are competent for fertilization (Sadler and Shakes 2000). We also performed a competition experiment by crossing males to *unc-119(ed3)* hermaphrodites for 16 h, transferred the hermaphrodites at 24 h intervals, and counted the total number of self and cross progeny at each time point. Male sperm from all genotypes and conditions were preferentially used over hermaphrodite self-sperm (Fig. 3d), suggesting that sperm derived following DPY-27 degradation maintains the capability to out compete hermaphrodite sperm (Ward and Carrel 1979; LaMunyon and Ward 1995). Together, these results indicate that spermiogenesis, sperm quality, quantity, and competitiveness are not affected following degradation of DPY-27 by the AID system.

Molecular and biochemical studies using males collected following DPY-27 degradation

We used the *dyp-27::AID* system to monitor gene expression in the presence and absence of auxin. We first examined the
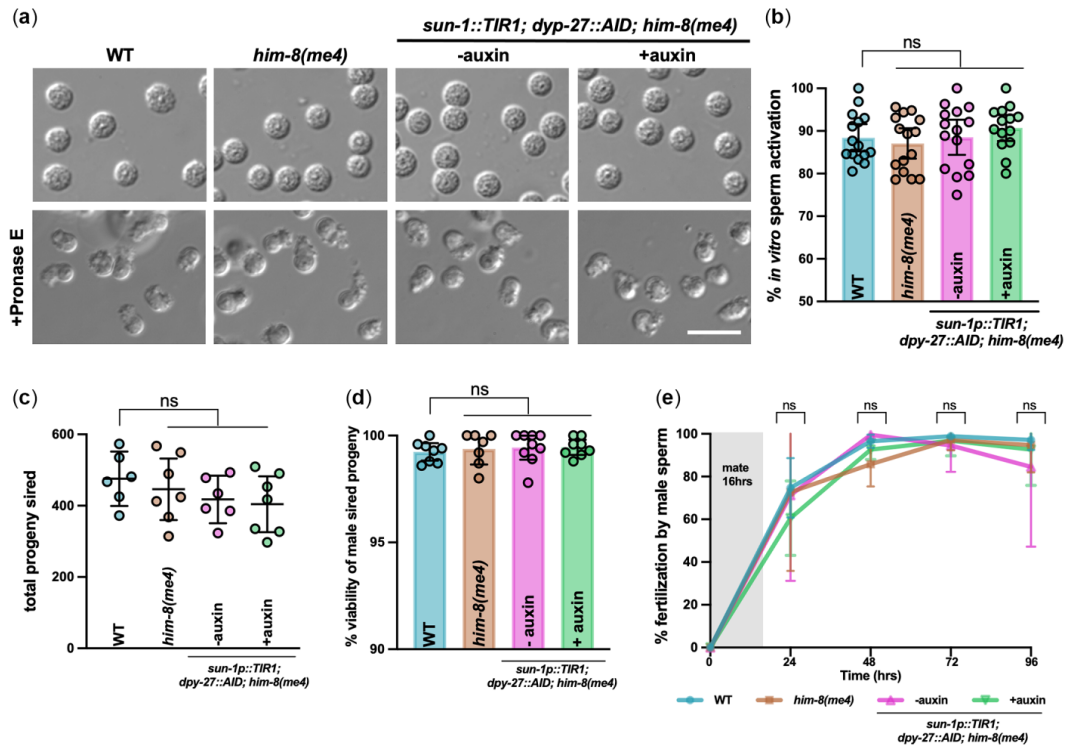
Fig. 3. Spermiogenesis, sperm quality, and competition are not perturbed following DPY-27 degradation in males. a) Micrographs of sperm isolated from N2 (WT), *him-8(me4)*, and *sun-1p::TIR1; dpy-27::AID; him-8(me4)* −auxin and +auxin and in the presence of Pronase E (+Pronase E), which leads to sperm activation. Scale bar = 10 microns. b) Quantification of sperm activation. Comparisons by Mann–Whitney revealed no statistical differences between the strains/conditions. The number of sperm examined: N2 (WT) = 544; him-8(me4) = 1,104; sun-1p::TIR1; dpy-27::AID; him-8(me4) −auxin = 602; sun-1p::TIR1; dpy-27::AID; him-8(me4) +auxin = 647. c) Total progeny sired. Mean and 95% confidence intervals are shown. Comparisons by Mann–Whitney revealed no statistical differences between the strains/conditions. Number of crosses examined: N2 (WT) = 6; him-8(me4) = 7; sun-1p::TIR1; dpy-27::AID; him-8(me4) −auxin = 6; sun-1p::TIR1; dpy-27::AID; him-8(me4) +auxin = 7. d) Embryonic viability of *fog-2(q71)* progeny sired by indicated males. Mean and 95% confidence intervals are shown. Comparisons by Mann–Whitney revealed no statistical differences between the strains/conditions. Number of crosses examined: wild type = 10; him-8(me4) = 8; sun-1p::TIR1; dpy-27::AID; him-8(me4) −auxin = 10; sun-1p::TIR1; dpy-27::AID; him-8(me4) +auxin = 9. e) Sperm competition assays were performed with *unc-119(ed3)* hermaphrodites. Mean and 95% confidence intervals are shown. Comparisons by Mann–Whitney revealed no statistical differences between the strains/conditions. Number of crosses examined: wild type = 10; him-8(me4) = 7; sun-1p::TIR1; dpy-27::AID; him-8(me4) −auxin = 7; sun-1p::TIR1; dpy-27::AID; him-8(me4) +auxin = 8.

expression of *vit-2*, 1 of 6 *vit* genes that encode vitellogenin (yolk proteins). Vit genes are expressed in the intestine of adult hermaphrodites, where the corresponding proteins are synthesized and then transported from the intestine into maturing oocytes (Kimble and Sharrock 1983; Grant and Hirsh 1999; Goszczynski *et al.* 2016). We collected adult worms from wild type (99.8% hermaphrodites/0.2% males) and *sun-1p::TIR1; dpy-27::AID; him-8* in the absence (60% hermaphrodites/40% males) and presence of auxin (0.5% hermaphrodites/99.5% males), extracted total RNA and analyzed *vit-2* expression using quantitative RT-PCR. We observed a small reduction in the expression of *vit-2* in *sun-1p::TIR1; dpy-27::AID; him-8* worms isolated from cultures grown in the absence of auxin compared to wild type (1.18-fold reduction), even though there was a 1.67-fold reduction in the number of hermaphrodites (Fig. 4a). This smaller than expected reduction in expression may be a consequence of the smaller body size of males compared to hermaphrodites, and/or due to inefficient collection of the male worms when a significant proportion of the

population is hermaphrodites. On the other hand, we observed a 300-fold reduction of *vit-2* expression in *sun-1p::TIR1; dpy-27::AID; him-8* worms isolated from cultures grown in the presence of auxin compared to wild type (Fig. 4a). These results are consistent with strong enrichment of males in our cultures.

We next examined the expression of a male-specific transcription factor *snpc-1.3*. *snpc-1.3* drives male piRNA expression and is expressed in the male germline (Choi *et al.* 2021). We observed a 4-fold enrichment of *snpc-1.3* expression in *sun-1p::TIR1; dpy-27::AID; him-8* worms isolated from cultures grown in the absence of auxin and a 60-fold enrichment of *snpc-1.3* in the presence of auxin compared to wild type (Fig. 4a). Thus, our enrichment procedure facilitates analyses of sex-specific gene expression profiles.

Gene expression studies can be performed on a relatively small number of worms; however, biochemical analyses require more material. To determine the utility of our male enrichment system in biochemical analyses, we isolated large numbers of
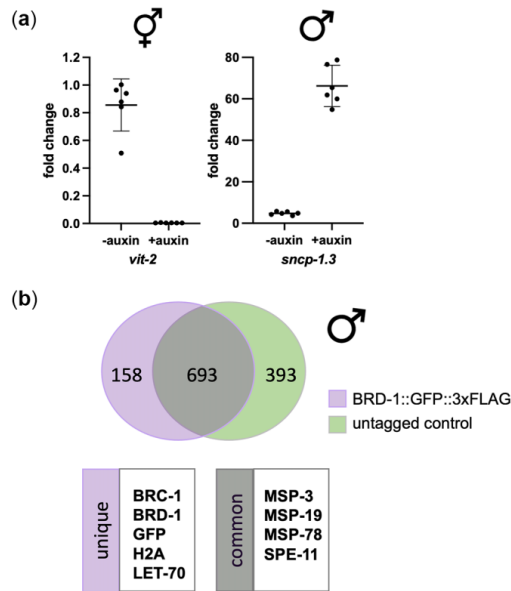
Fig. 4. Molecular and biochemical analyses of males isolated following DPY-27 depletion. a) Fold change of mRNA expression for *vit-2* (hermaphrodite enriched) and *sncp*-1.3 (male-enriched) in *sun-1p::TIR1; dpy-27::AID; him-8(me4)* in the absence and presence of auxin relative to wild type. Fold change was determined using the $2^{-\Delta\Delta Cq}$ method. *ama-1* (housekeeping) mRNA levels were used as a reference. Statistical comparisons by Mann–Whitney between − and + auxin for both *vit-2* and *sncp*-1.3, $P = 0.0022$. Raw Cq values and calculations are provided in Supplementary File 3. b) Mass spectrometry of peptides identified from male extracts (BRD-1 = 97.6% males; BRD-1::GFP::3xFLAG = 98.5% males). Venn diagram (generated by https://bioinfogp.cnb.csic.es/tools/venny/) shows unique peptides from BRD-1::GFP::3xFLAG and peptides from untagged control (BRD-1) with common peptides in middle. A small number of proteins with known interactions with BRC-1-BRD-1 (unique) as well as sperm proteins that are likely nonspecific interactions (common) are highlighted. The complete data set of nonspecific peptides and peptides unique to BRD-1::GFP::3xFLAG are available in Supplementary File 4.

males following DPY-27 degradation from worms expressing wild-type BRD-1 or BRD-1::GFP::3xFLAG, a component of the *C. elegans* BRCA1-BARD1 (BRC-1-BRD-1) complex. BRC-1-BRD-1 is an E3 ubiquitin ligase enriched in nuclei throughout the germline and in embryos. The complex regulates several aspects of meiotic recombination in both oogenesis and spermatogenesis (Boulton *et al.* 2004; Polanowska *et al.* 2006; Janisiw *et al.* 2018; Li *et al.* 2018, 2020).

We used magnetic anti-FLAG beads to pull-down proteins associated with BRD-1::GFP::3xFLAG from male whole worm lysates (see *Materials and Methods*). Mass spectrometry analyses of 2 independent pull-downs from both BRD-1 and BRD-1:: GFP::3xFLAG lysates identified enrichment of sperm proteins (Fig. 4b). While these sperm proteins are likely not specific interactors of BRD-1, their identification is consistent with the strong enrichment of male worms following DPY-27 degradation. In the BRD-1::GFP::3xFLAG pull-downs, we specifically identified its binding partner BRC-1, histone H2A, a known target of mammalian BRCA1-BARD1 ubiquitinylation, (reviewed in Witus *et al.* 2021), and the E2 ubiquitin-conjugating enzyme LET-70/UBC-2, which

had previously been shown to interact with the complex during DNA damage signaling in hermaphrodite worm extracts (Polanowska *et al.* 2006; Fig. 4b; Supplementary File 4). These results are consistent with a role for BRC-1-BRD-1 E3 ligase activity in male meiosis and demonstrate the utility of the system for examining protein interactions.

In conclusion, we describe a method to collect relatively pure populations of males that will facilitate future studies investigating how sex influences physiology. In combination with the large number of available mutants and continued improvement on the auxin-induced degradation system (Divekar *et al.* 2021; Hills-Muckey *et al.* 2022; Negishi *et al.* 2022), investigators can easily manipulate sex and determine the molecular processes that are differentially regulated in the sexes.

Data availability

Strains and reagents are available upon request. JEL1197 was deposited at CGC. The authors affirm that all data necessary for confirming the conclusions of this article are represented fully within the article and its tables and figures.

Supplemental material is available at *G3* online.

Conflicts of interest

The authors declare that there is no conflict of interest.

Literature cited

Ashley GE, Duong T, Levenson MT, Martinez MAQ, Johnson LC, Hibshman JD, Saeger HN, Palmisano NJ, Doonan R, Martinez-Mendez R, *et al.* An expanded auxin-inducible degron toolkit for *Caenorhabditis elegans*. Genetics. 2021;217(3):iyab006.

Boulton SJ, Martin JS, Polanowska J, Hill DE, Gartner A, Vidal M. BRCA1/BARD1 orthologs required for DNA repair in *Caenorhabditis elegans*. Curr Biol. 2004;14(1):33–39.

Cahoon CK, Libuda DE. Conditional immobilization for live imaging *Caenorhabditis elegans* using auxin-dependent protein depletion. G3 (Bethesda). 2021;11:jkab310.

Checchi PM, Lawrence KS, Van MV, Larson BJ, Engebrecht J. Pseudosynapsis and decreased stringency of meiotic repair pathway choice on the hemizygous sex chromosome of *Caenorhabditis elegans* males. Genetics. 2014;197(2):543–560.

Choi CP, Tay RJ, Starostik MR, Feng S, Moresco JJ, Montgomery BE, Xu E, Hammonds MA, Schatz MC, Montgomery TA, *et al.* SNPC-1.3 is a sex-specific transcription factor that drives male piRNA expression in *C. elegans*. Elife. 2021;10:e60681.

Chu DS, Liu H, Nix P, Wu TF, Ralston EJ, Yates JR, Meyer BJ. Sperm chromatin proteomics identifies evolutionarily conserved fertility factors. Nature. 2006;443(7107):101–105.

Colaiácovo MP, MacQueen AJ, Martinez-Perez E, McDonald K, Adamo A, La Volpe A, Villeneuve AM. Synaptonemal complex assembly in *C. elegans* is dispensable for loading strand-exchange proteins but critical for proper completion of recombination. Dev Cell. 2003;5(3):463–474.

Divekar NS, Davis-Roca AC, Zhang L, Dernburg AF, Wignall SM. A degron-based strategy reveals new insights into Aurora B function in *C. elegans*. PLoS Genet. 2021;17(5):e1009567.

Fielmich L-E, Schmidt R, Dickinson DJ, Goldstein B, Akhmanova A, van den Heuvel S. Optogenetic dissection of mitotic spindle positioning in vivo. Elife. 2018;7:e38198.

Goszczynski B, Captan VV, Danielson AM, Lancaster BR, McGhee JD. A 44 bp intestine-specific hermaphrodite-specific enhancer from the *C. elegans* vit-2 vitellogenin gene is directly regulated by ELT-2, MAB-3, FKH-9 and DAF-16 and indirectly regulated by the germline, by daf-2/insulin signaling and by the TGF-beta/Sma/Mab pathway. Dev Biol. 2016;413(1):112–127.

Grant B, Hirsh D. Receptor-mediated endocytosis in the *Caenorhabditis elegans* oocyte. Mol Biol Cell. 1999;10(12): 4311–4326.

Gray WM, del Pozo JC, Walker L, Hobbie L, Risseeuw E, Banks T, Crosby WL, Yang M, Ma H, Estelle M, *et al.* Identification of an SCF ubiquitin-ligase complex required for auxin response in *Arabidopsis thaliana*. Genes Dev. 1999;13(13):1678–1691.

Hansen JM, Chavez DR, Stanfield GM. COMP-1 promotes competitive advantage of nematode sperm. Elife. 2015;4:e05423.

Hills-Muckey K, Martinez MAQ, Stec N, Hebbar S, Saldanha J, Medwig-Kinney TN, Moore FEQ, Ivanova M, Morao A, Ward JD, *et al.* An engineered, orthogonal auxin analog/AtTIR1(F79G) pairing improves both specificity and efficacy of the auxin degradation system in *Caenorhabditis elegans*. Genetics. 2022;220(2):iyab174.

Hodgkin J, Horvitz HR, Brenner S. Nondisjunction mutants of the nematode *Caenorhabditis elegans*. Genetics. 1979;91(1):67–94.

Hubbard EJ, Greenstein D. The *Caenorhabditis elegans* gonad: a test tube for cell and developmental biology. Dev Dyn. 2000;218(1): 2–22.

Janisiw E, Dello Stritto MR, Jantsch V, Silva N. BRCA1-BARD1 associate with the synaptonemal complex and pro-crossover factors and influence RAD-51 dynamics during *Caenorhabditis elegans* meiosis. PLoS Genet. 2018;14(11):e1007653.

Jaramillo-Lambert A, Ellefson M, Villeneuve AM, Engebrecht J. Differential timing of S phases, X chromosome replication, and meiotic prophase in the *C. elegans* germ line. Dev Biol. 2007;308(1): 206–221.

Jaramillo-Lambert A, Engebrecht J. A single unpaired and transcriptionally silenced X chromosome locally precludes checkpoint signaling in the *Caenorhabditis elegans* germ line. Genetics. 2010; 184(3):613–628.

Jaramillo-Lambert A, Harigaya Y, Vitt J, Villeneuve A, Engebrecht J. Meiotic errors activate checkpoints that improve gamete quality without triggering apoptosis in male germ cells. Curr Biol. 2010; 20(23):2078–2089.

Kasimatis KR, Moerdyk-Schauwecker MJ, Phillips PC. Auxin-mediated sterility induction system for longevity and mating studies in *Caenorhabditis elegans*. G3 (Bethesda). 2018;8(8):2655–2662.

Kimble J, Sharrock WJ. Tissue-specific synthesis of yolk proteins in *Caenorhabditis elegans*. Dev Biol. 1983;96(1):189–196.

Kong AT, Leprevost FV, Avtonomov DM, Mellacheruvu D, Nesvizhskii AI. MSFragger: ultrafast and comprehensive peptide identification in mass spectrometry-based proteomics. Nat Methods. 2017;14(5):513–520.

Kurhanewicz NA, Dinwiddie D, Bush ZD, Libuda DE. Elevated temperatures cause transposon-associated DNA damage in *C. elegans* spermatocytes. Curr Biol. 2020;30(24):5007–5017.e4.

LaMunyon CW, Ward S. Larger sperm outcompete smaller sperm in the nematode *Caenorhabditis elegans*. Proc Biol Sci. 1998;265(1409): 1997–2002.

LaMunyon CW, Ward S. Sperm precedence in a hermaphroditic nematode (*Caenorhabditis elegans*) is due to competitive superiority of male sperm. Experientia. 1995;51(8):817–823.

L'Hernault SW, Shakes DC, Ward S. Developmental genetics of chromosome I spermatogenesis-defective mutants in the nematode *Caenorhabditis elegans*. Genetics. 1988;120(2):435–452.

Li Q, Hariri S, Engebrecht J. Meiotic double-strand break processing and crossover patterning are regulated in a sex-specific manner by BRCA1-BARD1 in *Caenorhabditis elegans*. Genetics. 2020;216(2): 359–379.

Li Q, Saito TT, Martinez-Garcia M, Deshong AJ, Nadarajan S, Lawrence KS, Checchi PM, Colaiacovo MP, Engebrecht J. The tumor suppressor BRCA1-BARD1 complex localizes to the synaptonemal complex and regulates recombination under meiotic dysfunction in *Caenorhabditis elegans*. PLoS Genet. 2018;14(11):e1007701.

Liu Z, Wang B, He R, Zhao Y, Miao L. Calcium signaling and the MAPK cascade are required for sperm activation in *Caenorhabditis elegans*. Biochim Biophys Acta. 2014;1843(2):299–308.

Meier F, Brunner A-D, Koch S, Koch H, Lubeck M, Krause M, Goedecke N, Decker J, Kosinski T, Park MA, *et al.* Online Parallel Accumulation-Serial Fragmentation (PASEF) with a Novel Trapped Ion Mobility Mass Spectrometer. Mol Cell Proteomics. 2018;17(12):2534–2545.

Meyer BJ. X-Chromosome dosage compensation. In: The *C. elegans* Research Community WormBook, editor. WormBook. 2005. p. 1–14.

Miller VM. Why are sex and gender important to basic physiology and translational and individualized medicine? Am J Physiol Heart Circ Physiol. 2014;306(6):H781–H788.

Negishi T, Kitagawa S, Horii N, Tanaka Y, Haruta N, Sugimoto A, Sawa H, Hayashi K-I, Harata M, Kanemaki MT, *et al.* The auxin-inducible degron 2 (AID2) system enables controlled protein knockdown during embryogenesis and development in *Caenorhabditis elegans*. Genetics. 2022;220(2):iyab218.

Nishimura H, L'Hernault SW. Spermatogenesis-defective (spe) mutants of the nematode *Caenorhabditis elegans* provide clues to solve the puzzle of male germline functions during reproduction. Dev Dyn. 2010;239(5):1502–1514.

Nishimura K, Fukagawa T, Takisawa H, Kakimoto T, Kanemaki M. An auxin-based degron system for the rapid depletion of proteins in nonplant cells. Nat Methods. 2009;6(12):917–922.

Paix A, Folkmann A, Rasoloson D, Seydoux G. High efficiency, homology-directed genome editing in *Caenorhabditis elegans* using CRISPR-Cas9 ribonucleoprotein complexes. Genetics. 2015;201(1):47–54.

Plenefisch JD, DeLong L, Meyer BJ. Genes that implement the hermaphrodite mode of dosage compensation in *Caenorhabditis elegans*. Genetics. 1989;121(1):57–76.

Polanowska J, Martin JS, Garcia-Muse T, Petalcorin MI, Boulton SJ. A conserved pathway to activate BRCA1-dependent ubiquitylation at DNA damage sites. EMBO J. 2006;25(10):2178–2188.

81

Porta-de-la-Riva M, Fontrodona L, Villanueva A, Ceron J. Basic *Caenorhabditis elegans* methods: synchronization and observation. J Vis Exp. 2012;64:e4019.

Ragle JM, Aita AL, Morrison KN, Martinez-Mendez R, Saeger HN, Ashley GA, Johnson LC, Schubert KA, Shakes DC, Ward JD, *et al.* The conserved molting/circadian rhythm regulator NHR-23/NR1F1 serves as an essential co-regulator of *C. elegans* spermatogenesis. Development. 2020;147:dev193862.

Rinaldo C, Bazzicalupo P, Ederle S, Hilliard M, Volpe AL. Roles for *Caenorhabditis elegans rad-51* in meiosis and in resistance to ionizing radiation during development. Genetics. 2002;160(2):471–479.

Ruegger M, Dewey E, Gray WM, Hobbie L, Turner J, Estelle M. The TIR1 protein of Arabidopsis functions in auxin response and is related to human SKP2 and yeast grr1p. Genes Dev. 1998;12(2):198–207.

Sadler PL, Shakes DC. Anucleate *Caenorhabditis elegans* sperm can crawl, fertilize oocytes and direct anterior-posterior polarization of the 1-cell embryo. Development. 2000;127(2):355–366.

Schedl T, Kimble J. *fog-2*, a germ-line-specific sex determination gene required for hermaphrodite spermatogenesis in *Caenorhabditis elegans*. Genetics. 1988;119(1):43–61.

Shakes DC, Wu J-C, Sadler PL, Laprade K, Moore LL, Noritake A, Chu DS. Spermatogenesis-specific features of the meiotic program in *Caenorhabditis elegans*. PLoS Genet. 2009;5(8):e1000611.

Singaravelu G, Chatterjee I, Marcello MR, Singson A. Isolation and in vitro activation of *Caenorhabditis elegans* sperm. J Vis Exp. 2011;47:2336.

Sulston JE, Albertson DG, Thomson JN. The *Caenorhabditis elegans* male: postembryonic development of nongonadal structures. Dev Biol. 1980;78(2):542–576.

Tsai CJ, Mets DG, Albrecht MR, Nix P, Chan A, Meyer BJ. Meiotic crossover number and distribution are regulated by a dosage compensation protein that resembles a condensin subunit. Genes Dev. 2008;22(2):194–211.

Ward S, Carrel JS. Fertilization and sperm competition in the nematode *Caenorhabditis elegans*. Dev Biol. 1979;73(2):304–321.

Witus SR, Stewart MD, Klevit RE. The BRCA1/BARD1 ubiquitin ligase and its substrates. Biochem J. 2021;478(18):3467–3483.

Yokoo R, Zawadzki KA, Nabeshima K, Drake M, Arur S, Villeneuve AM. COSA-1 reveals robust homeostasis and separable licensing and reinforcement steps governing meiotic crossovers. Cell. 2012;149(1):75–87.

Yu F, Haynes SE, Teo GC, Avtonomov DM, Polasky DA, Nesvizhskii AI. Fast quantitative analysis of timsTOF PASEF data with MSFragger and IonQuant. Mol Cell Proteomics. 2020;19(9):1575–1585.

Zhang L, Ward JD, Cheng Z, Dernburg AF. The auxin-inducible degradation (AID) system enables versatile conditional protein depletion in *C. elegans*. Development. 2015;142(24):4374–4384.

Communicating editor: J. Ward

Chapter 5

Differential requirement for BRCA1-BARD1 E3 ubiquitin ligase activity in DNA damage repair and meiosis in the *Caenorhabditis elegans* germ line

Qianyan Li, Arshdeep Kaur, Kyoko Okada, Richard J. McKenney, JoAnne Engebrecht

Arshdeep conducted genetic crosses to generate multiple strains used in this study. Kyoko Okada conducted the initial trial on and assisted with the purification of recombinant chimeric proteins. JoAnne performed male progeny and viability assays (Figure 1C-1E, 5A, 6E, 7A) and analyzed fluorescent BRC-1 fusion proteins foci number (Figure 6D) and overall pattern by coefficient of variation (Figure 5D and 7C). QL performed all other experiments.

Abstract

The tumor suppressor BRCA1-BARD1 complex functions in many cellular processes; of critical importance to its tumor suppressor function is its role in genome integrity. Although RING E3 ubiquitin ligase activity is the only known enzymatic activity of the complex, the *in vivo* requirement for BRCA1-BARD1 E3 ubiquitin ligase activity has been controversial. Here we probe the role of BRCA1-BARD1 E3 ubiquitin ligase activity *in vivo* using *C. elegans*. Genetic, cell biological, and biochemical analyses of mutants defective for E3 ligase activity reveal both E3 ligase-dependent and independent functions of the complex in the context of DNA damage repair and meiosis. We show that E3 ligase activity is essential for BRCA1-BARD1 to concentrate at both DNA damage and recombination sites in meiotic germ cells, but not at DNA damage sites in proliferating germ cells. While BRCA1 alone is capable of monoubiquitylation, BARD1 is required with BRCA1 to promote polyubiquitylation. We find that the requirement for E3 ligase activity and BARD1 in DNA damage signaling and repair can be partially alleviated by driving the nuclear accumulation and self-association of BRCA1. Our data suggest that in addition to E3 ligase activity, BRC-1 serves a structural role for DNA damage signaling and repair while BRD-1 plays an accessory role to enhance BRC-1 function.

Author Summary

BRCA1-BARD1 is a E3 ubiquitin ligase, which modifies proteins by the addition of the small protein ubiquitin. While mutations that disrupt E3 ligase activity and stability of the BRCA1-BARD1 complex lead to a predisposition for breast and ovarian cancer, the specific requirement for E3 ligase activity in tumor suppression is not known. Here we probe the function of E3 ligase activity and BARD1 in the maintenance of genome integrity by engineering point mutations that disrupt E3 ligase activity in *C. elegans* BRCA1 as well as a null mutation in BARD1. We find that while E3 ligase activity is important for genome integrity, the complex plays additional roles besides ubiquitylating proteins. Further, our data suggest that BRCA1 is the key functional unit of the complex while BARD1 is an accessory partner that enhances BRCA1's function. These findings may help explain why there is a higher prevalence of cancer-causing mutations in BRCA1 compared to BARD1.

Introduction

BReast CAncer susceptibility gene 1 (BRCA1) and its obligate partner BARD1 (BRCA1 Associated RING Domain protein 1) are RING domain-containing proteins, which when mutated are linked to elevated incidence of breast and ovarian cancer [1-6]. The BRCA1-BARD1 complex functions in a myriad of cellular processes, including DNA damage repair, replication, checkpoint signaling, meiosis, chromatin dynamics, centrosome amplification, metabolism, and transcriptional and translational regulation [7-13]. BRCA1-BARD1 regulates these pathways presumably through ubiquitylation of substrates via its RING domains, which function as an E3 ubiquitin ligase. BRCA1 specifically interacts with E2-conjugating enzymes for ubiquitin transfer, while BARD1 greatly stimulates the E3 ligase activity of BRCA1 [14, 15].

Multiple potential BRCA1-BARD1 substrates have been identified; however, the physiological significance of most of these substrates is currently unknown [16]. One well established substrate in the context of DNA damage signaling and transcriptional regulation is histone H2A [17-19]. Recent structural and molecular studies have led to mechanistic insight into recruitment of the complex to DNA damage sites and subsequent ubiquitylation of histone H2A. These studies have highlighted the targeting role of BARD1 to nucleosomes, where ubiquitylation of H2A by the complex promotes repair of DNA double strand breaks (DSBs). This most likely occurs by blocking recruitment of 53BP1, which promotes error-prone non-homologous end joining at the expense of homologous recombination [20-22]. However, the full spectrum of substrates and their relationship to regulation of different cellular processes are currently not known.

The role of BRCA1-BARD1 in DNA damage repair has been linked to its tumor suppressor function. Early studies suggested that BRCA1-BARD1 E3 ligase activity was not essential for either recombinational repair or tumor suppression. This conclusion was based on the analysis of a single isoleucine to alanine mutation at amino acid 26 (I26A) in the BRCA1 RING domain that abrogates its E3 ligase activity *in vitro* but maintains the stability of the BRCA1-BARD1 heterodimer, unlike many cancer-causing mutations that impair both E3 ligase activity and heterodimer stability [14, 23-26]. Mice expressing the BRCA1[I26A] mutant protein were not prone to tumor formation and mutant cells were proficient for homology-directed repair of DSBs, suggesting that E3 ligase activity is not essential for tumor suppressor function [27, 28]. In depth biochemical analyses, however, have shown that the BRCA1[I26A] mutant still exhibits residual E3 ligase activity when paired with a subset of E2 ubiquitin-conjugating enzymes in *in vitro* ubiquitin transfer assays. Mutation of two additional residues (leucine 63 and lysine 65 changed to alanines) within the BRCA1 RING domain in combination with I26A are required to completely abrogate E3 ligase activity *in vitro* without compromising the structural integrity of the complex [29]. These results suggest that BRCA1 harboring all three mutations is a true ligase dead mutant; however, the phenotypic consequence of this triple mutation has not been analyzed.

To define the requirement for E3 ligase activity *in vivo*, we focused on the *C. elegans* BRCA1 and BARD1 orthologs, BRC-1 and BRD-1. Previous analyses revealed that *C. elegans* BRC-1-BRD-1 is a functional E3 ubiquitin ligase that plays roles in DNA damage repair and meiotic recombination [30-40], as well as regulation of heterochromatin during embryogenesis [41]. Additionally, a recent study reported a role for BRC-1-BRD-1 in post-mitotic axon regeneration [42], consistent with the complex playing multiple roles *in vivo*. Here we analyzed the

requirement for BRC-1-BRD-1 E3 ubiquitin ligase activity by generating worms expressing BRC-1

mutant proteins containing the corresponding single (I23A) and triple (I23A, I59A, R61A)

mutations based on modeling with human BRCA1. We found both E3 ligase-dependent and

independent functions of BRC-1-BRD-1 in the context of DNA damage repair and meiosis.

Intriguingly, E3 ligase activity and BRD-1 function can be partially bypassed by independently

driving nuclear accumulation and self-association of BRC-1. Our data suggest that in addition to

E3 ligase activity, BRC-1 serves a structural role for DNA damage signaling and repair while BRD-

1 plays an accessory role to enhance BRC-1 function.

Results

brc-1(triA)* exhibits a more severe phenotype than *brc-1(I23A)

The *C. elegans* orthologs of BRCA1 and BARD1 are structurally conserved with the same key

domains as the human proteins: both BRC-1 and BRD-1 contain an N-terminal RING domain and

C-terminal BRCT repeat domains [31]. The RING domains specify E3 ubiquitin ligase activity, while

BRCT domains are phospho-protein interaction modules. Sequence alignment between human

BRCA1 and *C. elegans* BRC-1 RING domains reveals that residues essential for E3 ligase activity in

human BRCA1 (isoleucine 26, leucine 63, and lysine 65) correspond to amino acids isoleucine 23,

isoleucine 59 and arginine 61 in *C. elegans* BRC-1 (Fig 1A). While not identical, these amino acids

have similar chemical properties in terms of hydrophobicity and charge. To confirm that these

BRC-1 residues structurally align with the human residues critical for ubiquitin transfer, we used

AlphaFold to predict the structure of *C. elegans* BRC-1 RING domain, which was superimposed

onto the NMR structure of the human BRCA1 RING domain (Fig 1B) [14, 43, 44]. The predicted

structure overlay is consistent with the sequence alignment in that isoleucine 23, isoleucine 59 and arginine 61 in BRC-1 are the structural counterparts of isoleucine 26, leucine 63 and lysine 65 in human BRCA1.

To probe the *in vivo* function of BRC-1 E3 ligase activity, we generated *C. elegans* mutants *brc-1(I23A)* [isoleucine 23 mutated to alanine] and *brc-1(triA)* [isoleucine 23, isoleucine 59, arginine 61 mutated to alanines] at the endogenous *brc-1* locus using CRISPR-Cas9 genome editing and analyzed the mutant phenotypes with respect to meiosis and DNA damage repair. *brc-1* and *brd-1* mutants produce slightly elevated levels of male self-progeny (X0), a readout of meiotic X chromosome nondisjunction, have low levels of embryonic lethality under standard growth conditions, but display high levels of embryonic lethality after exposure to γ-irradiation (IR), which induces DNA DSBs [31, 32, 34]. For both male self-progeny and embryonic lethality under standard growth conditions, the *brc-1(I23A)* mutant produced similar levels to wild type, while *brc-1(triA)* worms gave rise to elevated levels compared to wild type but not to the extent of the *brc-1(null)* mutant [34] (Fig 1C, D). Following exposure to 75Gys of IR, *brc-1(I23A)* displayed higher levels of embryonic lethality compared to wild type, while *brc-1(triA)* produced inviable progeny at levels comparable to those observed in the *brc-1(null)* mutant, suggesting that E3 ligase activity is important when DNA damage is present.

While BRC-1-BRD-1 plays only a subtle role in an otherwise wild-type meiosis as evidenced by the low levels of male self-progeny and embryonic lethality (Fig 1C, D), we previously showed that the BRC-1-BRD-1 complex plays a critical role when chromosome synapsis and crossover formation are perturbed by mutation of either pairing center proteins, which are required for pairing and synapsis of homologous chromosomes, or components of the synaptonemal complex

89

(SC), the meiosis-specific protein structure that stabilizes homologous chromosome associations [33, 34]. To examine the phenotypic consequence of impairing BRC-1-BRD-1 E3 ligase activity when meiosis is perturbed, we monitored embryonic lethality in the different *brc-1* mutants in combination with mutation of ZIM-1, a zinc finger pairing center protein that mediates the pairing and synapsis of chromosomes *II* and *III* [45]. *zim-1* mutants produce 60-70% inviable progeny due to random segregation of chromosomes *II* and *III* in meiosis resulting in the formation of aneuploid gametes. We observed a progressive increase in embryonic lethality in *brc-1(I23A); zim-1*, *brc-1(triA); zim-1,* and *brc-1(null); zim-1* mutants, consistent with our previous observation that *brc-1(triA)* is more severely impaired for function than *brc-1(I23A)*. These results also suggest that neither *brc-1(I23A)* nor *brc-1(triA)* are null alleles (Fig 2A).

In addition to enhancing embryonic viability, BRC-1 and BRD-1 stabilize the RAD-51 filament at mid to late pachytene in the *zim-1* mutant [33, 34]. The RAD-51 recombinase assembles on resected single strand DNA at DSBs and is essential for homology search and strand invasion during homologous recombination [46-48]. In mutants where crossover formation is blocked by defects in pairing or synapsis (e.g., *zim-1*), RAD-51 filaments, visualized as nuclear foci by immunostaining, are extended into late pachytene [34, 48, 49]. Removal of BRC-1 in this context results in a "RAD-51 dark region" at mid to late pachytene due to a defect in RAD-51 filament stability [34] (Fig 2C, D). This is manifested in a reduction in both RAD-51 foci numbers (zone 3) and signal intensity (in dark region), followed by an increase in RAD-51 foci numbers (zone 4) in the *brc-1(null); zim-1* mutant (Fig 2B-F). To determine whether BRC-1 E3 ligase activity is required for RAD-51 stabilization when meiosis is perturbed, we monitored RAD-51 foci number and signal intensity in the different *brc-1; zim-1* mutants (Fig 2B). As with the increasing

severity of embryonic lethality in the putative E3 ligase dead alleles in *zim-1* mutants, impairment

of RAD-51 filament stability also showed increasing severity in the mutants (Fig 2D). In zones 2

and 3, *brc-1(I23A); zim-1* had slightly reduced numbers of RAD-51 foci compared to *zim-1*, but

significantly higher numbers than observed in *brc-1(null); zim-1*. More foci were observed in zone

4 in *brc-1(I23A); zim-1* than *zim-1* alone (Fig 2B, E; Supplemental Table 3). Additionally, average

RAD-51 foci intensity in the *brc-1(I23A); zim-1* was significantly reduced in the RAD-51 dark region

compared to *zim-1*, but not as reduced as in the *brc-1(null); zim-1* mutant ("in"; Fig 2C, F;

Supplemental Table 3). These findings suggest that *brc-1(I23A)* has a partial defect in RAD-51

filament stabilization. In contrast to *brc-1(I23A); zim-1*, *brc-1(triA); zim-1* showed a severe

reduction in the average number of RAD-51 foci in zone 3, although not to the same extent as in

brc-1(null); zim-1. There was also a significant reduction in average RAD-51 foci intensity in the

RAD-51 dark region in *brc-1(triA); zim-1* comparable to that observed in the *brc-1(null); zim-1*

mutant ("in"; Fig 2B-F; Supplemental Table 3). Taken together, *brc-1(I23A)* has a weak phenotype,

and *brc-1(triA)* is more severe, but still less severe compared to the *brc-1(null)*, suggesting that

while E3 ligase activity of BRC-1 is important in the context of defective meiosis, the presence

and structural integrity of the complex is critical.

BRC-1^{I23A} and BRC-1^{triA} are impaired for E3 ubiquitin ligase activity *in vitro*

To verify that BRC-1^{I23A} and BRC-1^{triA} are impaired for E3 ubiquitin ligase activity, we expressed

and purified a chimeric form of the RING domains of BRC-1 and BRD-1 (BRD-1-BRC-1) in *E. coli*,

modeled after studies of the human complex [23] (Fig 3A; Supplemental Fig 1A). The BRD-1-BRC-

1 chimera was incubated in the presence of human UBE1 E1 activating enzyme (50% identical to

C. elegans E1 UBA-1), UbcH5c E2 conjugating enzyme (94% identical to *C. elegans* E2 UBC-2), HA-ubiquitin (99% identical to *C. elegans* ubiquitin), and ATP and auto-ubiquitylation of the chimera was used as a readout for E3 ubiquitin ligase activity. Visualization with anti-HA antibodies revealed a characteristic ladder of bands due to the incorporation of multiple HA-ubiquitins into the chimera in the presence of ATP, indicating robust auto-polyubiquitylation catalyzed by the BRD-1-BRC-1 chimera (Fig 3B).

We next expressed and purified mutant chimeras harboring the I23A or triA (I23A, I59A, R61A) mutations (S1A Fig) and performed the auto-ubiquitylation assay. We observed a significant reduction in the incorporation of HA-ubiquitin into the mutant complexes. While no polyubiquitylation was observed, there was reduced but detectable monoubiquitylation of both I23A and triA chimeras by an end point assay (I23A = 14%, triA = 12% of wild-type auto-ubiquitylation; Fig 3C). Time course analyses with decreased concentrations of reaction components revealed a significant reduction in ubiquitin transfer by the I23A and triA chimeras. After 40 mins the I23A and triA chimeras showed only 4.1% and 2.8% of total ubiquitin incorporation as compared to the wild-type chimera (Fig 3D, E). While it did not reach statistical significance, the triA chimera showed consistently lower auto-monoubiquitylation than the I23A chimera. The physiological relevance of the residual auto-monoubiquitylation observed in the mutant chimeras is not clear as it was also observed in reactions lacking the E2 conjugating enzyme (S1B Fig).

Histone H2A is a known physiological substrate of human BRCA1-BARD1 [17, 19]. We next determined whether the wild-type and mutant chimeras could catalyze the incorporation of HA-ubiquitin into human histone H2A (90% identical to *C. elegans* H2A). Using antibodies directed

against histone H2A or HA, we observed incorporation of mono and di-ubiquitin into H2A in the wild-type reaction; however, no ubiquitin incorporation into H2A was detected with either of the mutant chimeras (Fig 3F; S1C Fig). From these experiments we conclude that BRC-1 harboring the I23A and the triA mutations are both significantly impaired for E3 ubiquitin ligase activity *in vitro*.

Nuclear accumulation and BRC-1-BRD-1 interaction are differentially affected by BRC-1[I23A] and BRC-1[triA]

The finding that the *brc-1(I23A)* mutant had considerably weaker phenotypes in DNA damage repair and meiosis compared to the *brc-1(triA)* mutant but displayed similar impairment in E3 ubiquitin ligase activity *in vitro*, led us to examine the consequence of these mutations in more detail. We first monitored the localization of the mutant complexes using antibodies directed against BRD-1[35]. BRC-1 and BRD-1 are mutually dependent for localization and are enriched in germ cell nuclei; in mitotic and early meiotic germ cells the complex is observed diffusely on chromatin and in foci. As meiosis progresses BRC-1-BRD-1 becomes associated with the SC and is then restricted to six small stretches on the six pairs of homologous chromosomes defined by the single crossover site [32, 34, 35] (Fig 4A). In the *brc-1(I23A)* mutant BRD-1 displayed a similar localization pattern as wild type, although the intensity of the signal was weaker and not as concentrated in the nucleus (nuclear enrichment in *brc-1(I23A)* was 79% of wild type; Fig 4A, B). Nuclear accumulation of BRD-1 was further impaired in the *brc-1(triA)* mutant in proliferating germ cells through mid pachytene, where the protein was enriched in the cytoplasm relative to the nucleus (Fig 4A, B). At late pachytene and diakinesis in the *brc-1(triA)* mutant, BRD-1 was observed in short stretches in the nucleus, in addition to the cytoplasmic signal (Fig 4A). A similar

localization pattern was observed by live cell imaging in the corresponding *brc-1* mutants expressing BRD-1::GFP at the endogenous locus [34] (S2A Fig). These results suggest that nuclear accumulation of the complex is impaired in the E3 ligase defective mutants. Significantly less BRD-1 accumulates in the nucleus in *brc-1(triA)* compared to *brc-1(I23A)*, and this difference likely contributes to the increased severity of the *brc-1(triA)* mutant observed *in vivo*.

Given the reduced signal of BRD-1 observed by immunofluorescence in the *brc-1(I23A)* and *brc-1(triA)* mutants, we next examined steady state protein levels by immunoblot analysis. For these experiments we used worms expressing BRD-1::GFP, which also contain 3 copies of the FLAG epitope, and monitored protein levels using anti-FLAG antibodies. We observed a modest reduction of BRD-1 steady state levels in the *brc-1(I23A)* and *brc-1(triA)* mutants compared to wild type (*brc-1(I23A) brd-1::gfp* = 81.5±6.2% and *brc-1(triA) brd-1::gfp* = 74.6±4.5% of *brd-1::gfp*) (Fig 4C, D). However, there was no significant difference between the two mutants (p=0.19), suggesting that the difference in phenotypes observed *in vivo* is not a consequence of altered steady state protein levels in the mutants, but likely reflects a change in subcellular distribution.

It has been reported that mutations of either I26 or I26, L63, K65 do not alter the interaction between human BRCA1 and BARD1 [29]. To determine whether this is also the case for the *C. elegans* orthologs, we examined interaction between full length BRC-1 and BRD-1 using the yeast two-hybrid system, which has previously been used to demonstrate interaction between these two proteins [31]. As expected, an interaction was detected between wild-type BRC-1 and BRD-1 using *his3* expression as a reporter by monitoring growth on medium lacking histidine. We observed slightly less growth on medium lacking histidine in the BRC-1^triA mutant,

suggesting that while BRC-1^{triA} interacts with BRD-1, there is some impairment (Fig 4E). Quantitative analysis of an independent reporter, b-galactosidase, revealed a ~50% decrease in the interaction between BRC-1^{I23A} and BRD-1 and a ~90% interaction defect between BRC-1^{triA} and BRD-1 (Fig 4F). Thus, in contrast to human BRCA1, mutations in BRC-1 residues important for ligase activity also affect interaction with BRD-1 and this interaction defect may contribute to the more severe phenotype of *brc-1(triA)*.

GFP fused to E3 ligase defective BRC-1 restores nuclear localization and partially rescues defects in DNA damage repair

In the course of our experiments we discovered that fusion of GFP to the N-terminus of the E3 ligase impaired *brc-1* mutants had less severe phenotypes in response to DNA damage compared to the non-tagged alleles, although only *gfp::brc-1(triA)* vs. *brc-1(triA)* reached statistical significance and was investigated further (p<0.0001; Fig 5A). Rescue in viability was specific to BRC-1, as C-terminal fusion of GFP to BRD-1 did not rescue embryonic lethality following IR in the E3 ligase defective mutants (S2B Fig). GFP::BRC-1 rescue was not a consequence of a change in BRC-1 expression, as there was no difference in steady state protein levels (S2C Fig). Interestingly, localization by live cell imaging revealed that unlike BRD-1 or BRD-1::GFP in the *brc-1(triA)* mutant, GFP::BRC-1^{triA} was enriched in the nucleus (-IR; Fig 5B, C), consistent with nuclear localization being important for function. As BRC-1-BRD-1 becomes enriched in nuclear foci in response to DNA damage [34, 35] and we observed improvement of function when GFP was fused to the BRC-1^{triA} following IR exposure, we examined localization of the mutant complex in response to IR-induced DNA damage. Two hours after exposure to IR, GFP::BRC-1^{triA} was largely nucleoplasmic

as well as concentrated into nuclear foci in mitotic germ cells, although foci formation was not as robust as in wild type (+IR; Fig 5B). Interestingly, within the same germ line, no distinct GFP::BRC-1[triA] foci were detected in meiotic nuclei following IR treatment. To quantify this, we calculated the coefficient of variation (CV), which provides a measure of the extent of foci above the nucleoplasmic GFP fluorescence signal. In mitotically-dividing *gfp::brc-1(triA)* mutant germ cells there was a significantly higher CV in IR treated worms compared to untreated worms; however, in meiotic cells there was no change in CV value following IR treatment (Fig 5D). These results suggest that independently recruiting BRC-1 to the nucleus by GFP fusion, where it can concentrate at DNA damage sites, partially suppresses the requirement for E3 ligase activity in proliferating germ cells.

BRC-1-BRD-1 E3 ligase activity is essential for recruitment of the complex to meiotic DSBs

In contrast to mitotic germ cells, essentially no GFP::BRC-1[triA] foci were observed in meiotic nuclei after exposure to IR, suggesting that meiosis is more sensitive to loss of E3 ligase activity in recruiting the complex to DNA damage sites (Fig 5B, D). To probe the requirement for BRC-1-BRD-1 E3 ligase activity in recruitment of the complex to meiotic DSBs, we monitored GFP::BRC-1[triA] localization in the *syp-1* mutant, where homologous chromosomes fail to synapse and no crossovers are formed [48]. As we previously reported, there were extensive GFP::BRC-1 nuclear foci in the *syp-1* mutant; these foci presumably represent meiotic recombination sites that are delayed in repair due to the absence of a homologous repair template [34]. In contrast to GFP::BRC-1, essentially no GFP::BRC-1[triA] foci were observed in the *syp-1* mutant (Fig 6A, D). This

result suggests that E3 ligase activity is critical for accumulation of BRC-1-BRD-1 at sites of meiotic recombination when chromosomes fail to synapse.

To determine whether the more severe defect in recruitment of GFP::BRC-1^{triA} to sites of recombination in meiosis was a consequence of barriers imposed by the specialized meiotic chromosome structure, we examined the requirement for BRC-1-BRD-1 E3 ligase activity in recruitment of the complex to DSBs in mutants defective in the formation of the chromosome axes. To that end, we monitored the localization of GFP::BRC-1 and GFP::BRC-1^{triA} when axis formation was impaired by mutation of the HORMA domain protein, HIM-3. HIM-3 is an axis component and is required for homolog pairing and synapsis and promotes crossover formation by biasing recombination to the homologous chromosome instead of the sister chromatid [50, 51]. While GFP::BRC-1 is recruited to both foci and the occasional track in the *him-3* mutant, as we have observed previously in mutants defective in meiotic recombination (e.g., *spo-11, mre-11, msh-5*) [33, 34], only tracks but no GFP::BRC-1^{triA} foci were observed in *him-3* (Fig 6B, D). Quantification of GFP::BRC-1 foci showed that the average number was lower in the *him-3* mutant compared to *syp-1* (29.4±4.0 vs. 16.9±3.5; p<0.0001), consistent with repair being more efficient in *him-3* mutants due to release of the barrier to inter-sister repair (Fig 6D). We also examined the consequence of impairing meiotic chromosome cohesion and hence axis formation by mutation of the meiosis-specific cohesin kleisin subunits, REC-8, COH-3, and COH-4 [52, 53]. Unlike *syp-1* and *him-3* mutants, *rec-8; coh-3 coh-4* triple mutants are not competent for meiotic DSB formation and therefore no GFP::BRC-1 foci were detected [53]. Consequently, we monitored recruitment of GFP::BRC-1 and GFP::BRC-1^{triA} to DNA breaks induced by IR and while we observed abundant GFP::BRC-1 foci, no GFP::BRC-1^{triA} foci were detected (Fig 6C, D). We also

observed a bright aggregate of both GFP::BRC-1 and GFP::BRC-1^{triA} in the *rec-8; coh-3 coh-4*

mutant in the presence and absence of IR, which is likely SC-like structures formed independently

of chromosomes (polycomplexes). These results suggest that the chromosome axis does not

impose a special requirement for BRC-1-BRD-1 E3 ligase-dependent recruitment of the complex

to DSBs.

We next examined the phenotypic consequence of the inability to recruit nuclear

GFP::BRC-1^{triA} to meiotic foci by examining progeny viability in the *zim-1* mutant. We observed

improved progeny viability of GFP::BRC-1^{triA} compared to BRC-1^{triA}, but not to the extent of what

was observed in response to IR (Fig 6E and Fig 5A). Thus, nuclear BRC-1-BRD-1 provides some

function despite its inability to accumulate at DSBs. Taken together, meiosis imposes a special

requirement for BRC-1-BRD-1 E3 ligase activity for recruitment to DNA damage and meiotic

recombination sites.

BRD-1 function can be partially bypassed by expressing GFP::BRC-1

The partial rescue of the E3 ligase impaired mutants by fusing GFP to BRC-1, but not to BRD-1,

prompted us to explore the contribution of BRD-1 to the function of the complex. To that end,

we constructed a null allele (*brd-1(null)*) by engineering multiple stop codons in the second exon

of *brd-1* as described [54], as available alleles of *brd-1* are in-frame deletions C-terminal to the

RING domain and helices where the two proteins interact [34]. *brd-1(null)* mRNA was unstable

and no GFP fluorescence was detected in *brd-1(null)* worms containing GFP fused to the C-

terminus of *brd-1*, providing evidence that it is a null allele (S3A, B Fig). Further, *brd-1(null)* was

phenotypically indistinguishable from *brc-1(null)* for male self-progeny and embryonic lethality in the absence and presence of IR (S3C and S4A Figs).

We next examined the phenotype of *gfp::brc-1 brd-1(null)* and saw a partial rescue of embryonic lethality following exposure to IR (Fig 7A). Consistent with this, GFP::BRC-1 was enriched in the nucleus and formed weak foci in response to IR in the absence of BRD-1, although there was reduced steady state levels of GFP::BRC-1 compared to in the presence of BRD-1 (Fig 7B, C; S4 Fig). These findings suggest that GFP::BRC-1 alone can provide some function without its binding partner. Rescue was specific to appending GFP to BRC-1, as neither GFP::BRD-1 nor BRD-1::GFP could provide partial function when BRC-1 was absent as measured by embryonic lethality following IR treatment (S4A Fig). Additionally, neither GFP::BRD-1 nor BRD-1::GFP accumulated in the nucleus in the absence of BRC-1 [34] (S4B Fig).

To determine the consequence of removing BRD-1 to BRC-1 E3 ligase activity we expressed and purified GFP::BRC-1 RING in *E. coli* (S4C Fig) and assayed auto-ubiquitylation *in vitro*. We observed significant auto-monoubiquitylation of GFP::BRC-1 RING, but no polyubiquitylation, suggesting that GFP::BRC-1 RING alone is competent to transfer a single ubiquitin onto itself (Fig 7D). To ascertain whether the lack of polyubiquitylation was due to the absence of BRD-1, we performed the *in vitro* assay using GFP::BRC-1 RING in the presence of the BRD-1-BRC-1[triA] chimera, which is incapable of polyubiquitylation (Fig 3B, C). Addition of BRD-1-BRC-1[triA] to the reaction resulted in both an increase in monoubiquitylation of the chimera and some polyubiquitylation (total ubiquitin signal was 2x the BRD-1-BRC-1[triA] ubiquitin signal alone; Fig 7D). These results suggest that BRC-1 can monoubiquitylate itself when fused to GFP in the absence of BRD-1, but that BRD-1 is required for polyubiquitylation of the complex.

To determine whether GFP::BRC-1-mediated monoubiquitylation was functionally important, we expressed GFP::BRC-1[triA] in *brd-1(null)* and monitored embryonic lethality following exposure to IR. No significant rescue was observed, suggesting that BRC-1-mediated monoubiquitylation is important in response to DNA damage (Fig 7A).

BRC-1 nuclear accumulation and self-association are important for function in the absence of BRD-1

To ascertain how fusion of GFP to the N-terminus of BRC-1 promotes function in the absence of BRD-1, we constructed an N-terminal fusion with mScarlet, a monomeric red fluorescent protein [55], at the endogenous BRC-1 locus. The mScarlet::BRC-1 fusion was fully functional (S4A Fig). However, expression of mScarlet::BRC-1 in *brd-1(null)* did not improve progeny viability following exposure to IR, even though mScarlet::BRC-1 was nuclear, could form foci in response to IR, and was as stable as GFP::BRC-1 in the *brd-1(null)* mutant (Fig 7B, C, S4D Fig). These results suggest that nuclear accumulation, while necessary, is not sufficient for BRC-1 function independent of BRD-1. As the name implies, mScarlet is monomeric, while GFP has the tendency to dimerize or oligomerize, particularly at high concentrations [56]. We next addressed whether association between GFP molecules was important for bypassing BRD-1 function. To that end, we modified the GFP fused to BRC-1 by substituting hydrophobic amino acids with charged amino acids on the surface interface (A206K, L221K, F223R) [57]; we refer to this as GFP[nd]::BRC-1 (nd for non-dimerizable). As with mScarlet::BRC-1, GFP[nd]::BRC-1 is fully functional in an otherwise wild-type worm (S4A Fig). However, expression of GFP[nd]::BRC-1 did not provide any rescue of the *brd-1(null)* mutant even though it was nuclear, could form foci in response to IR, and was as stable as

GFP::BRC-1 in the *brd-1(null)* mutant (Fig 7A, B, C; S4D Fig). These results indicate that nuclear accumulation and self-association of BRC-1 driven by GFP can partially bypass the requirement for BRD-1 in response to DNA damage.

Discussion

Here we take advantage of *C. elegans* to examine the requirement for BRCA1-BARD1 E3 ubiquitin ligase activity *in vivo* in the context of DNA damage signaling and meiosis. We find that mutants significantly impaired for E3 ligase activity *in vitro* still provide some function *in vivo*. We provide evidence that nuclear localization and BRC-1-BRD-1 association are critical for the function of the complex and these properties are impacted when E3 ligase activity is abrogated. Additionally, we show that GFP fusion to BRC-1 can drive protein accumulation in the nucleus and BRC-1 self-association, which partially rescue defects in DNA damage repair in the absence of BRD-1, indicating that BRC-1 is the key functional unit of the complex, while BRD-1 plays an accessory role to augment BRC-1 function.

A BRCA1 ligase dead mutant?

The role of BRCA1-BARD1 E3 ubiquitin ligase activity has remained enigmatic, due in part to the absence of a true ligase dead allele [27-29]. Based on extensive biochemical and structural work on RING-type E3 ligases in general, and the human BRCA1-BARD1 complex specifically, we constructed two BRC-1 mutants predicted to interfere with E3 ligase activity: I23A and triA [14, 23, 29, 58, 59] (Fig 1A, B). In human BRCA1 isoleucine 26 defines the binding site for E2 conjugating enzymes, while lysine 65 is the linchpin residue that activates E2-ubiquitin for ubiquitin transfer; human BRCA1 harboring the triple I26A, L63A, K65A mutation is an E3 ligase

dead mutant *in vitro* [29]. The corresponding isoleucine 23 and arginine 61 residues in *C. elegans* BRC-1 likely play analogous roles in E2 binding and activation of E2-ubiquitin and therefore the triA mutant is predicted to be a ligase dead enzyme (Fig 1B). Surprisingly, while both BRC-1[I23A] and BRC-1[triA] are significantly impaired for E3 ligase activity *in vitro* (Fig 3), they have different phenotypes *in vivo* (Figs 1, 2, 4). Further, neither *brc-1(I23A)* nor *brc-1(triA)* has a phenotype as severe as *brc-1(null)*, suggesting that in addition to E3 ligase activity, the complex serves a structural role to promote DNA damage signaling, repair, and meiotic recombination. This is consistent with studies of human BRCA1, where RING-less mutants maintain some homologous recombination function [60, 61].

Human BRCA1-BARD1 is capable of coupling with multiple E2s *in vitro* and different E2s define mono vs. polyubiquitylation of substrates and how polyubiquitin chains are linked to each other. The BRCA1[I26A] mutant has residual E3 ligase activity with a subset of E2s, including UbcH5c, which in complex with BRCA1-BARD1 promotes polyubiquitylation [23, 29]. We used UbcH5c in *in vitro* ubiquitylation assays and observed robust auto-polyubiquitylation as well as ubiquitylation of H2A with the wild-type chimera but no detectable self-polyubiquitylation with either I23A or triA chimeras, nor any ubiquitylation of histone H2A (Fig 3). However, there was significantly reduced but detectable auto-monoubiquitylation with the mutant chimeras. It is not clear whether monoubiquitylation represents residual activity that is only modestly reduced by mutation of I59A and R61A in the I23A mutant in *C. elegans* BRC-1 or is perhaps a consequence of the RING domains of BRD-1 and BRC-1 being physically tethered in the chimera. We did observe low levels of monoubiquitylation in the absence of any E2 (S1 Fig), suggesting that some

auto-monoubiquitylation may result from enhanced interaction between BRC-1 and BRD-1 RING domains within the chimera.

UbcH5c is orthologous to *C. elegans* UBC-2 (LET-70), which has previously been shown to couple with BRC-1-BRD-1 for ubiquitin transfer in the context of DNA damage signaling [35]. Similar to human BRCA1-BARD1, it is likely that *C. elegans* BRC-1-BRD-1 couples with multiple E2s to regulate different pathways (e.g., DNA damage signaling, meiosis, heterochromatin regulation, axon outgrowth) [31-37, 41, 42]. The *C. elegans* genome encodes 22 E2s and the entire spectrum of these E2s coupling to different E3 ligases is not clear [62]. Recently developed tools to conditionally deplete proteins in a tissue-specific manner could help define how different E2s couple with BRC-1-BRD-1, and other E3 ubiquitin ligases, to regulate different pathways *in vivo* [63-65].

While *C. elegans* BRC-1-BRD-1 shares many similarities with the human complex, it is not surprising that differences have evolved between worms and humans. For example, we found that in contrast to the human proteins, *C. elegans* E3 ligase defective BRC-1 show impaired interaction with BRD-1 [29] (Fig 4). One possibility is that these amino acid substitutions directly alter how BRC-1 and BRD-1 interact, although these do not reside in the helices required for binding between BRC-1 and BRD-1. Alternatively, BRC-1-BRD-1 auto-ubiquitylation may enhance interaction between these proteins, consequently ubiquitylation and interaction are impaired in E3 ligase defective BRC-1. Using physically tethered BRC-1 and BRD-1 RING domains in our chimeric proteins in the *in vitro* assay may have masked the interaction defect, leading to similar impairment of E3 ligase activity *in vitro* in BRC-1[I23A] and BRC-1[triA], but different phenotypes *in vivo*.

Nonetheless, continued analyses in *C. elegans* will be instrumental in defining the fundamental roles of BRC-1-BRD-1 in the context of a whole organism.

BARD1 serves an accessory role to ensure BRCA1-mediated polyubiquitylation and nuclear localization.

BARD1 was identified as a BRCA1 interacting protein and mutations in BARD1 also lead to an increased incidence of cancer [2, 6, 66]. Structural work defined the contact sites between the two proteins at the helices adjacent to the RING domains and demonstrated that only BRCA1 binds E2s for ubiquitin transfer, while BARD1 is required to stimulate BRCA1's E3 ligase activity [15, 67, 68]. We observed robust auto-polyubiquitylation of the wild-type chimera *in vitro;* however, assaying GFP::BRC-1 RING alone revealed significant auto-monoubiquitylation only, but no polyubiquitylation, in the presence of the same E2. Addition of the triA chimera to the GFP::BRC-1 RING reaction promoted the formation of polyubiquitylation, suggesting that BRD-1 is specifically required for BRC-1-mediated polyubiquitylation. Whether BARD1 also stimulates BRCA1 polyubiquitylation in mammalian cells is unclear; however, it has been shown that BRCA1-BARD1 auto-polyubiquitylation enhances the E3 ligase activity of the full-length complex *in vitro* [14, 15, 69].

In addition to promoting E3 ligase activity, BARD1 is important for the stability and nuclear retention of BRCA1 *in vivo*. Analysis of human BRCA1-BARD1 have revealed multiple mechanisms, including both regulated nuclear import and export driven by interaction between the two proteins, to ensure nuclear localization of the complex where it primarily functions [70, 71]. Similar to what has been reported in mammals, *C. elegans* BRD-1 is required for the stability and nuclear localization of BRC-1 [32, 72]. It was therefore surprising that appending GFP to the N-

terminus of BRC-1 could bypass the requirement for BRD-1 in promoting nuclear accumulation of BRC-1. GFP::BRC-1 alone could partially promote DNA damage signaling in the absence of BRD-1 and this was dependent on both nuclear localization and self-association driven by GFP. These results reinforce that BRCA1 is the primary functional unit of the complex and its key functions and targets are within the nucleus, while BARD1 serves an accessory role to bolster BRCA1-mediated polyubiquitylation and nuclear localization.

While both BRCA1 and BARD1 possess N-terminal RING and C-terminal BRCT domains, BARD1 uniquely contains conserved ankyrin repeats in the middle of the protein [10]. Recent molecular and structural studies have revealed that the BARD1 ankyrin and BRCT domains direct the interaction of BRCA1-BARD1 to N-terminal ubiquitylated histone H2A within the nucleosome, a chromatin mark associated with DSBs. Once bound, the complex mediates the ubiquitylation of the C-terminal tail of H2A, which opposes the binding of 53BP1 to promote repair by homologous recombination [20-22]. Given the unique requirement for BARD1 ankyrin domains in recruitment to damaged DNA, how does GFP::BRC-1 partially bypass the need for BRD-1 with respect to DNA damage signaling? One possibility is that there are redundant mechanisms for recruitment of BRC-1-BRD-1 to DSBs. Human BRCA1-BARD1 recruitment to DNA damage sites has been shown to be mediated through both BRCA1-BARD1 and RAP80 [73]. While no obvious RAP80 ortholog has been identified in *C. elegans*, other interacting proteins may serve a similar role in the recruitment of the complex to DSBs, and/or sequences within BRC-1 itself may facilitate concentration at DNA damage sites.

BRC-1-BRD-1 E3 ligase activity is required for recruitment of the complex to meiotic DSBs.

Our analysis of the E3 ligase defective mutants revealed that while GFP fusion to BRC-1[triA]

drives nuclear accumulation and the protein is capable of foci formation in response to DNA damage in the mitotic germ cells, E3 ligase activity is critical for the recruitment of the complex to DSBs in meiotic cells. Unique to meiosis is the pairing and synapsis of homologous chromosomes, which are essential for crossovers formation to ensure that the homologs segregate properly at Meiosis I. These events occur within the specialized structure of meiotic chromosomes, which includes the chromosome axes and the SC. Chromosome axes are extended filaments, which provide a scaffold for the organization of chromosomes as a linear array of loops [74, 75], and become the lateral elements of the SC. We found that blocking the formation of the chromosome axis, or the SC, did not alleviate the requirement for BRC-1-BRD-1 E3 ligase activity, suggesting that their presence does not impose an additional barrier for recruitment of the complex to meiotic DSBs (Fig 6). In addition to the specialized structure of meiotic chromosomes, the chromatin landscape is also different in meiotic cells and this unique chromatin environment may dictate the requirement for E3 ligase activity in recruiting the complex to meiotic DSBs [76]. Additionally, context-specific BRC-1-BRD-1 post-translational modifications and/or interacting proteins may exist that define redundant pathways for recruiting the complex to DNA damage sites in mitotic germ cells. Future work will provide insight into the context-dependent recruitment of BRC-1-BRD-1 in response to DNA damage.

Conclusion

BRCA1-BARD1 regulates a plethora of processes *in vivo* and mounting evidence indicates that BRCA1-BARD1 E3 ligase activity is critical for several aspects of the complex's function, including tumor suppression. However, the underlying molecular mechanisms are just beginning to be

revealed. Our findings that BRC-1 is the key driver for DNA damage signaling and repair within the heterodimer is consistent with the observed higher prevalence of pathogenic variants identified in BRCA1 as compared to BARD1 [77, 78]. Further, mutations in BRCA1 pose high risk for both breast and ovarian cancer, while BARD1 mutations are only a risk factor for breast, but not ovarian cancer [79-81]. Thus, as in *C. elegans*, human BRCA1 and BARD1 are not equivalent in function leading to different spectrum of cancers when mutated.

Materials and methods

Genetics: *C. elegans* strains used in this study are listed in Supplemental Table 1. Some nematode strains were provided by the Caenorhabditis Genetics Center, which is funded by the National Institutes of Health National Center for Research Resources (NIH NCRR). Strains were maintained at 20°C.

CRISPR-mediated allele construction: *brc-1(xoe4)*, *gfp::brc-1(xoe7)* and *brd-1::gfp(xoe14)* have been described [34]. *gfp::brc-1(xoe20[I23A])* and *mScarlet-i::brc-1(xoe34)* were generated using CRISPR-mediated genome editing with a self-excising cassette as described in [82] with modifications as follows: I23A was introduced at the same time with GFP knock-in by incorporating the corresponding mutation in the 3' homology arm on the repair template plasmid using the Q5 site-directed mutagenesis kit (New England Biolabs). GermLine Optimized mScarlet-i sequence (Fielmich *et al.* 2018) was cloned into the repair template plasmid in place of GFP by Gibson Assembly to generate *mScarlet-i::brc-1(xoe34)*. *gfp::brc-1(xoe48[triA])* was generated by introducing the corresponding I59A R61A mutations in the *gfp::brc-1(xoe20[I23A])* background

107

using the co-CRISPR method [83]. All other genome-edited strains were generated using the co-CRISPR method. *brd-1(xoe58[null-gfp::3xFLAG])* was generated by introducing the stop-in cassette into *brd-1::gfp(xoe14)* [34]. Guide sequence, repair template, and primers for genotyping are provided in Supplemental Table 2. All strains were outcrossed for a minimum of three times before analyses.

Embryonic lethality in the absence and presence of irradiation and male self-progeny: L4 hermaphrodites were transferred to individual plates (-IR) or exposed to 75Gys γ-irradiation from a ^{137}Cs source, and then transferred to individual plates. Individually plated hermaphrodites were transferred to new plates every 24hr for 3 days. Embryonic lethality was determined by counting eggs and hatched larvae 24hr after removing the hermaphrodite and calculating percent as eggs/(eggs + larvae). Males were scored after 72hr and calculating percent as males/(males + hermaphrodites + eggs).

Cytological analyses

Immunolabeling: Germ lines were immunolabeled as described [84]. The following primary antibodies were used at the indicated dilutions: rabbit anti-RAD-51 (2948.00.02; SDIX; 1:5,000; RRID: AB_2616441), rabbit anti-BRD-1 (1:500; from Dr. Simon Boulton[35]). Secondary antibodies Alexa Fluor 594 donkey anti-rabbit IgG from Life Technologies were used at 1:500 dilution. DAPI (2µg/ml; Sigma-Aldrich) was used to counterstain DNA.

Image capture: Collection of fixed images was performed using an API Delta Vision Ultra deconvolution microscope equipped with an 60x, NA 1.49 objective lens, and appropriate filters for epi-fluorescence. Z stacks (0.2μm) were collected from the entire gonad. Images were deconvolved using Applied Precision SoftWoRx batch deconvolution software and subsequently processed and analyzed using Fiji (ImageJ) (Wayne Rasband, NIH).

For live cell imaging, 18–24 hr post L4 hermaphrodites were anesthetized in 1mM tetramisole and immobilized between a coverslip and a 2% agarose pad on a glass slide. Z-stacks (0.33μm) were captured on a spinning-disk module of an inverted objective fluorescence microscope with a ~100Å, NA 1.46 objective, and EMCCD camera. Z-projections of stacks were generated, cropped, and adjusted for brightness in Fiji.

RAD-51 foci quantification: RAD-51 foci were quantified in a minimum of three germ lines of age-matched hermaphrodites (18-24hr post-L4). As the *zim-1* mutation results in an extended transition zone, we divided germ lines into four equal zones beginning from the first row with two or more crescent-shaped nuclei until the end of diplotene (Fig 2B). RAD-51 foci were quantified from half projections of the germ lines; the number of foci per nucleus was scored for each zone.

To measure pixel intensities of RAD-51, foci were identified by a prominence value between 10-20 using the "Find Maxima" function embedded in Fiji from half projections of germ lines. Pixel intensities were measured using ROI Manager in Fiji from defined regions of the gonad and the values were plotted on scatterplot with means and 95% CI using GraphPad Prism. A minimum of three germ lines for each genotype were used for quantification.

Nuclear to cytoplasmic ratio: Mean pixel intensity of BRD-1 immunolabeling or direct GFP fluorescence was measured from 80 nuclei and surrounding cytoplasm from three different germ lines in mitotic and meiotic (early to mid pachytene) regions of the gonad using Fiji. The nucleoplasmic to cytoplasmic ratio was calculated and the mean and 95% CI for the ratio was plotted.

Coefficient of variation: GFP::3xFLAG::BRC-1^{triA} fluorescence following exposure to 75Gys IR was quantified by measuring the mean fluorescence intensity and standard deviation (SD) in Fiji for individual nuclei [region of interest (ROI)] in mitotic germ cells (proliferative zone) and meiotic germ cells (early to mid pachytene). Coefficient of variation (CV) is defined as SD of intensity divided by mean intensity [85]. The CV describes the dispersion of pixel intensity values from a 2D ROI around the mean pixel intensity such that nuclei with more distinct foci will have high CV values, whereas nuclei with more uniform fluorescence will have low CV values.

GFP::BRC-1, and GFP::BRC-1^{triA} foci quantification: Foci were quantified in 10 mid pachytene nuclei from each of three half projections of germ lines of age-matched hermaphrodites (18-24hr post-L4).

Protein Constructs: The BRD-1-BRC-1 chimera, encoding amino acids 1-107 of BRD-1 and amino acids 2-106 of BRC-1 separated by a GGSGG-linker was synthesized as a G-block and cloned into pET28A vector containing a PreScission protease cleavage site, superfolder GFP (sfGFP) and a strepII-tag, using Gibson Assembly. Mutant BRD-1-BRC-1 chimeras harboring the single I23A and

triA mutations were similarly synthesized as G-blocks and cloned into pET28A as described above. The GFP::BRC-1 RING sequence in pET28A encodes amino acids 2-106 of BRC-1 and a N-terminal GFP followed by 3x FLAG-tag and a C-terminal strepII-tag. The protein expressed from this construct has identical amino acid sequences as the fusion protein expressed in *gfp::brc-1(xoe7)* allele with the exception of truncated BRC-1 RING domain and the addition of the strepII-tag.

Protein purification: The wild-type and mutant BRD-1-BRC-1 chimeras were expressed in BL21-CodonPlus (DE3)-RIPL cells (Agilent). The cells were grown at 37°C until OD600 0.6 and were induced by 0.2mM isopropyl-β-D-thiogalactoside in the presence of 100μM ZnCl2 at 37°C for 6 hrs. The GFP::BRC-1 RING was induced overnight at 18°C. After induction, cells were harvested and resuspended in buffer A (20mM HEPES-KOH pH 7.2, 300mM NaCl, 1mM EGTA) supplemented with 1mM DTT, 0.2% NP-40, protease inhibitors (1mM PMSF; protease inhibitor cocktail P83340; Sigma-Aldrich) and lysed using a Emulsiflex C-3 (Avestin) high pressure homogenizer. The lysates were centrifuged at 15000xg for 20min at 4°C. The supernatants were passed through Strep-Tactin XT (IBA) for affinity purification, and the column was washed with lysis buffer to remove unbound proteins before eluting the proteins with 50 μM biotin (Chem-Impex Int'l) in low salt buffer (20mM HEPES-KOH pH 7.2, 30 mM NaCl, 0.1% NP40). Proteins were further purified by anion exchange using HiTrap Q HP column equilibrated with 20mM HEPES-KOH pH7.2 with a linear NaCl gradient from 0mM to 600mM. Peak fractions were pooled and concentrated on Amicon-Ultra spin filters (EMD Millipore) and supplemented with 10% glycerol. Protein aliquots were snap frozen in liquid nitrogen and stored at -80°C. Protein concentration was measured using a Nanodrop One (ThermoFisher) based on the total amount of fluorophore (sfGFP or GFP).

E3 ligase activity assay: Ubiquitin transfer reactions were performed in 30μl reaction volume at 30°C for the indicated time with mild rocking. For end point auto-ubiquitylation assays, the reaction mixture contained 0.2μM E1 (hUBE1; E-305; bio-techne), 1mM E2 (hUbcH5c; E2-627; biotechne), 5μM BRD-1-BRC-1 chimera, 20μM HA-ubiquitin (U-110; bio-techne), 5mM ATP, 5mM MgCl$_2$ in reaction buffer (20mM Hepes pH 7.2; 150mM NaCl). To test ubiquitylation of histone H2A, 0.75μM human histone H2A (ab200295; Abcam) was added to the above reaction mixture. For time course experiments, 0.1μM E1, 0.5μM E2, 3μM BRD-1-BRC-1 chimera, 10μM HA-ubiquitin, 5mM ATP, 5mM MgCl$_2$ were mixed in a 150μl reaction volume and incubated with mild rocking at 30°C. 30μl were removed at 0, 5, 10, 20, 40min and the reactions stopped with 10μl 4X sample buffer followed by boiling. Reaction mixtures were visualized by immunoblot and analyzed by measuring pixel intensity of ubiquitylated species.

Immunoblot analysis: For steady state protein levels, whole worm lysates were generated from indicated genotypes. ~200 worms were collected in M9 buffer, washed 2x in M9 and then resuspended in equal volume of 2X Laemmli sample buffer (Bio-RAD) in a total volume of 40ml. Worm lysates or E3 ligase reaction mixtures were resolved on 4-20% stain-free SDS-PAGE gels (Bio-RAD) and transferred to Millipore Immobilon-P PVDF membranes. Membranes were blocked with 5% nonfat milk and probed with mouse anti-FLAG (MA1-91878; Invitrogen; 1:1000; RRID AB_1957945), rabbit anti-GFP (NB600-308; Novus Biologicals; 1:2000; RRID: AB_10003058), mouse anti-HA [12CA5; amino acids 98–106 of human influenza virus hemagglutinin protein; IgG2b mAb; 1:1000; RRID: AB_2532070; in-house (Trimmer Laboratory)], or rabbit anti-Histone-H2A (ab18255; Abcam; 1:1000; RRID:AB_470265) followed by IRDye800-conjugated anti-mouse

IgG secondary antibodies (962 32212; LI-COR Bioscience; 1:20000; RRID: AB_621847) or IRDye680-conjugated anti-rabbit IgG secondary antibodies (925-68073: ; LI-COR Bioscience; 1:20000; RRID: AB_2716687). Immunoblots were imaged on a LI-COR Odyssey Infrared Imager, signal was quantified using Image StudioLite and normalized with total protein input measured from the stain-free signal using BioRad Gel Doc^{TM} EZ System.

Yeast two-hybrid: Full length wild-type or mutant BRC-1 sequences were cloned into plasmid pBridge (Takara Bio), transformed into yeast strain Y2HGold (Takara Bio) and transformants were selected on medium lacking tryptophan. Full length BRD-1 sequences were cloned into plasmid pACT2.2, transformed into yeast strain Y187 (Takara Bio) and transformants were selected on medium lacking leucine. Wild type or mutant BRC-1 expressing strains were mated with BRD-1 expressing strain and the diploids selected on -Trp - Leu double dropout plate at 30°C. Diploid cells were grown in liquid -Trp - Leu double dropout medium overnight, and serial dilutions were plated on -His -Trp -Leu triple dropout and -Trp -Leu double dropout solid media. For quantitative measurement of wild type or mutant BRC-1 and BRD-1 interactions, b-galactosidase activity was measured. Cell lysates were incubated in the presence of CPRG (chlorophenol red-b-D-galactopyranoside, RocheApplied Science Cat. NO.10884308001) as substrate, color change was measure at OD_{578} and b-galactosidase units were calculated as described (Yeast Protocol Handbook, Takara Bio).

RT-PCR: Total RNA was isolated from 50 to 100 μl of packed worms from wild type and *brd-1(null)* using the RNeasy Mini Kit (74104; Qiagen) and QIAshredder (79654; Qiagen). 1 μg of RNA was

converted to cDNA using SuperScript III First-Strand Synthesis System for RT-PCR (18080-051; Invitrogen) primed with Oligo(dT)20. PCR was performed in a standard PCR machine with 20 cycles of amplification and resolved by gel electrophoresis.

References

1.   Futreal PA, Liu Q, Shattuck-Eidens D, Cochran C, Harshman K, Tavtigian S, et al. BRCA1 mutations in primary breast and ovarian carcinomas. Science. 1994;266(5182):120-2. Epub 1994/10/07. doi: 10.1126/science.7939630. PubMed PMID: 7939630.

2.   Ghimenti C, Sensi E, Presciuttini S, Brunetti IM, Conte P, Bevilacqua G, et al. Germline mutations of the BRCA1-associated ring domain (BARD1) gene in breast and breast/ovarian families negative for BRCA1 and BRCA2 alterations. Genes Chromosomes Cancer. 2002;33(3):235-42. Epub 2002/01/25. doi: 10.1002/gcc.1223. PubMed PMID: 11807980.

3.   Godwin AK, Vanderveer L, Schultz DC, Lynch HT, Altomare DA, Buetow KH, et al. A common region of deletion on chromosome 17q in both sporadic and familial epithelial ovarian tumors distal to BRCA1. Am J Hum Genet. 1994;55(4):666-77. Epub 1994/10/01. PubMed PMID: 7942844; PubMed Central PMCID: PMCPMC1918278.

4.   Hall JM, Lee MK, Newman B, Morrow JE, Anderson LA, Huey B, et al. Linkage of early-onset familial breast cancer to chromosome 17q21. Science. 1990;250(4988):1684-9. PubMed PMID: 2270482.

5.   Miki Y, Swensen J, Shattuck-Eidens D, Futreal PA, Harshman K, Tavtigian S, et al. A strong candidate for the breast and ovarian cancer susceptibility gene BRCA1. Science. 1994;266(5182):66-71. Epub 1994/10/07. doi: 10.1126/science.7545954. PubMed PMID: 7545954.

6.   Thai TH, Du F, Tsan JT, Jin Y, Phung A, Spillman MA, et al. Mutations in the BRCA1-associated RING domain (BARD1) gene in primary breast, ovarian and uterine cancers. Hum Mol Genet. 1998;7(2):195-202. Epub 1998/03/21. doi: 10.1093/hmg/7.2.195. PubMed PMID: 9425226.

7.   Bochar DA, Wang L, Beniya H, Kinev A, Xue Y, Lane WS, et al. BRCA1 is associated with a human SWI/SNF-related complex: linking chromatin remodeling to breast cancer. Cell. 2000;102(2):257-65. Epub 2000/08/16. doi: 10.1016/s0092-8674(00)00030-1. PubMed PMID: 10943845.

8.   Dizin E, Gressier C, Magnard C, Ray H, Decimo D, Ohlmann T, et al. BRCA1 interacts with poly(A)-binding protein: implication of BRCA1 in translation regulation. J Biol Chem. 2006;281(34):24236-46. Epub 2006/06/20. doi: 10.1074/jbc.M602176200. PubMed PMID: 16782705.

9.   Kais Z, Parvin JD. Regulation of centrosomes by the BRCA1-dependent ubiquitin ligase. Cancer Biol Ther. 2008;7(10):1540-3. PubMed PMID: 18927495; PubMed Central PMCID: PMCPMC2628548.

10.   Li Q, Engebrecht J. BRCA1 and BRCA2 Tumor Suppressor Function in Meiosis. Front Cell Dev Biol. 2021;9:668309. Epub 2021/05/18. doi: 10.3389/fcell.2021.668309. PubMed PMID: 33996823; PubMed Central PMCID: PMCPMC8121103.

11.   Mullan PB, Quinn JE, Harkin DP. The role of BRCA1 in transcriptional regulation and cell cycle control. Oncogene. 2006;25(43):5854-63. Epub 2006/09/26. doi: 10.1038/sj.onc.1209872. PubMed PMID: 16998500.

12.   Privat M, Radosevic-Robin N, Aubel C, Cayre A, Penault-Llorca F, Marceau G, et al. BRCA1 induces major energetic metabolism reprogramming in breast cancer cells. PLoS One.

2014;9(7):e102438. Epub 2014/07/11. doi: 10.1371/journal.pone.0102438. PubMed PMID: 25010005; PubMed Central PMCID: PMCPMC4092140.

13.   Tarsounas M, Sung P. The antitumorigenic roles of BRCA1-BARD1 in DNA repair and replication. Nat Rev Mol Cell Biol. 2020;21(5):284-99. Epub 2020/02/26. doi: 10.1038/s41580-020-0218-z. PubMed PMID: 32094664; PubMed Central PMCID: PMCPMC7204409.

14.   Brzovic PS, Keeffe JR, Nishikawa H, Miyamoto K, Fox D, 3rd, Fukuda M, et al. Binding and recognition in the assembly of an active BRCA1/BARD1 ubiquitin-ligase complex. Proc Natl Acad Sci U S A. 2003;100(10):5646-51. doi: 10.1073/pnas.0836054100. PubMed PMID: 12732733; PubMed Central PMCID: PMCPMC156255.

15.   Hashizume R, Fukuda M, Maeda I, Nishikawa H, Oyake D, Yabuki Y, et al. The RING heterodimer BRCA1-BARD1 is a ubiquitin ligase inactivated by a breast cancer-derived mutation. J Biol Chem. 2001;276(18):14537-40. doi: 10.1074/jbc.C000881200. PubMed PMID: 11278247.

16.   Witus SR, Stewart MD, Klevit RE. The BRCA1/BARD1 ubiquitin ligase and its substrates. Biochem J. 2021;478(18):3467-83. Epub 2021/10/01. doi: 10.1042/BCJ20200864. PubMed PMID: 34591954; PubMed Central PMCID: PMCPMC8763022.

17.   Kalb R, Mallery DL, Larkin C, Huang JT, Hiom K. BRCA1 is a histone-H2A-specific ubiquitin ligase. Cell Rep. 2014;8(4):999-1005. Epub 2014/08/19. doi: 10.1016/j.celrep.2014.07.025. PubMed PMID: 25131202; PubMed Central PMCID: PMCPMC4382519.

18.   Stewart MD, Zelin E, Dhall A, Walsh T, Upadhyay E, Corn JE, et al. BARD1 is necessary for ubiquitylation of nucleosomal histone H2A and for transcriptional regulation of estrogen metabolism genes. Proc Natl Acad Sci U S A. 2018;115(6):1316-21. Epub 2018/01/26. doi: 10.1073/pnas.1715467115. PubMed PMID: 29367421; PubMed Central PMCID: PMCPMC5819413.

19.   Thakar A, Parvin J, Zlatanova J. BRCA1/BARD1 E3 ubiquitin ligase can modify histones H2A and H2B in the nucleosome particle. J Biomol Struct Dyn. 2010;27(4):399-406. Epub 2009/11/18. doi: 10.1080/07391102.2010.10507326. PubMed PMID: 19916563.

20.   Becker JR, Clifford G, Bonnet C, Groth A, Wilson MD, Chapman JR. BARD1 reads H2A lysine 15 ubiquitination to direct homologous recombination. Nature. 2021;596(7872):433-7. Epub 2021/07/30. doi: 10.1038/s41586-021-03776-w. PubMed PMID: 34321663.

21.   Hu Q, Botuyan MV, Zhao D, Cui G, Mer E, Mer G. Mechanisms of BRCA1-BARD1 nucleosome recognition and ubiquitylation. Nature. 2021;596(7872):438-43. Epub 2021/07/30. doi: 10.1038/s41586-021-03716-8. PubMed PMID: 34321665; PubMed Central PMCID: PMCPMC8680157.

22.   Witus SR, Burrell AL, Farrell DP, Kang J, Wang M, Hansen JM, et al. BRCA1/BARD1 site-specific ubiquitylation of nucleosomal H2A is directed by BARD1. Nat Struct Mol Biol. 2021;28(3):268-77. Epub 2021/02/17. doi: 10.1038/s41594-020-00556-4. PubMed PMID: 33589814; PubMed Central PMCID: PMCPMC8007219.

23.   Christensen DE, Brzovic PS, Klevit RE. E2-BRCA1 RING interactions dictate synthesis of mono- or specific polyubiquitin chain linkages. Nat Struct Mol Biol. 2007;14(10):941-8. doi: 10.1038/nsmb1295. PubMed PMID: 17873885.

24.   Morris JR, Pangon L, Boutell C, Katagiri T, Keep NH, Solomon E. Genetic analysis of BRCA1 ubiquitin ligase activity and its relationship to breast cancer susceptibility. Hum Mol Genet. 2006;15(4):599-606. doi: 10.1093/hmg/ddi476. PubMed PMID: 16403807.

25.   Ransburgh DJ, Chiba N, Ishioka C, Toland AE, Parvin JD. Identification of breast tumor mutations in BRCA1 that abolish its function in homologous DNA recombination. Cancer Res. 2010;70(3):988-95. Epub 2010/01/28. doi: 10.1158/0008-5472.CAN-09-2850. PubMed PMID: 20103620; PubMed Central PMCID: PMCPMC2943742.

26.   Starita LM, Young DL, Islam M, Kitzman JO, Gullingsrud J, Hause RJ, et al. Massively Parallel Functional Analysis of BRCA1 RING Domain Variants. Genetics. 2015;200(2):413-22. Epub 2015/04/01. doi: 10.1534/genetics.115.175802. PubMed PMID: 25823446; PubMed Central PMCID: PMCPMC4492368.

27.   Reid LJ, Shakya R, Modi AP, Lokshin M, Cheng JT, Jasin M, et al. E3 ligase activity of BRCA1 is not essential for mammalian cell viability or homology-directed repair of double-strand DNA breaks. Proc Natl Acad Sci U S A. 2008;105(52):20876-81. Epub 2008/12/18. doi: 10.1073/pnas.0811203106. PubMed PMID: 19088202; PubMed Central PMCID: PMCPMC2603436.

28.   Shakya R, Reid LJ, Reczek CR, Cole F, Egli D, Lin CS, et al. BRCA1 tumor suppression depends on BRCT phosphoprotein binding, but not its E3 ligase activity. Science. 2011;334(6055):525-8. doi: 10.1126/science.1209909. PubMed PMID: 22034435; PubMed Central PMCID: PMCPMC3904783.

29.   Stewart MD, Duncan ED, Coronado E, DaRosa PA, Pruneda JN, Brzovic PS, et al. Tuning BRCA1 and BARD1 activity to investigate RING ubiquitin ligase mechanisms. Protein Sci. 2017;26(3):475-83. Epub 2016/12/16. doi: 10.1002/pro.3091. PubMed PMID: 27977889; PubMed Central PMCID: PMCPMC5326557.

30.   Adamo A, Montemauri P, Silva N, Ward JD, Boulton SJ, La Volpe A. BRC-1 acts in the inter-sister pathway of meiotic double-strand break repair. EMBO Rep. 2008;9(3):287-92. Epub 2008/01/26. doi: 10.1038/sj.embor.7401167. PubMed PMID: 18219312; PubMed Central PMCID: PMCPMC2267377.

31.   Boulton SJ, Martin JS, Polanowska J, Hill DE, Gartner A, Vidal M. BRCA1/BARD1 orthologs required for DNA repair in *Caenorhabditis elegans*. Curr Biol. 2004;14(1):33-9. PubMed PMID: 14711411.

32.   Janisiw E, Dello Stritto MR, Jantsch V, Silva N. BRCA1-BARD1 associate with the synaptonemal complex and pro-crossover factors and influence RAD-51 dynamics during *Caenorhabditis elegans* meiosis. PLoS Genet. 2018;14(11):e1007653. Epub 2018/11/02. doi: 10.1371/journal.pgen.1007653. PubMed PMID: 30383754; PubMed Central PMCID: PMCPMC6211622.

33.   Li Q, Hariri S, Engebrecht J. Meiotic Double-Strand Break Processing and Crossover Patterning Are Regulated in a Sex-Specific Manner by BRCA1-BARD1 in Caenorhabditis elegans. Genetics. 2020;216(2):359-79. Epub 2020/08/17. doi: 10.1534/genetics.120.303292. PubMed PMID: 32796008; PubMed Central PMCID: PMCPMC7536853.

34.   Li Q, Saito TT, Martinez-Garcia M, Deshong AJ, Nadarajan S, Lawrence KS, et al. The tumor suppressor BRCA1-BARD1 complex localizes to the synaptonemal complex and regulates recombination under meiotic dysfunction in Caenorhabditis elegans. PLoS Genet. 2018;14(11):e1007701. Epub 2018/11/02. doi: 10.1371/journal.pgen.1007701. PubMed PMID: 30383767; PubMed Central PMCID: PMCPMC6211623.

35.   Polanowska J, Martin JS, Garcia-Muse T, Petalcorin MI, Boulton SJ. A conserved pathway to activate BRCA1-dependent ubiquitylation at DNA damage sites. Embo J. 2006;25(10):2178-

88. Epub 2006/04/22. doi: 10.1038/sj.emboj.7601102. PubMed PMID: 16628214; PubMed Central PMCID: PMCPMC1462971.

36.   Toraason E, Salagean A, Almanzar DE, Rog O, Libuda DE. BRCA1/BRC-1 and SMC-5/6 regulate DNA repair pathway engagement during C. elegans meiosis. bioRxiv. 2022;doi: https://doi.org/10.1101/2022.06.12.495837.

37.   Trivedi S, Blazickova J, Siva N. PARG establishes a functional module with BRCA1-BARD1 that controls DNA repair pathway choice duirng gametogenesis. bioRxiv. 2022;doi: https://doi.org/10.1101/2022.06.14.496162.

38.   Garcia-Muse T, Galindo-Diaz U, Garcia-Rubio M, Martin JS, Polanowska J, O'Reilly N, et al. A Meiotic Checkpoint Alters Repair Partner Bias to Permit Inter-sister Repair of Persistent DSBs. Cell Rep. 2019;26(3):775-87 e5. Epub 2019/01/17. doi: 10.1016/j.celrep.2018.12.074. PubMed PMID: 30650366; PubMed Central PMCID: PMCPMC6334227.

39.   Kamp JA, van Schendel R, Dilweg IW, Tijsterman M. BRCA1-associated structural variations are a consequence of polymerase theta-mediated end-joining. Nat Commun. 2020;11(1):3615. Epub 2020/07/19. doi: 10.1038/s41467-020-17455-3. PubMed PMID: 32680986; PubMed Central PMCID: PMCPMC7368036.

40.   Meier B, Volkova NV, Hong Y, Bertolini S, Gonzalez-Huici V, Petrova T, et al. Protection of the C. elegans germ cell genome depends on diverse DNA repair pathways during normal proliferation. PLoS One. 2021;16(4):e0250291. Epub 2021/04/28. doi: 10.1371/journal.pone.0250291. PubMed PMID: 33905417; PubMed Central PMCID: PMCPMC8078821.

41.   Padeken J, Zeller P, Towbin B, Katic I, Kalck V, Methot SP, et al. Synergistic lethality between BRCA1 and H3K9me2 loss reflects satellite derepression. Genes Dev. 2019;33(7-8):436-51. Epub 2019/02/26. doi: 10.1101/gad.322495.118. PubMed PMID: 30804228; PubMed Central PMCID: PMCPMC6446544.

42.   Sakai Y, Hanafusa H, Shimizu T, Pastuhov SI, Hisamoto N, Matsumoto K. BRCA1-BARD1 Regulates Axon Regeneration in Concert with the Gqalpha-DAG Signaling Network. J Neurosci. 2021;41(13):2842-53. Epub 2021/02/18. doi: 10.1523/JNEUROSCI.1806-20.2021. PubMed PMID: 33593852; PubMed Central PMCID: PMCPMC8018897.

43.   Humphreys IR, Pei J, Baek M, Krishnakumar A, Anishchenko I, Ovchinnikov S, et al. Computed structures of core eukaryotic protein complexes. Science. 2021;374(6573):eabm4805. Epub 2021/11/12. doi: 10.1126/science.abm4805. PubMed PMID: 34762488; PubMed Central PMCID: PMCPMC7612107.

44.   Pettersen EF, Goddard TD, Huang CC, Meng EC, Couch GS, Croll TI, et al. UCSF ChimeraX: Structure visualization for researchers, educators, and developers. Protein Sci. 2021;30(1):70-82. Epub 2020/09/04. doi: 10.1002/pro.3943. PubMed PMID: 32881101; PubMed Central PMCID: PMCPMC7737788.

45.   Phillips CM, Dernburg AF. A family of zinc-finger proteins is required for chromosome-specific pairing and synapsis during meiosis in C. elegans. Dev Cell. 2006;11(6):817-29. doi: 10.1016/j.devcel.2006.09.020. PubMed PMID: 17141157.

46.   Alpi A, Pasierbek P, Gartner A, Loidl J. Genetic and cytological characterization of the recombination protein RAD-51 in Caenorhabditis elegans. Chromosoma. 2003;112(1):6-16. doi: 10.1007/s00412-003-0237-5. PubMed PMID: 12684824.

47.   Rinaldo C, Bazzicalupo P, Ederle S, Hilliard M, La Volpe A. Roles for *Caenorhabditis elegans rad-51* in meiosis and in resistance to ionizing radiation during development. Genetics. 2002;160(2):471-9. PubMed PMID: 11861554; PubMed Central PMCID: PMCPMC1461995.

48.   Colaiacovo MP, MacQueen AJ, Martinez-Perez E, McDonald K, Adamo A, La Volpe A, et al. Synaptonemal complex assembly in *C. elegans* is dispensable for loading strand-exchange proteins but critical for proper completion of recombination. Dev Cell. 2003;5(3):463-74. PubMed PMID: 12967565.

49.   Carlton PM, Farruggio AP, Dernburg AF. A link between meiotic prophase progression and crossover control. PLoS Genet. 2006;2(2):e12. doi: 10.1371/journal.pgen.0020012. PubMed PMID: 16462941; PubMed Central PMCID: PMCPMC1359072.

50.   Couteau F, Nabeshima K, Villeneuve A, Zetka M. A component of C. elegans meiotic chromosome axes at the interface of homolog alignment, synapsis, nuclear reorganization, and recombination. Curr Biol. 2004;14(7):585-92. Epub 2004/04/06. doi: 10.1016/j.cub.2004.03.033. PubMed PMID: 15062099.

51.   Zetka MC, Kawasaki I, Strome S, Muller F. Synapsis and chiasma formation in Caenorhabditis elegans require HIM-3, a meiotic chromosome core component that functions in chromosome segregation. Genes Dev. 1999;13(17):2258-70. Epub 1999/09/15. doi: 10.1101/gad.13.17.2258. PubMed PMID: 10485848; PubMed Central PMCID: PMCPMC317003.

52.   Severson AF, Ling L, van Zuylen V, Meyer BJ. The axial element protein HTP-3 promotes cohesin loading and meiotic axis assembly in C. elegans to implement the meiotic program of chromosome segregation. Genes Dev. 2009;23(15):1763-78. Epub 2009/07/04. doi: 10.1101/gad.1808809. PubMed PMID: 19574299; PubMed Central PMCID: PMCPMC2720254.

53.   Severson AF, Meyer BJ. Divergent kleisin subunits of cohesin specify mechanisms to tether and release meiotic chromosomes. Elife. 2014;3:e03467. Epub 2014/08/31. doi: 10.7554/eLife.03467. PubMed PMID: 25171895; PubMed Central PMCID: PMCPMC4174578.

54.   Wang H, Park H, Liu J, Sternberg PW. An Efficient Genome Editing Strategy To Generate Putative Null Mutants in Caenorhabditis elegans Using CRISPR/Cas9. G3 (Bethesda). 2018;8(11):3607-16. Epub 2018/09/19. doi: 10.1534/g3.118.200662. PubMed PMID: 30224336; PubMed Central PMCID: PMCPMC6222585.

55.   Bindels DS, Haarbosch L, van Weeren L, Postma M, Wiese KE, Mastop M, et al. mScarlet: a bright monomeric red fluorescent protein for cellular imaging. Nat Methods. 2017;14(1):53-6. Epub 2016/11/22. doi: 10.1038/nmeth.4074. PubMed PMID: 27869816.

56.   Tsien RY. The green fluorescent protein. Annu Rev Biochem. 1998;67:509-44. Epub 1998/10/06. doi: 10.1146/annurev.biochem.67.1.509. PubMed PMID: 9759496.

57.   Zacharias DA, Violin JD, Newton AC, Tsien RY. Partitioning of lipid-modified monomeric GFPs into membrane microdomains of live cells. Science. 2002;296(5569):913-6. Epub 2002/05/04. doi: 10.1126/science.1068539. PubMed PMID: 11988576.

58.   Brzovic PS, Rajagopal P, Hoyt DW, King MC, Klevit RE. Structure of a BRCA1-BARD1 heterodimeric RING-RING complex. Nat Struct Biol. 2001;8(10):833-7. doi: 10.1038/nsb1001-833. PubMed PMID: 11573085.

59.   Metzger MB, Pruneda JN, Klevit RE, Weissman AM. RING-type E3 ligases: master manipulators of E2 ubiquitin-conjugating enzymes and ubiquitination. Biochim Biophys Acta. 2014;1843(1):47-60. Epub 2013/06/12. doi: 10.1016/j.bbamcr.2013.05.026. PubMed PMID: 23747565; PubMed Central PMCID: PMCPMC4109693.

60.   Drost R, Dhillon KK, van der Gulden H, van der Heijden I, Brandsma I, Cruz C, et al. BRCA1185delAG tumors may acquire therapy resistance through expression of RING-less BRCA1. J Clin Invest. 2016;126(8):2903-18. Epub 2016/07/28. doi: 10.1172/JCI70196. PubMed PMID: 27454287; PubMed Central PMCID: PMCPMC4966325.

61.   Li M, Cole F, Patel DS, Misenko SM, Her J, Malhowski A, et al. 53BP1 ablation rescues genomic instability in mice expressing 'RING-less' BRCA1. EMBO Rep. 2016;17(11):1532-41. Epub 2016/11/04. doi: 10.15252/embr.201642497. PubMed PMID: 27670884; PubMed Central PMCID: PMCPMC5090706.

62.   Kipreos ET. Ubiquitin-mediated pathways in C. elegans. WormBook. 2005:1-24. Epub 2007/12/01. doi: 10.1895/wormbook.1.36.1. PubMed PMID: 18050424; PubMed Central PMCID: PMCPMC4781597.

63.   Ashley GE, Duong T, Levenson MT, Martinez MAQ, Johnson LC, Hibshman JD, et al. An expanded auxin-inducible degron toolkit for Caenorhabditis elegans. Genetics. 2021;217(3). Epub 2021/03/08. doi: 10.1093/genetics/iyab006. PubMed PMID: 33677541; PubMed Central PMCID: PMCPMC8045686.

64.   Zhang L, Ward JD, Cheng Z, Dernburg AF. The auxin-inducible degradation (AID) system enables versatile conditional protein depletion in C. elegans. Development. 2015;142(24):4374-84. doi: 10.1242/dev.129635. PubMed PMID: 26552885; PubMed Central PMCID: PMCPMC4689222.

65.   Hills-Muckey K, Martinez MAQ, Stec N, Hebbar S, Saldanha J, Medwig-Kinney TN, et al. An engineered, orthogonal auxin analog/AtTIR1(F79G) pairing improves both specificity and efficacy of the auxin degradation system in Caenorhabditis elegans. Genetics. 2021. Epub 2021/11/06. doi: 10.1093/genetics/iyab174. PubMed PMID: 34739048.

66.   Wu LC, Wang ZW, Tsan JT, Spillman MA, Phung A, Xu XL, et al. Identification of a RING protein that can interact in vivo with the BRCA1 gene product. Nat Genet. 1996;14(4):430-40. Epub 1996/12/01. doi: 10.1038/ng1296-430. PubMed PMID: 8944023.

67.   Chen A, Kleiman FE, Manley JL, Ouchi T, Pan ZQ. Autoubiquitination of the BRCA1*BARD1 RING ubiquitin ligase. J Biol Chem. 2002;277(24):22085-92. Epub 2002/04/03. doi: 10.1074/jbc.M201252200. PubMed PMID: 11927591.

68.   Xia Y, Pao GM, Chen HW, Verma IM, Hunter T. Enhancement of BRCA1 E3 ubiquitin ligase activity through direct interaction with the BARD1 protein. J Biol Chem. 2003;278(7):5255-63. Epub 2002/11/15. doi: 10.1074/jbc.M204591200. PubMed PMID: 12431996.

69.   Mallery DL, Vandenberg CJ, Hiom K. Activation of the E3 ligase function of the BRCA1/BARD1 complex by polyubiquitin chains. EMBO J. 2002;21(24):6755-62. Epub 2002/12/18. doi: 10.1093/emboj/cdf691. PubMed PMID: 12485996; PubMed Central PMCID: PMCPMC139111.

70.   Thompson ME. BRCA1 16 years later: nuclear import and export processes. FEBS J. 2010;277(15):3072-8. Epub 2010/07/09. doi: 10.1111/j.1742-4658.2010.07733.x. PubMed PMID: 20608972.

71.   Fabbro M, Rodriguez JA, Baer R, Henderson BR. BARD1 induces BRCA1 intranuclear foci formation by increasing RING-dependent BRCA1 nuclear import and inhibiting BRCA1 nuclear export. J Biol Chem. 2002;277(24):21315-24. Epub 2002/04/02. doi: 10.1074/jbc.M200769200. PubMed PMID: 11925436.

72.   Fielmich LE, Schmidt R, Dickinson DJ, Goldstein B, Akhmanova A, van den Heuvel S. Optogenetic dissection of mitotic spindle positioning in vivo. Elife. 2018;7. Epub 2018/08/16. doi: 10.7554/eLife.38198. PubMed PMID: 30109984; PubMed Central PMCID: PMCPMC6214656.

73.   Sherker A, Chaudhary N, Adam S, Heijink AM, Noordermeer SM, Fradet-Turcotte A, et al. Two redundant ubiquitin-dependent pathways of BRCA1 localization to DNA damage sites. EMBO Rep. 2021;22(12):e53679. Epub 2021/11/03. doi: 10.15252/embr.202153679. PubMed PMID: 34726323; PubMed Central PMCID: PMCPMC8647010.

74.   West AM, Rosenberg SC, Ur SN, Lehmer MK, Ye Q, Hagemann G, et al. A conserved filamentous assembly underlies the structure of the meiotic chromosome axis. Elife. 2019;8. Epub 2019/01/19. doi: 10.7554/eLife.40372. PubMed PMID: 30657449; PubMed Central PMCID: PMCPMC6349405.

75.   Zickler D, Kleckner N. Meiotic chromosomes: integrating structure and function. Annu Rev Genet. 1999;33:603-754. Epub 2000/02/26. doi: 10.1146/annurev.genet.33.1.603. PubMed PMID: 10690419.

76.   Wang L, Xu Z, Khawar MB, Liu C, Li W. The histone codes for meiosis. Reproduction. 2017;154(3):R65-R79. Epub 2017/07/12. doi: 10.1530/REP-17-0153. PubMed PMID: 28696245.

77.   Breast Cancer Association C, Dorling L, Carvalho S, Allen J, Gonzalez-Neira A, Luccarini C, et al. Breast Cancer Risk Genes - Association Analysis in More than 113,000 Women. N Engl J Med. 2021;384(5):428-39. Epub 2021/01/21. doi: 10.1056/NEJMoa1913948. PubMed PMID: 33471991; PubMed Central PMCID: PMCPMC7611105.

78.   Hu C, Hart SN, Gnanaolivu R, Huang H, Lee KY, Na J, et al. A Population-Based Study of Genes Previously Implicated in Breast Cancer. N Engl J Med. 2021;384(5):440-51. Epub 2021/01/21. doi: 10.1056/NEJMoa2005936. PubMed PMID: 33471974; PubMed Central PMCID: PMCPMC8127622.

79.   Knijnenburg TA, Wang L, Zimmermann MT, Chambwe N, Gao GF, Cherniack AD, et al. Genomic and Molecular Landscape of DNA Damage Repair Deficiency across The Cancer Genome Atlas. Cell Rep. 2018;23(1):239-54 e6. Epub 2018/04/05. doi: 10.1016/j.celrep.2018.03.076. PubMed PMID: 29617664; PubMed Central PMCID: PMCPMC5961503.

80.   Weber-Lassalle N, Borde J, Weber-Lassalle K, Horvath J, Niederacher D, Arnold N, et al. Germline loss-of-function variants in the BARD1 gene are associated with early-onset familial breast cancer but not ovarian cancer. Breast Cancer Res. 2019;21(1):55. Epub 2019/05/01. doi: 10.1186/s13058-019-1137-9. PubMed PMID: 31036035; PubMed Central PMCID: PMCPMC6489184.

81.   Suszynska M, Kozlowski P. Summary of BARD1 Mutations and Precise Estimation of Breast and Ovarian Cancer Risks Associated with the Mutations. Genes (Basel). 2020;11(7). Epub 2020/07/19. doi: 10.3390/genes11070798. PubMed PMID: 32679805; PubMed Central PMCID: PMCPMC7397132.

82.   Dickinson DJ, Pani AM, Heppert JK, Higgins CD, Goldstein B. Streamlined genome engineering with a self-excising drug selection cassette. Genetics. 2015;200(4):1035-49. doi: 10.1534/genetics.115.178335. PubMed PMID: 26044593; PubMed Central PMCID: PMCPMC4574250.

83.   Paix A, Folkmann A, Rasoloson D, Seydoux G. High efficiency, homology-directed genome editing in *Caenorhabditis elegans* ssing CRISPR-Cas9 ribonucleoprotein complexes. Genetics. 2015;201(1):47-54. doi: 10.1534/genetics.115.179382. PubMed PMID: 26187122; PubMed Central PMCID: PMCPMC4566275.

84.   Jaramillo-Lambert A, Ellefson M, Villeneuve AM, Engebrecht J. Differential timing of S phases, X chromosome replication, and meiotic prophase in the C. elegans germ line. Dev Biol. 2007;308(1):206-21. Epub 2007/06/30. doi: 10.1016/j.ydbio.2007.05.019. PubMed PMID: 17599823.

85.   Bishop HI, Guan D, Bocksteins E, Parajuli LK, Murray KD, Cobb MM, et al. Distinct cell-andlayer-specific expressionpatterns and independent regulation of Kv2 channel subtypes in cortical pyramidal neurons. J Neurosci. 2015;35(44):14922-42. Epub 2015/11/06. doi: 10.1523/JNEUROSCI.1897-15.2015. PubMed PMID: 26538660; PubMed Central PMCID: PMCPMC4635138.

86.   Li Q, Kaur A, Mallory B, Hariri S, Engebrecht J. Inducible degradation of dosage compensation protein DPY-27 facilitates isolation of Caenorhabditis elegans males for molecular and biochemical analyses. G3 (Bethesda). 2022;12(5). Epub 2022/04/12. doi: 10.1093/g3journal/jkac085. PubMed PMID: 35404452; PubMed Central PMCID: PMCPMC9073673.

87.   Branon TC, Bosch JA, Sanchez AD, Udeshi ND, Svinkina T, Carr SA, et al. Efficient proximity labeling in living cells and organisms with TurboID. Nat Biotechnol. 2018;36(9):880-+. doi: 10.1038/nbt.4201. PubMed PMID: WOS:000443986000031.

88.   Stewart MD, Duncan ED, Coronado E, DaRosa PA, Pruneda JN, Brzovic PS, et al. Tuning BRCA1 and BARD1 activity to investigate RING ubiquitin ligase mechanisms. Protein Sci. 2017;26(3):475-83. doi: 10.1002/pro.3091. PubMed PMID: WOS:000394992700008.

89.   Polanowska J, Martin JS, Garcia-Muse T, Petalcorin MIR, Boulton SJ. A conserved pathway to activate BRCA1-dependent ubiquitylation at DNA damage sites. Embo J. 2006;25(10):2178-88. doi: 10.1038/sj.emboj.7601102. PubMed PMID: WOS:000237590000013.
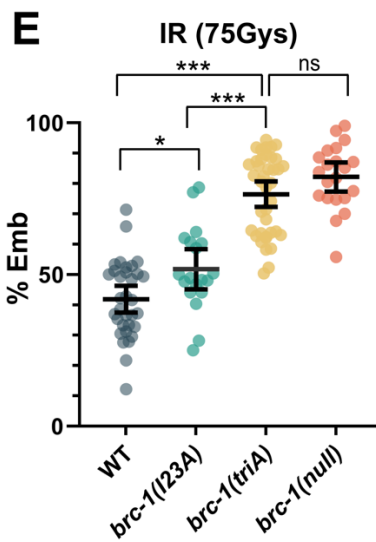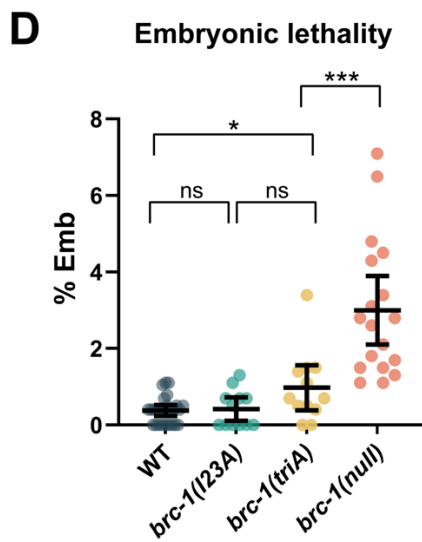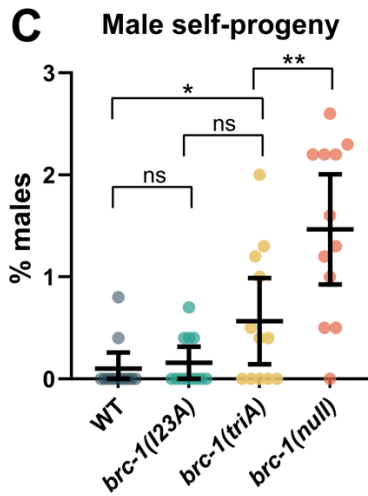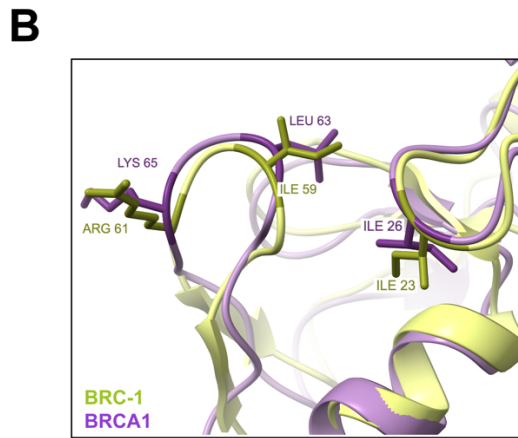
Figure 1. Mutation of three key amino acids in the BRC-1 RING domain leads to a more severe phenotype than the single I23A mutation.

(A) Sequence alignment reveals that amino acids isoleucine 23, isoleucine 59 and arginine 61 in *C. elegans* BRC-1 RING domain correspond to isoleucine 26, leucine 63 and lysine 65 in human

BRCA1 RING domain (yellow). (B) Structure of BRC-1 RING domain (green) predicted by AlphaFold superimposed onto the NMR structure of human BRCA1 RING domain (purple) showing the three amino acids occupy the same physical position. (C) Male self-progeny, (D) embryonic lethality (Emb), and (E) embryonic lethality in the presence of 75Gys IR were examined in wild type, *brc-1(I23A)*, *brc-1(triA),* and *brc-1(null)* animals. Number of animals examined in (C): n=12 for all genotypes; (D): WT n=26; *brc-1(I23A)* n=12; *brc-1(triA)* n=12; *brc-1(null)* n=18; (E) WT n=38; *brc-1(I23A)* n=19; *brc-1(triA)* n=39; *brc-1(null)* n=21. *** $p < 0.001$; ** $p < 0.01$; * $p < 0.05$; ns = not significant by Mann-Whitney.
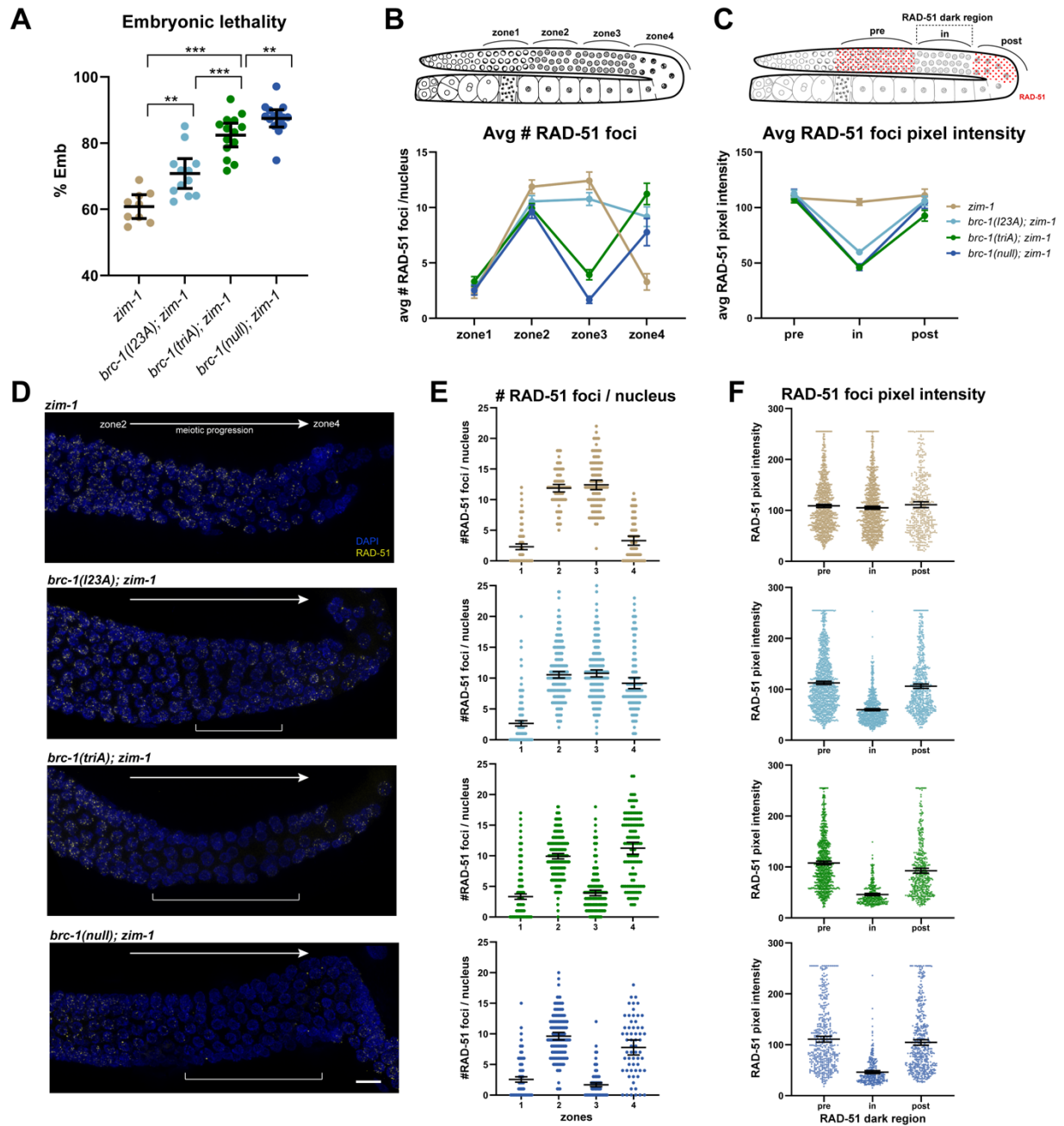
Figure 2. *brc-1(I23A)* and *brc-1(triA)* mutants show differential defects in promoting progeny

viability and RAD-51 filament stabilization in the *zim-1* mutant.

(A) Embryonic lethality of *brc-1* mutants in the *zim-1* mutant background. Embryonic lethality of *brc-1(triA); zim-1* mutant (n=14) is intermediate between *brc-1(I23A); zim-1* (n=12) and *brc-1(null); zim-1* mutants (n=15)*; zim-1* (n=9)*** p < 0.001; ** p < 0.01 Mann-Whitney. (B) Cartoon of gonad indicating the zones analyzed for RAD-51 foci numbers across the meiotic region. Graph depicts the average number of RAD-51 foci per nucleus quantified per zone from three germ lines of indicated genotypes. RAD-51 foci number only modestly declines in zone 3 in the *brc-1(I23A); zim-1* mutant. (C) Cartoon of gonad indicating regions analyzed for RAD-51 foci pixel intensity. Graph shows average pixel intensity of RAD-51 foci from pre, in and post RAD-51 dark region in three germ lines of the indicated genotypes. *brc-1(I23A); zim-1* contains nuclei with reduced RAD-51 foci intensity in the dark region but not to the extent of *brc-1(triA); zim-1* and *brc-1(null); zim-1* mutants. (D) Images showing part of the germ line from early/mid-pachytene (zone 2) to diplotene (zone 4) immunolabeled with RAD-51 antibody (yellow) and counterstained with DAPI (blue). Brackets indicate the presence and location of RAD-51 dark region in the mutant germ lines, which is not as pronounced in the *brc-1(I23A); zim-1* mutant. Scale bar = 10µm (E) Scatter plot of number of RAD-51 foci per nucleus across the four zones. (F) Scatter plot of RAD-51 foci pixel intensity from pre, in and post RAD-51 dark regions in the germ lines. Mean and 95% CI are indicated for all data sets; statistical comparisons between genotypes are shown in Supplemental Table 3.
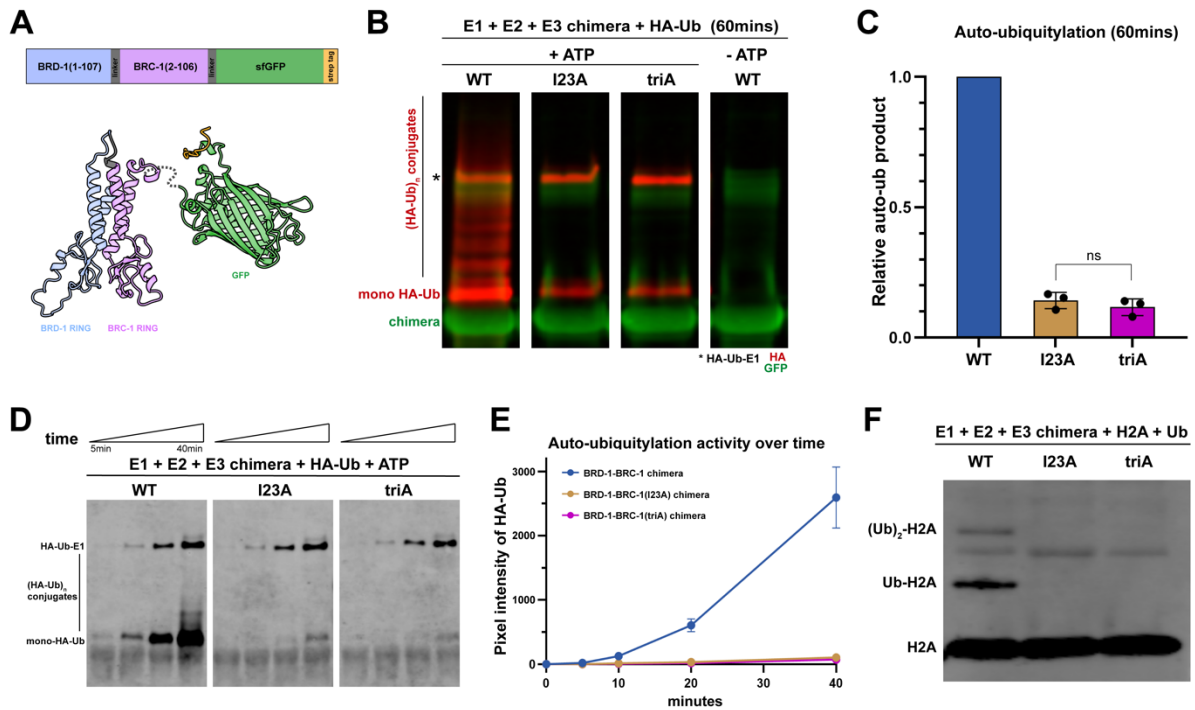
Figure 3. BRD-1-BRC-1^{I23A} and BRD-1-BRC-1^{triA} chimeras are defective for E3 ubiquitin ligase activity *in vitro*

(A) Construct and model based on AlphaFold of BRD-1-BRC-1 chimera: N-terminal BRD-1 RING domain (amino acids 1-107; blue), GGSGG linker (grey) and the BRC-1 RING domain (amino acids 2-106; purple) are connected to a superfold GFP (green) and strep II tag (orange) at the C terminus. Mutant chimera proteins contain either the single I23A or the I23A I59A R61A triple mutations (triA) in the BRC-1 RING. (B) Immunoblot showing auto-ubiquitylation (anti-HA-Ub, red) of BRD-1-BRC-1 chimera (anti-GFP, green) when incubated with E1, E2, HA-Ub and ATP for 60mins. *E1 incorporates HA-Ub (HA-Ub-E1) independently of E2 or E3s. Wild-type chimera promotes the formation of both auto-mono (mono HA-Ub) and polyubiquitylated (HA-Ub$_n$) conjugates while only reduced levels of auto-monoubiquitylated BRD-1-BRC-1 were present in mutant chimera

127

reactions. (C) Quantification of total HA-Ub signal at the end of 60mins showed that I23A and triA chimeras produced an average of 14% and 12% of total ubiquitylation, respectively, as compared to the wild-type chimera. The difference between I23A and triA is not significant (ns) by Student T test, p = 0.55. (D) Time-course experiment to compare the kinetics of E3 ligase activity of the wild-type and mutant chimeras. Immunoblot showing HA-Ub signal at 5, 10, 20, and 40mins after the respective chimera was incubated with E1, E2, HA-Ub and ATP. (E) Quantification of HA-Ub signals plotted against time in wild-type and mutant chimeras (At 40mins: I23A = 0.041±0.013, triA = 0.028±0.016 of wild-type auto-ubiquitylation). (F) Immunoblot of *C. elegans* ubiquitin incorporation into human histone H2A (anti-H2A) by WT and mutant chimeras; only WT was able to transfer ubiquitin to histone H2A protein to generate mono (Ub-H2A) and di ((Ub)$_2$-H2A) ubiquitylation, but no ubiquitin incorporation into H2A was observed with either the I23A or triA mutant chimeras.
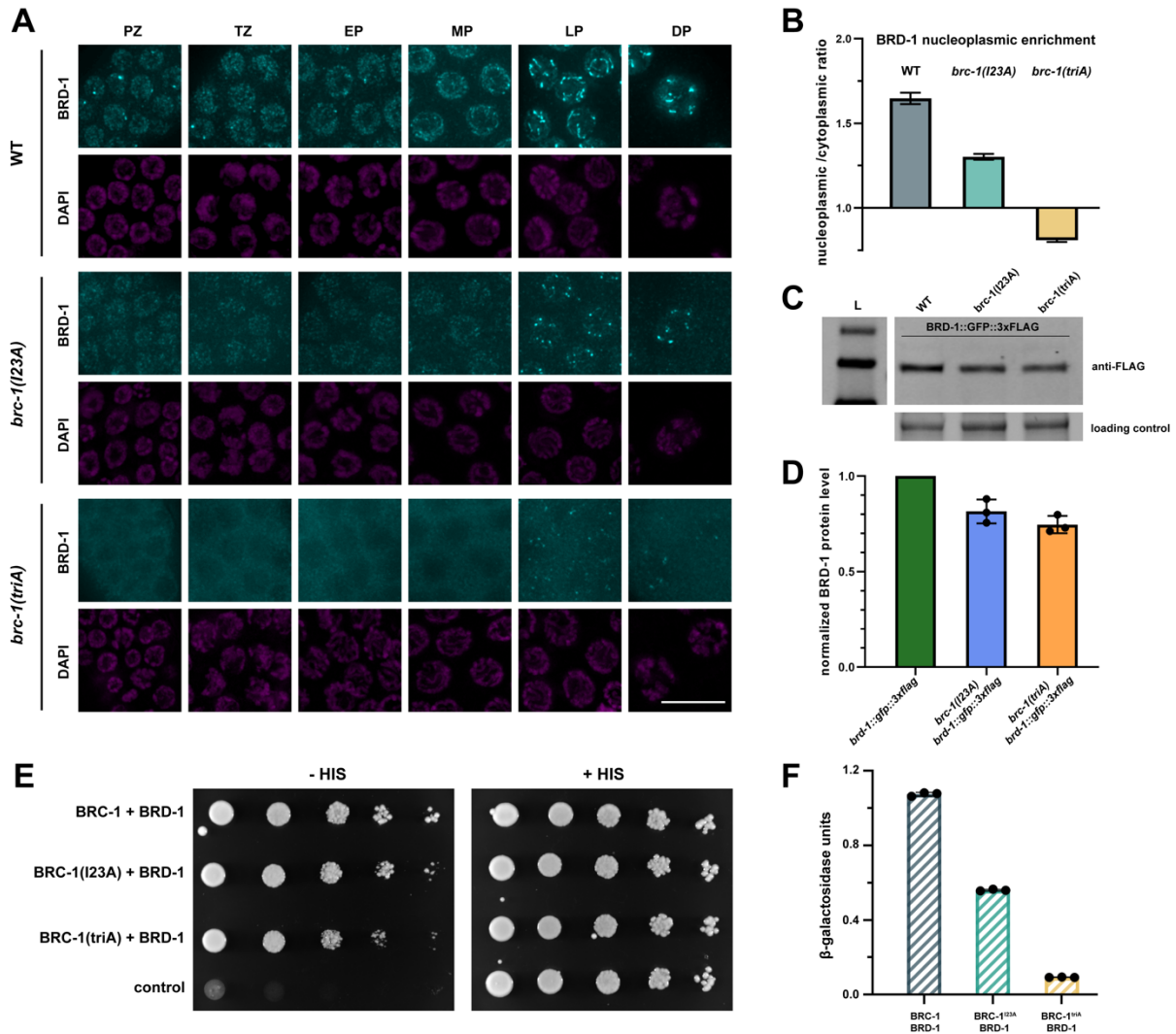
Figure 4. Nuclear accumulation and BRC-1-BRD-1 interaction are differentially affected by BRC-1^{I23A} and BRC-1^{triA} mutations

(A) Images of germline nuclei showing BRD-1 immunolabeling (cyan) by anti-BRD-1 antibodies and DAPI staining to visualize DNA (magenta). PZ = proliferative zone; TZ = transition zone; EP = early pachytene; MP = mid pachytene; LP = late pachytene; DP = diplotene stages in the germ line. Scale bar = 10μm. (B) Graph shows nucleoplasmic to cytoplasmic ratio of BRD-1 signal. (C) Immunoblot of BRD-1::GFP::3xFLAG from whole worm extracts. BRD-1::GFP::3xFLAG migrates

slower than its predicted size (112 kDa); molecular weight standards = 170, 130, 100 kDa, respectively. (D) Quantification of BRD-1::GFP::3xFLAG steady state levels in the *brc-1* mutants normalized to the wild type from 3 independent experiments. (E) Yeast two-hybrid interaction between BRC-1 and BRD-1 as measured by growth on medium lacking histidine (-HIS) with +HIS as control. (F) Relative b-galactosidase activity assay showing reduced interaction between mutant BRC-1 (I23A and triA) and BRD-1 in corresponding yeast strains.
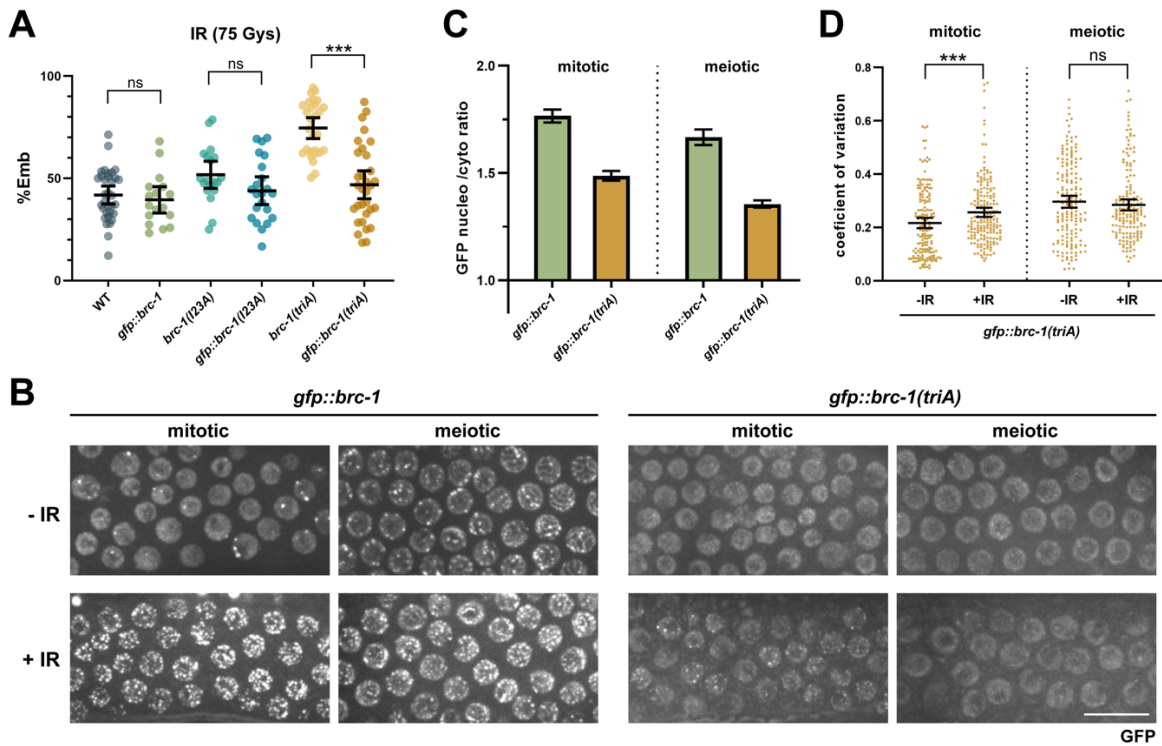
Figure 5. Nuclear accumulation of BRC-1 with impaired E3 ligase activity promotes viability in response to DNA damage.

(A) Embryonic lethality in the presence of 75Gys IR was examined in wild type (n=33), *gfp::brc-1* (n=17), *brc-1(I23A)* (n=19), *gfp::brc-1(I23A)* (n=22), *brc-1(triA)* (n=28)*,* and *gfp::brc-1(triA)* (n=32) animals. *** $p < 0.001$ Mann-Whitney. (B) Images of mitotic and meiotic (early pachytene - mid pachytene) germ cells expressing GFP::BRC-1 or GFP::BRC-1[triA] in the absence (-IR) and presence (+IR) of 75Gys radiation. Scale bar=10μm. (C) Graph shows nucleoplasmic to cytoplasmic ratio of GFP signal in *gfp::brc-1* and *gfp::brc-1(triA)* strains. A minimum of 60 nuclei from 3 germ lines were analyzed. (D) Coefficient of variation for GFP::BRC-1[triA] fluorescence to reflect changes in localization (foci formation) in response to IR in mitotic and meiotic nuclei in the germ line; five

germ lines were analyzed for each genotype. Statistical comparisons between - and + IR *** p <

0.001 Mann-Whitney.
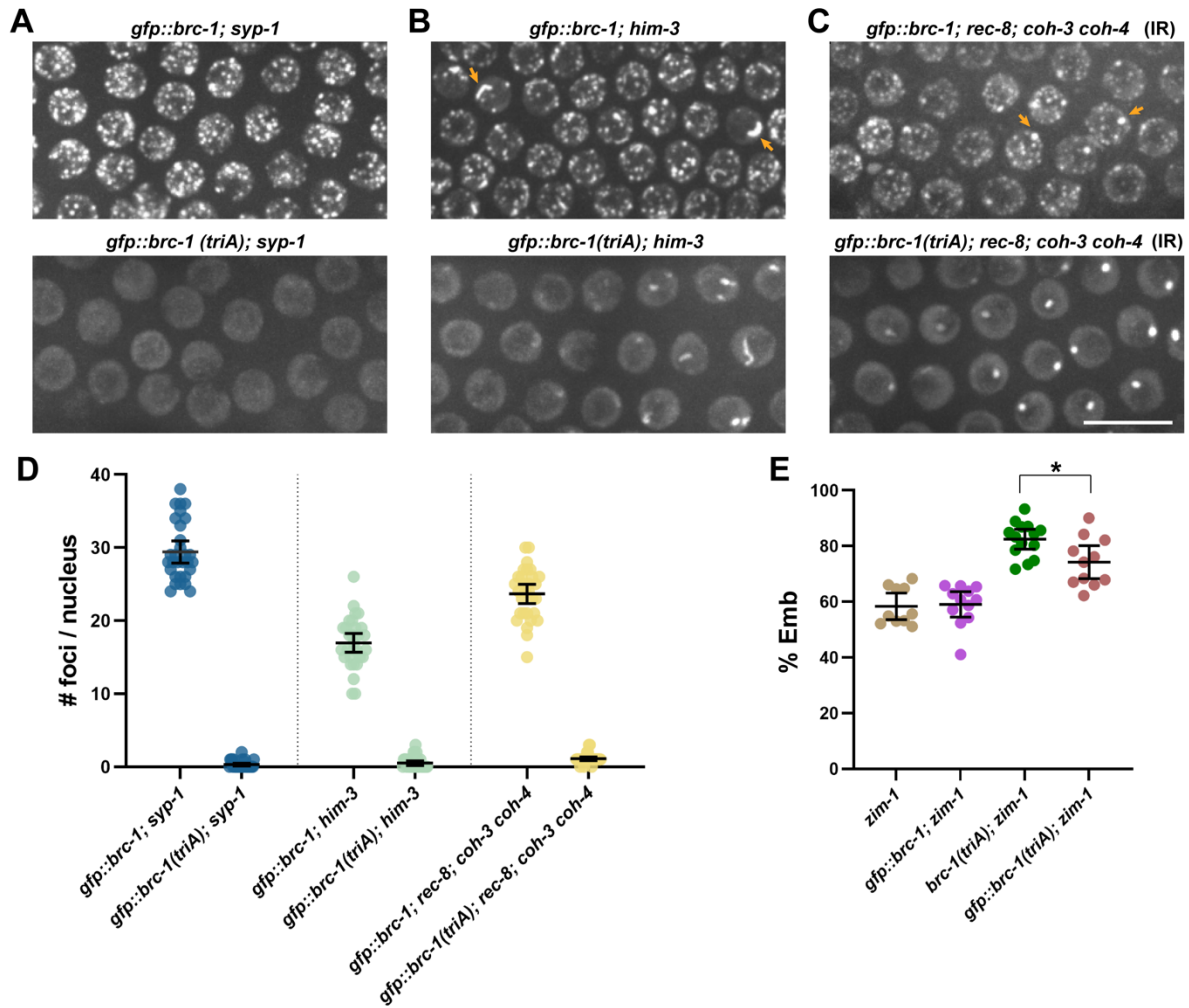
Figure 6. BRC-1-BRD-1 E3 ligase activity is essential for recruitment of the complex to DSBs on meiotic chromosomes.

Images of meiotic (early pachytene - mid pachytene) germ cells expressing GFP::BRC-1 or GFP::BRC-1^{triA} in *syp-1* (A) and *him-3* (B) mutants without IR, and *rec-8; coh-3 coh-4* mutants in the presence of 75Gys IR (C). Scale bar=10μm. (D) Quantification of GFP::BRC-1 or GFP::BRC-1^{triA} foci observed in the different mutants; a minimum of 3 germ lines from half-projections were scored. (E) Embryonic lethality in *zim-1* (n=10), *gfp::brc-1; zim-1* (n=12), *brc-1(triA); zim-1* (n=14), *gfp::brc-1(triA); zim-1* (n=11) mutants. * p < 0.05 Mann-Whitney.
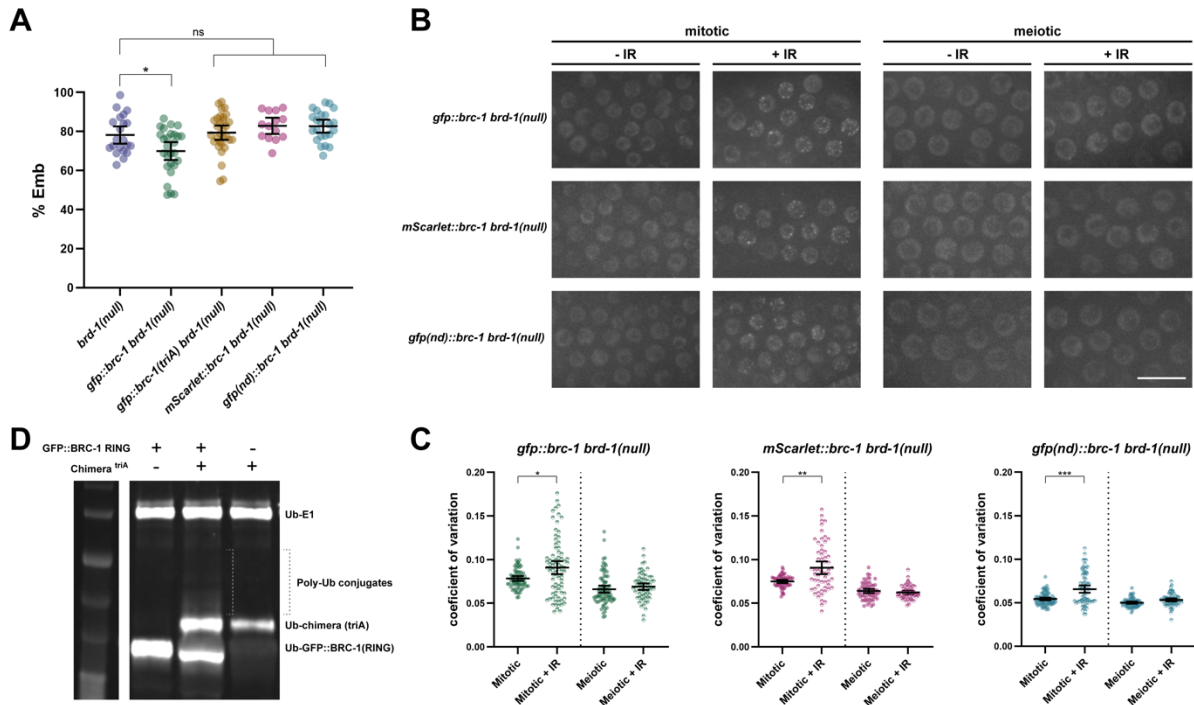
Figure 7. BRC-1 nuclear accumulation and self-association are required to partially bypass the requirement for BRD-1.

(A) Embryonic lethality in the presence of 75Gys IR was examined in *brd-1(null)* (n=21), *gfp::brc-1 brd-1(null)* (n=27), *gfp::brc-1(triA) brd-1(null)* (n=31), *mScarlet::brc-1 brd-1(null)* (n=14), *gfp(nd) brd-1(null)* (n=23). * $p < 0.05$ by Mann-Whitney. (B) Images of mitotic and meiotic (early pachytene - mid pachytene) *brd-1(null)* germ cells in the absence (-IR) and presence of IR (+IR) expressing either GFP::BRC-1, mScarlet::BRC-1 or GFP[nd]::BRC-1. Scale bar = 10µm. (C) Coefficient of variation for GFP::BRC-1, mScarlet::BRC-1, and GFP[nd]::BRC-1 fluorescence to reflect changes in localization (foci formation) in response to IR in the absence of BRD-1 in mitotic and meiotic germ cell nuclei; a minimum of 4 germ lines were analyzed for each genotype. Statistical comparisons between - and + IR by Mann-Whitney: * $p < 0.05$, ** $p < 0.01$, *** $p < 0.001$ by Mann-Whitney. (D) Immunoblot of auto-ubiquitylation (anti-HA-Ub) of GFP::BRC-1 RING, GFP::BRC-1 RING in the

presence of the BRD-1-BRC-1^{triA} chimera, and BRD-1-BRC-1^{triA} chimera alone. ~2x more monoubiquitylation on the BRD-1-BRC-1^{triA} chimera as well as polyubiquitylation were observed when GFP::BRC-1 RING was included in the reaction.
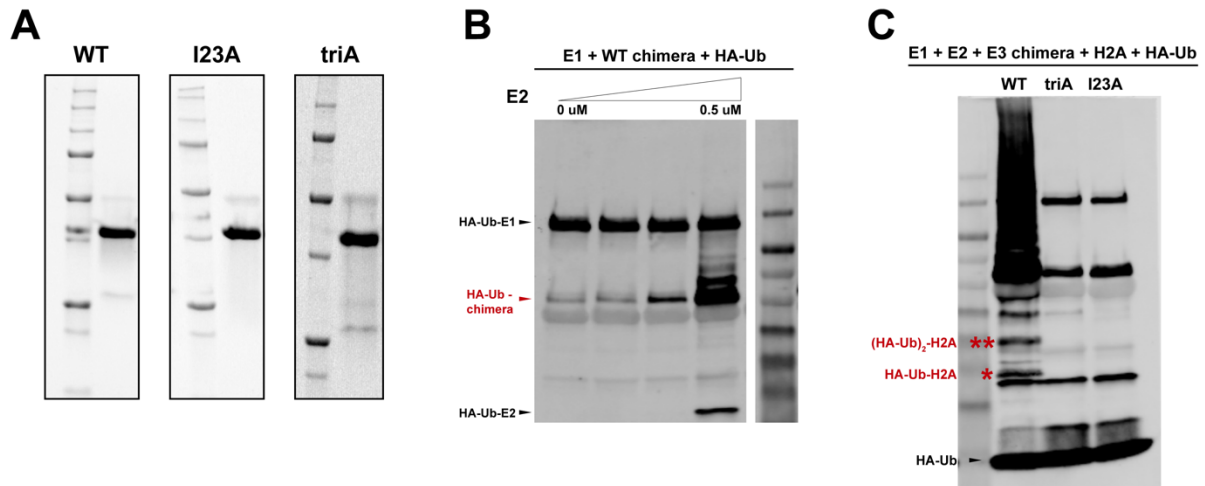
S1 Fig. BRD-1-BRC-1 chimera purification and E3 ubiquitin ligase assays.

(A) Purified chimeras visualized on stain-free gels (proteins do not run true to size as they were loaded on gel in sample buffer without heat denaturation). (B) Titration of E2 conjugating enzyme in E3 ubiquitin ligase assay shows a non-specific mono-Ub product in the absence of E2 enzyme (red). (C) Incorporation of mono- and di-HA-Ub into histone H2A as visualized by antibody against HA.
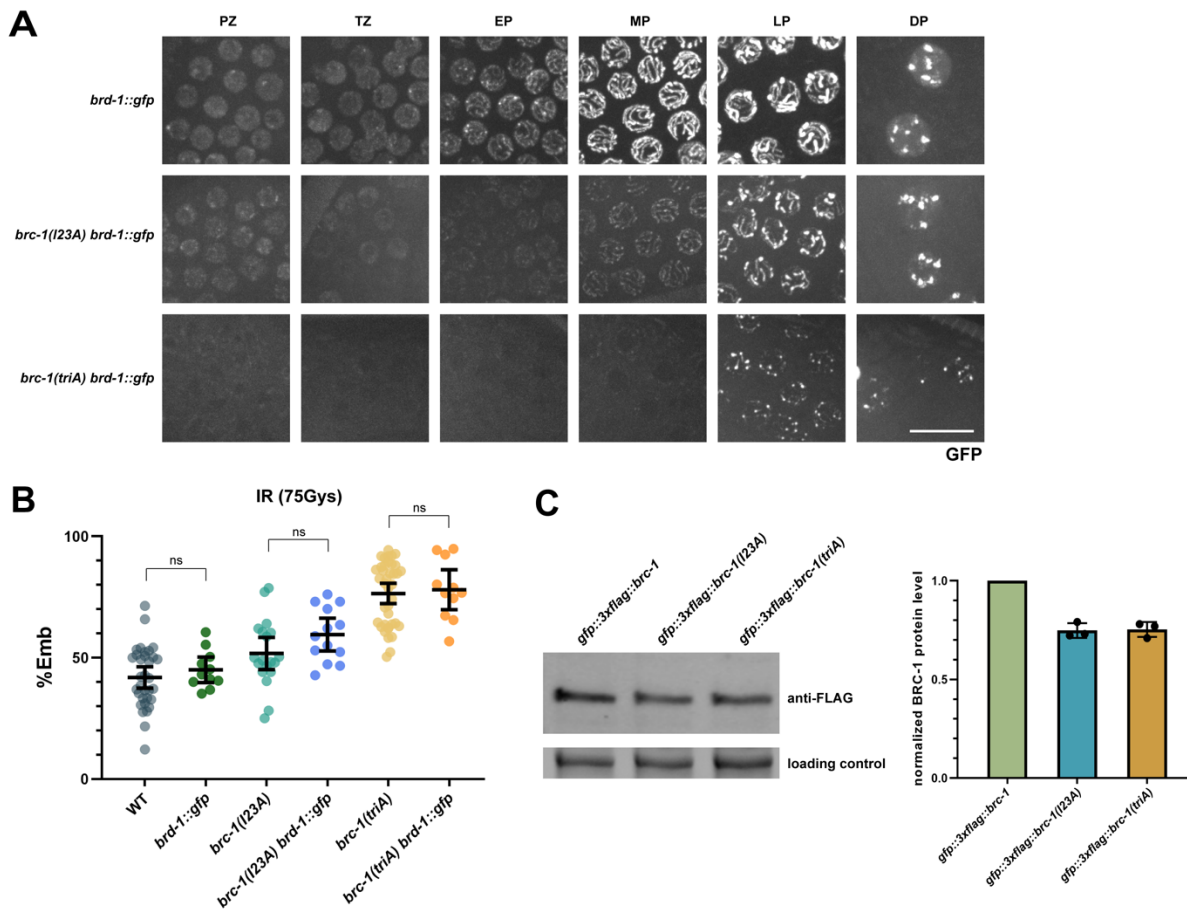
S2 Fig. C-terminal GFP fusion to BRD-1 does not promote nuclear accumulation of the complex nor rescue of embryonic lethality in response to IR treatment.

(A) BRD-1 protein localization shown by direct GFP fluorescence in wild-type and mutant *brc-1* worms in respective germ line regions. PZ = proliferative zone; TZ = transition zone; EP = early pachytene; MP = mid pachytene; LP = late pachytene; DP = diplotene. Scale bar = 10μm. (B) Embryonic lethality of worms treated with 75Gys IR. C-terminal GFP fusion to BRD-1 did not rescue viability in the *brc-1* mutants. (C) Immunoblot (left) showing steady state levels of BRC-1 proteins from wild type and mutant whole worm extracts. Levels of mutant BRC-1 proteins normalized to wild type protein from three independent experiments (right).
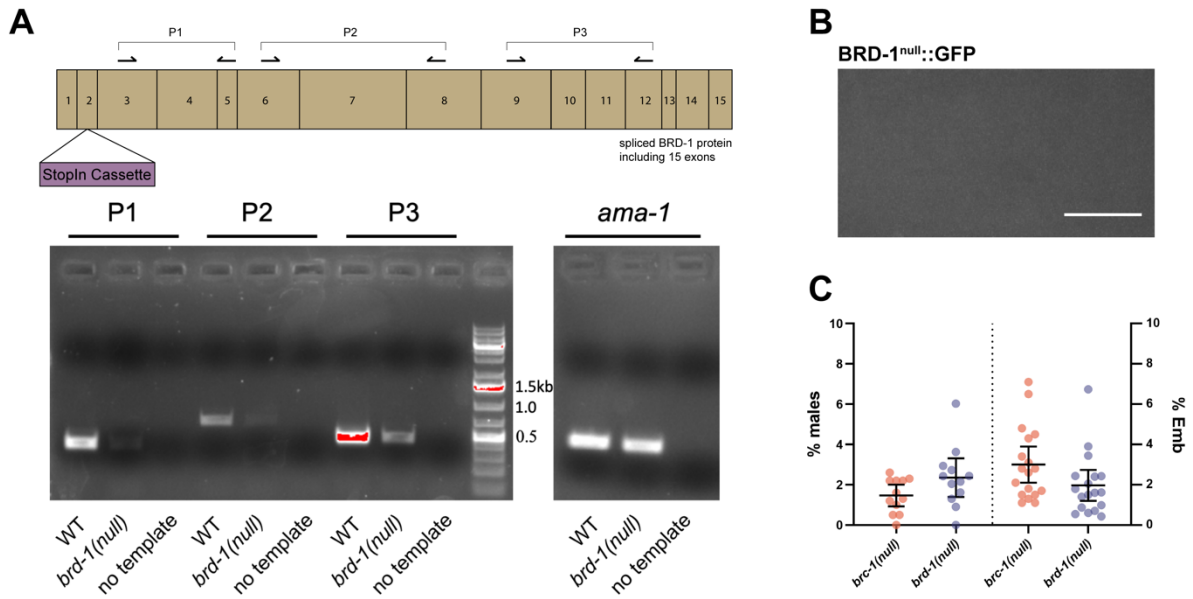
S3 Fig. Analysis of *brd-1(null)*.

(A) BRD-1 exon structure and position of insertion of the stop-in cassette. Primer pairs (P1-P3) used for RT-PCR of wild type and *brd-1(null)* cDNA are indicated. P1 Forward: cgccacatttcaacagaaacc, P1 Reverse: gcttctttgctgtagtcgtg; P2 Forward: cgcgtaattcgacaaaacgc, P2 Reverse: gcattaataactgcacccgc; P3 Forward: ggctcaacattagaaacaacgc, P3 Reverse: gatcaataatgcacgctctcag. *ama-1* was used as control [86]. B) No GFP fluorescence was observed in *brd-1(null)::gfp* worms. Scale bar = 10mm. (C) Male self-progeny (left Y axis; n=12) and embryonic lethality (right Y axis; n=18) of *brc-1(null)* and *brd-1(null)* worms.
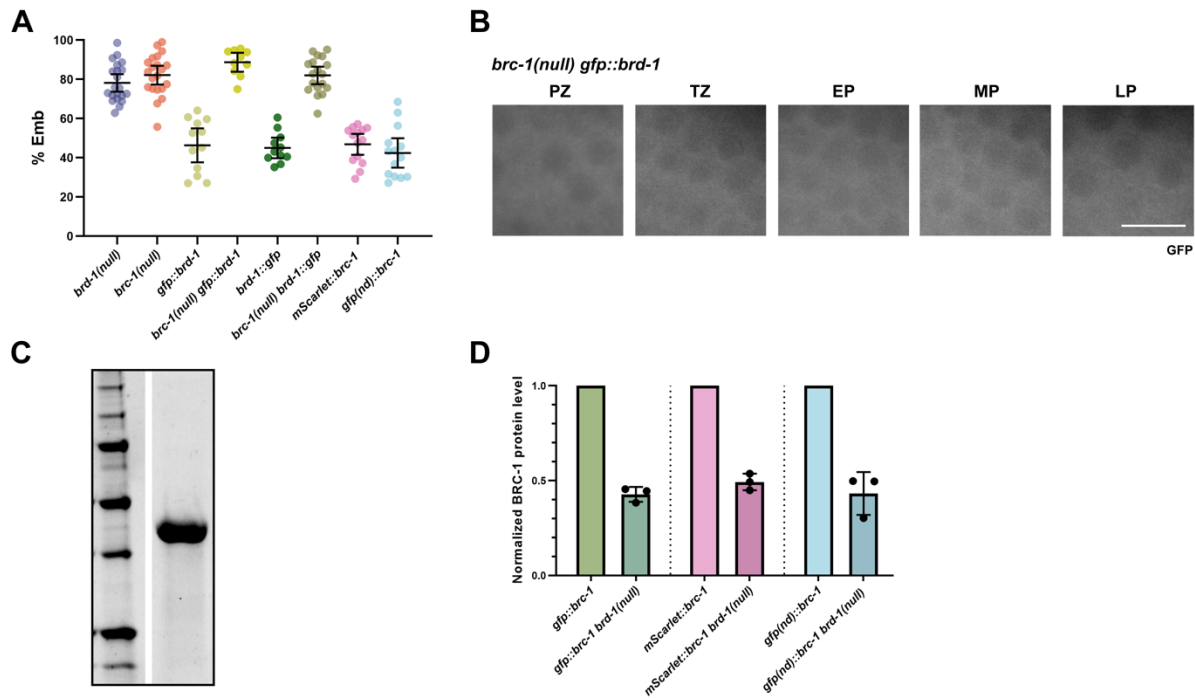
S4 Fig. Embryonic lethality of different fluorescent protein fusions and GFP::BRC-1 RING purification.

(A) Embryonic lethality in the presence of 75Gys IR was examined in *brd-1(null)* (n=21), *brc-1(null)* (n=21), *gfp::brd-1* (n=12), *brc-1(null) gfp::brd-1* (n=10), *brd-1::gfp* (n=11), *brc-1(null) brd-1::gfp* (n=18), *mScarlet::brc-1* (n=14), *gfp(nd)::brc-1* (n=14). (B) Direct GFP fluorescence of germ cell nuclei from *brc-1(null) gfp::brc-1*. Scale bar = 10μm. (C) Purified GFP::BRC-1 RING protein visualized on stain-free gel (protein does not run true to size as it was loaded on gel in sample buffer without heat denaturation). (D) Graph of relative steady state levels of GFP::BRC-1, mScarlet::BRC-1, and GFP[nd]::BRC-1 in the *brd-1(null)* mutant.

Chapter 6

Conclusions and future directions

Conclusions

I studied the meiotic roles of the tumor suppressor BRCA1-BARD1 in both oogenesis and spermatogenesis using *C. elegans* as a model for my dissertation work. In the first chapter, I reviewed recent studies that focused on meiotic functions of BRCA1-BARD1 in mice and worms. While evidence suggests mouse BRCA1-BARD1 is involved in meiotic recombination, both genes are essential and the use of viable hypomorphic alleles precludes in-depth analysis of phenotypic consequences resulting from complete loss of BRCA1-BARD1 function. Further, BRCA1-BARD-1 is essential for meiotic sex chromosome inactivation (MSCI) in mouse spermatogenesis, the disruption of which leads to pachytene arrest and apoptosis of germ cells. As a result, BRCA1-BARD1 function in meiotic recombination during spermatogenesis has not been previously reported. In *C. elegans*, BRC-1-BRD-1 is suggested to play a role in promoting inter-sister recombination during oogenesis but this function alone does not explain the phenotypes observed for the loss of function mutants. Additionally, it remains controversial whether E3 ubiquitin ligase activity of BRCA1-BARD1 is essential for its *in vivo* function, particularly with respect to DNA repair and recombination. With these gaps in knowledge in mind, I examined the roles of BRC-1-BRD-1 in *C. elegans* meiosis and reported my findings in the following chapters.

Chapter two focuses on the meiotic roles of BRC-1-BRD-1 in oogenesis. I described the localization pattern of BRC-1 and BRD-1 in the oogenic *C. elegans* gonad based on live cell imaging using worms expressing endogenous functional GFP fusions to the N-terminus of BRC-1 and the C-terminus of BRD-1. Both proteins form foci that colocalize with RAD-51 and concentrate to the short arm upon crossover designation in late pachytene, consistent with BRC-1-BRD-1 playing roles in both recombinational repair and crossover patterning. I found the complex is essential

for promoting viability when meiosis is impaired such as in the *zim-1* mutant background and reported a previously uncharacterized role of BRC-1-BRD-1 in stabilizing RAD-51 filaments to prevent their precocious disassembly in mid-late pachytene under situations where as few as one chromosome pair is not able to establish a crossover. I also discovered that BRC-1-BRD-1 regulates crossover numbers and distribution by SNP markers based genetic linkage analysis. In the *zim-1* mutant background, BRC-1-BRD-1 promotes the formation of extra crossovers accompanied by a high level of COSA-1 foci, and mutation of BRC-1 leads to a reduction in the number of double crossovers while the overall genetic map distance remains similar, suggesting a likely increase in the number of single crossovers. This observation indicates a previously unappreciated role for BRC-1-BRD-1 in regulating crossovers along with other key cellular components for chiasma formation under meiotic dysfunction.

In chapter three, I described the meiotic roles of BRC-1-BRD-1 during spermatogenesis in *C. elegans* males. I reported that, different from mice, *C. elegans* BRC-1-BRD-1 is not essential for MSCI, allowing functional analysis of the complex in meiosis using null mutants. I discovered that BRC-1-BRD-1 promotes HR by facilitating DNA resection on processed meiotic DSBs in early pachytene, and in the absence of BRC-1-BRD-1, non-homologous end joining (NHEJ) pathway is responsible for repairing a subset of meiotic DSBs. This role of BRC-1-BRD-1 in favoring HR at the expense of NHEJ resembles one of the established functions for the complex in mammalian somatic cells. Although BRC-1 and BRD-1 localization in the male germ line are very similar to what is observed in the female germ line, there are differences between the two sexes with respect to BRC-1-BRD-1 function. First, I found that functional BRC-1-BRD-1 is important in the male germ line for enhancing sperm quality in the *zim-1* mutant but this is not achieved by

stabilizing the RAD-51 filaments as in the female germ line. Moreover, I found that BRC-1-BRD-1 suppresses the formation of extra crossovers in the *zim-1* mutant background, evidenced by higher levels of COSA-1 foci and expanded map distance with increased numbers of double and triple crossovers when BRC-1-BRD-1 is inhibited. These findings are surprising because they are contrary to what I observed for BRC-1-BRD-1 function during oogenesis.

To further characterize the molecular mechanisms for BRC-1-BRD-1 function during male meiosis, particularly in identifying its binding partners at different stages of meiotic prophase, I described a method in chapter four that allows for collecting large quantities of male worms with high purity. This method takes advantage of the auxin-inducible degradation system to conditionally deplete DPY-27, a component of dosage compensation complex which is required for embryonic viability in hermaphrodites. This method solves a long-standing challenge in the field for collecting sufficient quantities of male worms with relative ease. I will discuss the application of this method in conjunction with other tools to answer remaining questions with respect to BRC-1-BRD-1 meiotic functions in the next section.

In chapter five, I studied the requirement of E3 ubiquitin ligase activity for BRC-1-BRD-1 *in vivo* function by examining the phenotypic consequences of mutating three key amino acids residing in the RING domain of BRC-1. I found that the *brc-1(triA)* mutant exhibits phenotypes that are close to, but not identical to the null, and the phenotypes are stronger than the *brc-1(I23A)* mutant. I showed that BRC-1^{triA} and BRC-1^{I23A} have similarly impaired *in vitro* E3 ligase activity but the interaction between BRC-1 and BRD-1 is weakened when BRC-1 contains the triple alanine mutations. Examination of protein localization revealed that E3 ligase activity is important for BRC-1-BRD-1 nuclear retention and also critical for the recruitment of the complex

to DNA damage sites in the meiotic region of the gonad but not in the proliferative region where cells divide mitotically. Further, I discovered that induced nuclear localization of BRC-1 and its self-association in the absence of BRD-1 is partially functional, resulting in phenotypic rescue in response to ionizing radiation. My findings confirm the essentiality of E3 ligase activity of BRC-1-BRD-1 in DNA damage repair and meiosis, and implicate BRC-1 as the major component in the complex while BRD-1 is an accessory partner to enhance BRC-1 function.

Future directions on sex-specific functions of BRC-1-BRD-1 during meiosis

As described in chapter two and three, BRC-1-BRD-1 exhibits different functions in meiotic DSB repair at specific substages of meiotic prophase in the oogenic and spermatogenic germ lines. Sex-specific differences of BRC-1-BRD-1 are also manifested in the opposing effects on crossover numbers and positioning. As BRC-1-BRD-1 shows similar localization patterns throughout meiotic prophase in the two sexes, the observed functional difference of BRC-1-BRD-1 may result from the complex ubiquitylating distinct substrates at various stages during oogenesis and spermatogenesis. To date, *bona fide* physiological substrates of BRC-1-BRD-1 in the *C. elegans* germ line have not been reported. In the ubiquitylation pathway, interaction between E3 and substrate is relatively transient, posing a challenge to identify substrates using traditional pull down assays. *In vivo* proximity labeling utilizing engineered enzymes such as TurboID, a biotin ligase [1], followed by streptavidin pulldown and mass spectrometry, can be used to identify potential substrates from hermaphrodite and male worms. This requires engineering worms expressing TurboID fused to BRC-1 or BRD-1 at their endogenous loci. For male-specific samples, proximity labeling and the auxin-inducible degradation method described in chapter four will be

combined together to collect pure populations of males for detecting potential BRC-1-BRD-1

substrates from the male germline, and the results will be compared to those identified from

pure hermaphrodite samples. Knowledge of physiological substrates will provide insight into the

molecular mechanisms of BRC-1-BRD-1 in regulating meiotic DSB repair and crossover patterning

in the two different sexes. Alternatively, BRC-1-BRD-1 may also pair with different E2 conjugating

enzymes in the female and male germ lines. As has been reported, mammalian BRCA1-BARD1

can function with multiple E2 enzymes *in vitro*, leading to the formation of different ubiquitin

modifications on substrates [3]. UBC-2 was identified from previous studies as an E2 enzyme that

functions with BRC-1-BRD-1 in DNA damage repair in hermaphrodite germlines [2]; however,

whether additional E2 enzymes pair with BRC-1-BRD-1 and are involved in crossover regulation,

or in the male germ line, remain enigmatic. Future investigation could use similar approaches as

mentioned above to identify potential E2 enzymes, and such information will help demystify the

various functions that BRC-1-BRD-1 play in *C. elegans* oogenesis and spermatogenesis.

Future directions on determining the role of the sequence deleted in *brc-1(tm1145)*

and its relationship to E3 ligase activity

In chapter five, I reported that neither *brc-1* null allele nor the E3 ligase defective *brc-1(triA)*

allele is able to stabilize the RAD-51 filaments in *zim-1* mutant background, suggesting that a

functional BRC-1 protein, and more specifically, its E3 ubiquitin ligase activity, is required to

prevent the RAD-51 filament from premature disassembly when meiosis is impaired. Further,

E3 ligase activity is essential for recruiting BRC-1-BRD-1 to DNA damage sites and form

concentrated foci in the meiotic region of the gonad, as GFP::BRC-1^{triA} protein does not form

foci in response to either SPO-11 or IR induced DNA DSBs. On the other hand, *brc-1(tm1145)* is a hypomorphic allele with an in-frame deletion of 71 amino acids C-terminal to, but not immediately next to, the RING domain of BRC-1. The deleted 213 bp sequence is specifically found in *Caenorhabditis* species and does not bear obvious homology with other mammalian BRCA1 orthologs. As reported in chapter two, the *brc-1(tm1145)* allele also displays a defect in RAD-51 filament stabilization, similar to the *brc-1(triA)* mutant. Additionally, live cell imaging on worms expressing a GFP fusion to the N-terminus of BRC-1^{tm1145} shows that the protein is not capable of forming foci in the meiotic region even when high levels of DSBs are present. Further, when worms are treated with hydroxyurea, BRC-1-BRD-1 are excluded from nuclei and relocated in the cytoplasm in an extended region from the proliferative zone into mid-pachytene. These observed phenotypes for *brc-1(tm1145)* highly resemble those of the *brc-1(triA)* allele and raise an interesting question if the region deleted in the *brc-1(tm1145)* is involved in E3 ubiquitin ligase activity, even though the sequence clearly is outside of the RING domain. One possibility is that this deleted region defines an interaction site with a BRC-1 binding partner in the context of DSB recombinational repair where E3 ligase activity is equally important. To elucidate the molecular basis of this sequence, a yeast-two-hybrid screen could be performed to identify potential binding partners. Although very unlikely, there is also a possibility that this sequence is directly involved in regulating the RING domains of BRC-1 and BRD-1, and therefore may affect E3 ligase activity. Using recombinant BRC-1 proteins in the presence or absence of the region deleted in *brc-1(tm1145)* and performing *in vitro* E3 ligase activity assay will provide insights into the functional connection between this sequence and the RING domain. Future directions described above will further our understanding of how BRC-

1 functions in a network of protein players during meiosis and how the regulation of BRC-1-

BRD-1 E3 ligase activity has evolved throughout evolution.

References

1.   Branon TC, Bosch JA, Sanchez AD, Udeshi ND, Svinkina T, Carr SA, et al. Efficient proximity labeling in living cells and organisms with TurboID. Nat Biotechnol. 2018;36(9):880-7. Epub 2018/08/21. doi: 10.1038/nbt.4201. PubMed PMID: 30125270; PubMed Central PMCID: PMCPMC6126969.
2.   Polanowska J, Martin JS, Garcia-Muse T, Petalcorin MI, Boulton SJ. A conserved pathway to activate BRCA1-dependent ubiquitylation at DNA damage sites. Embo J. 2006;25(10):2178-88. Epub 2006/04/22. doi: 10.1038/sj.emboj.7601102. PubMed PMID: 16628214; PubMed Central PMCID: PMCPMC1462971.
3.   Stewart MD, Duncan ED, Coronado E, DaRosa PA, Pruneda JN, Brzovic PS, et al. Tuning BRCA1 and BARD1 activity to investigate RING ubiquitin ligase mechanisms. Protein Sci. 2017;26(3):475-83. Epub 2016/12/16. doi: 10.1002/pro.3091. PubMed PMID: 27977889; PubMed Central PMCID: PMCPMC5326557.